TAILORING HMHDPE/LLDPE BLEND FOR HIGH PERFORMANCE APPLICATIONS: ROLE OF NANOZIRCONIA, SILICA NANOFIBERS

Thesis submitted to

Cochin University of Science and Technology

in partial fulfilment of the requirements

for the award of the degree of

Doctor of Philosophy

Shadiya M. A.

Department of Polymer Science and Rubber Technology
Cochin University of Science and Technology
Kochi- 682 022, Kerala, India

August 2017

Tailoring HMHDPE/LLDPE Blend for High Performance Applications: Role of Nanozirconia, Silica Nanofibers

Ph. D Thesis

Author

Shadiya M. A.
Research Scholar
Department of Polymer Science and Rubber Technology
Cochin University of Science and Technology
Cochin- 682 022, Kerala, India
E-mail: shadiya.ashraf@gmail.com

Supervising guide

Dr.K. E. George
Professor (Retd.)
Department of Polymer Science and Rubber Technology
Cochin University of Science and Technology
Cochin- 682 022, Kerala, India
E-mail:principal@aisat.ac.in

Department of Polymer Science and Rubber Technology
Cochin University of Science and Technology
Cochin- 682 022, Kerala, India

August2017

Department of Polymer Science and Rubber Technology
Cochin University of Science and Technology
Cochin- 682 022, Kerala, India

Dr.K. E. George
Retd. Professor

Phone: +91 9446447851
Email:rani@cusat.ac.in

04/08/2017

Certificate

     This is to certify that the thesis entitled **"Tailoring HMHDPE/LLDPE Blend for High Performance Applications: Role of Nanozirconia, Silica Nanofibers"** is an authentic record of research work carried out by **Shadiya M. A.** under my supervision and guidance in the Department of Polymer Science and Rubber Technology, Cochin University of Science and Technology, Cochin-22. No part of the work reported in this thesis has been presented for any other degree from any other institution. All the relevant corrections and modifications suggested by the audience during the pre-synopsis seminar and recommended by the Doctoral committee have been incorporated in the thesis.

Dr.K. E. George
(Supervising Guide)

Declaration

I hereby declare that the thesis entitled **"Tailoring HMHDPE/LLDPE Blend for High Performance Applications: Role of Nanozirconia, Silica Nanofibers"** is the bonafide work carried out by me under the supervision of **Dr. K. E. George** Rtd. Professor, Department of Polymer Science and Rubber Technology, Cochin University of Science and Technology, Cochin-22 and has never been included in any other thesis submitted previously for the award of any degree.

Cochin – 22   *Shadiya M. A.*
04/08/2017

Dedicated to

ALLAH, *The God Almighty*

The most beneficent and merciful

Who gave me such a wonderful family members and friends

Acknowledgements

acquaintance. The enthusiasm and research aptitude of teacher has lit a positive vibe in my life till now. Teacher, thank you for being with me for all your friendship and motherly affection. Next I would like to thank our Bindhu teacher who inspired me by her vibrant presentation skills and readiness to take up all challenges given whether it is life or academics. She is my conference pal! Teacher guided me in writing papers and inspired a lot and builds confidence in me to present my work in conferences and has taken special interest in making sure that I complete my work in the time bound. Julie chechi and her family…I have no words to extend my gratitude to them…… Binuchettan and kids have shown high degree of care in supporting me complete my thesis at this moment. Julie chechi is a strong pillar of support to rely upon even at midnight and is more cautious in helping me to complete this tedious task. Despite her busy life she had time and concern for me for which I have always felt blessed. Thank you chechi for your unconditional love and care.

I thank Sreedevichechi for being my elder sister scolding me for my kiddish demands and for being the soul who lifted me up as and when I felt desperate and disappointed. She taught me to handle and manage tasks at its best ever possible way. I am definitely going to miss your guidance and love. Words are inadequate to thank Nisha as she was always with me even after her submission. Throughout this long journey of research life Neenachechi and my classmate Neena are two other special duals who have left their benchmark in my thesis. Whenever a theoretical doubt or guidance is required neenachechi is there with a solution and a novel idea every time. And my Neena is always there as an anchor of my flawless journey. Renjuchechi is another personality to whom I would love to extend gratitude and thanks for her calm and sweet support which has always made me feel that I am not alone, chechi has taught me to manage, to overcome all those pains and difficulties I met within and around me during my stay at the department.

Dhanyachechi… thank you for your selfless assistance in making my thesis and for all those pain you have taken in making my thesis perfect. I would like to extend my sincere gratitude to Jolly sir, a caring brother for his help during my difficult times. A similar kind of concern and friendship was shown by Venu sir and Gean sir ….thanks a lot. Bipin sir was there as a well wisher during my stay at the PS&RT, I thank you for being there. Bhagyesh, its because of you I could keep the thread of my research lively, even in my hardships. You carried out all those tasks as

||||| Preface |||||

Modification of polymer blends with nanofillers has opened up infinite ways to develop materials of choice. Polyolefins are the most widely used matrix for polymer nanocomposites becomes general due to their wide spectrum of properties finding applications in diverse fields.

The various spectrums of nanomaterials include metal oxides, nanoclay, nanocellulose, carbon nanotubes, graphene, etc. Nanozirconia is a versatile nanomaterial with diverse applications due to its innate mechanical and thermal stability. Zirconia has three well-defined polymorphs: the tetragonal, monoclinic and cubic form. The aim of this study is to demonstrate a polymeric surfactant assisted sol- gel method for the preparation of highly stabilized t- ZrO_2. Since polymeric surfactant acts as a dispersing medium, the very frequent crisis of nanoparticles agglomeration can be completely avoided. Further the role of mode of addition leading to the formation of monoclinic crystallite phase with spheroid morphology is also well explored.

Nanosilica, like any other nanomaterial has gained great interest in the field of food industry, catalysis, chromatography, coatings, stabilizers, emulsifiers and biological sciences. The conventional synthesis of nanosilica includes vapour-phase reaction, sol–gel and thermo-decomposition methods. In most of these methods alkyl orthosilicates or sodium silicates are the silicon source. But the limited availability of crude oils and high processing cost has initiated a considerable interest in sustainable and renewable resources for the development of nanosilica. Silica deposited in plants as opal phytolith can be easily leached by acid hydrolysis. The novel green chemical route for the isolation of fibrous nanosilica by exploiting the vast and abundant green sources like Indian grass, flowers of pampas grass and bamboo.

The reinforcing effect of the synthesized nanozirconia (both t and m-ZrO_2 forms) and the isolated silica fibers on HMHDPE/ LLDPE blends

are discussed in detailed. The mechanical, thermal and rheological properties of nanocomposites are investigated. Improvements are observed in the compressive, impact and flexural properties. Commendable increase in wear resistance of the composites is also noted.

The thesis entitled **"Tailoring HMHDPE/LLDPE blend for High Performance Applications: Role of Nanozirconia, Silica nanofibers"** consist of eight chapters.

A brief introduction on polymer blends, polymer nanocomposites, polyolefins, nanofillers, nanozirconia, and nanosilica etc. is given in **Chapter 1**. The scope and objective of the work is also presents in the chapter. A review of thermoplastics polymer nanocomposites is provided. Scope and objectives of the present work are also included.

Chapter 2 of the thesis gives the details of materials used in the present work and the experimental techniques employed for the preparation and characterization of the fillers and nanocomposites are described.

The synthesis of nanozirconia by a surfactant assisted sol-gel method is given in **Chapter 3**. Poly vinyl alcohol (PVA) is used as the polymeric surfactant for size reduction of the nanomaterial synthesized and different weight % PVA was chosen to control the size of the final product. By varying the mode of addition of the reactants, different crystalline form and morphology for nanozirconia can be derived. By changing the reaction conditions like final calcination temperatures, a notable change in particle size, morphology, degree of agglomeration and crystallinity are observed.

The isolation of silica nanofibers from three different grass sources namely Indian grass, Pampas grass and Bamboo is described in **Chapter 4**. Acid pre-treatment followed by calcination is employed for the isolation of silica and the optimum conditions and the detailed characterizations of the isolated fibrous nanosilica are discussed in detail.

Chapter 5 is divided into part A and part B. Part A focuses on the optimization of the polymer blend by evaluating its mechanical, thermal and rheological parameters. High molecular weight high density polyethylene (HMHDPE) and linear low density polyethylene (LLDPE) are selected for the preparation of blend and 80/20 HMHDPE-LLDPE (HL-2) blend is chosen for further nanocomposite fabrication. PartB describes the fabrication and evaluation of the synthesized nanozirconia on the mechanical, thermal, morphological and rheological behavior of the blend.

Chapter 6 of the thesis deals with the fabrication and evaluation of fibrillar nanosilica composite of HL-2 blend. The effects of CGS, PGNS and BMS silica in modifying the HL-2 matrix are discussed in **Part A**, **Part B** and **Part C** respectively.

The zirconia and silica filled nanocomposites of HL-2 blend for high performance applications like load bearing in biomedical field is described in **Chapter 7**. Detailed descriptions of the mechanical properties like compressive modulus, fracture toughness and wear resistance are also described.

The summary and conclusions and the future outlook of the study is presented in **Chapter 8**.

<p style="text-align:center">||||| **Contents** |||||</p>

Chapter **2**

MATERIALS AND METHODS **45- 60**

Chapter 5
HMHDPE/LLDPE BLEND: EFFECT OF NANOZIRCONIA .... 119 - 162

Part A

**HMHDPE/LLDPE BLENDS: PREPARATION AND EVALUATION OF
MECHANICAL, THERMAL AND RHEOLOGICAL CHARACTERISTICS**

Part B

**PREPARATION AND EVALUATION OF MONOCLINIC AND
TETRAGONAL NANOZIRCONIA REINFORCED HMHDPE/LLDPE BLEND**

Chapter 6

FIBRILLAR NANOSILICA REINFORCED HMHDPE-LLDPE BLEND: FABRICATION AND EVALUATION OF NOVEL NANOCOMPOSITES

Part A

HMHDPE/LLDPE/CGS NANOCOMPOSITES

Chapter 7
**POLYMER BLEND NANOCOMPOSITES FOR HIGH
PERFORMANCE APPLICATIONS**

Chapter 8
SUMMARY AND CONCLUSIONS

List of Abbreviations and Symbols

ASTM	American Society for Testing and Materials
BET	Brunauer-Emmett-Teller
DMA	Dynamic mechanical analysis
DRA	Dynamic Rheological Analysis
DSC	Differential Scanning Calorimetry
EDS	Energy dispersive X-ray analysis
FTIR	Fourier transform infrared spectroscopy
FWHM	Full width at half maximum
HDPE	High density polyethylene
HMHDPE	High molecular weight high density polyethylene
IPA	Isopropyl alcohol
LDPE	Low density polyethylene
LLDPE	Linear low density polyethylene
MFI	Melt flow index
MPa	Mega Pascal
MMT	Montmorillonite
N	Normality
PE	Polyethylene
PEEK	Polyether ether ketone
PP	Polypropylene
PVA	Poly vinyl alcohol
rpm	revolutions per minute
SEM	Scanning electron microscopy
TEM	Transmission electron microscopy
TGA	Thermogravimetric analysis
UHMWPE	Ultra high molecular weight polyethylene
XRD	X-ray diffraction
ZrO_2	Zirconia
E'	Storage modulus

E"   Loss modulus

G'   Shear storage modulus

G"   Shear loss modulus

ΔH_f Enthalpy of fusion

ΔH_c Enthalpy of crystallization

ΔH_{mix} Enthalpy of mixing

ΔS_{mix} Entropy of mixing

K_{IC} Critical intensity fracture toughness

$\tan \delta$ Loss tangent

Tc   Peak crystallisation temperature

$Tc_{,endset}$ Crystallisation temperature(endset)

$Tc_{,onset}$ Crystallisation temperature(onset)

T_g Glass transition temperature

T_m Peak melting temperature

$T_{m,onset}$ Melting temperature(onset)

$T_{m,endset}$ Melting temperature(endset)

Ws   Wear rate

η^* Complex viscosity

ω Angular frequency

λ Wavelength of X ray

wt %   Weight percentage

θ Angle corresponding to the peak

μm Micrometer

nm   Nanometer

ºC   Degree celcius

.....ೞ೦ಌ.....

Chapter 1

INTRODUCTION

General aspects of polymer blends and nanofillers as modifiers are presented in this chapter. Recent developments in polymer nanocomposites are also outlined. The material progresses into the Scope and objectives of the present work.

1.1 Introduction

Rapid advancement in nanoscience and nanotechnology has profoundly influenced day to day life of mankind. The properties of polymers can be tailored by the incorporation of nanofillers. Since nanofiller have large surface area it can effectively affect the polymer even at the molecular level and has evolved a new class of engineering material namely 'Nanocomposites'. In the current era of composites, nanocomposites are finding applications in a variety of fields such as aerospace, biomedical field etc. Among the various nanofillers, nanosilica and nanozirconia possess a unique position in the owing to their fine properties.

Blending of two polymers has obvious attractions since it provides a new material with desired set of properties which may not be observed in constituent polymers. On account of economical and technical uncertainties associated with synthesis of new polymeric material, blending technique is a very easy and cost effective approach. Over the past decades modification of polymer blends with nanofillers opens innumerable ways to generate technologically innovative products. In the thermo-mechanical performance of the polymer blend can be enhanced by the addition of nanofillers owing to their better filler matrix interactions.

The properties of polymer/polymer blend nanocomposites are equally determined by the molecular structure of the polymer/polymer blend, the processability of nanocomposite and also the filler-matrix interactions. Since various kinds of nanofillers in enormous quantity are required for technological applications, nowadays scientists are interested in cost effective large scale synthesis of nanoparticles with less than 100 nm in diameter. In this aspect bio fillers assume increasing importance because of their renewable source and low cost.

1.2 Polymer blends

The first polymer blend was a mixture of natural rubber and gutta percha developed and patented by Thomas Hancock in 1846 [1]. The term *polymer blend* can be used to describe a mixture of two or more polymers or copolymers [2] and can be interchanged with the term *polymer composite*. A polymer alloy explains an immiscible polymer blend with a distinct phase-morphology [2]. An *interpenetrating polymer network* is a polymer blend in which one or more components undergo polymerization in the

presence of the other [3]. Other terms can be used to depict polymer blends and these primarily relate to state of miscibility of the blend.

A polymer blend is obtained by combining at least two or more macromolecular substances, polymers or copolymers in which the individual component is more than 2 wt %. Blending provides a smart approach of developing new materials with improved properties like chemical resistance, impact strength etc. Blending reduces the number of grades that need to be manufactured and stored, so saving space and capital investment. Blending also helps in rapid formulation changes and thereby ensures better plant flexibility and high productivity. Furthermore processability of materials can be improved by blending which are otherwise limited in the ability to be transformed into products. Consequently the development of new polymer blends is found to increase at a rate about three times in the plastic industry.

1.2.1 Thermodynamics of blending

The most important characteristic of a polymer blend is the phase beavior. Polymer blends can exhibit miscibility or phase separation or various levels of mixing in between the extremes (e.g., partial miscibility). The most important factor leading to miscibility in low molecular weight materials is the combinatorial entropy contribution which is very large compared to high molecular weight polymers. The most important relationship governing mixtures of dissimilar components 1 and 2 is:

$$\Delta G_m = \Delta H_m - T\Delta S_m \text{ ....(1.1)}$$

where ΔG_m is the free energy of mixing, ΔH_m is the enthalpy of mixing (heat of mixing) and ΔS_m is the entropy of mixing. For miscibility to occur,

ΔG_m must be smaller than 0. For low molecular weight materials, increasing temperature generally leads to increasing miscibility as the $T\Delta S_m$ term increases, thus driving ΔG_m to more negative values. For higher molecular weight components, the $T\Delta S_m$ term is small and other factors (such as non-combinatorial entropy contributions and temperature dependant ΔH_m values) can dominate and lead to the reverse behavior, decreasing miscibility with increasing temperature.

1.2.2 Types of blends

According to the thermodynamic point of view polymer blends are broadly classified as miscible, partially miscible and immiscible blends [4]. Miscible blends are characterized by the presence of a single glass transition temperature (T_g), single phase and thermodynamic solubility. Mostly their properties can be predicted as weighed average of the properties of individual components. Polystyrene-Polypropylene oxide (PS-PPO) is one of the examples for a miscible blend with miscibility over a wide range of temperature and in all compositions, the inflammability, heat resistance and toughness of PPO is combined with the good processability and low cost of PS.

Immiscible blends exhibit T_g and/or melting temperature of both components, and are phase separated. The overall performance of the blend not only depends on the properties of the individual components but also the morphology of the blends and the interfacial properties between the blend phases. Most of the polymer blends are immiscible due to the negligibly small entropy of mixing. When small amount of one component is added, many polymer systems are miscible but immiscible a higher loading [4-6].

For partially miscible blends one of the components of the blends is dissolved in the other. This kind of blends display excellent phase morphology and improved properties and is compatible. Both components of the blend are homogeneous and possess their own T_g and both the T_gs are shifted from the values for the pure blend components towards the T_g, of the other component. An example for partially miscible blend is Polycarbonate- Acrylonirile butadiene styrene (PC–ABS) blends, which combine the heat resistance and toughness of PC with the processability, stress cracking resistance, low temperature impact and low cost of ABS.

The adverse effects are so pronounced that the resultant material is most likely unusable. The main reason is that most polymer pairs are immiscible and blending leads to a phase separated material. This material has three inherent problems [4],

1) Instability of immiscible polymer blends

2) Weak interfacial adhesion between the two phases

3) Poor dispersion of one polymer phase in the other

1.3 Polymer blends from thermoplastics

Thermoplastics account for about 80 percent of all polymers produced. Relatively low cost and easy processability, they are most extensively used in plastic industry. Among thermoplastics, polyolefins such as polyethylene (PE), polystyrene (PS), Polypropylene (PP) occupy an important position in the commodity plastics market. It is anticipated that about 70% of polyethylene enters into the market as blends. As a result, miscibility of polyethylene blends has been a ubiquitous research topic in the

polymer community over the past two decades. At the present instant the usages of polyolefin blends have augmented due to the increased applications in packaging and medicine.

Polyolefins can be divided into two main types, polyethylene and polypropylene, which are subdivided into several grades for different applications. Commercial polyethylene resins, despite their name, are most often copolymers of ethylene, with varying fractions of α-olefin co-monomer. The generally used α-olefins are 1-butene, 1-hexene, and 1-octene. They are used to decrease the density and crystallinity of the polyolefin, while changing its physical properties and applications. Among polyolefins HDPE, LLDPE, LDPE, and PP are the most widely used polymers for blending. Based on the density and branching, polyethylenes are classified into different categories and are shown below. Type of branching, crystal structure and molecular weight significantly reflect the mechanical and other physical properties. Mainly polyethylenes are used for packaging industries. Nowadays much attention is given to biomedical field.

- Ultra high molecular weight polyethylene (UHMWPE)
- Ultra low molecular weight polyethylene (ULMWPE)
- High density polyethylene (HDPE)
- High density cross linked polyethylene (HDXLPE)
- High molecular weight polyethylene (HMWPE)
- High molecular weight high density polyethylene (HMHDPE)
- Medium density polyethylene (MDPE)
- Very low density polyethylene (VLDPE)
- Low density polyethylene (LDPE)

- Linear low density polyethylene (LLDPE)
- Ethylene ionomers

Ultra high molecular weight polyethylene (UHMWPE) is similar in structure to HDPE, produced by the Ziegler process and its molecular weight range between 3.1 and 5.7 million. As a result of large molecular weight, high degree of polymer chain entanglements, it has high melt viscosity and therefore relatively difficult to process. Consequently their usage is limited, but it can easily be drawn into fibers. The benefits of using UHMWPE arise from the superior impact properties, high abrasion resistance, low creep and good resistance to stress-cracking. The outstanding properties make UHMWPE find applications in various fields, especially moving parts of weaving machines, gears, bearings etc. Its high impact strength leads them used for armor and radar domes. Currently, the main application of UHMWPE is in biomedical applications as artificial joints.

The most sold volume among different grades of polyethylene is HDPE, LDPE and LLDPE. By volume of consumption, HDPE is the top among the three different grades of PEs [7]. HDPE with density 0.94 to 0.97 g/cm^3 has short or very low degree of branching, making it highly crystalline and confers unique mechanical properties. HDPE is stiffer and stronger than LDPE. Its molecular weight ranges from 100,000 to 200,000. HDPE is prepared using Ziegler and Natta catalyst at low temperature and pressure. It is mainly is used for packaging applications. Since HDPE is a safe plastic material, it can also be used for the manufacturing of toys. Superior mechanical properties make it suitable for biomedical field, especially in bone implant applications [8, 9].

LLDPE is considerably a linear polymer with short branches or side chains, stiffer than LDPE with different melt processability. Its density ranges between 0.915 to 0.925 g/cm^3 and have high puncture and impact resistance. LLDPE is a copolymer of ethylene and an alpha conventional LDPE. It is well known that LLDPE has superior properties (tensile strength, environmental stress crack resistance, etc.) compared to conventional LDPE. Major applications of LLDPE are in packaging industry due to its flexibility, transparency and better toughness. It also finds use in the manufacture of toys, lids and cable covering. Recently, LLDPE has been used as a blend with other polyethylenes or to completely replace other grades for certain specified applications [10, 11].

LDPE is formed by free radical polymerization. It is characterized by high degree of long and short chain branching, for this reason the chains do not pack well into the crystal structure [9]. Thus the density is small compared to the above ones, ranging from 0.925-0.940 g/cm^3. Consequently the intermolecular force of attraction is less, since instantaneous-dipole induced-dipole attraction is low. This creates lower tensile strength and superior ductility. This tough and flexible polymer mainly used for packaging film, general purpose moulding of domestic products such as bottles and tubes, depending on the molecular weight [9].

HMHDPE is a type of HDPE, having much higher molecular weight and a broader molecular weight distribution than HDPE which imparts enhanced toughness and good stiffness along with superior abrasion and chemical resistance [12]. Therefore, HMHDPE is widely used in a variety of bearing applications, at low temperature conditions with good chemical resistance [13].

1.3.1 Polyethylene blends

Datta and Birley were the first researchers to study the compatibility of HDPE-LDPE and HDPE-LLDPE blends in the solid state, particularly their crystalline phase, using DSC, XRD, and mechanical property testing [14]. Y. Zhao *et al.* studied the effect of branches of LLDPE on the miscibility of HDPE-LLDPE blend, and reported in blends with low content of branches, the two components are mixed perfectly and form co-crystals. It also implies that the miscibility of the linear and branched polyethylenes is affected not only by the content of branches but by the distribution of branches in branched polyethylene [15]. H. S. Lee and M. M. Den reported the rheological properties of the blends of linear and branched polyethylenes. The most significant observation of this study is that, HDPE, which is miscible in at least some composition with both LLDPE and LDPE, can be used as a compatibilizing agent for LLDPE-LDPE blends to create a ternary system that appears to be fully miscible [16].

M. Munaro and L. Akcelrud demonstrated considerable enhancement in the stress crack resistance of HDPE based materials attained by blending with other types of polyethylene. Better results were found for the combination of HDPE with LLDPE as compared to LDPE, possibly due to co-crystallization [17]. The addition of UHMWPE to HDPE with different proportions hopefully improved the mechanical properties of HDPE film in a two-step processing way as reported by J. Zuo *et al.* [18]. Gongde Liu *et al.* also showed that addition of PP to UHMWPE improved the processability of the blend compared to UHMWPE alone or its blend with HDPE [19].

Several authors agree with the assumption that resistance to environmental stress crack is directly related to the density of molecules which in turn is related to the number of short branches and the molar mass of the polymer. It has also been reported that for PE blends, the miscibility and crystallinity play an important role in the blends behavior [20-22]. The use of nanoscale indentation with the AFM for the identification of phases in blends of LLDPE and HDPE M.S has been studied by Bischel *et al.* [23].

G. Sarkhel *et al.* investigated the mechanical and rheological properties of HDPE-LDPE blends and reported that percentage of crystallinity of the blends decreased with increasing LDPE content, but the rate of crystallization of HDPE was unaffected [24]. A lower content of HDPE containing blend showed better miscibility compared to the blend containing higher HDPE; this was due to the relatively poor compatibility of crystalline HDPE phase with LDPE.

Polyethylene blends have been extensively investigated in terms of their rheological properties. Several research work has been broadly explored the rheological beavior of HDPE -LLDPE as well as HDPE - LDPE and LLDPE -LDPE blends. These works established that polyolefin blends can be miscible, partially-miscible or immiscible.

1.4 Composites

Composites are another class of material system combined of two materials. One of the component is called the reinforcing phase embedded in the other component called the matrix phase. The reinforcing materials can be in the form of fiber, sheets or particle and the matrix material can be

metal, ceramic or polymer. Typically, reinforcing materials are strong with low densities, while the matrix is usually a ductile or tough material. Natural composite materials are complex structures consisting of continuous or discontinuous fibrous or particulate material embedded in an organic matrix acting as glue. Wood is a composite of fibrous cellulose and lignin. Bone is a composite of collagen and other proteins and calcium phosphate salts. The shells of mollusks are made of layers of hard mineral separated by a protein binder.

1.4.1 Classification of composites

Composites can be classified in different ways [25]

I. **Depending on the matrix system**

    a) Metal matrix composites(MMC)

    b) Ceramic matrix composites (CMC)

    c) Polymer matrix composites (PMC)

    d) Rubber matrix composites(RMC)

II. **Depending on the occurrence of composites**

    a) Natural composites-(e.g., jute, silks, wood, bamboo)

    b) Man-made composites-(e.g., glass reinforced fiber)

III. **Depending on the size of constituents**

    a) Macrocomposites - consisting of macro sized particle like galvanized steel, helicopter blades etc.

    b) Microcomposites – comprising of metallic alloys, reinforced Plastics etc.

    c) Nanocomposites – composite system having at least one of the components in the nanometer size range.

IV. Depending on structural components

    a) Fibrous composites(compound of fibrous filler in matrix)

    b) Laminar composites(compound of layer of materials)

    c) Particulate composites(compound of particulate fillers in matrix)

    d) Skeletal composites(composed of continuous skeletal matrix filled with a second matrix)

1.4.1.1 Nanocomposites

With the advancement in nanotechnology, nanocomposites prevail over all other composite materials. In nanocomposites one of its constituents called the reinforcing filler is having dimension less than 100 nm and is continuously dispersed in the matrix phase. The effectiveness of the nanocomposites is reliant upon the properties of the reinforcing constituents, the volume fraction of the nanomaterial, shape and arrangement of inclusions and finally the interfacial interaction between matrix and particulates. The nanoscale dimension of the reinforcing filler offers ultra large interfacial area per volume resulting in extraordinary properties to the nanocomposites.

The major advancement of nanocomposites over other conventional composite materials is:

- Light weight due to low filler loading

- Economical due to less amount of filler used

- Superior properties such as mechanical, optical, thermal, barrier, electrical etc., over conventional composites even at very low filler loading [26]

1.5 Nanomaterials

Nanotechnology has the potential to produce significant changes in areas such as resources and manufacturing, energy and environment, electronics and chemicals, computation and information technology, medicine and healthcare, pharmaceutical, biotechnology and agriculture, etc. The advancement of nanoscience and nanotechnology has developed extensive range of novel nanomaterials. Nanomaterials serve as a bridge between the molecular and condensed phase [27]. The outstanding properties of nanocomposites offered by the nanomaterials are mainly due to their surface to volume ratio of nanomaterial. When the particle size decreases the number of atoms present on the surface anonymously increases; as a result, the interatomic forces like the electrostatic as well as magnetic attraction becomes stronger [27-29]. Their chemical and physical properties differ from those of the bulk solids. Since the surface energy of nanoparticles is much higher they will easily agglomerate or aggregated. Therefore proper dispersion of nanoparticles in the polymer matrix is a challenging problem in developing nanocomposites.

1.5.1 Classification of nanomaterials

The nano-scale materials are categorized on the basis of origin, number of dimensions which exist in the nanometer range and structural configuration.

1.5.1.1 Based on origin

a) **Natural nanomaterials:** Nanomaterials from natural source like corals, shells, etc are exploited for creating nanocomposites.

b) **Artificial nanomaterials**: Nanomaterials synthesized artificially

- Engineered nanoparticles- Nanomaterials prepared to meet specific properties. eg- carbon nanotubes, nano silica, nano zirconia, quantum dots etc.

- Incidental nanomaterials- Nanoparticles produced as a by-product of manmade process.

1.5.1.2 Based on dimension

a) **One dimensional (1-D):** These have one of the dimensions of the nanostructure in the nanometer range. These include nanoplatelets, nano sheets, and nanolayers. Example: clay nanoplatelets, graphite nanoplatelets.

b) **Two dimensional (2-D**): In which two of the dimensions of the nanomaterials are in nanometer scale and the third one outside the nanometer range. Nanorods, nanowires and nanotubes come under this category. Example: carbon nanofibers and carbon nano tubes.

c) **Three dimensional (3-D):** All the three dimensions are inside the nano meter scale. These include nanoparticles, nanocrystals. Example: Fullerenes.

1.5.1.3 Based on structural configuration

a) **Carbon based nano materials:** These are nanomaterials having carbon origin, and are ellipsoids, spherical or cylindrical in shape. Example: fullerenes, nanotubes (SWCNTs and MWCNTs)

b) **Metal based nano materials**: The nanomaterials having metal origin and these include nanogold, nanosilver and other metal oxides, such as titanium dioxide, iron etc.

1.5.2 Preparation of nanomaterials

There are two general ways offered to produce nanomaterials [30]. The first way is to start with bulk material and then break it in to small pieces using mechanical, chemical or other form of energy (Top down). An opposite approach is to synthesis the material from atomic or molecular species via chemical reactions and allows the precursor particle to grow in to size (Bottom up). Both approaches can be done in either gas, liquid, super critical fluids, solid state or in vacuum. Bottom-up process is economical and creates less waste. Most of the manufactures are interested to control a) particle size b) particle shape c) particle distribution d) particle composition e) degree of particle agglomeration.

Numerous methods for the preparation of nanomaterials have previously been reported which comprise sol-gel technique , micro emulsion processes, spray pyrolysis and drying, self assembling, mechano chemical processing, super critical water processing, vapour transport process, sonochemical process, homogeneous precipitation, solid-state reaction, wet-chemical precipitation method, chemical vapour deposition method and thermal decomposition etc.

Some of the main techniques generally used are:

1.5.2.1 Sol – gel process

The sol-gel technique is a long established industrial process for generation of colloidal nano particles from liquid phase by reactions like hydrolysis, polycondensation and drying [31, 32]. The method consist of the generation an inorganic framework via the formation a colloidal suspension, called the sol followed by the gelation of the sol leads to the

generation of net work in the continuous liquid phase called gel. The process has been further developed in last year for the production of advanced nanomaterials and coating. The main advantages of sol-gel techniques for the preparation of the materials are low temperature processing, versatility and flexible rheology allowing easy shaping and the embedding. This method is mainly adopted for the preparation of ceramic nanomaterials like metal oxide nanoparticles.

1.5.2.2 Chemical vapour deposition (CVD)

CVD consist in activating a chemical reaction between the substrate surface and a gaseous precursor. Activation can be achieved either with temperature (thermal CVD) or with plasma (PECVD - Plasma Enhanced Chemical Vapour Deposition). The main advantage is the non directive aspect of this technology [33, 34].

1.5.2.3 Atomic or molecular condensation

This method is used mainly for metal containing nanoparticles. A bulk material is heated in vacuum to produce a stream of vaporized and atomic matter, which is directed to a chamber containing either inert or reactive gas atmosphere. Rapid cooling of the metal atoms due to their collision with the gas molecules results in the condensation and formation of nanoparticles.

1.5.2.4 Super critical fluid synthesis

Methods using supercritical fluids are also potent for the synthesis of nanoparticle. For these methods, the properties of a super critical fluid (fluid forced into supercritical state by regulating its temperature and pressure) are used to form nanoparticles by a rapid expansion of a supercritical solution [35, 36].

1.5.2.5 Wet chemical precipitation

This method involves the mixing of desired precursors in a controlled manner in liquid phase. The main advantages of this method are the ease of production, high purity of the synthesized product, low working temperature, and inexpensive synthetic requirements [37, 38].

1.5.2.6 Mechanical process

These include grinding, milling and mechanical alloying technique [39]. These processes utilize the age-old technique of physically pounding coarse powders into finer ones, which is similar to the grinding flour mills. The advantages of these techniques are that they are simple and require low cost equipment. However, there can be difficulties such as agglomeration of the powders, broad particle size distributions and contamination from the process equipment itself.

1.5.2.7 Using templates to form nanoparticles

Any materials containing regular nano-sized pores or voids can be used as templates to form nano particles [40]. Examples of such templates include porous alumina, zeolites, diblock co-polymer, dendrimers, proteins and other molecules. The template need not be a 3D object. Artificial templates can be created on a plane surface or on a gas liquid interface by forming self–assembled mono layers.

1.6 Nanosilica

Among the various nanomaterials, the most extensively investigated particulates are layered silicates (nanoclay) and carbon nanotubes, which are two- and one- dimensional in geometry, with large aspect ratio (usually

100). Recently attention is paid to low aspect ratio, such as spherical or cubic shaped nanoparticles, especially, nanosilica (nano-SiO_2) due to its wide range of potential applications and low cost. Due to the inherent properties of nanosilica, it plays crucial role in the field of ceramics, optoelectronics, sensors, rubber technology, food materials, aeronautical and biomedical materials, in addition to its promising use in catalysis and chemical separations (41-47).

Some major roles of nanosilica in different applications include:

- As a reinforcing material

   In polymers to improve their properties for specific applications nanosilica reinforced polymers such as polymethacrylates, polyimides, polyamides, polyacrylics, polyoleifns, elastomers etc. show better resistance to staining and remarkable barrier properties to gases and moisture and also exhibit good mechanical properties. The addition of small amounts of silica nanoparticles to the cement paste can reduce the calcium leaching rate of the cement paste. Portland cement composite with nanosilica has a more solid, dense and stable bonding framework [43].

- In opto-electronic applications

   Silica nanotubes draw special attention in this aspect. It has potential applications such as nano containers and nano reactors and in photo induced energy transfer and electron transfer [44]. Nanosilica films (Xerocoat), when applied to mirror/glass materials help to prevent unwanted reflections which allow the passage of light through glass

thereby improving the vision. It is used as an encapsulation and protective coatings in electro-optically active materials and also in optoelectronic applications.

▪ In biomedical field

Silica nanoparticles especially mesoporous nanosilica is used in various biomedical applications, such as in protein adsorption, separation, nucleic acid detection, molecular imaging, gene therapy, drug delivery, tissue engineering, scaffolds and regenerative medicine applications [48, 49].

Because of this the large scale industrial and engineering applications, nanosilica with controlled size and shape is required. Therefore recently much attention is given to the synthesis and characterization of nanosilica suitable for specific application. The major routes for the production of synthesizing amorphous silica are the wet chemical and thermal route [50-52]. These processes are time consuming and energy intensive. More over the reagents requisite for the intention are usually sodium silicate, alkyl orthosilicates etc, are not the best commercial sources of silica owing to their flammability, high cost, difficulties in handling and storage and also the exposure of silicon alkoxides precursor [53-55]. Therefore, their replacement with a comparatively less expensive and robust inorganic silica source is required [56-59]. Also the properties of nanosilica depend strongly on the synthetic conditions like the time of reaction, synthesis temperature, pH, addition of surfactants, and the manner of washing and drying. These factors manipulate the size and morphology of the SiO_2 particles, and also their aggregation, specific surface area and porosity.

Increasing demand and inflexible performance requirements have given thrust for finding new sources for the isolation of silica for the preparation of nanocomposites [60,61].

1.6.1 Significance of green /renewable sources for nanosilica synthesis

Currently, the tuning of agricultural residues into value-added nanomaterials is of immense attention to all researchers because of their properties, such as biocompatibility, eco-friendliness, biodegradability, sustainability and cost effectiveness. For the last few years, due to the easy availability, low cost, rapidly increasing environmental awareness, growing global waste problem, limited availability of crude oils and high processing cost trigger the development concepts of sustainability and reconsideration of renewable resources, and ecological concerns, researchers have initiated a considerable interest in natural materials to produce 'green' products.

Due to the inconvenience in handling the chemicals and their high cost we are forced to develop an economically viable method to fabricate nanosilica from a silicon-containing biomass material. Silica has long been known to be present in plants. Silica showed the greatest variation between plants, plant parts, and species of plants. Plant varieties, soil type, water uptake as well as the conditions influence the concentration of silica in plants [62,63]. In addition to this, grass inflorescence also influences the silica content [64,65]. In continuing attempts to reduce processing cost and time, many research works have been published on the use of rice husk as a raw material for producing silica nano particles [61, 66-72]. Silica can be successfully isolated from Stenotaphrum secundatum (St. Augustine) grass using an annelid-based biotransformation process as reported by Espindola *et al.* [73].

1.7 Nanozirconia

Nanomaterials has been explored more attention due to their lower size and large surface area. Nanozirconia alone has increased manifold applications. Zirconia has three well-defined polymorphs; tetragonal, monoclinic and cubic phases (t-ZrO_2, m-ZrO_2 and c-ZrO_2). Zirconia exists in monoclinic form at room temperature and gets converted to the tetragonal phase at 1447 K. The tetragonal phase is further converted to the cubic phase at around 2643 K.

Nanozirconia can be exploited as a catalyst in a variety of reactions like alkylation, amination, condensation, isomerisation, cracking, hydration, oxidation, etc. Owing to the excellent properties like high strength, high fracture toughness, excellent wear resistance, high hardness, and good chemical resistance, zirconia nanoparticles find applications in different fields.

Some major areas of its interest include:

▪ Catalysis

Zirconia mixed oxide systems find applications as a catalyst and as a catalyst support [74]. Sulfated zirconia has been explored in catalytic processes owing to its use as a 'super acid' [75, 76].

▪ Electronic field

Zirconia finds applications in optoelectronic field, since 95% of the ferrules, the most vital part of the optical fiber connectors, are made of zirconia and the extreme precision was obtained by using nanozirconia, instead of its micro particles [77, 78] buffer layers for growing super conductors [79, 80], improve the quality of the plates

CTP (Computer To Plate) [81]. Nanoporous zirconia is used typically as a good sensor material for oxygen [99]. NASICON, a solid ionic conductor containing zirconia is for electrochemical applications as solid electrolyte or sensitive membranes for potentiometric detection of alkaline cations [82-84].

- Polymer modifiers

  Reinforcement of nanozirconia with polymers and other materials produce composites with enhanced performance for specific applications. Nanozirconia in its pristine form as well as its mixed oxide systems is used as a component of wear resistant/protective coatings. In order to extend the service life of UHMWPE based artificial implant, the wear resistance can be enhanced by the incorporation of ZrO_2. The friction and wear behavior of other polymeric materials can also be improved by the incorporation of nanozirconia.

- Biomedical field

  Because of its extremely low wear and excellent biocompatibility offer nanozirconia, a viable material for use in ceramic joints [85-87]. Tetragonal nanozirconia has been successfully used as a good sorbent in the development of radionuclide (for example: $^{68}Ge/^{68}Ga$ and $^{99}Mo/^{99m}Tc$) generators for biomedical applications [88, 89].

Among the different polymorphs of zirconia t-ZrO_2 and m-ZrO_2 are of more importance for its catalytic applications because of high thermal stability, high BET surface area and amphoteric nature [90, 91]. Since tetragonal and cubic phases are unquenchable at high temperature, obtaining them at lower temperatures has gained importance due to their potential

applications [88, 92, 93]. Several attempts have been made to achieve stabilized tetragonal and cubic phases by doping zirconia with a variety of metal oxides like CaO, Y_2O_3, CeO_2, Ce_2O_3, La_2O_3, MgO, CuO, Cr_2O_3, MnO_2, NiO, SnO_2 etc. [94-97]. However it is very difficult to control the dopant and the synthesis proceeds through a tedious route. In some cases t- ZrO_2 exists at room temperature and the condition of its stability is still a subject of arguments [98, 99].

1.7.1 Synthesis of nanozirconia

Researchers have explained many synthetic routes like precipitation, sol-gel method, chemical vapor synthesis, micro emulsion method, glycothermal process, and hydrothermal precipitation process to obtain these polymorphs even without adding the dopant metal. For realizing industrial production, the most familiar and simple method used to prepare nanozirconia is the "Sol-Gel" technique [100, 101] and is often in top-priority because of easy processability, low energy consumption, inexpensive, simple methods and equipments.

No matter which method is used to prepare nanopowder but the problem to be solved is, to overcome agglomeration and precipitation. Recently, a great deal of interest was focused on the synthesis of the nanostructured mesoporous oxides using a surfactant-assisted route to conquer the agglomeration [102, 103]. Sintering temperature is another factor which affects aggregations; lower being the better, because when sintering is done at lower temperature, the crystallite size collapse is less frequent. Furthermore the key role in stabilizing the tetragonal phase of the nanozirconia is played by 'the small crystallite size'.

1.7.1.1 Surfactant assisted synthesis

Nanomaterials can be synthesized by precipitation or sol-gel method using the requisite reagents in presence of a polymeric dispersing agent. The medium used for carrying out the reaction is a big challenge because almost all the wet chemical methods face two major problems i.e., agglomeration and also ZrO_2 particles containing phase mixtures with high amount of monoclinic phase along with existence of amorphous hydrous ZrO_2 [104, 105]. Presence of dispersing agents with large number of hydroxyl groups per molecule would produce a matrix into which synthesized particle would be incorporated, thus producing materials in the nanoscale. This occurs by the interaction between the hydroxyl groups of dispersing medium and the hydroxyl groups of reagent which results in co-condensation. The synthesized material after complete drying is proposed to be calcined to remove the dispersing medium matrix and hence obtaining nanoparticles. Generally poly vinyl alcohol (PVA), starch and carboxy methyl cellulose (CMC) are used as good dispersing agent for the synthesis of nanomaterials. Nanocrystalline zirconia powder with high surface area, pure tetragonal phase and mesoporous structure was prepared by a surfactant-assisted route by using Pluronic P123 block copolymer as the surfactant by M. Rezaei *et al.* [106]. NanoBaSO$_4$ was successfully synthesisized by using PVA as polymeric surfactant as reported by Nisha et.al [107].

1.8 Polymer nanocomposites

Polymers are considered to be good hosting matrices for composite materials because they can easily be tailored to yield a variety of bulk physical properties. Moreover, organic polymers generally have long-term stability and good processability. Inorganic nanoparticles possess outstanding

optical, catalytic, electronic and magnetic properties, which are significantly different their bulk states. By combining the attractive functionalities of both components (organic polymers and inorganic nanoparticles), nanocomposites are expected to display synergistically improved properties.

Moreover in the case of polymer nanocomposites, where the reinforcement particles are in nanometer scale, they have ultra large interfacial area per volume, and the distances between the polymer and filler components are extremely short. Polymer coils are 40 nm in diameter and the nanoparticles are of the same order of magnitude as the polymer. As a result, the molecular interactions between the polymer and the nanoparticles will be effective leading to polymer nanocomposites with unusual material properties. The resultant nanocomposites exhibit enhanced optical, magnetic, mechanical and optoelectronic properties. Consequently, the composites have been extensively used in the areas such as military equipments, protective garments, aerospace, electronics, safety, automotive, optical devices and biomedical field.

1.8.1 Preparation of polymer nanocomposites

After the selection of a particular polymer matrix and appropriate nanoparticles for species applications, the next challenge is to determine the proper synthesis method to create the desired polymer nanocomposite. In general, for solid thermosetting reactive polymers or thermoplastic polymer with solid nanoparticles, the following processing methods are recommended

- Solution intercalation
- Melt intercalation
- Roll milling

For liquid thermosetting reactive pre polymers or thermoplastic polymers with solid nanoparticles, the following processing methods are recommended:

- Emulsion polymerisation
- In-situ polymerisation
- High-shear Mixing

1.8.1.1 Solution intercalation

The layers silicate is exfoliated into single layers using a solvent in which the polymer (or a thermosetting reactive pre polymer, in the case of insoluble polymers such as polyimide) is soluble. It is well known that such layered silicates (due to the weak forces that stack the layers together) can be easily dispersed in an adequate solvent. The polymers then absorb onto the delaminated sheets and when evaporated (or the mixture precipitated), the sheet reassembles, sandwiching the polymer to form an ordered multilayered structure [108].

1.8.1.2 Melt intercalation

The layered silicate is mixed with the solid polymer matrix in the molten state. Under these conditions, if the silicate layers are sufficiently compatible with the selected polymer and the polymer can be inserted into the interlayer space forming either an intercalated or an exfoliated nanocomposite. No solvent is required for this method [109].

1.8.1.3 Roll milling

Three-roll milling is considered as low-shear mixing for incorporating nanoparticles into masticated polymer, as compared to high-shear mixing [109].

1.8.1.4 Emulsion polymerization

In a manner analogous to the solution intercalation technique, the layered silicate is dispersed in the aqueous phase, and the polymer nanocomposites are formed. The emulsion polymerization technique has been used to study the intercalation of water soluble polymer with in Na^+-MMT, which is well known to readily delaminate in water [108].

1.8.1.5 In-situ polymerization

The layered silicate is swollen within the liquid monomer (or a monomer solution) so that the polymer formation can occur between the intercalated sheets. Polymerization can be initiated by different polymerization methods such as heat or radiation, diffusion of suitable initiator or an organic initiator or catalyst fixed through cationic inside the layer before the swelling step [110-112].

1.8.1.6 High-shear mixing

The solid or liquid nanoparticles are mixed with the liquid polymer matrix using high–shear equipment (e.g., an IKA mixer, IKA Wilmington, NC). High–shear mixing will disrupt the nanoparticle aggregates and disperse into the polymer matrix resulting in an intercalated or an exfoliated nanocomposite. This technique may or may not, (especially in the case of water based polymer) require solvent [110].

1.8.2 Application of polymer nanocomposites

Table 1.1 Potential applications of polymer-based inorganic particulates nancomposites (modified from Refs. [113,114]).

Nanocomposites	Applications
Polycarprolactone/SiO_2	Bone-bioerodible for skeletal tissue repair.
Polyimide/SiO_2	Microelectronics.
PMMA/SiO_2	Dental application, optical devices.
POLYETHYLACRYLATE/SIO_2	Catalysis support, stationary phase for chromatography.
Poly(p-phenylene vinylene)/SiO_2	Non-linear optical material for optical waveguides.
Poly(amide-imide)/TiO_2	Composite membranes for gas separation.
Poly(3,4-ethylene-dioxythiphene)/ V_2O_5	Cathode materials for rechargeable lithium batteries.
Polycarbonate/SiO_2	Abrasion resistant coating.
Shape memory polymers/SiC	Medical devices for gripping or releasing therapeutics within blood vessels.
Nylon-6/LS	Automotive timing-belt-TOYOTA.
Nylon-6/clay	Barrier films – Bayer AG
Nylon-6/clay	Films and bottles - Honeywell
Nylon-6, 12, 66/clay	Auto fuel systems - Ube
Nylon-6/PP/clay	Electrically conductive
UHMWPE/clay	Earthquake-resistance pipes – Yantai Haili Ind.& Commerce of China
Polypropylene/clay	Packaging - Clariant
PEO/LS	Airplane interiors, fuel tanks, components in electrical and electronic parts, brakes and tires.
PLA/LS	Lithium battery development.
PET/clay	Food packaging application. Specific examples include packaging for processed meats, cheese, confectionery, cereals and boil-in-the-bag foods, fruit juice and dairy products, beer and carbonated drinks bottles.
Thermoplastic olefin/clay	Beverage containers.
Polyimide/clay	Automotive step assists – GM Safari and Astra Vans.
Epoxy/MMT	Materials for electronics.
SPEEK/laponite	Direct methanol fuel cells.
EVA/clay	Wires and cables – Kabelwerk Eupen of Belgium
Unsaturated polyester/clay	Marine, transportation – Polymeric Supply

1.8.3 Nanocomposites based on polyethylenes and their blends

HDPE is the largest of the different types of polyethylenes by volume consumption. K. Li and S. C. Tjong reported that the mechanical and crystallization behavior were improved by the addition of Hydroxyapetite (HA) on HDPE. They also stated that thermal stability and wear resistance were considerably improved [115]. S. Nath *et al.* demonstrated the significant improvement in properties like hardness, stiffness, as well as the biocompatibility of HDPE by the combined reinforcement of both bioinert and bioactive ceramic fillers like Al_2O_3 and HA [116]. A. Y. Sadi *et al.* investigated the effect of HA and the combined effect of HA and partially stabilized zirconia (PSZ) particle on the mechanical properties of HDPE. Partial replacement of HA with PSZ led to improvement in both strength and toughness in HDPE/HA composite. As the ceramic counterpart increase in the sample a ductile to brittle transition was observed [117].

G. Malucelli *et al.* studied the effect of two different alumina powders on the thermal and mechanical behavior of LDPE- Al_2O_3 composites. The thermo-oxidative stability, stiffness and abrasion resistance of neat LDPE were enhanced by the presence of nanoalumina [118]. V. M. Khumalo *et al.* investigated the effect of synthetic boehmite alumina (BA) on the thermal, morphological and rheological behavior of HDPE and LDPE. BA was found to be a weak nucleating agent for both PEs. Thermo-oxidative stability was improved by the addition of BA to PE while unexpected melt rheological properties were observed [119]. M. E. A. Mohsin reported that the use of MMT as secondary filler improved the thermal, mechanical and morphological properties of CNT/HDPE

nanocomposite [120]. Tensile, wear and friction properties of the crosslinked UHMWPE were enhanced by the incorporation of nano HA, by L. Xiong *et al.* [121]. B. Jongsomjit *et al.* synthesized LLDPE-SiO$_2$ and LLDPE-ZrO$_2$ nanocomposite via in situ polymerization and reported that productivity improved five times more when nano ZrO$_2$ filler was applied [122]. A. Durmus studied the effect of nanoclay on the mechanical properties of LLDPE, and reported that both the tensile yield strength and modulus improved on filler loading [123]. D. Pedrazzoli *et al.* reported the viscoelastic and fracture toughness behavior of LLDPE by nanoalumina [124]. Tai jin-hua *et al.* reported the enhanced properties of LLDPE-MWNT composites [125].

In order to reduce the high melt viscosity of UHMWPE X.Ren *et al.* prepared UHMWPE-LLDPE blend and studied the effect of carbon nanofibers (CNFs) on the blend. The results stated that addition of CNFs decreased the degree of crystallinity, whereas the crystalline structure of the blend matrix was unaffected. The tensile properties, thermal stability as well as thermal conductivity of the blend were also enhanced [126]. Nanokaolin clay was found to be a good reinforcing filler for PS -HDPE blend as reported by Sunitha *et al.* [127].

1.8.4 Polymer nanocomposites for high performance applications

Polymer nanocomposites play a crucial role in engineering applications, where the properties of wear and friction predominant. The advantage of light weight, self lubricity, ease of processability, corrosion resistance of polymers along with the high mechanical and wear and friction properties offered by the inorganic counter parts have allowed them to be the perfect

choice. According to the specific end-use requirements, nanocomposites can be carefully tailored/tuned, thus create the required device characteristics of new and improved materials. They can be extensively applied even in aerospace applications, medicine and biotechnology, as well as in the food and cosmetics industries. Applications include devices, implants and supporting materials (e.g. artificial organs, prostheses and sutures) in orthopedic applications.

Being a distinct polymer with highest mechanical properties and chemical resistance over other polymers UHMWPE was excellent choice among other PEs for most of the engineering applications like valves, automotive, and engineering bearing. Along with above properties, its high biocompatibility coupled with wear resistance makes UHMWPE an attractive component in biomedical applications such as artificial joint replacements.

Despite the suitability of polymers for engineering applications, the wear problem still a challenge can be better solved by the incorporation of nanofillers. Literature supports that the incorporation of nano fibers or inorganic nanoparticles, other ceramic and bio-material into a UHMWPE matrix would considerably reduce the wear rate under sliding wear conditions thus improving the service life of the material [128-136]. B.P Chang *et al.* have carried out a comparative study of micro and nano sized ZnO reinforced UHMWPE under dry sliding abrasive wear conditions, and reported that both the composites shows improved wear resistance [137]. Wear resistance of UHMWPE can be further improved by adding natural

biocompatible particles like natural coral particles for the application of acetabular cups by S. Ge and co-workers [138].

Polyetheretherketone (PEEK) is another strong semi-crystalline thermoplastic polymer with outstanding mechanical properties and, thus has been apply as matrix material for high performance composites. It is an attractive bearing material under different loading conditions. Reinforcing effect of short glass fibers and CNF on PEEK was studied by Voss and Friedric, and reported that compared to the glass fibers, carbon fibers showed excellent wear resistance properties [139]. Incorporation of nanosilica effectively reduces the friction and wear of PEEK [140]. Abrasion resistance of LDPE was improved by the addition of nanoalumina [118] HDPE is a ubiquitous material widely used for packaging applications. With the emergence of HDPE-HA composite (HAPEX) by Bonefield and co-workers, much research is still going on to develop this composite for high performance application like bone implant applications [141]. B.B. Johnson *et al.* demonstrated the reinforcing effect of CNTs on HDPE matrix. They reported that wear resistance and frictional properties of HDPE was improved by the addition of CNTs [142]. K. Li and S. C. Tjong studied mechanical, thermal and tribological behavior of HDPE based nanocomposites reinforced with nanoHA. The major conclusion drawn from their work is that HA increased the crystallization temperature along with other enhanced mechanical properties. NanoHA also caused a substantial improvement in the load bearing capacity of HDPE [115].

Fouad and Elleithy [143] developed HDPE-graphite nanocomposites as load bearing materials for total joint replacement by utilizing the solid lubricant potential of graphite nanoparticles (GNPs). They reported that crystallinity of HDPE was amplified due to the heterogeneous nucleation effect of GNPs, and the tensile strength, Young's modulus and shear modulus of the nanocomposites were enhanced to reach corresponding properties of UHMWPE. Inorganic nanofillers like nanoZnO have also been investigated by many researchers for their capability to develop the tribological properties of polymer matrices like PTFE [144], polyester [145], and nylon [146]. Polymer matrix tribological properties were improved by the addition of nanoAg by K.S. Morley and co-workers [147].

1.9   Scope and objectives of the present work

Nanocomposites based on polymer blends are the subject of this study. The upgradation of PE based polymer blends by incorporating nanofillers for critical applications is the main objective of this study. It is proposed to synthesize nanozirconia by sol-gel method and silica nanofibers from different biomasses as modifiers for high molecular weight high density polyethylene-linear low density polyethylene (HMHDPE-LLDPE) blend to widen the spectrum of its use. Different blend compositions of HMHDPE-LLDPE are proposed to be developed by melt mixing followed by injection moulding. Optimization of the blend is proposed to be done by evaluating its mechanical, thermal, rheological, and morphological properties.

Nanozirconia is a versatile material with diverse applications due to its innate mechanical property and thermal stability. Zirconia has three well-defined polymorphs. Since tetragonal phase (t- ZrO_2) is unquenchable

at high temperature, obtaining them at lower temperatures without the presence of any dopant metal oxides has gained importance due to their potential applications. A specific objective of this study is to attempt a polymeric surfactant assisted sol-gel method for the preparation of highly stabilized t-ZrO_2. Since a polymeric surfactant acts as a dispersing medium, the very frequent crisis of nanoparticles agglomeration can be completely avoided, thus promising zirconia having size lower than 10 nm can be prepared. Furthermore the role of mode of addition leading to the formation of monoclinic crystallite phase with spheroid morphology is also proposed to be well explored.

Recently, applications of nanosilica as a potential nanomaterial have gained immense interest among the material researchers. But the common methods for the synthesis of nanosilica are time consuming, energy extensive and also involve toxicity exposure of silicon containing alkoxides precursor. Bio fillers are assuming increasing importance nowadays because of their renewable source and low cost. Thus we propose to develop a novel green chemical route by exploiting the vast and abundant silica sources namely Indian grass, Pampas grass and Bamboo for the isolation of mesoporous nano silica fibers. Thus the present work proposes to address the environmental issue of grass junk remediation by an ecofriendly method for the synthesis of fibrous nanosilica. Another objective is to develop a cost effective method in place of costly templates used for growing nano wires, nano tubes etc. [40, 148, 149]. It is proposed to investigate whether the frame work of grass itself can act as a template for nano synthesis. The product is likely to have high potential for prepairing polymer based composite materials.

The synthesized nanozirconia [both tetragonal (t-ZrO$_2$) and monoclinic (t-ZrO$_2$) zirconia] and silica nanofibers (from the three different sources) are proposed to be used as modifiers in the HMHDPE-LLDPE blend. The mechanical, thermal, rheological and morphological properties of the modified nanocomposites are proposed to be investigated to test its suitability for high performance applications in the biomedical field.

The specific objectives of the present work are:

1) To synthesis suitable biocompatible nanofillers and their characterization

   - To synthesis nanozirconia by a surfactant assisted sol-gel method with spherical morphology, low particle size and mesoporous structure.

   - To isolate silica nanofibers from different grass sources namely Indian grass, Pampas grass and Bamboo.

2) To prepare the blends of HMHDPE and LLDPE

3) To optimise the blend composition by evaluating its physical, mechanical, thermal, and rheological behavior.

4) To investigate the reinforcing effect of nanozirconia in HMHDPE-LLDPE blend

5) To investigate the potential of silica nanofiber to develop nanocomposites based on HMHDPE-LLDPE blend.

6) To optimise the nanocomposites for high performance applications.

References

[1]   Utracki LA. Polymer Alloys and Blends, Carl HanserVerlag, Munich, 1989.

[2]   Utracki LA, Walsh DJ, Weiss RA. Polymer alloys, blends, and Ionomers: an overview, J. Am. Chem. Soc1989; 1-35.

[3]   Utracki LA, Weiss RA, editors. Multiphase polymers: blends and ionomers. 1989 Jul 21.Utracki LA, Weiss RA., Washington DC, 1989, pp. 1-35.

[4]   Franck A, Germany TI. Viscoelasticity and dynamic mechanical testing. TA Instruments, New Castle, DE, USA; AN004.

[5]   Sadiku-Agboola O, Sadiku RE, Adegbola AT, Biotidara OF. Mater. Sci. Appl. 2011; 2:30-41.

[6]   Koning C, Van Duin M, Pagnoulle C, Jerome R. Progress in polym. sci.1998; 23:707-757.

[7]   Ali S, Garforth AA, Harris DH, Rawlence DJ, Uemichi Y. Catal. Today. 2002; 75:247-55.

[8]   Murata K, Hirano Y, Sakata Y, Uddin MA. J. Anal. Appl. Pyrolysis 2002; 65:71-90.

[9]   Peacock A. Handbook of polyethylene: structures, properties, and applications. CRC Press; 2000.

[10]   Gabriel C, Lilge D. Polymer. 2001; 42:297-303.

[11]   Chiu FC, Fu Q, Peng Y, Shih HH. J. Polym. Sci. B. Polym. Phy. 2002; 40: 325-37.

[12]   Chanda M, Roy SK, Plast. Technol. Handbook, Marcel Dekker, New York; 1998.

[13]   Anderson JC. Tribol.Int.1982; 15:43-7.

[14]   Datta NK, Birley AW. TA of polyethylene blends. Plast. Rub. Proc. Appl. 1982; 2:237-45.

[15]   Zhao Y, Liu S, Yang D. Macromol.Chem.Physic 1997; 198:1427-36.

[16]   Lee HS, Denn MM. Polym. Eng. Sci. 2000; 40:1132-42.

[17]   Munaro M, Akcelrud L. Polym. Degrad. Stabil. 2008; 93:43-9.

[18]   Zuo JD, Zhu YM, Liu SM, Jiang ZJ, Zhao JQ.Polym.Bull. 2007; 58:711-22.

[19]   Liu G, Chen Y, Li H. J. Appl. Polym. Sci. 2004; 92:2628-32.

[20]   Fu Q, Men Y, Strobl G. Polymer. 2003; 44:1927-33.

[21]   Munaro M, Akcelrud L. J. Polym.Res. 2008; 15:83-8.

[22]   Minick J, Moet A, Baer E. Polym. 1995; 36:1923-32.

[23]   Bischel MS, Vanlandingham MR, Eduljee RF, Gillespie JW, Schultz JM. J. Mater. Sci. 2000; 35:221-8.

[24]   Sarkhel G, Banerjee A, Bhattacharya P. Polym. Plast. Technol. Eng. 2006; 45:713-8.

[25]   Chung D. DL: Composite materials, functional materials for modern technologies. London, Springer; 2003.

[26]   Stephen R.Ph.D Thesis, Mahatma Gandhi University; 2005.

[27]   Rao CN, Müller A, Cheetham AK, editors. The chemistry of nanomaterials: synthesis, properties and applications. John Wiley & Sons; 2006.

[28]   Siegel RW. Nanostruct. Mater. 1993; 3:1-8.

[29]   Gleiter H. Nanostruct. Mater. 1992; 1:1-9.

[30]   Gaertner GF, Miquel PF. Nanostruct. Mater. 1993;4:559

[31]   Brinker CJ, Scherer GW. Sol-gel science: The physics and chemistry of sol-gel processing. Academic press; 2013.

[32]   Brinker CJ, Scherer GW. Sol-Gel Science: The Physics and Chemistry of Sol-Gel Processing. Academic, San Diego, CA; 1990.

[33]   Lyu SC, Zhang Y, Ruh H, Lee HJ, Shim HW, Suh EK, Lee CJ. Chem. Phy. Lett. 2002; 363:134-8.

[34] Rataboul F, Nayral C, Casanove MJ, Maisonnat A, Chaudret B. J.Organomet. Chem. 2002; 643:307-12.

[35] Koh YW, Lin M, Tan CK, Foo YL, Loh KP. J. Phy. Chem. B.2004; 108:11419-25.

[36] Yu W, Li X, Gao X. Cryst. growth des. 2005; 5:151-5.

[37] Rodrıguez-Paez JE, Caballero AC, Villegas M, Moure C, Duran P, Fernandez JF. J.Eur.Cer.Soc. 2001; 21:925-30.

[38] Purica M, Budianu E, Rusu E, Danila M, Gavrila R. Thin Solid Films. 2002; 403:485-8.

[39] Okuyama K, Lenggoro IW. Chem. Eng. Sci. 2003; 58:537-47.

[40] Mokoena EM, Datye AK, Coville NJ. J.Sol-gel Sci. Technol. 2003; 28:307-17.

[41] Pajonk GM. Appl. Catal. 1991; 72:217-66.

[42] Rao AV, Hegde ND, Hirashima H. J. Colloid Interface Sci.2007; 305:124-32.

[43] Tang Q, Xu Y, Wu D, Sun Y. J. Solid state Chem.2006; 179:1513-20.

[44] BernArdos A, KouřimsKá L. Czech J. Food Sci. 2013; 31.

[45] Wang ZL, Gao RP, Gole JL, Stout JD. Adv. Mater. 2000; 12:1938-40.

[46] Manivannan R, Ramanathan S. Appl. Surf. Sci. 2009; 255:3764-8.

[47] Torney F, Trewyn BG, Lin VSY, Wang K. Nat. Nanotechnol. 2007; 2:295-300.

[48] Lin YS, Haynes CL. Chem.mater. 2009; 21:3979-86.

[49] Jugdaohsingh R, Tucker KL, Qiao N, Cupples LA, Kiel DP, Powell JJ. J.Bone.Miner.Res. 2004; 19:297-307.

[50] Jesionowski T. J.Mater.Proc.Technol. 2008; 203:121-8.

[51] Naik SP, Sokolov I. Solid State Commun. 2007; 144:437-40.

[52] Yang M, Wang G, Yang Z. Mater.Chem.Phys. 2008; 111:5-8.

[53]   Singh LP, Bhattacharyya SK, Mishra G, Ahalawat S.Appl.NanoSci. 2011; 1:117-22.

[54]   Rahman IA, Vejayakumaran P, Sipaut CS, Ismail J, Bakar MA, Adnan R, Chee CK.Colloids Surf. A. Physicochem. Eng. Asp. 2007; 294:102-10.

[55]   Do Kim K, Choi KY, Yang JW. Colloids Surf. A. Physicochem. Eng. Asp. 2005; 254:193-8.

[56]   Sarawade PB, Kim JK, Hilonga A, Kim HT. Powder Technol. 2010; 197:288-94.

[57]   Essien ER, Olaniyi OA, Adams LA, Shaibu RO. J.Met.Mater. Miner. 2011; 21:7-12.

[58]   Adam F, Chew TS, Andas J. J.Sol-gel Sci. Technol. 2011; 59:580-3.

[59]   Adams LA, Shaibu RO, Essien RE, Oki A. . J.Met.Mater.Miner 2011; 21:1-6.

[60]   Chakraverty A, Mishra P, Banerjee HD. J.Mater.Sci. 1988; 23:21-4.

[61]   Kalapathy U, Proctor A, Shultz J. Biores.Technol. 2002; 85:285-9.

[62]   Jones LH, Handreck KA. Adv. Agron. 1967; 19:107-49.

[63]   Parry DW, Hodson MJ, Sangster AG, Jones WC, O'Neill CH. Phil. Trans.R.Soc. Lon.B.1984; 304:537-49.

[64]   Lanning FC, Ponnaiya BW, Crumpton CF. Plant Physiol. 1958; 33:339.

[65]   Lanning FC, Linko YY. J.Agr.Food Chem. 1961; 9:463-5.

[66]   Rafiee E, Shahebrahimi S, Feyzi M, Shaterzadeh M. Int. Nano Lett. 2012; 2:29.

[67]   Liou TH, Yang CC. Mater.Sci.Eng.B. 2011; 176:521-9.

[68]   An D, Guo Y, Zhu Y, Wang Z. Chem. Eng.J. 2010; 162:509-14.

[69]   Umeda J, Kondoh K, Michiura Y. Mater. Transactions. 2007; 48:3095-100.

[70]   Li D, Chen D, Zhu X. Biores.Technol. 2011; 102:7001-3.

[71]   Liou TH, Yang CC. Mater.Sci.Eng.B. 2011; 176:521-9.

[72]   Zulkifli NS, Ab Rahman I, Mohamad D, Husein A. Ceram. Int. 2013; 39:4559-67.

[73]   Espíndola-Gonzalez A, Fuentes-Ramirez R, Martínez-Hernández AL, Castaño VM, Velasco-Santos C. Adv.Mater.Sci.Eng. 2014; 2014.

[74]   Yamaguchi T. Catal. Today. 1994; 20:199-217.

[75]   Arata K. Adv.Catal. 1990; 37:165-211.

[76]   Arata K, Hino M. Mater.Chem.Phy.1990; 26:213-37.

[77]   Sathyaseelan B, Manikandan E, Baskaran I, Senthilnathan K, Sivakumar K, Moodley MK, Ladchumananandasivam R, Maaza M. J.Alloys Compd. 2017; 694:556-9.

[78]   Carberry J. Zirconia and ceramic engineering questions relating to the reliability of ceramic ferrules in the outside plant. Technical Documents White paper, NeptecLLc.

[79]   Bardal A, Zwerger M, Eibl O, Wecker J, Matthee T. Appl.Phy.Lett. 1992; 61:1243-5.

[80]   Phillips JM. J.Appl.Phy. 1996; 79:1829-48.

[81]   Chen W, Shi P, Liu Y, Zhang C. In Photonics and Optoelectronics Symposium. 2009; IEEE.

[82]   Khireddine H, Fabry P, Caneiro A, Bochu B. Sens. Actuators. B. Chem.1997; 40:223-30.

[83]   Mauvy F, Gondran C, Siebert E. Electrochim. Acta. 1999; 44:2219-26.

[84]   Yang Y, Liu CC. Sens. Actuators. B. Chem. 2000; 62:30-4.

[85]   Chen H, Zhang Y, Ding C. Wear. 2002; 253:885-93.

[86]   Gashti MP, Almasian A, Gashti MP. Sens. Actuators. B. Phys. 2012; 187:1-9.

[87]   Gashti MP, Almasian A. Compos.Part. B. Eng. 2013; 52:340-9.

[88] Chakravarty R, Shukla R, Tyagi AK, Dash A, Venkatesh M. Appl.Radiat. Isotopes. 2010; 68:229-38.

[89] Chakravarty R, Shukla R, Ram R, Tyagi AK, Dash A, Venkatesh M. Nucl. Med. Biol. 2011; 38:575-83.

[90] Chraska T, King AH, Berndt CC. Mater.Sci.Eng. A. 2000; 286:169-78.

[91] Luo TY, Liang TX, Li CS. Mater.Sci.Eng.A. 2004; 366:206-9.

[92] Tan D, Lin G, Liu Y, Teng Y, Zhuang Y, Zhu B, Zhao Q, Qiu J. J. Nanoparticle Res.. 2011; 13:1183-90.

[93] Centi G, Cerrato G, D'Angelo S, Finardi U, Giamello E, Morterra C, Perathoner S. Catal.Today. 1996; 27:265-70.

[94] Rodaev VV, Zhigachev AO, Golovin YI. Ceram.Int. 2017; 43:1200-4.

[95] Chandradass J, Han KS, Bae DS. J.Mater.Proc.Technol. 2008; 206:315-21.

[96] Vasylkiv OO, Sakka Y, Skorokhod VV. Powder Metall.Met.Ceram. 2005; 44:228-39.

[97] Lin JD, Duh JG. J.Amer.Ceram.Soc. 1997; 80:92-8.

[98] Štefanić G, Musić S, Popović S, Sekulić A. J.Mol.Struc. 1997; 408:391-4.

[99] Roy S. J.Sol-gel Sci. Technol.2007; 44:227-33.

[100] Wang JA, Valenzuela MA, Salmones J, Vázquez A, Garcıa-Ruiz A, Bokhimi X. Catal. Today. 2001; 68:21-30.

[101] Aguilar DH, Torres-Gonzalez LC, Torres-Martinez LM, Lopez T, Quintana P. J. Solid State Chem. 2001; 158:349-57.

[102] Zheng JY, Pang JB, Qiu KY, Wei Y. Microporous Mesoporous mater. 2001; 49:189-95.

[103] Blin JL, Flamant RK, Su BL. Int.J.Inorg.Mater. 2001; 3:959-72.

[104] Tsukada T, Venigalla S, Morrone AA, Adair JH. J.Amer.Ceram. Soc. 1999; 82:1169-74.

[105] Sōmiya S, Akiba T. J.Eur.Ceram Soc. 1999; 19:81-7.

[106] Rezaei M, Alavi SM, Sahebdelfar S, Yan ZF. Powder Technol. 2006; 168:59-63.

[107] Nandakumar N, Kurian P. Powder Technol. 2012; 224:51-6.

[108] Koo JH. Polymer nanocomposites. McGraw-Hill Professional Pub.; 2006.

[109] Mittal V, editor. Synthesis techniques for polymer nanocomposites. John Wiley & Sons; 2014.

[110] Gao F, editor. Advances in polymer nanocomposites: types and applications. Elsevier; 2012.

[111] Zeng C, Lee LJ. Macromolecules. 2001; 34:4098-103.

[112] Ou Y, Yang F, Yu ZZ. J.Polym.Sci.Part B.Polym.Phys. 998; 36:789-95.

[113] Sanchez C, Julián B, Belleville P, Popall M. J.Mater.Chem. 2005; 15:3559-92.

[114] Camargo PH, Satyanarayana KG, Wypych F. Mater.Res. 2009; 12:1-39.

[115] Li K, Tjong SC. J. Macromol. Sci. Part B. 2011;50:1325-37.

[116] Nath S, Bodhak S, Basu B. J.Biomed.Mater.Res.Part.B:Appl.Biomater 2009; 88:1-1.

[117] Sadi AY, Homaeigohar SS, Khavandi AR, Javadpour J. J.Mater.Sci. Mater.Med. 2004; 15:853-8.

[118] Malucelli G, Palmero P, Ronchetti S, Delmastro A, Montanaro L. Polym.Int. 2010; 59:1084-9.

[119] Khumalo VM, Karger-Kocsis J, Thomann R. Express Polym. Lett. 2010; 4:264-74.

[120] Mohsin MA, ArsadA, Alothman OY. World Acad. Sci. Eng. Technol., Int. J. Chem. Mol. Nucl. Mater. Metall. Eng. 2014; 8:117-20.

[121] Xiong L, Xiong D, Yang Y, Jin J. J.Biomed.Mater.Res.Part.B:Appl. Biomater. 2011; 98:127-38.

[122] Jongsomjit B, Panpranot J, Praserthdam P. Mater. Lett. 2007; 61:1376-9.

[123] Durmus A, Kasgoz A, Macosko CW. J. Macromol. Sci., Part B: Phys. 2008;47:608-19.

[124] Pedrazzoli. D, Ceccato. R, Kerger-Kocsis.J, Pegoretti.A, Express Polym Lett.2013;7:652-66.

[125] Jin-hua T, Guo-qin L, Huang C, Lin-jian S. Mater.Res. 2012; 15:1050-6.

[126] Ren X, Wang XQ, Sui G, Zhong WH, Fuqua MA, Ulven CA. J.Appl. Polym.Sci. 2008; 107:2837-45.

[127] George TS, Krishnan A, Anjana R, George KE. Polym. Compos. 2012; 33:1465-72.

[128] Dangsheng X. Mater. Lett. 2005; 59:175-9.

[129] Plumlee K, Schwartz CJ. Wear. 2009; 267:710-7.

[130] Guofang G, Huayong Y, Xin F. Wear. 2004; 256:88-94.

[131] Xiong D, Lin J, Fan D, Jin Z. J.Mater.Sci.Mater.Med. 2007; 18:2131-5.

[132] Xiong DS, Lin JM, Fan DL. Biomed.Mater. 2006; 1:175.

[133] Zoo YS, An JW, Lim DP, Lim DS. Tribol. Lett. 2004; 16:305-9.

[134] Schwartz CJ, Bahadur S, Mallapragada SK. Wear. 2007; 263:1072-80.

[135] Fang L, Leng Y, Gao P. Biomaterials. 2006; 27:3701-7.

[136] Liu JL, Zhu YY, Wang QL, Ge SR. J.China.Univ.Mining.Technol. 2008; 18:606-12.

[137] Chang BP, Akil HM, Nasir RB. Wear. 2013; 297:1120-7.

[138] Ge S, Wang S, Huang X. Wear. 2009; 267:770-6.

[139] Voss H, Friedrich K. Wear. 1987; 116:1-8.

[140] Wang Q, Xue Q, Shen W. Tribol.Int. 1997; 30:193-7.

[141] Bonfield W, Grynpas MD, Tully AE, Bowman J, Abram J.Biomaterials. 1981; 2:185-6.

[142] Johnson BB, Santare MH, Novotny JE, Advani SG. Mech.Mater. 2009; 41:1108-15.

[143] Fouad H, Elleithy R. J.Mech.Behav. Biomed.Mater. 2011; 4:1376-83.

[144] Li F, Hu KA, Li JL, Zhao BY. Wear. 2001; 249:877-82.

[145] Bahadur S, Zhang L, Anderegg JW. Wear. 1997; 203:464-73.

[146] Wang S, Ge S, Zhang D. Wear. 2009; 266:248-54.

[147] Morley KS, Webb PB, Tokareva NV, Krasnov AP, Popov VK, Zhang J, Roberts CJ, Howdle SM. Eur. Polym. J. 2007; 43:307-14.

[148] Ono Y, Nakashima K, Sano M, Kanekiyo Y, Inoue K, Hojo J,Shinkai S. Chem. Commun. 1998; 1477-8.

[149] Wang L, Tomura S, Ohashi F, Maeda M, Suzuki M, Inukai K. J.Mater.Chem. 2001; 11:1465-8.

[150] Liu L, Kou HZ, Mo W, Liu H, Wang Y. J.Phys.Chem B. 2006; 110:15218-23.

.....ഇരു.....

Chapter **2**

MATERIALS AND METHODS

The materials and experimental techniques used for the preparation of nanomaterials and nanocomposites are described in this chapter. The characterization techniques are also outlined.

2.1   Materials

2.1.1 Polymer matrix for blend preparation

2.1.1.1 High molecular weight high density polyethylene (HMHDPE)

HMHDPE (F00952 with a melt flow index of 0.05 gm/10 min and density of 0.952 g/cc) was supplied by Sabic, India.

2.1.1.2 Linear low density polyethylene (LLDPE)

LLDPE (O19010 with a melt flow index of 0.90 gm/10 min and density of 0.918g/cc), was purchased from Reliance industries Ltd, Mumbai, India.

2.1.2 Materials for preparation of nanofillers

2.1.2.1 Nanozirconia

The reagents required for the synthesis of nanozirconia were of analytical grade such as

a) Zirconium oxychloride ($ZrOCl_2.8H_2O$) was supplied by Spectro Chem Pvt. Ltd. Mumbai, India.

b) Ammonium hydroxide (NH_4OH) was purchased from Merck specialties Pvt. Ltd. Mumbai, India.

c) Isopropyl alcohol (IPA) was obtained from Sd fine chem. Pvt. Ltd. Mumbai, India.

d) Poly (vinyl alcohol) (hot, molecular weight 14000) was supplied from Spectro Chem Pvt. Ltd. Mumbai, India.

2.1.2.2 Nanosilica

a) Indian grass collected from our campus

b) Pampas grass collected from the river bank of Bharathapuzha near Shornoor, Kerala, India.

c) Bamboo from local area.

d) Hydrochloric acid (HCl) of assay 37% purchased from Merck specialties Pvt. Ltd. Mumbai.

2.2 Experimental methods

2.2.1 Preparation of blends and composites

Melt mixing technique was employed for composite preparation. Thermo Haake Rheomix 600 (Figure 2.1) mixing chamber with a volumetric

capacity of 69 cm^3 fitted with roller rotors (Figure 2.2) was used for the process. The temperature was set at 160 ^{o}C. The roller rotors in the chamber rotate in opposite directions so as to affect a shearing force on the material. Initially HMHDPE and LLDPE granules were placed in an air oven set at 100 ^{o}C for four hours to remove any moisture present and allowed to cool to room temperature in desiccators. Then the required quantities of the polymer pellets initially weighed were fed into the chamber. After 2 minutes of mixing, requisite amount of fillers were added according to their corresponding weight %. Two types of composites (nanozirconia composites, fibrous nanosilica composites) were fabricated by this method. A mixing time of 8 minutes at a counter rotating rotor speed of 50 rpm was used for the mixing of the polymers and the fillers. The hot polymer nanocomposites taken out from the mixing chamber were pressed in a hydraulic press and were cut into small pieces.

Figure 2.1 Thermo Haake Polylab System

Figure 2.2 Roller type rotors for melt compounding

2.2.2 Preparation of test specimen

Figure 2.3 DSM 12cc Micro Injection moulding machine

The test specimens were prepared using a semi automatic type injection moulding machine (Model JIM 1 H series 4508, Figure 2.3) with a barrel temperature of 170 $^{\circ}$C. Using appropriate moulds, dumb-bell shaped specimens for tensile study and rectangular specimens for impact, flexural and fracture toughness studies were prepared. Cylindrical specimens for compressive property and pin for the wear resistance property studies (Pin on disc) were also prepared in the same manners. The specimens were

moulded at identical conditions and the properties were taken as the average property of ten samples.

2.3 Characterization techniques

2.3.1 Mechanical properties

2.3.1.1 Tensile properties

Tensile properties were evaluated using Shimadzu Autograph AG-1 series universal testing machine equipped with a 50 kN load cell capacity at a displacement rate of 50 mm/min according to ASTM D 638 on dumb – bell shaped specimens. The gauge length between the jaws at the start of each test was fixed to 40 mm. A minimum of ten samples were tested in each composite and the average results were recorded.

2.3.1.2 Flexural properties

Flexural strength means the ability of the material to withstand bending forces applied perpendicular to its longitudinal axis. Flexural modulus is used as an indication of material's stiffness when flexed. Flexural test was conducted by three point loading system using UTM (Shimadzu AG-1) with a load cell capacity of 50kN according to ASTM D 790, using rectangular shaped samples at a crosshead speed of 5 mm/min. The rectangular specimens were placed on a three-point bending apparatus with two supports spanning 40 mm from each other and loaded by means of a loading nose midway between the supports until failure. A minimum of five samples were tested in each sample and the average results were recorded.

The flexural strength is given by

$$S = 3PL/2bd^2$$

where S = flexural strength, P = maximum load at the moment of break, b = width of the specimen, L = length of the span and d = the thickness of the specimen.

The flexural modulus is calculated from the slope of initial portion of the flexural stress-strain curve.

2.3.1.3 Hardness

Hand-operated durometer was used to measure the surface hardness (shore D) of the material according to ASTM D 785. Hardness test measures the penetration of a specified indenter into the material under specified conditions of force and time.

2.3.1.4 Impact strength

The Izod impact strength was measured using notched samples as per ASTM D 256 on a Ceast Resil Impact Analyser (Junior) using a hammer of 4 J at a striking rate of 3.96 m/s. The impact strength is calculated as the ratio of impact absorption to test specimen cross-section. Toughness is dependent upon temperature and the shape of the test specimen. The area under the stress-strain curve is directly proportional to the toughness of the material. The notched rectangular specimen is fixed vertically in the base of the machine, a pendulum swings on its course, released and strikes the sample, and the impact energy is directly read from the machine.

Impact strength = Impact energy (J)/Thickness (m)

2.3.1.5 Fracture toughness

A single-edge notch three-point-bending (SEN-TPB) test was carry out to get the critical stress intensity factor toughness (KIC) of the material according to ASTM D 5045 by using the rectangular specimen [Figure 2.4] at a crosshead speed of 10 mm/min. The notches were prepared first by the formation of saw cut slots having rectangular shape with a width of ~1 mm in the midsection of specimens. Before testing, the samples were pre-cracked by inserting a fresh razor blade into the sawed notch and impacting by a hammer. The total notch length of SEN-TPB specimen was in such a way that (a/w) should be in between 0.45-0.55, where 'a' is the initial crack length (crack pre-notch plus razor tapping notch) and 'w' is the specimen width. Equations (2.1) and (2.2) were used to evaluate the fracture toughness of the composites by taking 'P' as the critical load for crack propagation and 'B' as the specimen thickness.

$$K_{IC} = \frac{P}{BW^{1/2}} f\left(\frac{a}{w}\right), \ (x=a/w) \ \text{.......................................(2.1)}$$

$$f\left(\frac{a}{w}\right) = \{6x^{1/2} \ [1.99 - x(1-x)(2.15 - 3.93x + 2.7x^2)]\} \ / \ [\ (1+2x)(1-x)^{3/2}] \ \text{....(2.2)}$$
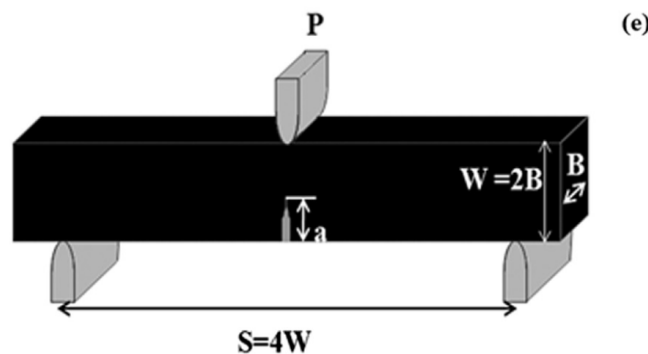
Figure 2.4   Schematic representation of the Specimen for SEN-TPB fracture toughness test

2.3.1.6 Compressive strength

Compressive testing was carried out in accordance to ASTM D 695-02a. Cylindrical specimens were moulded so that their length was twice their diameter and their two ends were flat and perpendicular to their long axis. The compressive test was done using UTM (Instron, model 3345) with a cross head speed of 1mm/min using a load cell capacity of 5 kN. The prepared specimens had dimensions of 6 mm diameter and 12 mm length and were compressed along their long axis until failure occurred. The force and displacement were recorded throughout the compression and converted to stress and strain on the basis of the initial specimen dimensions. The compressive modulus was calculated as the slope of the initial linear portion of the stress–strain curve. The offset compressive yield strength was determined as the stress at which the stress–strain curve intersected with a line drawn parallel to the slope defining the modulus, beginning at 1.0% strain (offset). The compressive strength was defined as the maximum stress carried by the specimen during the compression testing.
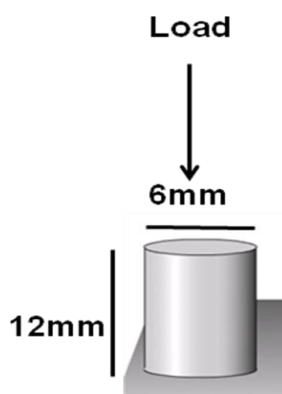
Figure 2.5 Schematic representation of sample for analysis of compressive modulus
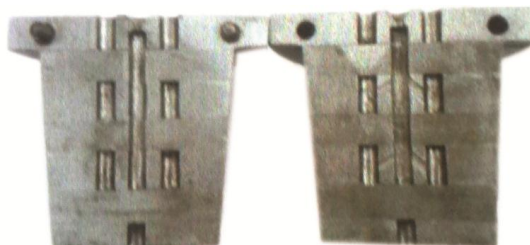
Figure 2.6 Mould used for the preparation of sample

2.3.1.7 Wear resistance

The tribological characteristics (wear resistance) were measured on a test device (Figure 2.7) under dry friction and with a load of 5 N at a shaft rotation velocity of 100 rpm. The polymeric samples in the form of a pin are abraded against the rough phase in the form of a disc without the presence of any lubricant. The wear resistance of the materials during sliding was found using a shaft–block arrangement according to ASTM standards G99 and DIN 50324. The sample friction tracks were studied on SEM.

Figure 2.7 PIN ON DISC test for wear resistance test apparatus

During the course of wear process, takes a few material away from the specimen. This mass loss can accurately measured by an analytical balance with a resolution of 0.1 mg. The weight of the sample before and

after the experiment was measured. A characteristic value, that describes the wear performance under the chosen conditions for a tribo-system is the specific wear rate(K_s):

$$K_s \;=\; \frac{\Delta m}{\rho . F . L} \;(\text{mm}^3\text{N}^{-1}\text{m}^{-1})$$

Where Δm is the mass loss, ρ is the measured density of the sample, F is the normal load applied, and L is the sliding distance. In order to get the actual picture of the wear performace the test was conducted with four samples and an average of these four readings was adapted in our results.

2.3.2 Thermal Properties

2.3.2.1 Thermo gravimetric analysis (TGA)

Thermo gravimetric analysis is a thermal analysis technique for understanding the thermo-physical properties of materials. TGA aims at the investigation of pyrolysis and thermal degradation of solids [1]. It monitors the mass of a sample as a function of temperature or time while the substance is subjected to a controlled temperature programme [2]. The integral (TGA) and derivative (DTG) thermogravimetric curves give information about thermal stability and extent of degradation of the polymeric material. The heating process brings a lot of changes in the material and finally leaves behind the inorganic filler as the inert residue.

Thermal analysis of the material was determined using Thermo Gravimetric Analyzer (TGA Q-50, TA instruments) in which approximately 7 mg of the sample was heated from ambient temperature to 600 °C at a heating rate of 20 °C/min, in an inert (nitrogen) atmosphere.

2.3.2.2 Differential scanning calorimetry (DSC)

Differential scanning calorimeter (DSC) is a technique for studying the thermal behavior of a material as a function of temperature as they go through physical or chemical changes with absorption or evolution of heat. It is used to investigate thermal transitions, including phase changes, crystallization, melting, glass transitions of a material as a function of temperature [3,4,5]. Heat flow, heat absorption (endothermic) or heat emission (exothermic), are measured as a function of time or temperature of the sample and the result is compared with that of a thermally inert reference. The materials, as they undergo changes in chemical and physical properties, which are detected by transducers, which changes into electrical signals that are collected and analyzed to give thermograms. DSC directly gives a recording of heat of flow rate (Cp) against temperature. The kinetics of phase transformation can also be studied by DSC. The melting and crystallization parameter, such as melting point (T_m), Heat of fusion (ΔH_f) temperature of crystallization (T_m), and Heat of crystallization (ΔH_c) were used for the comparison of composites.

The degree of crystallinity (X) can be measured as a function of time,

$$X = \Delta H_f \text{ (observed) } / (1-\phi) \, \Delta H_f \text{ (100\% crystalline)} *100$$

where ΔH_f (100% crystalline)* for HMHDPE is taken as 293J/g, and (1-ϕ) for 80/20 HMHDPE-LLDPE blend as 0.8. DSC measurements were made on a DSC Q 100 (TA instruments). The samples were heated from 30 ºC to 250 ºC at the rate of 50 ºC/min and kept at isothermal for 3 minutes in order to remove the thermal history, cooled from 250 ºC to room

temperature then reheated from room temperature to 250 ℃ at heating rate of 10 ℃ /min under nitrogen atmosphere (60mL/min flow.

2.3.3 Structural characterizations

2.3.3.1 Fourier transform infrared spectroscopy (FTIR)

FTIR is a powerful analytical tool used to determine the structure and functional groups in a molecule. FTIR aims at determining the molecular structure by detecting the characteristic vibrational frequencies of molecules. For a vibrational mode in a molecule to be IR active, it must be associated with changes in the permanent dipole. FTIR spectrum was recorded on a Fourier transform Infrared Spectroscope, Bruker, Tensor 27 model in ATR mode at wave numbers 4000-400 cm^{-1}.Here transmittance % is presented as the function of wave number (cm^{-1}).

2.3.3.2 X-ray diffraction analysis (XRD)

XRD is a unique technique for the characterization of crystalline materials and their structure determination. The characteristic XRD pattern obtained from each crystalline solid may be considered as a "fingerprint" for its identification [6]. By using Bragg's equation, $n\lambda= 2d \sin\theta$, where d is the spacing between the atomic planes in the crystal phase and λ is the wave length of X-rays used, the intensity of the diffracted X-ray is measured as a function of diffraction angle 2θ and specimen orientation. The value of d spacing gives an indication of the type of the composite formed. The crystallite size from XRD was calculated by X-ray line broadening technique using Debye-Scherrer equation $D=k\lambda/\beta\cos\theta$, where k=0.9, β is the full width at half maximum (FWHM) of an hkl X-ray

diffraction peak at θ value, and θ is half of the diffraction angle 2θ corresponding to the peak and D corresponds to the crystallite size.

The XRD patterns were recorded using X-Ray Diffractometer, Bruker, D8 Advance model, employing Cu K_α radiation (λ =1.54 Å) as radiation source and Ni filter operating at 30 kV and 20 mA at a 2θ scan speed of 10 °/min. The samples were scanned in the range of 3-80º at an increment step of scanning 0.020º.

2.3.4 Elemental analysis

2.3.4.1 Energy dispersive X-ray spectroscopy (EDS)

EDS a qualitative elemental analysis, standard less quantitative analysis, X-ray line scans and mapping, gives the chemical purity of the sample. EDS was performed along with SEM equipment. JOEL model JSM-6390LV is the specification for EDS.

2.3.5 Morphological Analysis

2.3.5.1 Scanning electron microscopy (SEM)

Scanning electron microscopy is used for the surface analysis of the nanomaterial. The method uses a focused beam of high-energy electrons to generate a variety of signals at the surface of solid specimens. These signals include secondary electrons, back scattered electrons, and diffracted backscattered electrons, photons, visible light, and heat. Of these, the signals produced by secondary electrons are the most important for studying the morphology and topography of the samples. SEM was also used to measure the mechanically performed fractured surface of the polymer nanocomposites [7].

The morphological characterization was carried out using a JEOL Model JSM 6390LV scanning electron microscope. Prior to SEM analysis sample surface were gold coated with the help of gold sputtering unit to avoid the charging effect and enhance the emission of secondary electrons.

2.3.5.2 Transmission electron microscopy (TEM)

Direct imaging of individual nanoparticles is made possible by TEM. TEM is unique since it provides a real space image on the atom distribution in the nanocrystal and on its surface. The morphology, porosity and particle size were observed using high resolution TEM (HRTEM) analysis on a Philips TEM CM200 model.

2.3.6 Surface analyses by BET

Brunauer–Emmett–Teller (BET) surface area analyzer was used to estimate surface area and pore size distribution of the nanomaterials and it was carried out using Quanta chrome Quandraorb automatic volumetric measurement system at 77K using ultra pure nitrogen gas.

2.3.7 Melt rheological analysis

2.3.7.1 Melt flow index (MFI)

An extrusion plastometer was used for measuring the melt flow index of polymer melts [8]. The rate of extrusion through a die of specified length and diameter was measured under prescribed conditions of temperature and load as a function of time. Melt flow index was calculated and reported as g/10min. This index is inversely proportional to molecular weight.

The MFI of the polymer and the nanocomposites were performsed on a CEAST Modular Line Melt Flow Indexer in accordance with ASTM D 1238 using 2.16 kg load at a melt temperature of 190 °C.

2.3.7.2 Dynamic rheological analysis (DRA)

Rheological characterization was performed on a parallel plate oscillatory rheometer, Anton Paar Rheometor MCR 102 (Figure 2.8) using 25 mm parallel plate fixtures, with a gap of 1-2 mm at 200 °C. The software used is Rheoplus version 32. The small pieces of melt compounded material were placed in the gap between the plates.

Figure 2.8 Rheometer (MCR 102)

The rheometer was operated in both amplitude sweep and frequency sweep test. In the amplitude sweep, angular frequency is kept at a constant value of 10 rad/s and amplitude is varied from 0.01 to 100% log values. The amplitude is kept at a constant value of 2.5% and frequency is varied from 100 to 0.1 rad/s in a log scale for frequency sweep experiment. The

elastic modulus (E'), loss modulus (E") and complex viscosity (η*) were measured as functions of the angular frequency (ω) from the frequency sweep data. At least two trials were run for each experimental condition to check for reproducibility of the results.

References

[1]   Flynn JH. Thermochimi. Acta. 1974; 8: 69-81.

[2]   Allen G, Bevington JC. Comprehensive Polym. Sci.: The Synthesis, Characterization, Reaction and Application of Polymers. Polym. properties. 1989; 2.

[3]   Busigin C, Lahtinen R, Martinez GM, Thomas G, Woodhams RT. Polym. Eng. Sci. 1984; 24: 169-74.

[4]   Zhu WP, Zhang GP, Yu JY, Dai G, J. Appl. Polym. Sci. 2004; 91:431.

[5]   Labour T, Vigier G, Seguela R, Gauthier C, Orange G, Bomal Y. J.Polym. Sci. Part B Polym. Phys. 2002; 40: 31-42.

[6]   Chandran S. Ph.D Thesis, Cochin University of Science and Technology, India; 2008.

[7]   Woodward AE. Atlas of polymer morphology. Hanser Publishers; 1988.

[8]   Annual Book of ASTM Standards, D 1238, 08.01; 2004.

.....ഇൗ.....

Chapter 3

PREPARATION AND CHARACTERIZATION OF NANOZIRCONIA BY POLY VINYL ALCOHOL ASSISTED SOL-GEL METHOD

Monodispersed tetragonal nanocrystalline zirconia (t-ZrO_2) with spherical morphology and monoclinic zirconia (m-ZrO_2) with spheroid morphology were synthesized by adopting a facile template assisted sol-gel method. The medium assisting growth of nanoparticles mainly consisted of $ZrOCl_2.8H_2O$ and NH_4OH as reactants in a 1:2 mixture of Isopropyl alcohol (IPA)-polyvinyl alcohol (PVA) as the dispersing agent. PVA being a macromolecular surfactant containing large number of hydroxyl groups per molecule acts as a template for particle growth and assists size control and can be easily removed after synthesis by calcination. The calcined nanopowders were characterized by X-ray diffraction (XRD), Particle size analyser, Zeta potential measurement, Fourier transform infrared spectroscopy (FTIR), Scanning electron microscopy (SEM), Transmission electron microscopy (TEM), Nitrogen adsorption (BET) and Thermo gravimetric analysis (TGA). The studies reveal that the size of the t-ZrO2 and m-ZrO_2 particles is highly reliant on PVA content and calcination temperature. More over reacting medium and calcination temperature has a vital role in determining the crystallinity and morphology of ZrO_2. The sample prepared under optimized conditions (2% w/v PVA) shows pure tetragonal crystallite phase with an average particle size of 5 nm, surface area of 56 m^2 g^{-1}, and a mesoporous structure after calcination at 600 ^{o}C for 5 h. The tetragonal phase is stable and show spherical morphology up to 600 ^{o}C after which the nanostructure is disturbed drastically; the agglomeration leads to structure collapse forming hard conglomerates leading to monoclinic crystalline phase. Changing the mode of addition of the reacting medium followed by calcination provides mesoporous, spheroid, monoclinic zirconia (m-ZrO_2) with an average particle size of 15 nm and surface area 73.5 m^2 g^{-1}.

3.1 Introduction

Nanotechnology can be considered as a state of the art tool which combines chemistry, physics, material science, electronics and biosciences. It is a state of the art of twenty first century, ranging from novel building materials in aerospace technology to life saving medicines. Normally, the term nano encompasses the range 1–100 nm. With respect to diversity in the application, nanotechnology offers uniqueness and flexibility not observed in any other field of technological innovations.

Nanomaterials are being considered for various applications due to their small size and large surface area. Out of the nanomaterials nanozirconia, has increased manifold applications. Owing to its high mechanical and thermal stability nanozirconia materials can be exploited in various applications like wear resistant/protective coatings [1–3], gate dielectric materials [4,5], and buffer layers for growing super conductors [6,7]. Zirconia mixed oxide systems find yet more attention as catalyst and as catalyst support [8], furthermore sulfated zirconia has been explored as a 'super acid' [9,10]. Partly or completely stabilized zirconia ceramic used as gas sensors [11], and as solid electrolyte in electronic instruments [12]. Nanozirconia was also successfully used as sorbents in the preparation of radionuclide generators and as sorbent for biomedical applications [13-15]. With unparalleled properties in optics, electronics, mechanics and calorifics, nanozirconia is an important inorganic material and it is of relevant to explore its preparation.

Zirconia has three well-defined polymorphs; the tetragonal and cubic phases are of more importance for its catalytic applications because

of high thermal stability, high BET surface area and amphoteric nature. The monoclinic form of zirconia exists in room temperature gets converted into the tetragonal phase at 1447 K. The tetragonal phase is further converted to the cubic phase around 2643 K [16, 17]. These high temperature tetragonal and cubic phases are, unquenchable and obtaining them at lower temperatures has gained importance over the past decade due to their potential applications [13-15, 18]. Several attempts have been made to achieve stabilized tetragonal and cubic phases by doping zirconia with a variety of metal oxides like CaO, Y_2O_3, CeO_2, Ce_2O_3, La_2O_3, MgO, CuO, Cr_2O_3, MnO_2, NiO, SnO_2 etc. [19-23]. However it is very difficult to control the dopant and the synthesis proceeds through a tedious route. In some cases t-ZrO_2 could exist at room temperature and the condition of its stability was still a subject of arguments [24]. Chakravarty *et al.* [14, 15] synthesized t-ZrO_2 for their potential utility as a new generation sorbent for the preparation of 99Mo/99mTc and 68Ge/68Ga generators for biomedical applications. Roy synthesized t-ZrO_2 using polyacryl amide as a gelling agent and a matrix, and the final product investigated had a particle size of about~20 nm [25]. The key role in stabilizing the tetragonal phase of the nano crystalline zirconia is played by 'the small crystallite size'.

Researchers have explained many synthetic routes like precipitation [26], sol-gel [27,28], chemical vapor synthesis [29], micro emulsion method [30], glycothermal process [31], and hydrothermal precipitation process [32] to obtain these polymorphs even without adding the dopant metal. For realizing industrial production, the most familiar and simple method used to prepare nanozirconia is the "Sol-Gel" technique [27,28] and is often in top-priority because of its easiness, while others have disadvantages in high

energy consumption, costly material, complex techniques, long production period, intricate equipments etc. No matter which method is used to prepare nanopowder, the crucial question is how to overcome conglomeration and precipitation. Recently, a great deal of interest was focused on the synthesis of the nanostructured mesoporous oxides using a surfactant-assisted route to conquer the agglomeration [33, 34]. Shukla *et al.* [35] prepared t- ZrO_2 having a crystallite size of about 65 nm through a sol gel process involving hydrolysis and condensation of zirconium (IV) n-propoxide in an alcohol solution using hydroxyl propyl cellulose (HPC) polymer as a steric stabilizer.

The aim of this study is to explore a polymeric surfactant assisted sol-gel method for the preparation of highly stabilized t-ZrO_2. Since polymeric surfactant act as a dispersing medium, the very frequent crisis of nanoparticles agglomeration is completely avoided. The addition of dispersing medium would produce a matrix into which synthesized incipient zirconia, would be incorporated still in the early stages of the reaction, thus producing zirconia in the nanoscale.

Even though the preparation of zirconium dioxide nanopowders by different methods has also been extensively studied, the exploration of facile synthesis of porous, spherical and monodispersed tetragonal nanocrystalline zirconia powders in a very dilute alcoholic (Isopropyl alcohol, IPA) media at ambient conditions is not yet regulated. Until now, there have been no reports on the preparation of homodispersed spherical tetragonal nano crystalline ZrO_2 in PVA supported medium at room temperature. The synthesis of tetragonal nanozirconia using PVA as the polymeric surfactant via sol-gel method is proposed to be attempted in this

study. We also propose to investigate the influence of PVA on morphology, size and its role in yielding porous nanomaterials. The influence of experimental conditions such as concentration of PVA and calcination temperatures on the nature of zirconia formed at constant molar ratio of reactants is proposed to be investigated. Furthermore the role of the sequence of addition is also proposed to be investigated.

3.2 Experimental

3.2.1 Chemicals

The chemicals used for the analysis are given in Table 3.1.

Table 3.1 Chemical used for the preparation of nanozirconia

Chemical	Source	Purity
$ZrOCl_2.8H_2O$	Spectro Chem Pvt. Ltd.	99.99%
NH_4OH	Merck specialities Pvt. Ltd.	99.99%
Poly (vinyl alcohol) (hot)	Spectro Chem Pvt. Ltd.	Molecular weight-14000
Isopropyl alcohol	Sd fine Chem. Pvt. Ltd.	AR grade
Ethanol	Alpha chemicals	AR grade

3.2.2 Preparation of nanozirconia

All the chemicals were used without further purification. The preparations were carried out at ambient temperature (ca.25 °C) in a glass beaker. In the synthesis of nanopowders two methods have been used. Method I: Initially 50 mL of 0.19 M zirconium oxychloride ($ZrOCl_2.8H_2O$) was thoroughly mixed with 50 mL of IPA-PVA mixtures. The medium selected was a 1:2 mixture of IPA-PVA with % w/v (weight by volume percentage) of PVA varied from 0-7 % w/v. (i.e., 50 mL IPA + 100 mL PVA, % w/v of PVA were 1% w/v, 2% w/v, 3% w/v, 5% w/v and 7% w/v

respectively). All solutions except 0% w/v showed a turbid appearance soon after mixing, though no visible precipitation was observed and it was taken in a micro burette. 50 mL of 2.9 M NH_4OH was taken in a beaker and the precipitation was done by adding a very dilute alcoholic (IPA) solution of zirconium oxychloride containing requisite % w/v PVA, drop wise at a rate of 0.2 mL/30 sec under vigorous magnetic stirring. This mode of addition is essential as, formation of zirconia precipitate in alkaline environment helps in stabilization of precursor to tetragonal nanoparticles [36]. After precipitation, the slurry was stirred for another 30 min keeping the pH of the reaction mixture in the range 11-12 by further addition of ammonia and then refluxed at 86 °C under vigorous stirring overnight, prior to formation of white gel. The digestion of the basic solution in the glass vessel by refluxing overnight at high temperature leads to stabilization of small-size tetragonal crystals. The vigorous stirring of the reaction medium prevents agglomeration of the precipitate and hence facilitates the formation of the nanoparticles. After refluxing the mixture it was cooled to room temperature and the gel was washed thoroughly with an alcoholic (ethanol) solution to remove unused PVA, soluble byproducts and unreacted reagents. The mixture was filtered and dried at 70 °C for 12 h prior to calcination at 400 °C, 600 °C and 800 °C for 5 h. A second method (Method II) was adopted in which: optimized PVA (2% w/v PVA) was taken in the beaker, and the precipitant NH_4OH was taken in the burette. After the gelation reaction the gel was refluxed, aged, washed, dried and calcined at 600 °C for 5 h. Synthesis strategy of nanozirconia was clearly depicted in Figure 3.1. The conditions were optimized and large scale preparation was done using 3000 mL borosil beaker as reactor. The yield of this process is 96%. An overview of the entire

reaction is given in Figure 3.1. Different batches for the preparation of nanozirconia are given in Table 3.2.
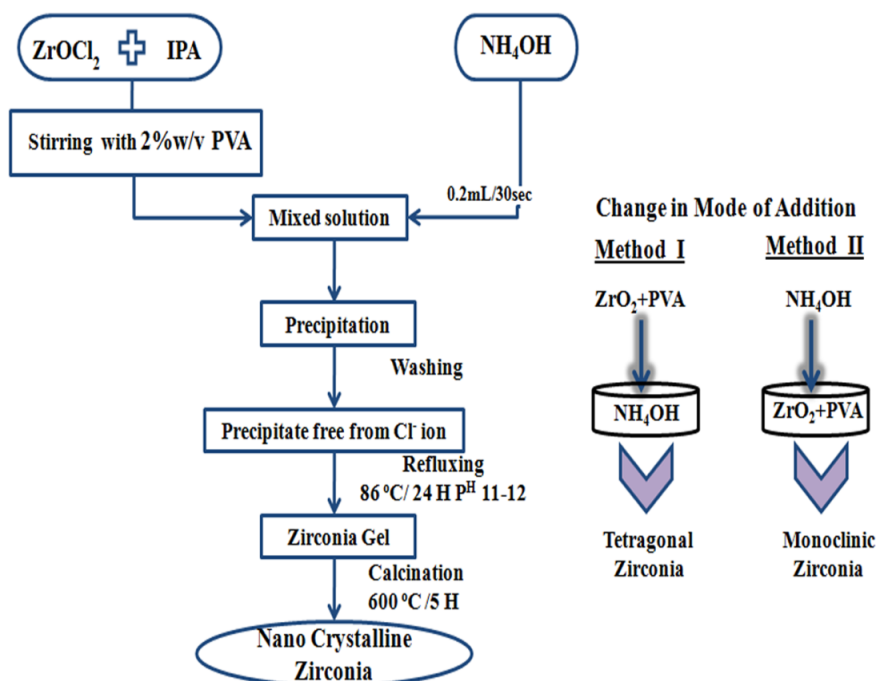
Figure 3.1 Schematic diagram for the preparation of nanozirconia

Table 3.2 Different batches for the preparation of nanozirconia
(The code used, NZRx-yDI ,'NZR'represents nanozirconia; 'x' stands for w/v% of PVA solution; 'y' stands for temperature of calcination,'D' for degree Celsius, I signify method I)

Sample name	w/v % of PVA	Calcination temperature
NZR0-600DI (by method I)	0	600 °C
NZR1-600DI (by method I)	1	600 °C
NZR2-600DI (by method I)	2	600 °C
NZR3-600DI (by method I)	3	600 °C
NZR5-600DI (by method I)	5	600 °C
NZR7-600DI (by method I)	7	600 °C
NZR2-400DI (by method I)	2	400 °C
NZR2-800DI (by method I)	2	800 °C
NZR2-600DII (by method II)	2	600 °C

3.3 Characterization of nanozirconia

The techniques used for the characterization of nanozirconia are discussed in Chapter 2.

3.4 Results and discussion

3.4.1 X-ray diffraction (XRD) studies

3.4.1.1 Influence of dispersion medium (PVA concentration) on XRD

The XRD patterns of the zirconia powders synthesized with 0, 1, 2, 3, 5 and 7% w/v aqueous solutions of PVA as mediums are shown in Figure 3.2. Only ZrO_2 peaks are observed in the XRD spectra. This indicates that all the powders are of high purity and results also suggest that the obtained product has high degree of crystallinity.
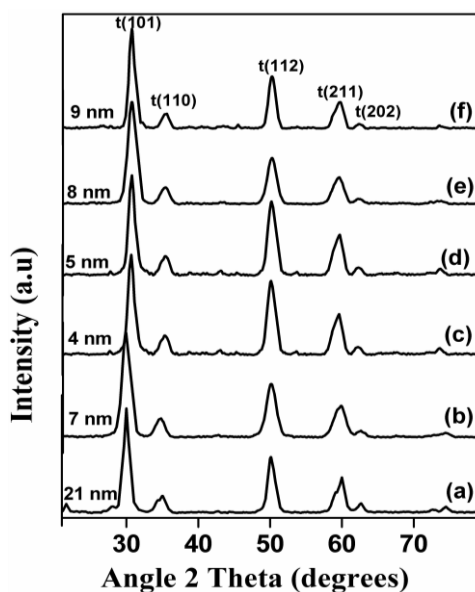
Figure 3.2 X-ray diffraction spectra of nanozirconia prepared in alcoholic (IPA) medium with different %w/v of PVA, by method I and all calcined at 600°C (a) NZR0-600DI, (b) NZR1-600DI, (c) NZR2-600DI, (d) NZR3-600DI, (e) NZR5-600DI, and (f) NZR7-600DI.

The relatively broad peaks are attributed to the very small crystallite size of the material. The XRD studies show that the major constituent phase in all the samples displays the typical tetragonal structure of ZrO_2. XRD discloses that as the PVA concentration increases there is not much decrease in the intensity and crystallinity of the peaks as indicated by the shortening and broadening of peaks. The average crystallites size of t-ZrO_2 in the presence of polymeric surfactant PVA as determined from the XRD pattern are presented in the figure 3.2. Much reduced size (~4 nm) was obtained for the t-ZrO_2 nanomaterial (NZR2-600DI) by 2% w/v aqueous PVA assisted sol-gel method of Zr^{2+} and OH^-.

Moreover all the powders prepared in the presence of PVA show smaller grain size than the ZrO_2 prepared without PVA indicating that the presence of PVA has a dispersive and protective effect on the powders. During the reaction period when $ZrOCl_2$ concentration increases, more $ZrO(OH)_2$ gels form at once and they are surrounded by the macromolecular chains of PVA which make them individually dispersed, giving little or no chance for aggregation. Thus XRD assisted analysis reveals that 2%w/v PVA solution is an optimum medium for nano synthesis. This may be the concentration which gives efficient polymer coating on each mole of the reactant and every single Zr^{2+} ion coated in PVA reacts with a single OH^- leading to reduced agglomeration of powders formed. Another factor aiding size reduction may be ethanol washing instead of water washing for the ZrO_2 hydrogel. Since Wang *et al.* [26] reported that rigid agglomerates are elevated by ethanol washing than water washing. They also reported that the gelation reaction carried out in water formed hard agglomerates during drying and calcination processes. Furthermore since PVA, is a

macromolecular chain having large number of OH groups provides suitable medium for the gelation. Thus the bottom line of the modified processes is that the crystallite size of t-ZrO$_2$ can be reduced to less than 10 nm in all the cases**.**

3.4.1.2 Influence of mode of addition in the sol-gel process
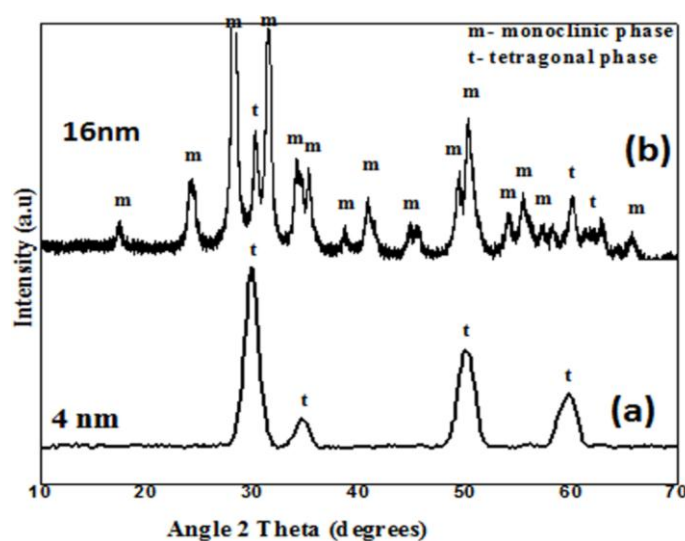
Figure 3.3 XRD pattern of nanoZrO$_2$ synthesized with 2%w/v PVA by (a) method I, NZR2-600DI and (b) method II, NZR2-600DII

However it can be observed that the mode of addition is critically important to get highly stabilized t-ZrO$_2$, because the reverse mode of addition (in Method II) of the sol-gel synthesis results in a mixture of monoclinic and tetragonal polymorphs of ZrO$_2$, with more monoclinic phase (m-ZrO$_2$) [powder XRD of the calcined sample shown in Figure 3.3] Broad nature of the peaks indicates nano crystalline nature of the sample and the crystallites size calculated as (~16 nm). Thus the synthesizing medium is very critical, to get whether the phase of ZrO$_2$ is tetragonal or

monoclinic. The reaction conducted in highly basic medium provides the t-ZrO_2 which further stabilizes the phase also [36]. The average particle sizes calculated by Debye–Scherrer equation are summarized in Table 3.3.

3.4.1.3 Influence of calcination temperature on XRD
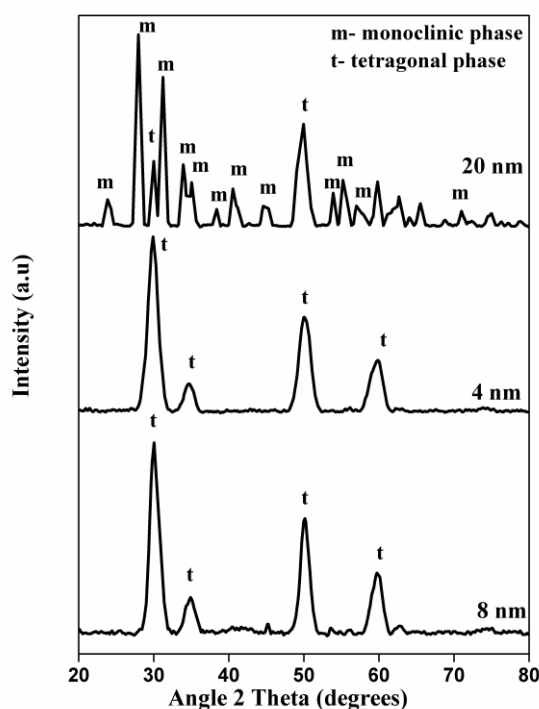
Figure 3.4 XRD spectra of nanoZrO$_2$ synthesized in IPA medium with 2%PVA solution calcined at different temperatures (a) at 400°C, NZR3-400DI (b) at 600°C, NZR3-600DI and (c) at 800°C, NZR7-800DI

The influence of calcination temperature on the particle size was analyzed using XRD-spectra of nanoZrO$_2$ synthesized in 2%w/v PVA solution at different calcination temperatures viz.400 °C, 600 °C and 800 °C for 5 h (Figure 3.4). Only ZrO$_2$ peaks are observed in the XRD spectra of all samples except for a calcination temperature of 400 °C. This

indicates that all other powders are of high purity and also only crystalline zirconia peaks are observed. The intensity and width of diffraction peaks differ between samples calcined at different temperatures. The spectra reveals that as the calcination temperature increases the crystallinity of the sample increases and grain size increases, whereas at 600 °C the grain size falls into 4 nm range as calculated using the Scherrer formula from broadening of XRD for {101}peak. At 400 °C the grain size is small as indicated by the broadening and shortening of peaks. Appearance of the impurity peaks in nanoZrO$_2$ synthesized in 2%w/v PVA solution calcined at 400 °C clearly indicates that complete removal of all the carbonaceous species from the polymeric surfactant PVA, is not possible at this temperature, and hence is not sufficient for post synthesis treatment. Calcination at 800 °C results in monoclinic than pure tetragonal phase for ZrO$_2$. Powder calcined at 600 °C yields small grain size with high purity. It is the optimum temperature that ensures complete removal of PVA template and other impurities from the nanoZrO$_2$ and the peaks in the spectra indicate the formation of controlled monodispersed t-ZrO$_2$ powder at this temperature. It is well recorded in literature that tetragonal phase of ZrO$_2$ is unstable at lower temperatures and can only be stabilized at lower temperatures by using additives such as Y$_2$O$_3$, MgO and CaO. Since none of these additives were used, it is inferred that the small size of the particles is responsible for the stabilization of the tetragonal phase, as explained in literature [37, 38].

Zirconia nanomaterial from NZR2-600DI is named as t- ZrO$_2$ and NZR2-600DII as m-ZrO$_2$ hereafter.

Table 3.3 Average particle size of zirconia nanomaterials

Sample name	Average particle size (nm)
NZR0-600DI	21
NZR1-600DI	7
NZR2-600DI (t-ZrO$_2$)	4
NZR3-600DI	5
NZR5-600DI	8
NZR7-600DI	9
NZR2-400DI	8
NZR2-800DI	20
NZR2-600DII (m-ZrO$_2$)	16

3.4.2 Particle size distribution and Zeta potential
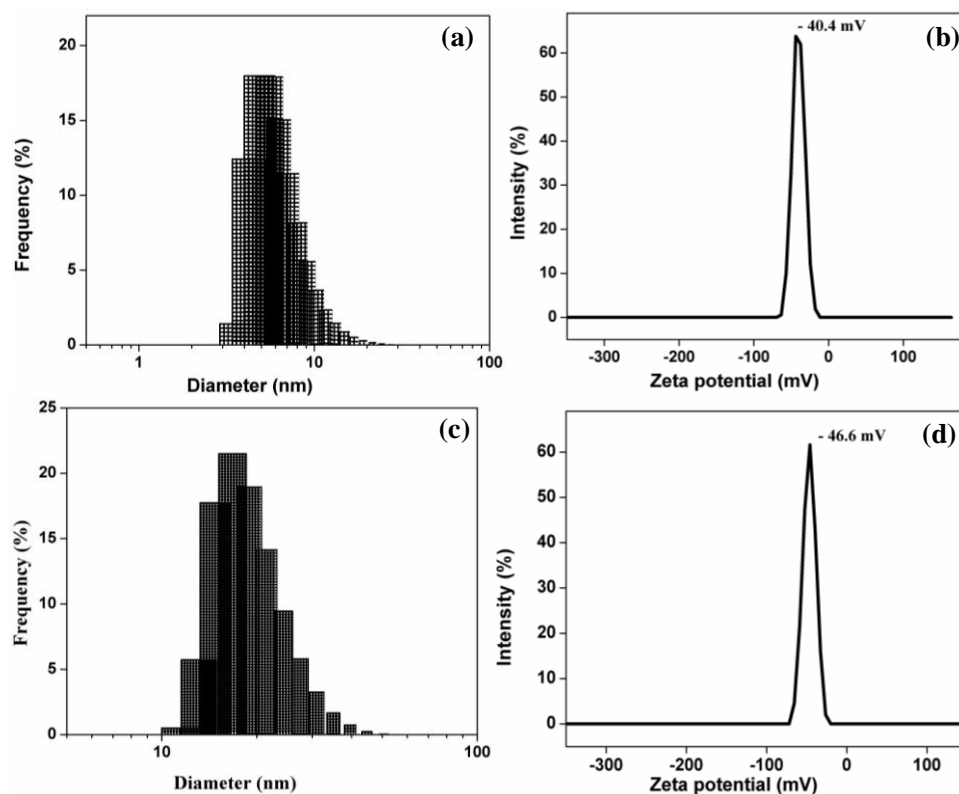
Figure 3.5 (a) particle size distribution of t-ZrO$_2$ synthesized by Method I (optimized condition), (b) Zeta potential of t-ZrO$_2$ measured at neutral pH, (c) Particle size distribution of m-ZrO$_2$ by Method II (optimized condition), and (b) Zeta potential of m-ZrO$_2$ measured at neutral pH.

The particle size distribution of zirconia nanoparticles was analysed by dynamic light scattering (DLS) and is shown in Figure 3.5. The synthesized t-ZrO_2 nanoparticles have a normal size distribution [Figure 3.5 (a)] with an average diameter of 6 nm, while m-ZrO_2 particle shows the expected size distribution [Figure 3.5 (c)] pattern in which most of the particles have particle size less than 18 nm. Additionally the zeta potential of both t-ZrO_2 and m-ZrO_2 were determined at neutral pH and was found to be -40.4 mV and -46.6 mV respectively [Figure 3.5 (b) for t-ZrO_2 and (d) m-ZrO_2]. From the DLS analysis the average particle size calculated was found comparable with size calculated from XRD and TEM (~5 nm for t- ZrO_2 and ~15 nm for m- ZrO_2). The high Zeta potential value at neutral pH indicates better dispersibility of powders.

3.4.3 Scanning electron microscopy (SEM)
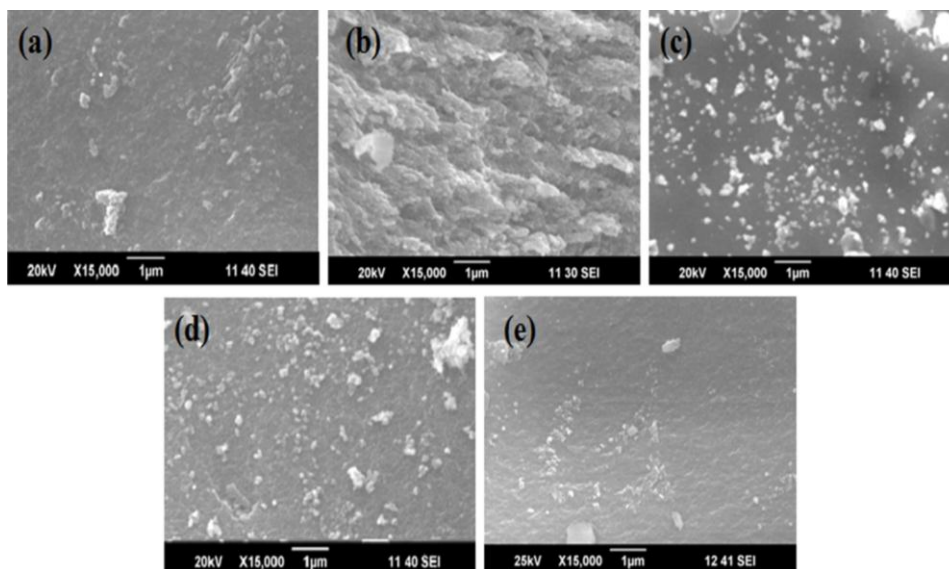
Figure 3.6 SEM photographs of monodispersed porous ZrO_2 nanomaterial synthesized in IPA medium with (a) NZR0-600DI (b) NZR2-400DI, (c) NZR2-600DI, (d) NZR2-800DI and (e) NZR2-600DII

Figure 3.6 shows SEM images of the synthesized ZrO_2 with and without the presence of PVA. Morphological investigation using SEM photograph of these sample shows that all nanopowders are spheroid except that of the reaction without PVA assisted medium. Figure 3.6 (a) shows the synthesized zirconia without the presence of PVA by method I calcined at 600 °C has a flaky structure with high degree of conglomeration and microstructures. The dependence of structure on temperature of calcination is clear from SEM photographs of nanoZrO_2 prepared in 2%w/v PVA calcined at 3 different temperatures. Figure 3.6 (b), (c) and (d) represent the SEM micrographs of zirconia synthesized with 2% w/v aqueous PVA solution calcined at 400 °C, 600 °C and 800 °C respectively. The nanopowder obtained after calcinations at 600 °C [Figure 3.6(c)] has a spherical morphology with uniformly arranged particles of almost similar shape and size. Thus the nanostructures of the synthesized powders have a uniform pattern in the presence of PVA, which leads directly to the formation of monodispersed porous nanopowders. At a lower calcination temperature at 400 °C the crystals had smaller size as it is clear from Figure 3.6(b). As the calcination temperature increased from 600 °C to 800 °C, structure collapses leading to agglomeration is clearly depicted in Figure 3.6(d). Hence it can be concluded that up to a calcination temperature of 600 °C, the spheroid monodispersed structure is stable and after there is a drastic change in the texture due to agglomeration. This agglomeration of nanopowders is due to structure collapse at higher temperature owing to the rapid removal of PVA from the surface. From the SEM micrograph shown in Figure 3.6(e), the nanozirconia obtained through method II with 2% w/v aqueous PVA solution calcined at 600°C, any information

regarding the morphology, size and distribution of particles, is not got since we observed highly agglomerated micrographs.

3.4.4 Elemental analysis (EDS)
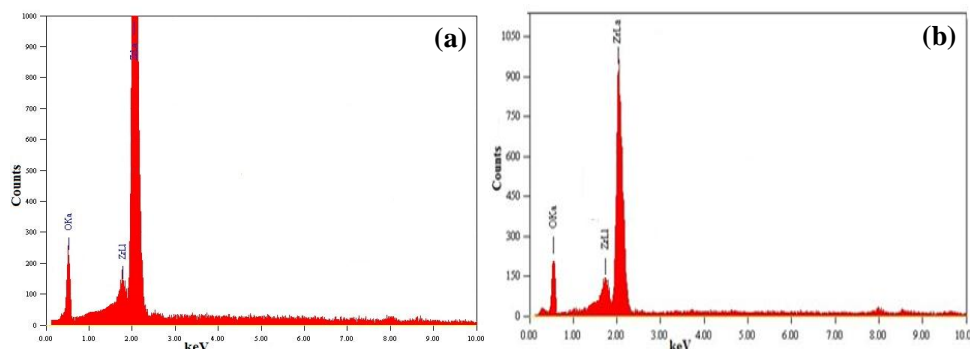
Figure 3.7 EDS spectra of ZrO$_2$ nanomaterial (a) NZR2-600DI (b) NZR2-600DII

The related EDS analysis spectrum of samples prepared in 2% w/v aqueous PVA solution via method I and II calcined at 600 °C is shown in Figure 3.7 (a) and (b). The EDS spectrum contains only peaks for Zirconium (Zr) and Oxygen (O), the absence of Carbon(C) peaks indicate the complete removal of coated PVA from nanopowders during calcination. This is indicative of the purity of the material from both the method of preparation. Thus it can be deduced that pure ZrO$_2$ is formed during the synthesis.

3.4.5 Transmission electron microscopy (TEM) analysis

The TEM images of t-ZrO$_2$ (NZR2-600DI) [Figure 3.8 (a) and (b)] confirm the formation of spherical nanoparticles with uniform size and shape. The particle size obtained from TEM was 5nm which is in good agreement with the XRD result. The uniformly distributed small pores in the particle, evidenced the porous nature of sample, and the pores appear brighter than the surroundings because they have absorbed less electrons [39].
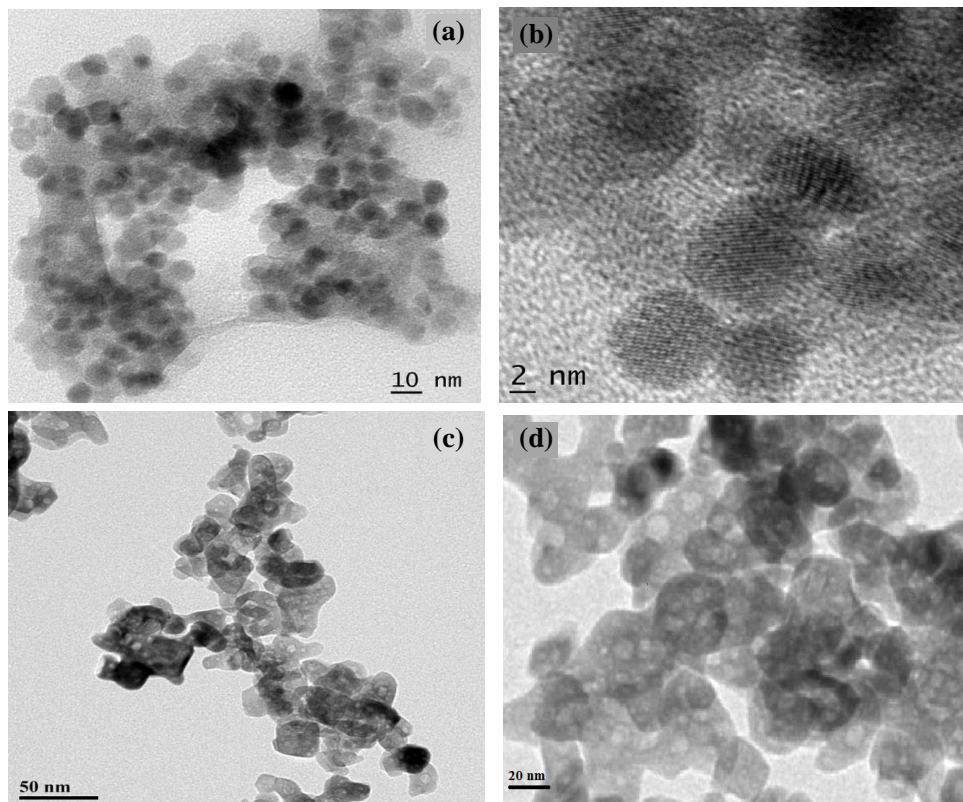
Figure 3.8 (a) and (b) TEM photographs of NZR2-600DI (t-ZrO$_2$)
(c) and (d) TEM photographs of NZR2-600DII (m-ZrO$_2$).

While the TEM micrograph [Figure 3.8 (c) & (d)] of the m-ZrO$_2$ (NZR2-600DII, mostly monoclinic phase by XRD results) indicates that nano crystalline zirconia has spheroid morphology and the result also pointed out that the synthesized nanozirconia is slightly agglomerated and the particles are somewhat uniform in size and shape. The average particle size of nanocrystalline m-ZrO$_2$ as determined by TEM measurement [Figure 3.8(c)] is found to be in the range of 10-15 nm which is in agreement with the results obtained from XRD. From the TEM images at high resolution [Figure 3.8(b) and (d)] it is clear that nanozirconia as we obtained

through both the methods are highly porous in nature and can clearly observe the pores from the TEM images.

3.4.6 Fourier transform infrared resonance (FTIR) studies
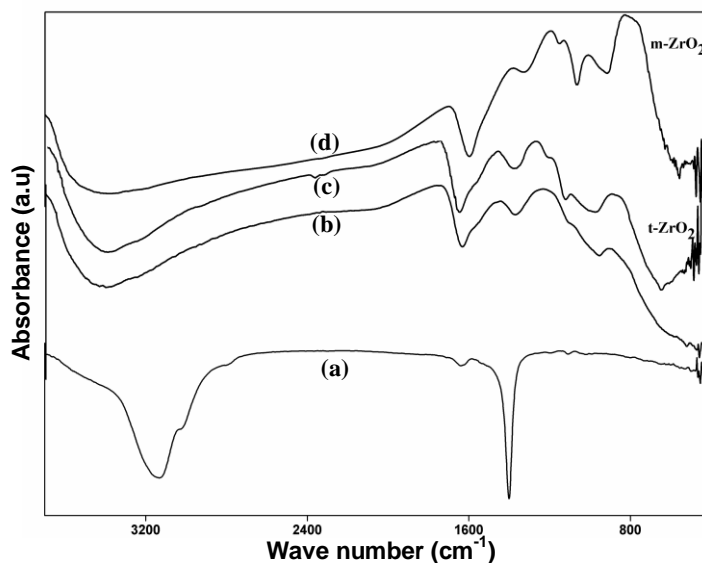
Figure 3.9 FTIR-spectra of ZrO$_2$ prepared via method I with 2% w/v PVA (a) dried at 80 °C and (b) NZR2-400DI (c) NZR2-600DI (t-ZrO$_2$) and (d) NZR2-600DII (m-ZrO$_2$).

The FTIR spectrum of the sample prepared via method I with 2%w/v PVA dried at 80°C is shown in Figure 3.9(a) and that calcined at 400 °C for 5 h is shown in Figure 3.9(b). Figure 3.9(c) and (d) represent the FTIR spectra of ZrO$_2$ prepared using method I and II prepared in 2% w/v PVA solution calcined for 5 h at 600 °C. The weak absorption bands in Figure 3.9 (a) at 3000, 2798 cm^{-1} are due to stretching vibrations of methyl (υ_{CH2}) groups from PVA which disappeared as calcination temperature increased indicating that PVA is removed from nano t-ZrO$_2$ powders at 400 °C itself [Figure 3.9(b)]. The infrared spectrum of synthesized t-ZrO$_2$ and m-ZrO$_2$ is

shown in Figure 3.9(c) and (d) show a broad absorption peak in the range 3,300–3,000 cm^{-1}, which is due to the sum of the contributions of hydroxyl groups and water molecules. Absorption peak at 1,630 cm^{-1} is due to the bending mode of OH$^-$ group attached to the matrix. The bands at 1,100 cm^{-1}, 1370 cm-1 are attributed to Zr–O–Zr bond. Figure 3.8(d) shows the FT-IR spectrum of calcined sample at 600 °C from method II, where absorption peak at 745 cm^{-1} is typical of monoclinic zirconia [40]. The unique peaks correspond to Zr-O bonds around 470-520 cm^{-1} and broad band at 520 cm^{-1} exhibits t-ZrO$_2$ phase [41]. All the above facts indicate that during the reaction, Zr^{2+} ions are encapsulated in PVA; the state at which the reactive chloride ions meet their counter ion in a dilute isolated state leading to reduced agglomeration. And the powders formed will be surrounded by PVA as indicated in IR spectra [Figure 3.9 (a)] which can be removed in the final stage by calcination as shown in Figure 3.9(c) and (d).

3.4.7 Surface area and Pore structure analysis
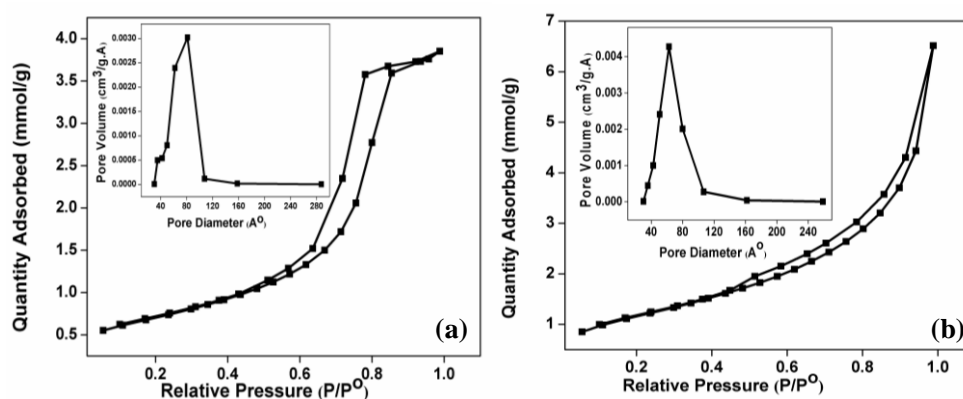
Figure 3.10 Nitrogen adsorption-desorption (BET) isotherm of (a) t-ZrO$_2$ obtained via Method I and (b) m-ZrO$_2$ from Method II; Inset shows the corresponding pore volume distribution curve.

Figure 3.10 (a) and (b) demonstrate typical nitrogen adsorption–desorption isotherm of t-ZrO_2 and m-ZrO_2 respectively. The inset shows their pore size distribution curves. In the nitrogen adsorption isotherm, both figures illustrate that the desorption branch does not follow the adsorption branch, but gives a distinct hysteresis loop, where the amount adsorbed is greater along the desorption branch compared to the adsorption branch. The isotherm belonged to the type IV category according to the International Union of Pure and Applied Chemistry (IUPAC) classification of different types of hysteresis loops. The type IV isotherm profile is generally associated with mesoporous adsorbents [42]. Figure 3.10 also reveals that the type IV isotherm consists of a narrow H1 hysteresis loop which confirms the narrow and uniform pore distribution in the sample. The Brunauer–Emmett–Teller (BET) surface area calculated from the nitrogen adsorption–desorption analysis for t-ZrO_2 is 56 m²/g with a pore volume of 0.1336 cc/g and pore diameter around 8.5 nm. Whereas m-ZrO_2 having BET surface area of 73.5 m²/g with a pore volume of 0.1661 cc/g and a pore diameter around 8 nm.

The measured specific surface areas are converted to equivalent primary particle size as, $D_{BET} = 6000/S_{BET} \times \rho$ [43]; D_{BET} is the particle size in nm, S_{BET} BET surface area and ρ the theoretical density in g/cc and the results are ~ 14.5 nm for m-ZrO_2 and 19nm for t-ZrO_2 which directly reflects trend with surface area. The values are contradictory to all other size calculation modes .This is because from BET we are calculating surface area by nitrogen adsorption after degassing at a low temperature. This process may sometimes leave certain internal mesoporous zones (as seen in TEM) closed, hiding those surfaces to be active so size calculation is erroneous for comparative studies with other sophisticated analyses.

3.4.8 Thermogravimetric analysis (TGA)
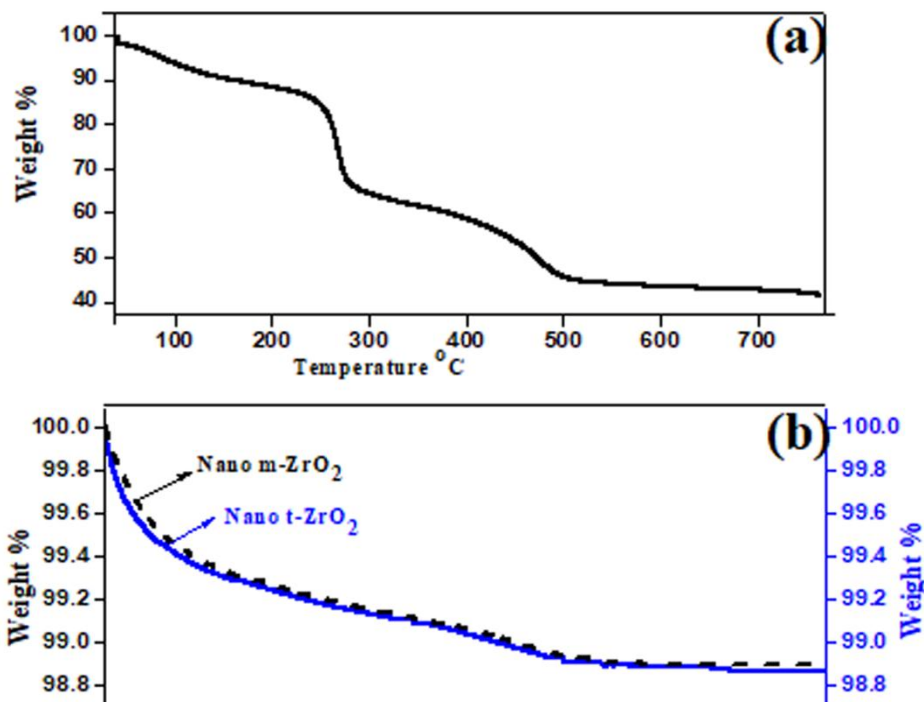
Figure 3.11 TGA patterns of monodispersed porous nanozirconia synthesized in alcoholic medium with 2% w/v PVA by Method I (a) dried at 80 °C, (b) calcined at 600 °C for 5h nano t-ZrO₂ (solid line), and by Method II calcined at 600 °C 5h, nano m-ZrO₂ (dotted line).

Thermo gravimetric analysis of the dried and calcined samples prepared via method I with 2% w/v PVA solution was carried out in the temperature range from 40 °C to 800 °C. The thermal behavior of these powders is shown in Figure 3.11. Figure 3.11 (a) gives the TGA patterns of the powder dried at 80 °C synthesized in 2% w/v PVA solution by method I and in (b) the solid line indicates that of nano t-ZrO_2 synthesized with 2% w/v PVA calcined at 600 °C. It can be seen from the thermogram (a) that at a temperature of 100–180 °C; the material shows a loss of its

initial weight. This weight loss is due to the removal of physically adsorbed water. After that weight loss prolongs up to 550 °C mainly due to the removal of organic moieties of PVA. On increasing the temperature from 400 to 600°C the weight loss of ~0.50% accounts for the removal of coordinated organic groups. Moreover on further increasing the temperature from 600°C, the weight loss is negligible. But since such a high temperature may lead to structure collapse and also from the XRD analysis, it can be inferred that the tetragonal phase is stable up to 600 °C and 800 °C calcined samples shows monoclinic phase to the material, a minimum calcination temperature of 600 °C is accepted in practice for the complete removal of impurities with consistent nanostructure. In Figure 3.11 (b) the solid line represents nano t-ZrO$_2$ and dotted line for nano m-ZrO$_2$ respectively, both the thermograms show the similar trend and observe a weight loss up to 200 °C and after that they do not show further reduction in weight. The loss of weight is due to the removal of physically adsorbed moisture present in the materials as it is clear from the FT-IR analysis which shows the presence of absorption bands of OH group. Furthermore on increasing the temperature from 200 °C, the weight loss is insignificant which prolong up to 600 °C, indicates that the both the nanomaterials are purer and all the impurities and the organic moieties present can be removed during the calcination process.

3.4 Conclusions

Pure tetragonal monodispersed zirconia powder having spherical morphology and mesoporous structure can be obtained by an optimization of the surfactant assisted sol-gel route. The particle size and morphology of

the synthesized nanoparticles were characterized using XRD, SEM as well as TEM. The study shows that 2%w/v aqueous PVA solution is an optimum medium for the synthesis. Further, ZrO_2 particles formed are also encapsulated with PVA which prevents agglomeration. PVA assists the formation of nanoparticles with smaller grain size and excess PVA can be removed at the final stage by calcination. The calcined powders yielded small grain size with high purity monodispersed tetragonal phase as indicated by the zirconia structure in XRD spectra and elemental composition in EDS analysis. The purity of the nanomaterial is confirmed from XRD, FTIR and TGA analysis. The stabilization of the tetragonal phase in the prepared sample is most likely due to the low surface energy of the tetragonal phase relative to the monoclinic phase. The small size of the particles is also responsible for the stabilization of the tetragonal phase. XRD studies as well revealed that while increasing the calcination temperature from 600 °C to 800 °C the crystallite phase changes. The results also concluded that the mode of addition is also an important factor to get highly stabilized tetragonal zirconia with spherical morphology, reverse order results in monoclinic zirconia with spheroid structure. The particle size of t-ZrO_2 is 4 nm and that for t-ZrO_2 is 16 nm from TEM, both are in good agreement with XRD results.

References

[1]   Chen H, Zhang Y, Ding C. Wear. 2002; 253:885-93.

[2]   Wang Q, Xue Q, Shen W, Zhang J. J. Appl. Polym. Sci. 1998; 69: 135-41.

[3]   Izumi K, Murakami M, Deguchi T, Morita A, Tohge N, Minami T. J. Amer. Ceram. Soc. 1989; 72:1465-8.

[4]   Afanas' ev VV, Houssa M, Stesmans A, Heyns MM. Appl. Phys. Lett. 2001; 78:3073-5.

[5]   Wilk GD, Wallace RM, Anthony JM. Appl. Phys. 2001; 89:5243-5275.

[6]   Bardal A, Zwerger M, Eibl O, Wecker J, Matthee T. Appl. Phys. Lett. 1992; 61:1243-5.

[7]   Phillips JM. J. Appl. Phys. 1996; 79:1829-48.

[8]   Yamaguchi T. Catal. Today. 1994; 20:199-217.

[9]   Arata K. Adv.Catal. 1990; 37:165-211.

[10]   Arata K, Hino M. Mater.Chem. Phys. 1990; 26:213-37.

[11]   Plashnitsa VV, Elumalai P, Fujio Y, Miura N. Electrochim.Acta 2009; 54: 6099-106.

[12]   Mori M, Abe T, Itoh H, Yamamoto O, Takeda Y, Kawahara T. Solid State Ionics. 1994; 74:157-64.

[13]   Chakravarty R, Shukla R, Tyagi AK, Dash A, Venkatesh M. Appl.Radia. Isotopes. 2010; 68:229-38.

[14]   Chakravarty R, Shukla R, Ram R, Tyagi AK, Dash A, Venkatesh M. Nucl. Med. Biol. 2011; 38:575-83.

[15]   Chakravarty R, Shukla R, Ram R, Tyagi AK, Dash A, Venkatesh M. Chromatographia. 2010; 72:875-84.

[16]   Chraska T, King AH, Berndt CC. Mater. Sci. Eng. A. 2000; 286:169-78.

[17]   Luo TY, Liang TX, Li CS. Mater. Sci. Eng.A. 2004; 366:206-9.

[18]   Centi G, Cerrato G, D'Angelo S, Finardi U, Giamello E, Morterra C, Perathoner S. Catal. Today. 1996; 27:265-70.

[19]   Clearfield A. J. Mater. Res. 1990; 161-2.

[20]   Chandradass J, Han KS, Bae DS. J. Mater. Proc. Technol. 2008; 206:315-21.

[21]   Sarkar D, Mohapatra D, Ray S, Bhattacharyya S, Adak S, Mitra N. Ceram. Int. 2007; 33:1275-82.

[22] Vasylkiv OO, Sakka Y, Skorokhod VV. Powder Metall. Met. Ceram. 2005; 44:228-39.

[23] Lin JD, Duh JG. J. Amer. Ceram. Soc. 1997; 80:92-8.

[24] Štefanić G, Musić S, Popović S, Sekulić A. J. Mole.Struc. 1997; 408:3 91-4.

[25] Roy S. J.Sol-Gel Sci. Technol. 2007; 44:227-33.

[26] Wang S, Li X, Zhai Y, Wang K. Powder Technol. 2006; 168:53-8.

[27] Wang JA, Valenzuela MA, Salmones J, Vázquez A, Garcıa-Ruiz A, Bokhimi X. Catal. Today. 2001; 68:21-30.

[28] Aguilar DH, Torres-Gonzalez LC, Torres-Martinez LM, Lopez T, Quintana P. J. Solid State Chem. 2001; 158:349-57.

[29] Srdić VV, Winterer M, Hahn H. J. Amer. Ceram. Soc. 2000; 83:729-36.

[30] Ma T, Huang Y, Yang J, He J, Zhao L. Mater. Des. 2004; 25:515-9.

[31] Jun-Seop KI, Dong-Hae LE, Sung KA, Dong-Sik BA, Hoy-Yul PA, Moon-Kyeung NA. Trans.Nonferrous Met. Soc. China. 2009; 19: 88-91.

[32] Vasylkiv O, Sakka Y. J. Amer. Ceram. Soc. 2001; 84:2489-94.

[33] Zheng JY, Pang JB, Qiu KY, Wei Y. Microporous Mesoporous Mater. 2001;49:189–195.

[34] Blin JL, Flamant RK, Su BL. Int. J.Inorg. Mater. 2001; 3:959-72.

[35] Shukla S, Seal S, Vij R, Bandyopadhyay S. J. Nanoparticle Res. 2002; 4: 553-9.

[36] Yin SF, Xu BQ. Chem. Phys. Chem. 2003; 4:277-81.

[37] Garvie RC. J.Phy. Chem. 1978; 82:218-24.

[38] Oleinikov NN, Pentin IV, Murav'eva GP, Ketsko VA. Zh. Neorg. Khim. 2001; 46:1413-20.

[39] Bala H, Fu W, Zhao J, Ding X, Jiang Y, Yu K, Wang Z. Colloids Surf. A. Physicochem. Eng. Asp. 2005; 252:129-34.

[40] Mondal A, Ram S. Ceram. Int. 2004; 30:239-49.

[41] WongMS, Huang HC, Ying JY. Chem. Mater. 2002; 14:1961-73.

[42] Sing KSW, Everett DH, Haul RAW, Moscou L, Pierotti RA, Rouquerol J,Siemieniewska T. Pure Appl. Chem. 1985; 57:603-619.

[43] Rezaei M, Alavi SM, Sahebdelfar S, Yan ZF. Powder Technol. 2006; 168: 59-63.

.....ജ്ഞ.....

ISOLATION AND CHARACTERIZATION OF FIBRILLAR NANOSILICA OF NATURAL ORIGIN: INDIAN GRASS, CORTADERIA SELLOANA FLOWERS AND BAMBOO AS THE SILICA SOURCES

The increase in the use of silica based nanocomposites has led to the search for new sources of silica. Silica has long been known to be present in plants. It is stored primarily as opaline phytoliths in the epidermis of plant tissue. In this study a novel green chemical route is proposed for the isolation of silica nanofibers by exploiting the vast and abundant grass varieties. The three different grass varieties like Indian grass (Sorghastum nutans, CG), Pampass grass (Cortaderia selloana, PG), and Bamboo (BM) have been selected for the isolation of nanosilica. To attain high-purity silica from these sources, leaching in hydrochloric acid of three different normalities and running water were conducted followed by air combustion. Diversified morphology was seen in the isolated silica from different grass sources. Highly pure, uniformly distributed fibrous silica was obtained from the optimized acid concentration from Scanning electron microscopy and energy-dispersive X-ray spectroscopy studies. The chemical purity, crystallinity and morphology are confirmed by FTIR, XRD, and TEM analysis. Thermal stability of the fiber was studied by TGA analysis and surface area noted by Brunauer–Emmett–Teller analysis. HR-TEM analysis reveals that actual morphology of isolated silica is rich in nano fibrillar channel network for PGNS silica and fibrous morphology for silica from Indian grass and Bamboo. This cost effective environment friendly pathway opens a new vista for utilization of bio-precursors as nanosilica source.

4.1 Introduction

Nanotechnology has contributed to the creation of smart functional materials, devices and systems through manipulation of matter in the nanometer scale and exploitation of novel phenomena and properties which arise because of the nanometer size. Nanomaterials are cornerstones of nanoscience and nanotechnology. Recently, applications of nanosilica as other nanomaterials have gained great interest among the material researchers, and also in the field of food industry, catalysis, chromatography, coatings, stabilizers, emulsifiers and biological sciences [1-3].

An enormous quantity of nanosilica powder with controlled shape, size and porosity is required for large-scale engineering applications. The nanosilica powder is generally prepared by using vapour-phase reaction, sol–gel and thermo-decomposition methods. In most of the above mentioned methods, it is synthesized mainly using alkyl orthosilicates as raw materials, which enables easy size control, shape and purity of the material. However, they are not the best commercial sources of silica due to their high cost, flammability, difficulties in handling and storage. Moreover these methods are costly, energy intensive and involve toxicity exposure from silicon alkoxide precursors [4-6]. Therefore, their replacement with a comparatively less expensive and robust inorganic silica source is desired [7-11].

Sodium silicate (water-glass) compared to the more commonly used tetraethoxysilane (TEOS) or tetramethoxysilane (TMOS) could be a good source of silica for industrial, large-scale production of nanosilica powders. Moreover, by using a purely aqueous medium, the expensive and very often toxic solvent could be avoided. However, sodium silicate produced

by smelting quartz sand and sodium carbonate at $1300^{\circ}C$ requires a large amount of energy [12]. Energy obtained from fossil fuels may not be sustainable in the future. Therefore, in an effort towards minimizing the use of toxic chemicals and reduce the generation of hazardous waste, novel or enhanced synthetic techniques are constantly being sought. Hence due consideration should be given to revolutionize the ways in which nanosilica are created and the range and nature of raw materials that can be used. For the last few years, due to their easy availability, low cost and ecological concerns researchers have initiated a considerable interest in natural materials to produce 'green' products. The rapidly increasing environmental awareness, growing global waste problem, limited availability of crude oils and high processing cost trigger the development concepts of sustainability and reconsideration of renewable resources.

Silica is one of the macronutrient in plants. In general, living plants contain silicon in three basic forms (i) Insoluble amorphous silica (SiO_2) (more than 90%), (ii) Silicate ion (about 0.5% to 8%), and (iii) Colloidal silicic acid (about 0% to 3.3%) [13]. This amorphous silica is found in epidermal cells of the plants in dumb-bell shaped cells called opal phytolith or silica phytolith. Phytoliths exist in abundance in grasses, including rice, wild rice, maize and wheat. [14, 15]. Grass species and their water uptake also influence the silica content in plants. The uptake of more water results in more silica content in the plant, thus cool-season grasses (canary grass) that require more up take of water hence having large amount of silica content. Soil type and condition also has an influence on the concentration of silicon in the plant [13, 16]. Typically, grass inflorescence contains five times more and leaves contain three times more the silica content of stems [14, 15].

Several attempts have been made to produce bulk silica from the most eco-friendly and economical source rice husk [17-19]. In recent years attempts have been made to prepare nanosilica powder from rice husk ash [11, 20-25]. Teresa and Dickon (2007) [26] demonstrated conversion of an inexpensive Luk Bamboo into biomorphic composites containing high-purity cristobalite-SiO_2 and β-silicon carbide (SiC) nanowires at different temperatures. Silica had been successfully extracted from Stenotaphrum secundatum (St. Augustine) grass using an annelid-based biotransformation process [27]. Although extensive literature exists on the physical and chemical phenomena of silica produced from sodium silicate precipitated with acids and also from rice husk. To date no work has been reported on the direct production of nanosilica from those grass sources like Indian grass Pampas grass and bamboo by a simple chemical treatment.

Present study proposes a simple chemical process for the isolation of nanosilica from non-conventional raw materials like grass sources. Three different types of grasses namely Indian grass, Pampas grass and Bamboo are proposed to be selected. Among these Indian grass is abundant in our country and contains silica opal. Sorghastrum nutans (Indian grass) belongs to the species s. nutans, genus sorgastrum under Poaceae family and is a perennial bunch grass. A perennial bunch grass contains large amount of silica [13,16]. Along with Indian grass, Pampas grass also appears to be a promising material because of its abundance and adaptability to grow in a wide range of environments and climates. The botanical name for Pampas grass is Cortaderia selloana, which belongs to the species, c.selloana, and genus cortaderia under the same family as Indian grass and is a flowering plant native to South America and is also believed to have originated in

Pampas region after which it is named. The plant was introduced to other continents as an ornamental grass and to a lesser extent it provides food for grazing animals. The feathery flowers when it dried are widely used in flower arrangements and other ornamental displays; otherwise it has no economical usages. In India, Pampas grass is mainly located in the river banks of almost all states. As recognized, bamboo plants are native to East Asia but are now planted in all subtropical regions of the world. It is a perennial plant in the grass family Poaceae. The large availability of bamboo plants makes them an attractive biomass resource for activated carbons [28]. Luk Bamboo had been converted into biomorphic composites containing high-purity cristobalite-SiO_2 and β-silicon carbide (SiC) nanowires after sintering at 1200 °C and 1400 °C, respectively [29]. The utilization of the nanosilica from these grass sources in polymeric composites may open up a new way of disposing off a waste product into the bio originated source of the nanosilica. This also offers a non toxic method of generating the filler, suitable for the preparation of biocompatible polymer nanocomposites. A better understanding of chemical composition, morphology, physical and thermal properties of the nanofibers after isolation from those sources will be useful in developing new bio nanocomposites.

Thus the objective of this work is to prepare fibrous nanosilica from bio resources by reducing disposal and pollution problems without compromising the purity of the nanomaterials obtained. In most of the conventional methods, fibrous silica is prepared by using expensive chemicals and with the aid of surfactants [30] through tedious procedures. The proposed techniques of isolating silica from these biomass is acid treatment followed by water washing and calcination for controlling the product purity. Effect of

strength of hydrochloric acid (HCl) to produce high purity amorphous nanosilica powder is also proposed to be investigated and the conditions for getting high-purity fibrous nanosilica are proposed to be optimized. The nanosilica powder prepared, will be characterised using Scanning electron microscopy (SEM), Energy-dispersive X-ray spectroscopy (EDS), Fourier transform infrared spectroscopy (FTIR), X-ray diffraction (XRD), Transmission electron microscopy (TEM), BET surface area analyzer, and Thermo gravimetric analysis (TGA), to explore the structure, morphology, size, purity, stability and other properties.

4.2 Experimental

4.2.1 Materials

Indian grass [Figure 4.1(a)] collected from our campus (CUSAT), Pampas grass [Figure 4.1(b)] collected from the river bank of Bharathapuzha near Shornoor, Kerala. Bamboo [Figure 4.1(c)] was collected from Aluva locality plantation. Tip of Indian grass (CG), flowers of Pampas grass (FPG) and stem of Bamboo (BM) were used for the isolation of nanosilica fibers. They were thoroughly cleaned with tap water to remove adhering soil and dirt. HCl (37%) from Merck was used for leaching purpose.

(a) Indian grass, CG
Sorghastum nutans

(b) Pampas Grass, PG
Cortaderia selloana

(c) Bamboo, BM

Figure 4.1 (a) CG-Indian grass, (b) PG-Pampas grass and (c) BM-Bamboo

4.2.2 Methods

4.2.2.1 Isolation of nanosilica from CG, FPG and BM

(a)   Isolation of fibrous nanosilica from Indian grass

Tips of Indian grass (CG) [Figure 4.2(a)] were removed, washed with water and dried in an oven at 100 °C. It was calcined in a muffle furnace at 650 °C for 6 h followed by acid treatment. HCl solutions of different normality (0.01 N, 0.1 N and 1 N) were added to the previously washed and dried CG. The solutions were agitated using magnetic stirrer at 80°C for 3 h. A reddish color was developed for the solution during acid treatment indicating the removal of metallic ions as soluble colored complexes. The acid treatment was continued till the color disappeared, ensuring complete removal of all the metallic impurities. Then the reaction vessel was kept overnight in an oven at 60 °C. The treated CG was washed thoroughly with distilled water and dried overnight at 110 °C in an oven. The samples were then calcined in a muffle furnace at 650 °C for 6 h and ground to fine powder.

(b)   Isolation of fibrous nanosilica from Pampas grass

Flowers of pampas grass [FPG, Figure 4.2(b)] were washed thoroughly with water and dried in an oven at 100 °C. The experimental procedure was repeated as in the case of CG.

(c)   Isolation of fibrous nanosilica from Bamboo

Stems of Bamboo (BM) [Figure 4.2(c)] were cut into small pieces, washed and dried. The same experimental procedure was repeated as discussed above.
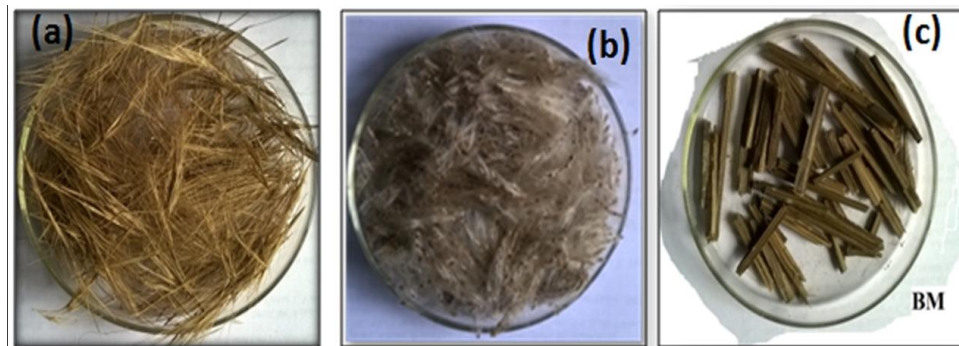
Figure 4.2 Dried grass sources (a) CG (b) FPG and (c) BM

4.2.3 Characterization

The detailed characterization techniques were discussed in Chapter 2.

4.3   Results and discussion

4.3.1 Elemental analysis by EDS spectra

(a)   Effect of HCl solution leaching and water rinsing conditions on removal of metallic impurities of CG

One of the main hurdles in obtaining high purity silica from any grass sources including rice husk by the direct incineration process is the presence of metallic substances or other impurities in the material. Pre-treatment can be carried out using either acidic solutions or basic ones. Pre-treatment with concentrated acidic materials can dissolve or leach the metallic impurities present in the materials and improve the concentration of silacious compounds. Several kinds of acids, both mineral and organic, have been reported to be used for pre-treatment of rice husk before other value addition processes such as incineration are carried out [31-36]. HCl is suggested as a better choice for acid treatment for the removal of metallic impurities; since it also provides higher

surface area and structure sustenance and so it is by far the most widely used method [17, 37-40]. HCl of three varied normalities was selected for pretreatment of our present grass sources.

The composition and morphology of the ash obtained from pre-treated CG after calcination were examined individually. All the different normalities of HCl treatments on CGs followed by calcination produced a white material which shows the purity of the sample from aforementioned materials on acid leaching.

Table 4.1 Composition of ash obtained after the calcination of HCl treated CG

Weight % of elements	Strength of HC1 used		
	1 N	**0.1 N**	**0.01 N**
Silicon (Si)	70.6	70.01	77.02
Oxygen (O)	29.4	29.99	22.78

Chemical composition of the acid pre-treated CG ash is given in Table 4.1 with amount of silicon and oxygen in mass percentage and the corresponding EDS spectrum shown in Figure 4.3. One of the main problems in obtaining high purity silica from biomass by the direct incineration process is the presence of metallic impurities in the grass sources itself. Here acid treatment with different normalities results in only silicon and oxygen as the elements, which shows that metallic impurities have been removed through acid leaching.
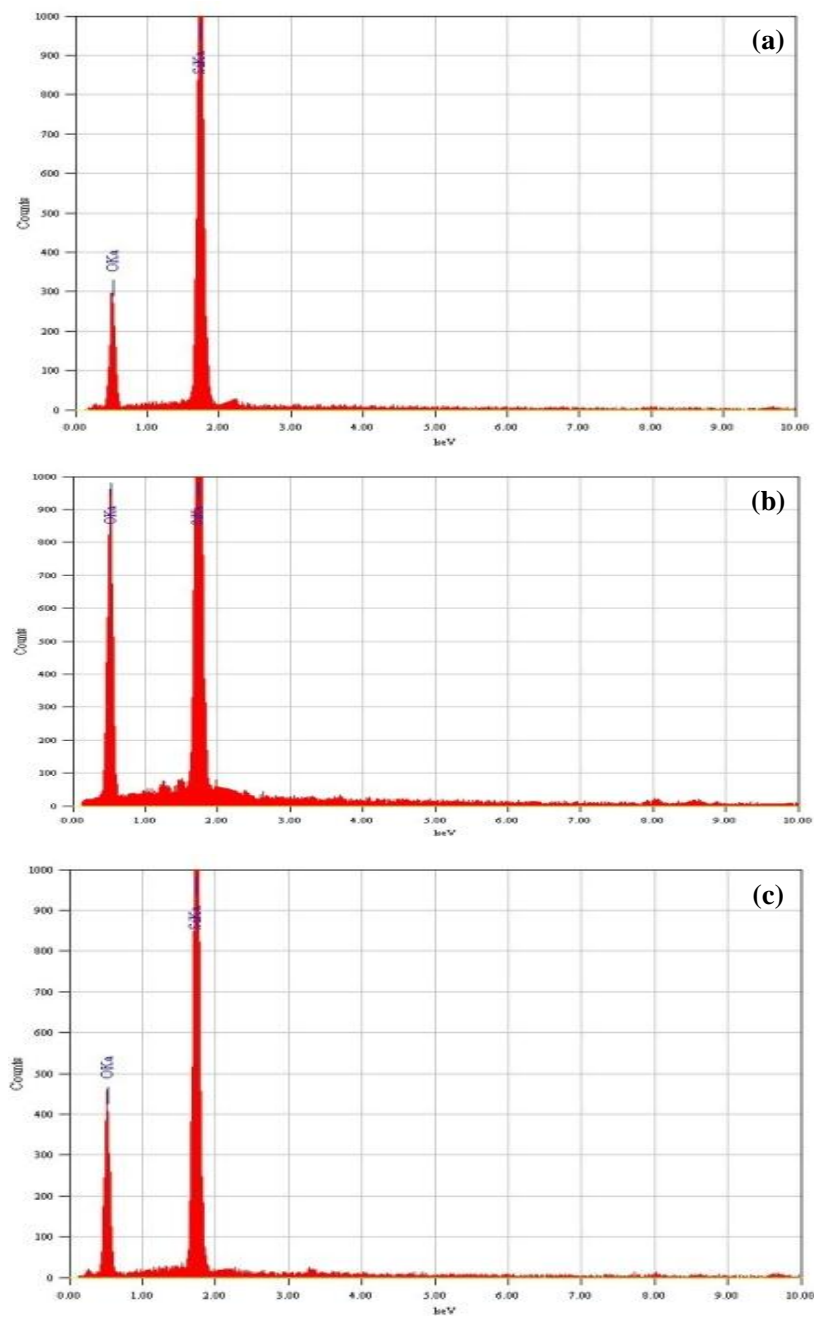
Figure 4.3 EDS spectrum of ash after calcination of (a) 1 N HCl treated CG (b) 0.1 N HCl treated CG and (c) 0.01 N HCl treated CG.

(b)   Effect of acid pre-treatment on FPG

The composition and morphology of the ash obtained from pre-treated FPG after calcination were examined individually; Chemical composition of the untreated FPG ash is displayed in Table 4.2 with amount of silicon, oxygen and metal impurities in mass percentage and the corresponding EDS spectrum was shown in Figure 4. 4.

Table 4.2 Composition of ash obtained after the calcination of pre-treated FPG

Weight % of elements	Strength of HC1 used		
	1 N	0.1 N	0.01 N
Silicon (Si)	49.9	49.12	42.43
Oxygen (O)	50.1	50.88	38.69
Potassium (K)	0.00	0.00	6.37
Calcium (Ca)	0.00	0.00	7.48
Magnesium (Mg)	0.00	0.00	5.02
Iron (Fe)	0.00	0.00	0.00
Manganese (Mn)	0.00	0.00	0.00
Chromium (Cr)	0.00	0.00	0.00

Even though 0.01 N HCl is effective in removing the most prominent metallic impurities, it cannot remove all other metallic impurities like K, Ca and Mg as evident from Table 4.2. The action of 0.1 N HCl removed all metallic impurities from FPG. This is confirmed from EDS analysis, and the elemental composition of the ashes which remains unchanged between the treated FPG's obtained after 0.1 N and 1 N HCl treatment.
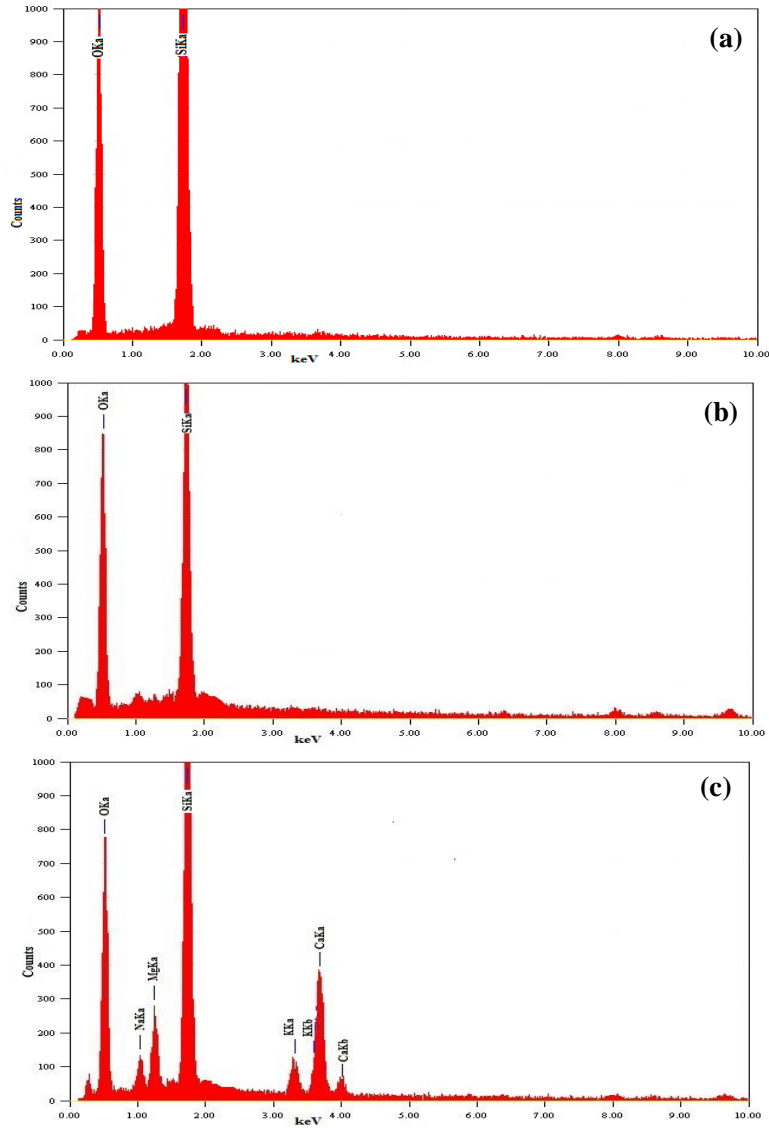
Figure 4.4 EDS spectrum of ash after calcination of (a) 1 N HCl treated FPG (b) 0.1 N HCl treated FPG and (c) 0.01 N HCl treated FPG.

 (c)   Effect of acid pre-treatment on BM

As in the above cases, acid treatment was carried out on BM and the elements with their mass % are displayed in Table 4.3 and the EDS spectrum is shown in Figure 4.5.

Table 4.3 Composition of ash obtained after the calcination of pre-treated BM

Weight % of elements	Strength of HC1 used		
	1 N	0.1 N	0.01 N
Silicon (Si)	70.6	68.99	42.58
Oxygen (O)	29.4	29.99	29.79
Potassium (K)	0.00	0.00	9.93
Calcium (Ca)	0.00	1.02	4.67
Magnesium (Mg)	0.00	0.00	3.14
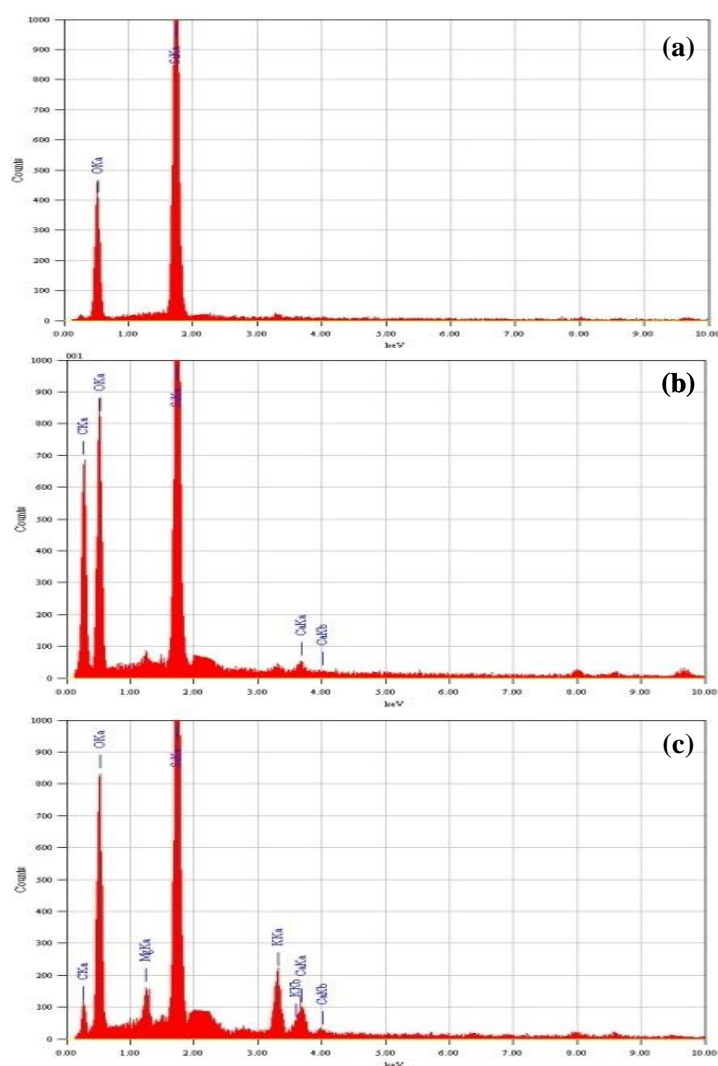
Figure 4.5   EDS spectrum of ash after calcination of (a) 1 N HCl treated BM (b) 0.1 N HCl treated BM and (c) 0.01 N HCl treated BM

From the elemental anaylysis it is clear that 1N HCl washing is enough to remove all the metallic impurities producing only silicon and oxygen.

4.3.2 SEM analysis

(a)   Effect of acid treatment on the morphology of CG ash

Figure 4.6   SEM photographs of the ashes from (a) and (b) 0.01 N HCl treated CG, (c) and (d) 0.1 N HCl treated CG and (e) 1 N HCl treated CG

The morphological analysis of acid treated CG after calcination was analysed through SEM and is displayed in Figure 4.6. 0.01N HCl treated CG ash shows [Figure 4.6(a) and (b)] the presence of nearly fibrillar structures. Bundles of fibers with micro meter size are shown in its higher magnification [Figure 4.6(b)] and the size of the fibrous bundle is as approximately 7μm. As the strength of acid increases to 0.1N [Figure 4.6 (c) and (d)] fibrous morphology remains the same as in the above case but more fiber breakage occurs due to the higher concentration of the acid. SEM studies also reveal a different morphology for 1 N HCl treated CG ash, since the acid concentration increases more and more fiber breakage takes place, resulting in hazy morphology. Hence from the SEM and EDS analysis it can be concluded that 0.01 N HCl pre-treatment is the optimum concentration for isolating fibrous, high purity silica from CG. The detailed characterization of the pure fibrous silica obtained after   0.01 N HCl treatment (CGS) was carried out, and is presented in detailed in the following portions.

The yield of silica obtained after 0.01 N HCl leaching followed by calcination is 13 g silica per 100 g CG. Here the choice of matrix is apt in the sense that the fibrillar nature of the biomass itself act as a template for getting fibrous morphology for the isolated silica through an undemanding route.

(b)   Effect of acid treatment on the morphology of FPG ash
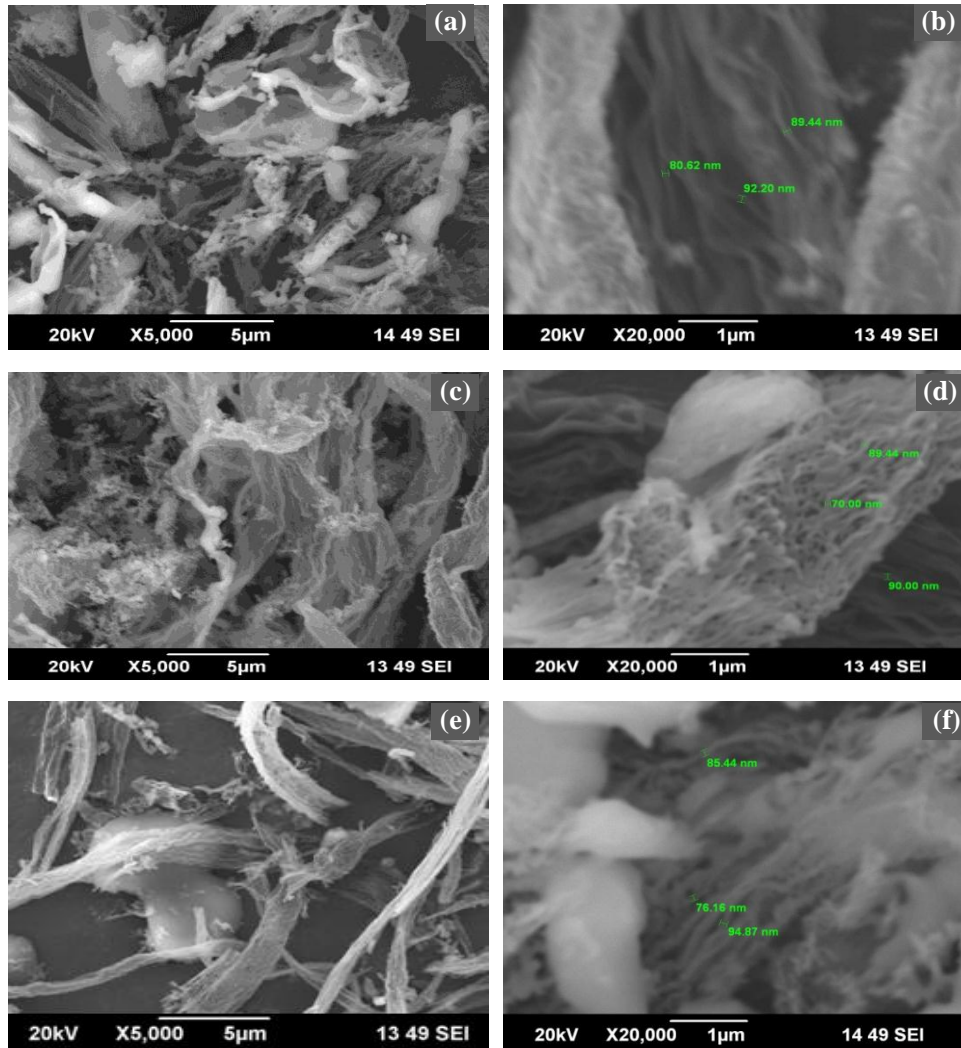
Figure 4.7 SEM photographs of the ashes from (a) and (b) 0.01 N HCl treated FPG, (c) and (d) 0.1 N HCl treated FPG and (e) and (f)1 N HCl treated FPG

SEM studies reveal a diverse morphology for the acid treated FPG ash than CG ash. 0.01 N HCl treated FPG gives fibrillar structure [Figure 4.7 (a)] with an individual fiber diameter less than 100 nm as it is clear in Figure 4.7(b). As the acid normality increases to 0.1 N, well defined puffy fibrous structure is observed even at lower magnification [Figure 4.7(c)]. The fibrous silica (PGNS) with less than 100 nm hair width could be extracted as vividly seen from Figure 4.7(d). On further increase of acid normality to 1 N [Figure 4.7(e) and (f)], the distinct fibrous structure is lost leading to stacked structure. The individual width can be hardly measured, though nominal fibers fall to the size range less than 100 nm. Moreover fiber breakage also occurs due to the deterioration of nano structure on increased strength of acid. Hence it is confirmed that 0.1 N HCl pre-treatment is the optimum concentration for isolating fibrous, high purity nano silica from FPG as seen from SEM analysis and EDS data. The detailed characterization of the pure fibrous nanosilica obtained after 0.1 N HCl treatment (PGNS) is carried out.

The yield of silica obtained after 0.1 N HCl leaching followed by calcination is found to be 6 g silica per 100 g flowers. Here also the choice of matrix is relevant in the sense that the biomass itself acts as a template for nano growth, since in most of the techniques used for the synthesis of fibrous nano silica either expensive chemicals are used or template assisted crystal growth is demanded [30].

(b)   Effect of acid treatment on the morphology of BM ash

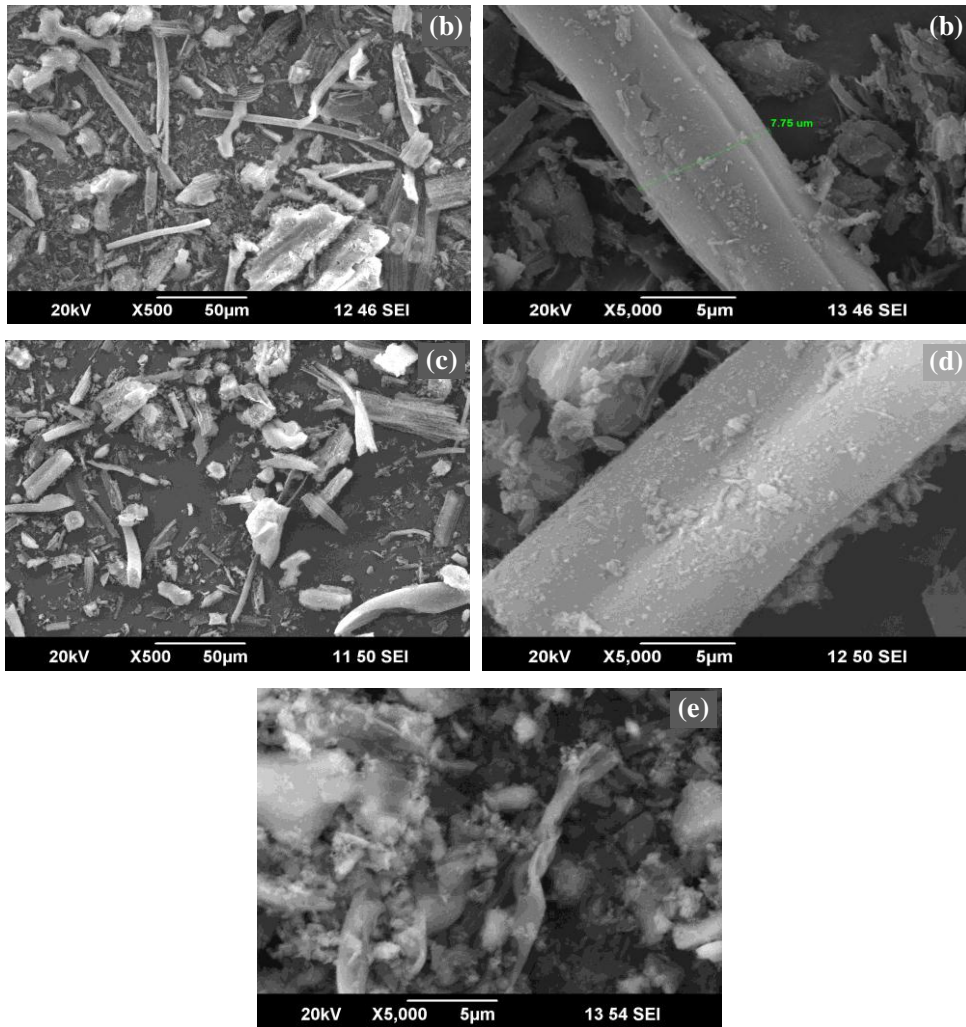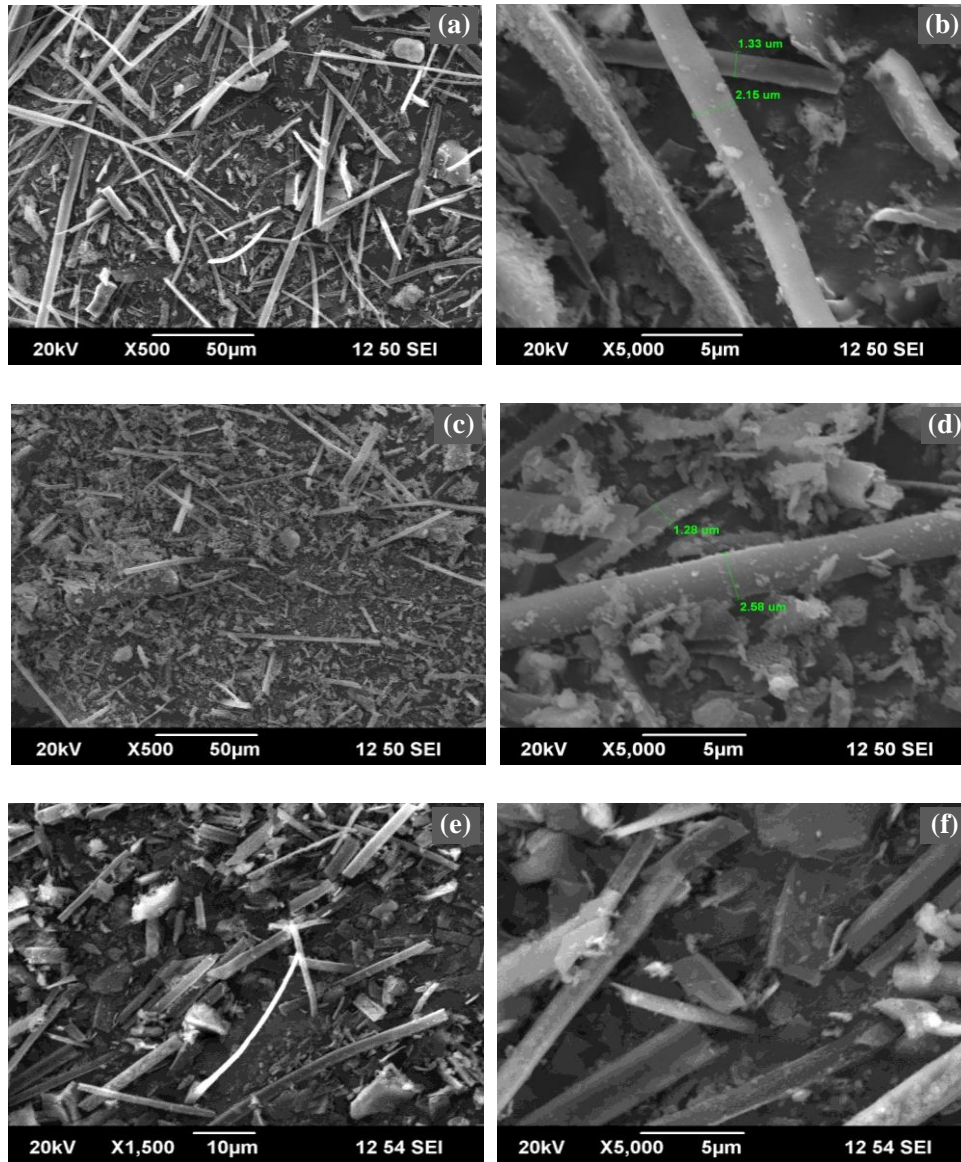**Figure 4.8   SEM photographs of the ashes from (a) and (b) 0.01 N HCl treated BM, (c) and (d) 0.1 N HCl treated BM and (e) and (f) 1 N HCl treated BM.**

The morphological analysis of acid treated BM shows fibrous morphology in all the acid treated cases as shown in Figure 4.8. Bundles of fibers in micrometer range are observed in all the three cases. The individual width cannot be measured, though nominal fibers falls to the size range less than 2 μm. But from the elemental analysis by EDS shows that 1N HCl pretreatment is necessary to remove all the metallic impurities present in the original bamboo flakes (BM). Hence the optimum concentration for isolating high purity silica fibers from BM is formed to be 1N. The detailed characterization of the pure fibrous silica obtained after 1 N HCl treatment (BMS) was carried out and presented further.

The yield of silica obtained after 1 N HCl leaching followed by calcination is found to be 3 g silica per 100 g BM. Here also the choice of matrix is justified since the biomass itself acts as a template for fibrous silica isolation. Hence fibrous silica can be isolated in a very easy and cost effective route.

4.3.3 Characterizations of optimized fibrous nanosilica

4.3.3.1 Characterizations of CGS

Figure 4.9(a) shows the FTIR spectrum of the silica obtained after 0.01N HCl pretreatment followed by calcination. The broad band around 3400 cm^{-1} for silica is due to silanol -OH groups and adsorbed water. The bending mode of this was seen at around 1631 cm^{-1}. The predominant peak at 1103 cm^{-1} is due to siloxane bonds (Si-O-Si). The peaks between 1000 and 700 cm^{-1} are attributed to vibration modes of the gel network. The presence of an absorption band at 803 cm^{-1} is assigned to the symmetric

stretching vibration of Si–O–Si bond. Another peak at 469 cm^{-1} is the bending mode of O-Si-O bond. Thus it can be concluded that the sample consists predominantly of silicon oxide.
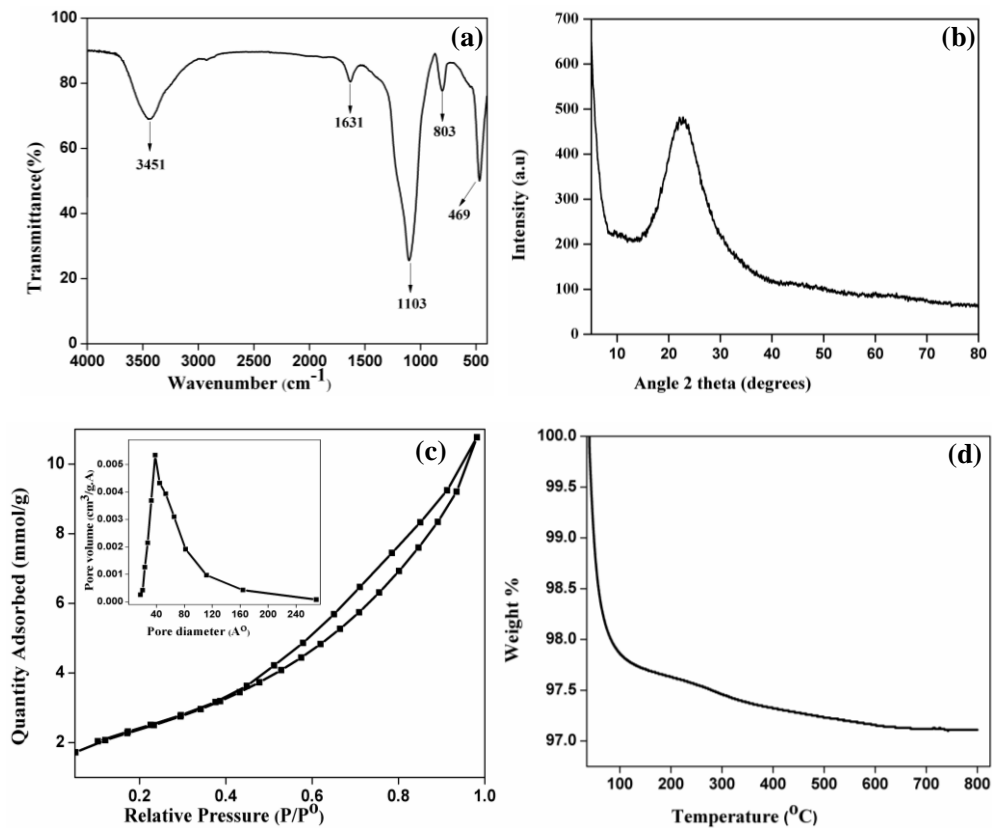
Figure 4.9 (a) FTIR spectrum (b) XRD pattern (c) Nitrogen adsorption–desorption isotherm (Inset shows the pore size distribution) (d) and TGA pattern of CGS.

X-Ray is an important tool to identify the crystalline nature, purity and size of the materials. The X-Ray diffraction patterns of the CGS silica samples are shown in Figure 4.9(b). The characteristic of amorphous SiO$_2$

is observed due to the strong broad peak around 22-23° is. This shows that the isolated silica is in amorphous state.

Figure 4.9(c) shows the nitrogen adsorption- desorption isotherm of CGS. From the figure it is clear that in the nitrogen adsorption isotherm, the desorption branch does not follow the adsorption branch, but gives a distinct hysteresis loop, where the amount adsorbed is greater along the desorption branch compared to the adsorption branch. The isotherm belonged to the type IV category in the International Union of Pure and Applied Chemistry (IUPAC) classification of different types of hysteresis loops. The type IV isotherm profile is generally associated with mesoporous adsorbents [41]. Figure 4.9(c) also reveals that the type IV isotherm consists of a narrow H1 hysteresis loop which confirms the narrow and uniform pore distribution in the sample. The Brunauer–Emmett–Teller (BET) surface area calculated from the nitrogen adsorption–desorption analysis is 195 m²/g with a pore diameter around 7.6 nm.

Thermogravimetric analysis of isolated silica CGS was carried out in the temperature range from 40 to 800 °C. The thermal behavior is shown in Figure 4.9(d). The thermogram shows a weight loss within 150 °C and after that it does not show further reduction in weight. Moreover on increasing the temperature from 150 °C, the weight loss is negligible which continues up to 600 °C, which indicates that CGS is purer and all the metallic impurities are removed during HCl pre-treatment and all the organic moieties present can be removed during the calcination process.

4.3.3.2 Characterizations of PGNS
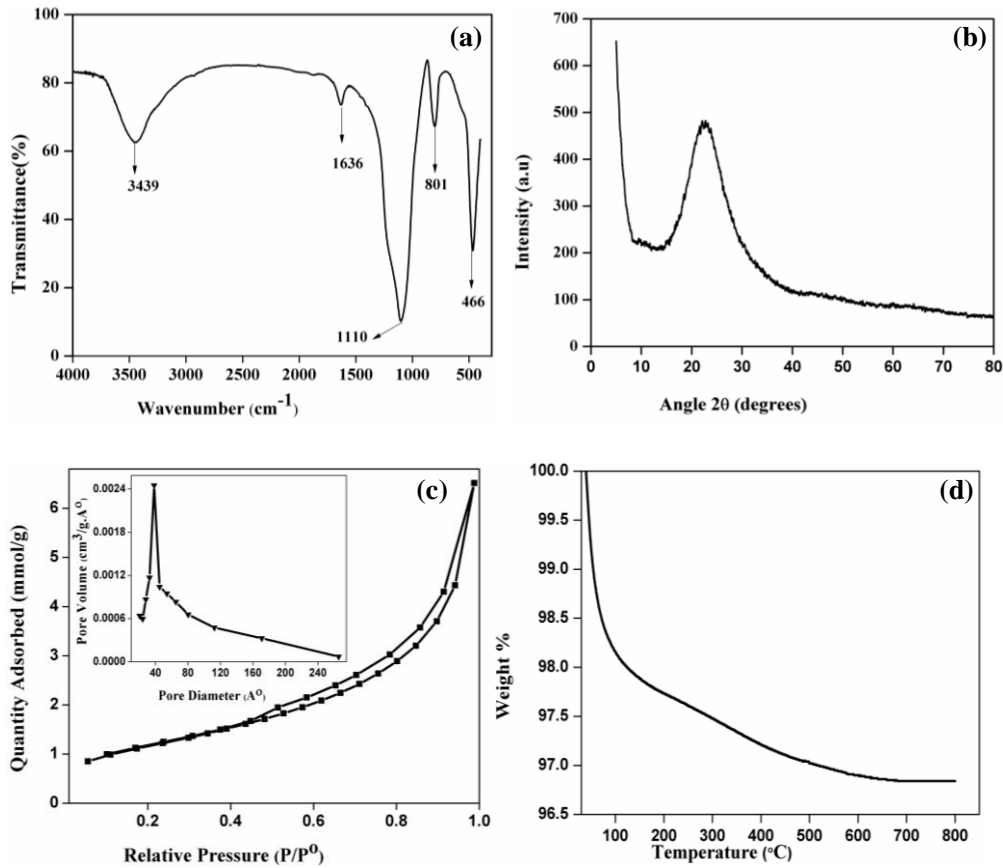
Figure 4.10 (a) XRD pattern (b) FTIR spectrum (c) Nitrogen adsorption–desorption isotherm (inset Pore size distribution) and (d) TGA pattern of PGNS

The XRD pattern of the CGS powder is shown in Figure 4.10 (a). The characteristic strong broad peak centers at 2Ɵ angle of ~22° and thus confirms the amorphous nature of silica. The absence of a sharp peak indicates the absence of crystallinity in the so called isolated sample.

The FTIR spectrum of the PGNS is shown in Figure 4.10(b). The peaks appearing in 450–1300 cm^{-1} are characteristic of silica samples. The band centered at 466 cm^{-1} corresponds to the bending frequency of O-Si-O. Also the strong peak at 1,110 cm^{-1} corresponds to the asymmetric vibration of the siloxane bond, Si–O–Si. This bond forms the backbone of the silica matrix. The presence of an absorption band at 801 cm^{-1} is assigned to the symmetric stretching vibration of Si–O–Si bond. The bands at 3,439 and 1,636 cm^{-1} correspond to the –O-H stretching and bending vibrations. The band around 3,439 cm^{-1} is due to –O-H stretching vibration of the silanol or adsorbed water molecules on the silica surface. The bending vibration of the trapped water molecules in the silica matrix is detected as an intense peak at 1,636 cm^{-1}. This band cannot be completely removed by heating, however its intensity is decreased. No peak is found between 2,800 and 3,000 cm^{-1} indicating that there are no original organic compounds in the silica after controlled combustion and extraction. Thus, it is possible to produce a highly pure nanosilica powder from FPG using 0.1 N HCl treatment followed by calcination at 650 °C for 6 h.

Figure 4.10 (c) shows typical nitrogen adsorption–desorption isotherm of PGNS. The nitrogen adsorption isotherm of PGNS also follows the same trend as explained in the case of CGS, where the amount adsorbed is greater along the desorption branch compared to the adsorption branch. The isotherm belongs to the type IV category IUPAC classification of different types of hysteresis loops which reveals that type IV isotherm consists of a narrow H1 hysteresis loop. This can be confirmed from the narrow and uniform pore distribution in the sample. The Brunauer–Emmett–Teller (BET) surface area calculated from the nitrogen adsorption–desorption

analysis is 126 m²/g with a pore volume of 0.29 cc/g. Adsorption in between 0.2 and 0.9 relative pressure (P/P$_0$) clearly indicates the presence of large number of mesopores [Figure 4.10(c) inset] with pore diameter around 3.6 nm.

The thermogravimetric curve obtained for PGNS is given in Figure 4. 10(d). The thermogram shows weight losses within 150 °C, but it does not show further reduction in weight. The negligible or nearly absence of weight loss after 150 °C confirmed that the isolated silica is purer and all the metallic impurities and the organic moieties present could be removed during HCl pre-treatment and the calcination process.

4.3.3.3 Characterizations of BMS

Figure 4.11(a) shows the FTIR spectrum of the silica obtained after 1N HCl pretreatment followed by calcination. The broad band around 3437 cm^{-1} is due to silanol –O-H groups and adsorbed moisture. The bending mode of -O-H is seen at around 1630 cm^{-1}. The prime peak at 1102 cm^{-1} is due to siloxane bonds (Si-O-Si). The presence of an absorption band at 803 cm^{-1} is assigned to the symmetric stretching vibration of Si–O–Si bond, and the peak at 469 cm^{-1} is the bending mode of O-Si-O bond. Thus from these observations it can be concluded that the sample consists predominantly of silicon oxide, further the purity of isolated BMS was established.
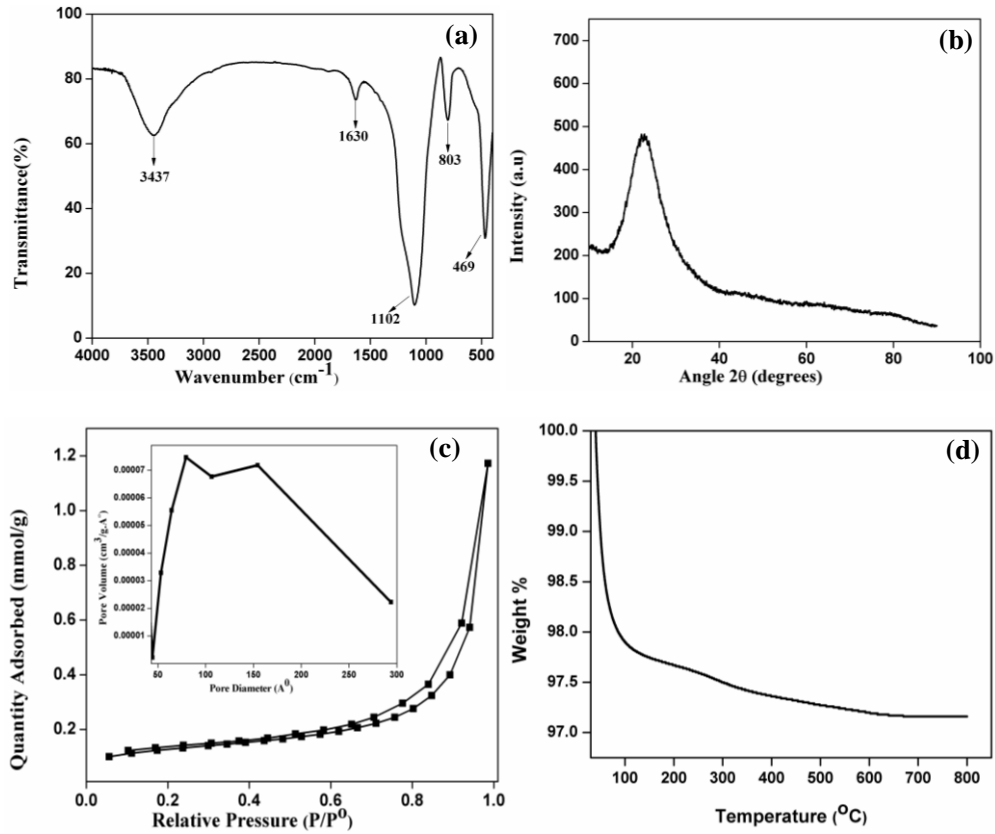
Figure 4.11 (a) FTIR spectrum (b) XRD pattern (c) Nitrogen adsorption–desorption isotherm (inset shows the pore size distribution) (d) TGA pattern.

Figure 4.11(b) XRD pattern of BMS clearly shows that a broad absorption band at 2θ around 22° is the characteristic of amorphous silica. Thus the isolated silica BMS is highly amorphous in nature.

The nitrogen adsorption-desorption isotherm [Figure 4.11(c)] clearly indicates the type IV isotherm as in the case of CGS and PGNS. The Brunauer–Emmett–Teller (BET) surface area calculated from the analysis is 180 m²/g and a pore diameter around 16 nm.

Thermogravimetric analysis of BMS was carried out in the temperature range from 40 to 800 °C and the thermal behavior is shown in Figure 4.11(d). The thermogram shows a weight loss within 150 °C and after that it does not show further reduction in weight. The loss of weight is due to the adsorbed moisture in the sample. On increasing the temperature from 150°C, the weight loss is negligible which indicates that BMS is purer and all the metallic impurities were removed during HCl pre-treatment and all the organic moieties present could be removed during the calcination process.

4.3.4 Transmission electron microscopy (TEM)

4.3.4.1 TEM analysis of CGS
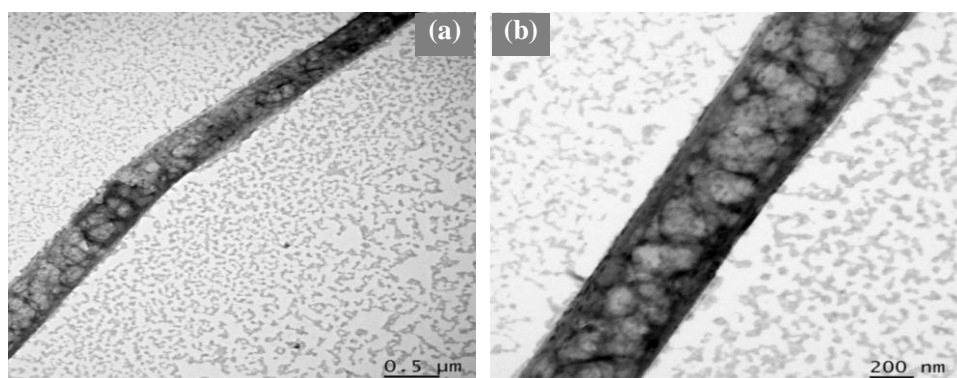
Figure 4. 12 (a) and (b) TEM images of CGS

The TEM images of CGS at lower resolution [Figure 4.12(a)] reveal that the isolated silica has a fibrous morphology. TEM at higher resolution [Figure 4.12 (b)] confirms porous fibrous structure to CGS. The uniformly distributed pores as revealed from BET analysis are also confirmed from the TEM images.

4.3.4.2 TEM analysis of PGNS
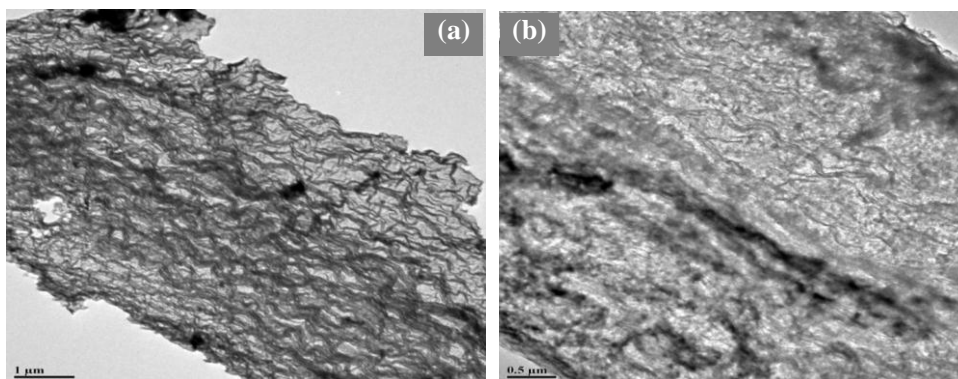
Figure 4.13 (a) and (b) TEM images of PGNS

The TEM images of PGNS [Figure 4.13 (a) and (b)] reveal that the isolated nanosilica mainly consists of nano channel network. TEM analysis confirms that porous nanoparticles are interconnected to form the fibrous nanochannel network. The individual channels are less than 100 nm in width. The uniformly distributed pores as revealed from BET analysis are also well established from the TEM images.

4.3.4.3 TEM analysis of BMS
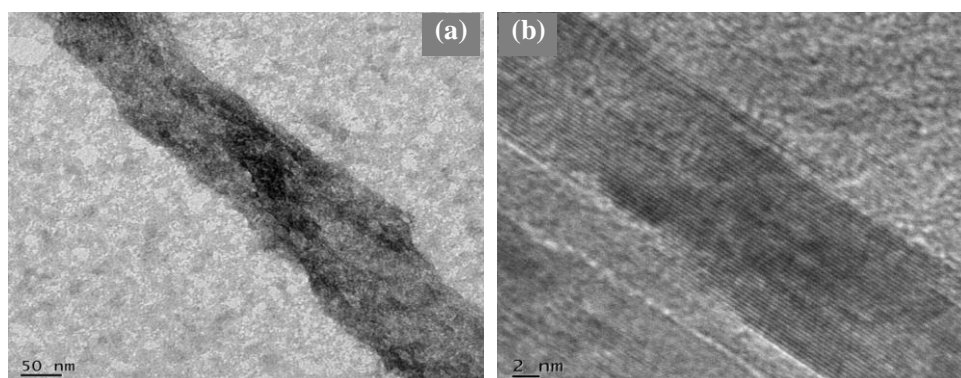
Figure 4. 14 (a) and (b) TEM images of BMS

The TEM analysis of BMS depicts a fibrous morphology for the isolated silica. Bundles of fibers with a few micrometers in width were observed in the SEM image, whereas TEM analysis gives a vivid picture of individual fibers having width in nanometer range.

4.4 Conclusions

Three different grass sources viz Indian grass, Pampas grass and Bamboo were used for the isolation of fibrous silica via an acid pre treatment followed by calcination. The optimized acid concentration for pretreatment was 0.01N HCl for CG and 0.1N HCl for FPG and 1N HCl for BM respectively. The metallic impurities were removed with mild acid solution and silica thus isolated has nano fibrous morphology as evident from SEM and EDS analysis in the case of PGNS, whereas bundles of fibers were obtained for CGS and BMS. Fibrous morphology for all the silica is confirmed from TEM analysis. Surface area and pore size distribution were studied by using BET surface area analysis and it is obtained as $195 m^2/g$ for CGS, $126 m^2/g$ for PGNS and $180 m^2/g$ for BMS. The yield of nanosilica from various raw materials in their dried form is as follows: CGS 130 g/kg, FPG 60 g/kg and BM 30 g/kg respectively. Thus the study has identified a potential route for preparing high-purity mesoporous fibrous silica materials by utilizing an abundant bio-precursor like tip of Indian grass, flowers of Pampas grass and stem of Bamboo. The method is simple and well suited for mass production, and may help to reduce the waste from these grass sources.

References

[1]   Wang ZL, Gao RP, Gole JL, Stout JD. Adv. Mater. 2000; 12:1938-40.

[2]   Manivannan R, Ramanathan S. Appl. Surf. Sci. 2009; 255:3764-8.

[3]   Torney F, Trewyn BG, Lin VS, Wang K. Nat. Nanotechnol. 2007; 2:295-300.

[4]   Singh LP, Bhattacharyya SK, Mishra G, Ahalawat S. Appl. Nano. Sci. 2011; 1:117-22.

[5]   Rahman IA, Vejayakumaran P, Sipaut CS, Ismail J, Bakar MA, Adnan R, Chee CK. Colloids Surf. A. Physicochem. Eng. Asp. 2007; 294:102-10.

[6]   Do Kim K, Choi KY, Yang JW. Colloids Surf. A. Physicochem. Eng. Asp. 2005; 254:193-8.

[7]   Sarawade PB, Kim JK, Hilonga A, Kim HT. Powder Technol. 2010; 197:288-94.

[8]   Essien ER, Olaniyi OA, Adams LA, Shaibu RO.J. Met. Mater. Miner. 2011; 21:7-12.

[9]   Adam F, Chew TS, Andas J. J.Sol-gel Sci. Technol. 2011; 59:580-3.

[10]   Adams LA, Shaibu RO, Essien RE, Oki A. J. Met. Mater. Miner. 2011; 21:1-6.

[11]   Rafiee E, Shahebrahimi S, Feyzi M, Shaterzadeh M. Int. Nano. Lett. 2012; 2:29.

[12]   Affandi S, Setyawan H, Winardi S, Purwanto A, Balgis R. Adv. Powder Technol. 2009; 20:468-72.

[13]   Jones LH, Handreck KA. Adv. Agro. 1967; 19:107-49.

[14]   Lanning FC, Ponnaiya BW, Crumpton CF. Plant Physiology. 1958; 33:339.

[15]   Lanning FC, Linko YY. J. Agri. Food Chem. 1961; 9:463-5.

[16]   Parry DW, Hodson MJ, Sangster AG, Jones WC, O'Neill CH. Phil.Trans. R. Soc. Lon. B: Biol. Sci. 1984; 304:537-49.

[17]   Chakraverty A, Mishra P, Banerjee HD. J. Mater. Sci. 1988; 23:21-4.

[18]   James J, Rao MS. Thermochim. Acta 1986; 97:329-36.

[19]   Kamiya K, Oka AI, Nasu H, Hashimoto T. J..Sol-gel Sci. Technol. 2000; 19:495-9.

[20]   Conradt R, Pimkhaokham P, Leela-Adisorn U. J. Non-Cryst. Solids. 1992; 145:75-9.

[21]   Liou TH. Mater. Sci. Eng. A. 2004; 364:313-23.

[22]   Zaky RR, Hessien MM, El-Midany AA, Khedr MH, Abdel-Aal EA, El-Barawy KA. Powder Technol. 2008; 185:31-5.

[23]   Li D, Chen D, Zhu X. Biores. Technol. 2011; 102:7001-3.

[24]   Liou TH, Yang CC. Mater. Sci. Eng. B. 2011; 176:521-9.

[25]   Carmona VB, Oliveira RM, Silva WT, Mattoso LH, Marconcini JM. Ind. Crops Prod. 2013; 43:291-6.

[26]   Cheung TL, Ng DH. J. Amer. Ceram. Soc. 2007; 90:559-64.

[27]   Espíndola-Gonzalez A, Fuentes-Ramirez R, Martínez-Hernández AL, Castaño VM, Velasco-Santos C. Adv. Mater. Sci. Eng. 2014; 2014.

[28]   Zhu J, Jia J, Kwong FL, Ng DH, Tjong SC. Biomass and bioenergy. 2012; 36:12-9.

[29]   Cheung TL, Ng DH. J.Amer.Ceram. Soc. 2007; 90:559-64.

[30]   Wu SH, Mou CY, Lin HP. Chem. Soc. Rev. 2013; 42:3862-75.

[31]   Umeda J,Kondoh K, Michiura Y. Mater. Trans. 2007; 48:3095-100.

[32]   Nakata Y, Suzuki M, Okutani T, Kikuchi M, Akiyama T. J. Ceram. Soc. Japan. 1989; 97:842-9.

[33]   Chandrasekhar S, Pramada PN, Praveen L. J. Mater. Sci. 2005; 40:6535-44.

[34]   Proctor A. J. Amer. Oil Chem. Soc. 1990; 67:576-84.

[35]   Real C, Alcala MD, Criado JM. J. Amer. Ceram. Soc. 1996; 79:2012-6.

[36] Krishnarao RV, Subrahmanyam J, Kumar TJ. J. Eur. Ceram. Soc. 2001; 21: 99-104.

[37] Liou TH, Yang CC. Mater. Sci. Eng. B. 2011; 176:521-9.

[38] Kalapathy U, Proctor A, Shultz J. Biores. Technol. 2000; 73:257-62.

[39] Chakraverty A, Banerjee HD, Mishra P. AMA, Africa and Latin America. 1990; 21:69-75.

[40] Kalapathy U, Proctor A, Shultz J. Biores. Technol. 2002; 85:285-9.

[41] Sing KSW, Everett DH, Haul RAW, Moscou L, Pierotti RA, Rouquerol J, Siemieniewska T. Pure Appl. Chem. 1985; 57:03-619.

.....ഇന.....

HMHDPE/LLDPE BLEND: EFFECT OF NANOZIRCONIA

Part A

HMHDPE/LLDPE BLENDS: PREPARATION AND EVALUATION OF MECHANICAL, THERMAL AND RHEOLOGICAL CHARACTERISTICS

Polyethylene based blends have become commercially important for optimizing its mechanical and rheological parameters. High molecular weight high density polyethylene (HMHDPE) and Linear low density polyethylene (LLDPE) based blend was prepared by melt mixing in a Thermo Haake Rheocord mixer. HMHDPE possess high stiffness but is difficult to process due to its high molecular weight while LLDPE has high impact strength and good processability. Processability of HMHDPE can be improved by blending with LLDPE. Further if properties like toughness and stiffness can also be averaged their blends can be commercially usefull. Mechanical properties like tensile, flexural, hardness and impact properties of the blends have been studied. Thermal analysis like DSC and TGA were also conducted. Melt rheological analysis on a parallel plate rheometer also explored. Mechanical properties fall in between HMHDPE and LLDPE. Thermo gravimetric analysis (TGA) shows improved thermal stability by the addition of LLDPE to HMHDPE.

5.A.1 Introduction

The blending of two or more polymers to form a new material is widely established as a means to produce new materials with tailored properties. Other than economical and environmental incentives, blending of polymers is often aimed at improving a weak property of a component resin such as impact strength or processability [1]. The miscibility of the constituent polymers determines the compatibility of the blend on a molecular level that, in turn, determines the ultimate properties [2-4].

Polyolefins are important polymers in industry. In recent years blends of various polyolefins have received more and more attention for many reasons. A vast number of blends of polyolefins have been used in agricultural and packaging industries. Among different grades of polyethylenes, ultra high molecular weight polyethylene (UHMWPE) being high molecular weight and density provides superior mechanical properties, but the processability of this PE is very difficult [5, 6]. Owing to its better mechanical performance and chemical inertness it has been long established as a bone substituent along with metal part or with nanofillers [7]. Due to the difficulties like processability and high cost of UHMWPE it will be advantageous to develop produce a new blend of PEs matching the properties of UHMWPE [8]. With the advancement of nanotechnology and innovative manufacturing techniques for the preparation of nanocomposites, HDPE based nanocomposites were recently investigated for the utilization in total hip artificial joints [9-14].

Polyethylene blends have become commercially important for optimizing the mechanical properties and processability of individual

members. High molecular weight high density polyethylene (HMHDPE) is widely used because of its versatile properties and is widely used due to its mechanical strength, low cost and resistance to chemical and biological attack [15-17]. Linear low density polyethylene (LLDPE) has better mechanical properties like elongation at break, impact strength and also has higher resistance to puncture and tearing than LDPE, and hence finds applications in different fields [18, 19]. Blends of LDPE and LLDPE are for last 20 years considered as excellent materials for film manufacture since they merge the processability of LDPE and the better mechanical and environmental cracking resistance of LLDPE [20-22]. The blend of HMHDPE, which has a few side chains per 1000 carbons, LLDPE, which has short chain branching can be easily realized; the characteristics can be varied by the mixing method or the mixing condition. While many studies have been undertaken on LDPE-LLDPE, HDPE-LDPE and HDPE-LLDPE blends, no studies are reported on HMHDPE-LLDPE blends. However, it is reported that a blend of HDPE and LLDPE exhibited a crystallization exotherm of a single peak which indicates that it is a compatible system [23]. In view of the continued and increasing importance of polyethylene blends as a means of developing new materials with desirable properties, the current work is aimed at the preparation of binary blends of HMHDPE and LLDPE and investigating their mechanical, thermal and rheological properties.

5.A.2 Methodology

5.A.2.1 Materials

The details of the polymers used for the study are discussed in Chapter 2.

5.A.2.2 Preparation of the blend

HMHDPE and LLDPE granules were placed in an air oven set at 100°C for four hours to remove any moisture present and allowed to cool to room temperature in desiccators. Five blend compositions were selected namely HL-1, HL-2, HL-3, HL-4, HL-5 and the granules were weighed out. For melt blending granules were fed into the mixing chamber of a Thermo Haake Rheomix Poly Lab system equipped with roller type rotors set at 160°C. The blender was fitted with roller rotor blades counter rotating at 3:2 speed ratio. Table 5.A.1 represents the sample description and the corresponding weight % for blend preparation. A mixing time of 8 minutes was allowed to complete each blending operations. During this time the torque would become steady. The hot polymer blend taken out from the mixing chamber was pressed by hydraulic press and was cut into small pieces. The material was then injection molded using a semi automatic type injection molding machine with a barrel temperature of 180°C.

Table 5.A.1 Composition of the polyethylene blends made by melt mixing in the Thermo Haake Rheomix Poly Lab system

Sample Code	Sample description	HMHDPE content in blends (weight in g)	LLDPE content in blends (weight in g)
HL-0	100% HMHDPE	43.77	0
HL-1	90% HMHDPE- 10% LLDPE	39.25	4.36
HL-2	80% HMHDPE-20% LLDPE	34.76	8.69
HL-3	70% HMHDPE- 30% LLDPE	30.35	12.97
HL-4	60% HMHDPE- 40% LLDPE	25.92	17.28
HL-5	50% HMHDPE-50% LLDPE	21.48	21.48
LH-0	100% LLDPE	0	42.20

The samples were injection moulded and characterized according to the techniques discussed in Chapter 2.

5.A.3 Results and discussion

5.A.3.1 Mechanical properties

5.A.3.1.1 Tensile properties

The tensile stress-strain curves of the HMHDPE-LLDPE blends of different compositions and the pure components are shown in Figure 5. A.1(a). The tensile properties of the blends vary smoothly between those of the parent polymers. LH-0 has a lower yield stress than HL-0, but a much higher elongation at break. The obvious effects of adding LH-0 to the blends are to lower the yield stress and increase the elongation at break. The strain hardening during plastic flow is similar for both polymers and the blends. The very high elongation at break of LH-0 is due to its stable necking behavior [24]. In the case of LH-0, elongation of the neck occurs as a result of the transfer of material from the wider part of the specimen, while in the case of HL-0 it occurs by deformation of the already transformed material.
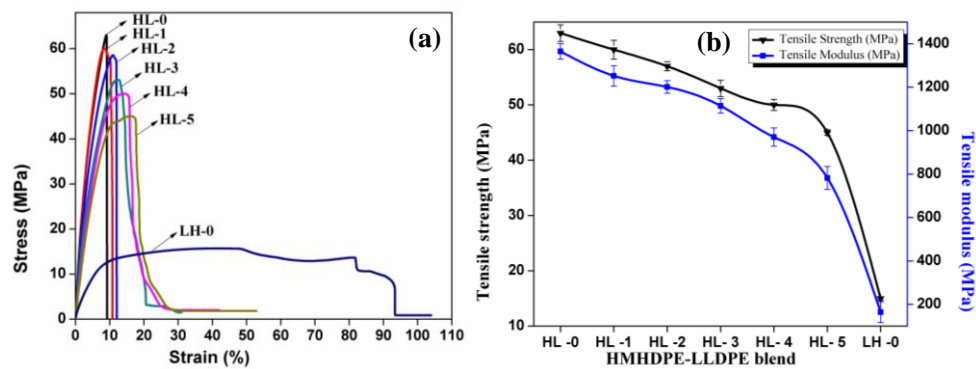
Figure 5.A.1 Tensile properties of HMHDPE/LLDPE blends (a) stress-strain curve (b) variation of tensile strength and tensile modulus by different blend compositions

The ultimate tensile strength and modulus of binary blends falls with incorporation of higher amount of LLDPE [Figure 5. A.1 (b)]. The break strength of HMDPE-LLDPE blends was observed to vary between 63 and 15 MPa and the tensile modulus was between 1365 and 164 MPa. These observations are in agreement with those made for blends of HDPE with LLDPE where the break strength was found to increase with increasing LLDPE content in the blend [25]. At higher concentration of LLDPE, the modulus does not change significantly. The tensile behavior of the HMHDPE-LLDPE blends suggests that the blends exhibit sufficient compatibility between HMHDPE and LLDPE in the solid phase. The ability to co-crystallize may be a strong driving force for the miscibility of these blends [26].

5.A.3.1.2 Flexural properties
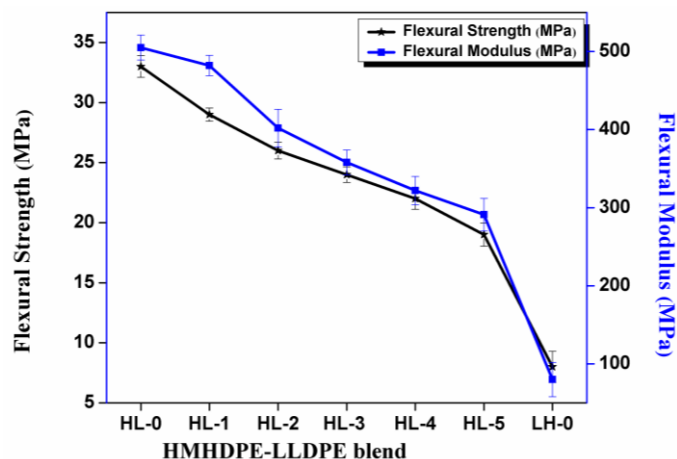
Figure 5.A.2 Variation of flexural strength and flexural modulus by different blend compositions

The flexural properties like flexural strength and modulus with the blend composition for HMHDPE-LLDPE are shown in Figure 5. A.2. Both

the properties are found to decrease with the increase in LLDPE content. The flexural strength changes from 33 MPa to 22 MPa as the LLDPE content increases from 0% to 40 weight%. Further addition of LLDPE shows a sharp drop in the flexural strength, reaching a value of 19 MPa for the 50/50 HMHDPE-LLDPE blend, and finally reaching to 8MPa for 100% LLDPE. Flexural modulus also shows the same trend.

5.A.3.1.3 Impact strength
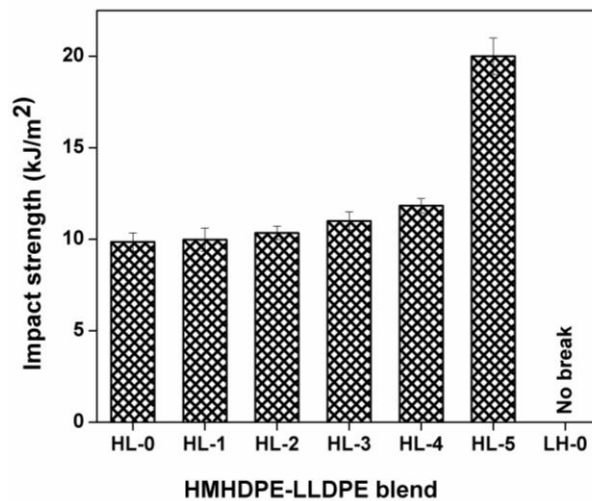
Figure 5.A.3 variation of impact strength by different blend compositions

The notched Izod impact strength versus composition for blends of HMHDPE with LLDPE is shown in Figure5. A.3. Impact strength increases for the HMHDPE-LLDPE blends with increasing LLDPE phase; LLDPE phase acts as an impact modifier for HMHDPE. When the LLDPE content varies from 0 to 40 weight%, a significant change in impact strength is not observed. But, as the LLDPE content in the blend exceeds 40%, a remarkable increase in impact strength is observed, attaining the values

419 J/m at 50 weight% LLDPE content in the blends. For 100% LLDPE, no break was observed under the test conditions. This suggests that the LLDPE has superior impact properties.

5. A.3.1.4 Surface hardness
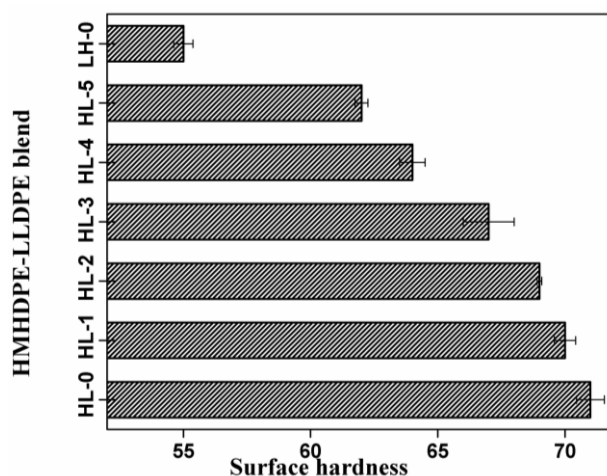
Figure 5.A.4 variation of impact strength by different blend compositions

Surface hardness values of the blends obtained from a hand operated durometer as shown in Figure 5.A.4. The hardness value represents the ability of the material to stand firm to the local surface deformation. LH-0 has the least hardness and HL-0 has the highest value, the blends show hardness in between that of HMHDPE and LLDPE.

5.A.3.2 Melt rheological properties

5.A.3.2.1 Melt flow index

The MFI of a polymer or polymer blend is related to its relative molecular weight and is often used to characterize its processability [27-29]. Melt flow index of HMHDPE-LLDPE blends of four different compositions

namely HL-0, HL-1, HL-2, HL-3, HL-4, HL-5 were obtained from Melt flow Indexer at a temperature of 190 °C. A plot of MFI versus composition for HMHDPE-LLDPE blends is shown in Figure5. A.5.
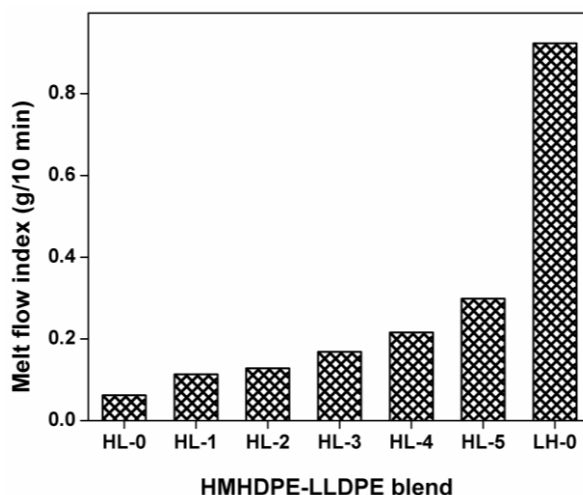
Figure 5.A.5 variation of MFI for different blend compositions

It is observed that for the HMHDPE-LLDPE blends, this plot shows an upward trend in the MFI. The MFI of HL-2 blend is 0.128 gm/10 min. When the LLDPE content increases to 50% the MFI value is 0.298 gm/10 min. The Melt Flow Index of polymer blends depends upon interfacial adhesion, interfacial thickness and the characteristics of the components forming the blend [27]. When shear stress is applied on polymer blends, there will be interlayer slip along with orientation and disentanglement. Further, the blend can undergo elongational flow. If the interface is strong, the deformation of the dispersed phase will be effectively transferred to the continuous phase. If the interface is weak, interlayer slip occurs. The psuedoplastic behavior of a polymer is due to the random and entangled nature of polymer chains [30]. The reduction in MFI of polymer blends

indicates an increase of shear viscosity. This is probably due to the fact that both phases in a polymer blend have an elastic response and can store a part of the elastic energy applied by the testing apparatus. But discrete domains would dissipate less energy while flowing in the apparatus than the continuous phase that wets the walls. They will offer less resistance to flow and resulting lower viscosity. The viscosity will be much lower if the dispersed phase gets deformed by the flow [31, 32]. In any polymer melt, flow occurs when polymer molecules slide past each other. The ease of flow depends upon the mobility of molecular chains and the forces or entanglements holding the molecules together. The complete occurrence of interlayer slip and consequent decrease in viscosity may be contributing to the increased MFI of HMHDPE-LLDPE blends rich in LLDPE content.

5.A.3.2.2 Dynamic rheological analysis (DRA)

The knowledge of rheological properties of the melt and the blend morphology are important to control the processing parameters for the desired end-use applications [33]. The compatibility or miscibility between phases is an important factor affecting the rheological characteristics of polymer melts. The dispersion and distribution of the components in the blends as well as the mixing conditions are also related [34]. Rheological properties are governing the flow behavior of polymers when they are processed in the molten state. It is particularly concerned with the properties of matter that determine its behavior when a mechanical force is exerted on it. Rheology is distinguished from fluid dynamics because it is concerned with the three traditional states of matters rather than only liquid and gases. It is the rheological properties that govern the flow behavior of polymers when they are processed in the molten state. In order to measure

a material's rheology, five criteria must be met: geometric boundary conditions, stress, strain, strain rate and mode of deformation. For a good understanding of the rheological properties of the materials, it is necessary to either assess the deformation resulting from a specified force or compute the force essential to create a given deformation. Since a measure of force, one can utilize the stress which is defined as the ratio of applied force to the cross sectional area on which the force acts. Deformation can be illustrated in term of strain or strain rate [35-40].
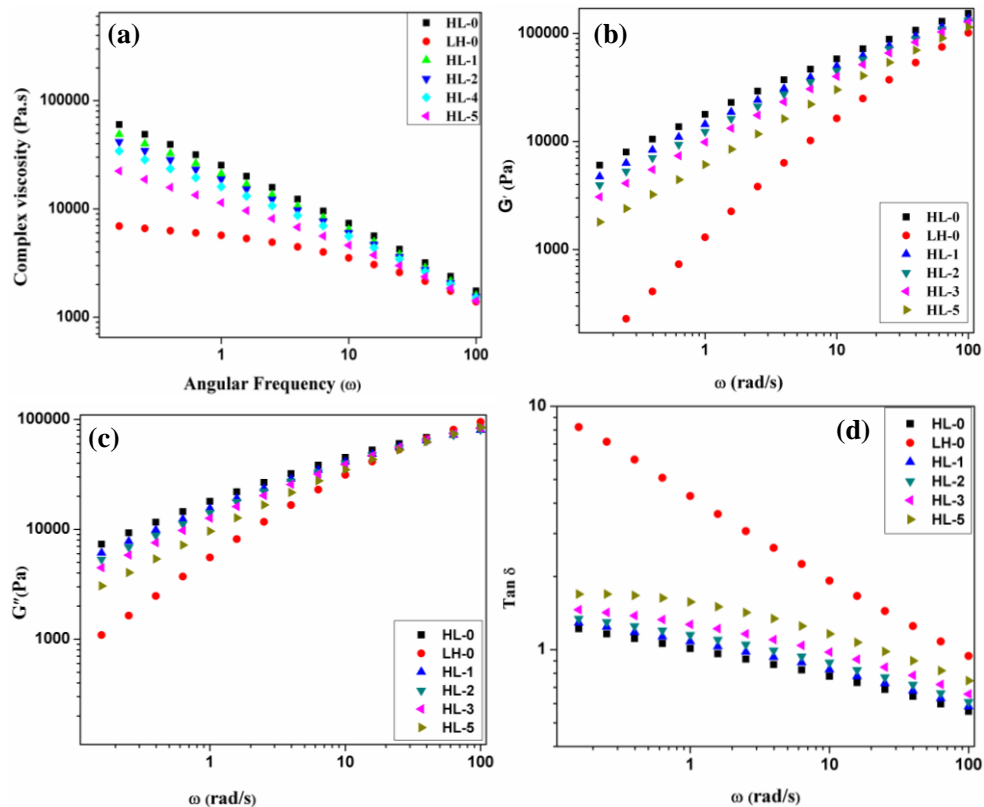
Figure 5.A.6 Dynamic rheological analysis of the pure polymer and the blends
(a) variation of complex viscosity against angular frequency,
(b) variation of storage modulus against angular frequency,
(c) variation of loss modulus against angular frequency,
(d) variation of tan δ against angular frequency

In Figure5. A.6(a) the variations of complex viscosity (η) with frequency on a log scale for the blend as well as the polymers is plotted. As it can be seen, for all the cases, complex viscosity decreases with increase in frequency. HL-0 has the highest complex viscosity and thus it is somewhat difficult to process. Blend shows complex viscosity in between that of HL-0 and LLDPE as expected. The variations of storage modulus (G') with frequency for the pure polymer as well as the blends are shown in Figure5. A.6 (b). Similar to the observations made in the case of mechanical properties, rheological properties also lies in between that of pure HL-0 and LLDPE. HL-0 has the highest storage modulus and LLDPE as the least value. Figure5. A.6 (c) and (d) show the variation of loss modulus (G") and tan δ against angular frequency for the polymer and the blend , which also follow the same trend in the case of storage modulus, that we already expected.

5.A.3.3 Thermal properties of the blend

5.A.3.3.1 Thermogravimetric analysis
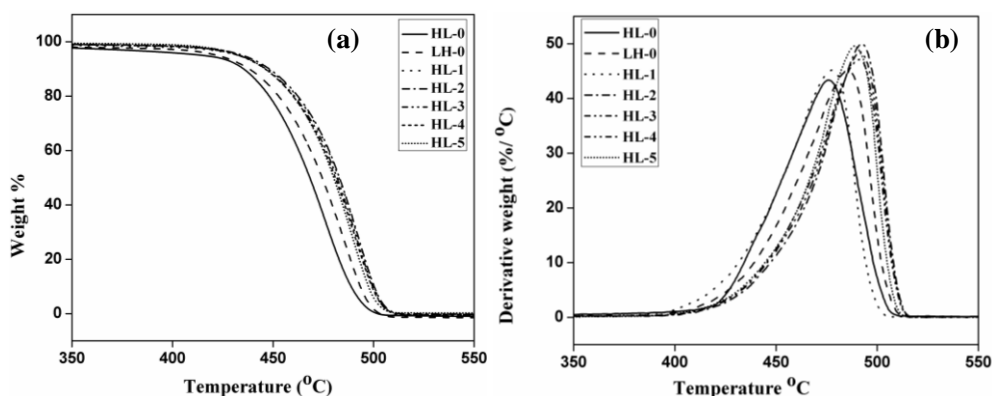
Figure 5. A.7 Thermogravimetric curve of HMHDPE-LLDPE blend

The thermal stability and degradation studies of polymer blends and polymer compounds are essential both for the processing and application purposes. Thermal analysis is considered as an important analytical method to understand the structure-property relationship and mastering the technology for the industrial production of different polymeric materials. Thermal degradation of PEs suggests that the degradation is initiated by chain scission of C-C bonds. All samples showed single step degradation pattern in the range of 290 to 530°C. Blends show superior thermal stability than the pure polymers.

5.A.3.3.2 Differential scanning calorimetry

The melting and crystallization behavior of the HMHDPE-LLDPE blends is shown in Figure 5.A.8.
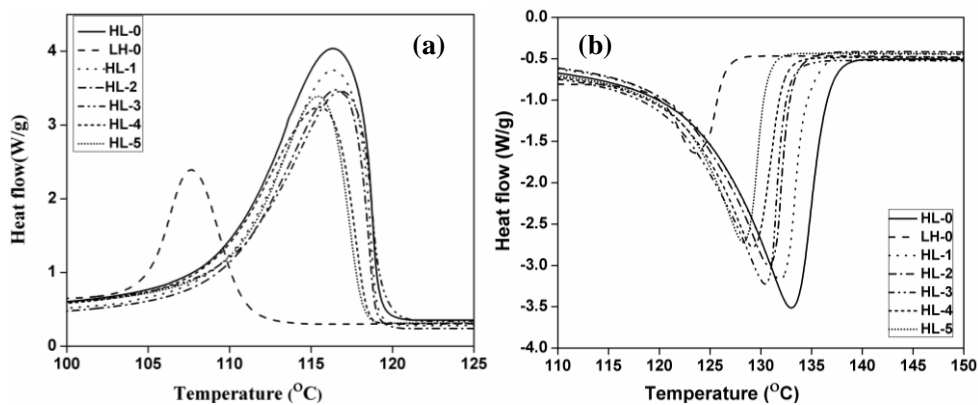
**Figure 5.A.8 Non isotherm crystallization curve of HMHDPE/LLDPE blend
(a) cooling behavior, (b) melting behavior**

HMDPE-LLDPE blends exhibit a single melting peak at all compositions, which is consistent with the report that HDPE/LLDPE blends co-crystallize to form a single phase [41]. As the HMHDPE content

increases, the single peak shifts to intermediate between the melting point of the pure components. The same tendency is noted in a cooling cycle for overall blend compositions. Thus the system can be considered to be miscible in the crystalline phase. Thermal study (DSC) on the melting and crystallization of the binary blends of HDPE/LLDPE system shows one melting endotherm by Lee *et al.* indicate that the blend system is miscible in the crystalline phase [42].

5.A.3.4 High performance studies of HL-2 blend

Based on the mechanical, thermal and rheological properties of the HMHDPE-LLDPE blends, the 80/20 blend HL-2 was selected for further studies. HMHDPE possesses the maximum stiffness and melting temperature while LLDPE has the highest impact strength. Addition of LLDPE also improves thermal stability and processability. So HL-2 blend which possesses high mechanical properties as well as good processability was selected to study it's suitability for high performance applications.

5.A.3.4.1 Compressive strength

Compressive property was measured using cylindrical shaped specimens with 12mm length and 6mm diameter by the application of compressive load. Here the polymeric materials being ductile, a clear point of failure is not observed. Hence compressive modulus is usually monitored to evaluate the compressive properties. Figure 5.A.9 (a) shows the compressive modulus of the pure polymers and the HL-2 blend.
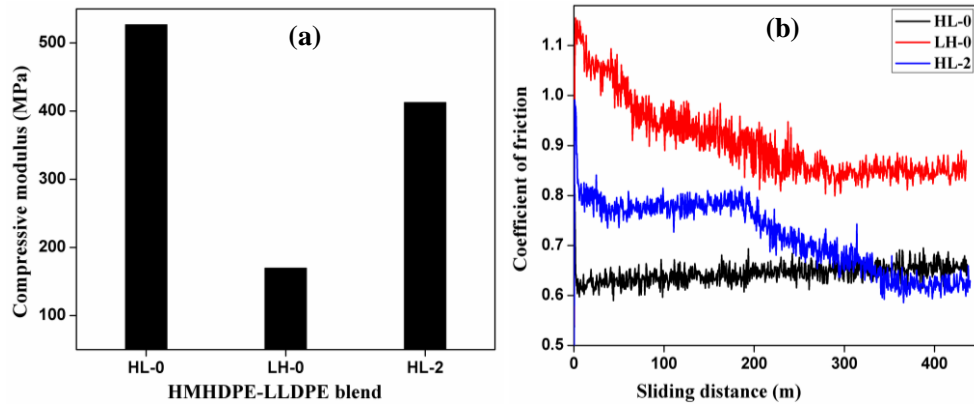
Figure 5.A.9 (a) Variation of compressive modulus (b) Coefficient of friction as a function of sliding distance

HL-0 has the highest compressive modulus and LH-0 has the least value, while the blend shows properties in between. As in the case of other mechanical performance here also the longer chains of HMHDPE transfer load more effectively to the polymer back bone by strengthening the intermolecular interactions under compressive load. HL-2 blend shows the compressive modulus 413 ± 15 MPa.

5.A.3.4.2 Wear resistance

Figure 5. A.9 (b) shows the variation of friction coefficient with sliding distance. As the coefficient of friction decreases the wear resistance of the material increases. It is observed that initially friction coefficient of LH-0 is high signifying better wear material. However with longer times (or the distance increases) coefficient of friction slightly decreases. HL-0 shows no significant change in the coefficient of friction against the sliding distance, which implies that HL-0 shows better wear resistance property. HL-2 initially shows coefficient of friction in between that of HL-0 and LH-0, but it decreases rapidly within short sliding distance, followed a

relatively steady-stage sliding until the friction coefficient remains unchanged due to the formation of the steady transfer films between contact surfaces of friction pair during the repetitive sliding action.

5.A.4 Conclusions

HMHDPE and LLDPE are sufficiently miscible in the solid phase as well as in the melt to take advantage of the attractive properties of the both. All mechanical properties other than impact strength are higher for HMHDPE than LLDPE. Blending HMHDPE with LLDPE enhances the toughness of HMHDPE with only marginal decrease in the yield stress. Also due to its high molecular weight HMHDPE is difficult to process. Processability of HMHDPE can be improved by blending with LLDPE. Thermal stability of HMHDPE improves by blending. To take advantage of the high mechanical performance with better processability 80/20 HMHDPE-LLDPE blend was selected for further studies.

References

[1]   Utracki LA, Favis BD. Polymer alloys and blends, Marcel Dekker, New York; 1989.

[2]   Andrews GD, Subramanian PM. Emerging technologies in plastics recycling. Amer. Chem. Soc.; 1992.

[3]   George J, Joseph R, Thomas S, Varughese KT. J. Appl.Polym. Sci. 1995; 57:449-65.

[4]   Rudin A. The Elements of Polymer Science and Engineering, Academic Press; 1982.

[5]   Chen J, Yang W, Yu GP, Wang M, Ni HY, Shen KZ. J. Mater. Process Technol.2008; 202:165-9.

[6] Wood WJ, Maguire RG, Zhong WH. Compos. Part B Eng. 2011; 42:584-91.

[7] Westby MD, Backman CL. BMC health services Res. 2010; 10:119.

[8] Xue Y, Wu W, Jacobs O, Schädel B. Polym. Test. 2006; 25:221-9.

[9] Wroblewski BM, Lynch M, Dowson D, Isaac GH. Bone Joint J. 1987; 69:61-3.

[10] Isaac GH, Atkinson JR, Dowson D, Wroblewski BM. Eng. Med. 1986; 15:19-22.

[11] Johnson BB, Santare MH, Novotny JE, Advani SG. Mech. Mater. 2009; 41:1108-15.

[12] Fouad H, Elleithy R, Al-Zahrani SM, Ali MA. Mater. Des. 2011; 32:1974-80.

[13] Fouad H, Elleithy R. J. Mech. Behav. Biomed. Mater. 2011; 4:1376-83.

[14] Wang M, Ladizesky NH, Tanner KE, Ward IM, Bonfield W. J. Mater. Sci. 2000; 35:1023-30.

[15] Krishnaswamy RK. Technical papers of the annual technical conference-society of plastics engineers incorporated 2001;1:111-115.

[16] Chanda M,Roy SK. Plastics Technology Handbook, Marcel Dekker, New York; 1998.

[17] Anderson JC. Tribol. Int. 1982; 15:43-7.

[18] Kontou E, Niaounakis M. Polym. 2006; 47:1267-1280.

[19] Kim S, Do I, Drzal LT. Polym. Compos. 2010; 31:755-61.

[20] Dutta N K, Birley AW. Plast. Rubb. Proc. Appln. 1983; 3:237.

[21] La Mantia FP, Acierno D. Eur. Polym. J. 1985; 21:811-3.

[22] La Mantia FP, Valenza A, Acierno D. Eur.Polym. J. I986; 22:647-52.

[23] Zhao Y, Liu S, Yang D. Macromol. Chem. Phys. 1997; 198:1427-36.

[24] Philip K, George KE. Doctoral dissertation, Cochin University of Science & Technology; 1992.

[25] Datta NK, Birley AW. Plast. Rubber Process. Appl. 1982;2:237-245.

[26] Laguna O, Collar EP, Taranco J. J. Appl.Polym. Sci. 1989; 38:667-85.

[27] Brydson JA. Plastics materials. Butterworth-Heinemann, 1999;205-246.

[28] Bremner T, Rudin A, Cook DG. J. Appl. Polym. Sci. 1990; 41:1617-27.

[29] Spalding MA, Kirkpatrick DE, Hyun KS. Polym. Eng. Sci. 1993; 33:423-30.

[30] Fujiyama M, Kawasaki Y. J. Appl. Polym. Sci. 1991; 42:481-8.

[31] Han CD. Multiphase Flow in Polymer Processing, Academic Press, New York; 1981.

[32] Liang JZ, Ness JN. Polym. Test 1997; 16:379-89.

[33] Dumoulin, MM, Uttracki LA, Carreau PI. Two Phase Polymer Systems,Hanser Publishers, Munich; 1991.

[34] Wang X, Jin R, Li H. J. Mater. Sci. Technol. 1995; 46-52.

[35] Rohn CL. Analytical polymer rheology: structure-processing-property relationships,Hanser; 1995.

[36] Robeson ML. Polymer Blends: Comprehensive Review,Hanser Gardner Publisher; 2007.

[37] Utracki LA. Polymer Blends, RAPRA Review Reports. 2000; 11:1-170.

[38] Velankar S, Van Puyvelde P, Mewis J, Moldenaers P. J. Rheol. 2004; 48:725-44.

[39] Zheng Q, Zuo M, Peng M, Shen L, Fan Y. Front Mater. Sci. China 2007; 1:1-6.

[40] Utracki LA. Polymer Blends Handbook, Kluwer Academic Publishers; 2002.

[41] Hu SR, Kyu T, Stein RS. J. Polym. Sci. Part B Polym. Phys. 1987; 25:71-87.

[42] Lee H, Cho K, Ahn TK, Choe S, Kim IJ, Park I, Lee BH. J. Polym. Sci. Part B Polym. Phys. 1997; 35:1633-42.

PREPARATION AND EVALUATION OF MONOCLINIC AND TETRAONAL NANOZIRCONIA REINFORCED HMHDPE/LLDPE BLEND

Nanocomposites based on 80/20 HMHDPE/LLDPE blend were fabricated by melt mixing in a Thermo Haake Rheocord mixer with two different zirconia nano powders (m-ZrO$_2$ and t-ZrO$_2$), followed by injection moulding. These two different fillers were dispersed in the matrix in order to investigate the influence of the crystalline phase, size and morphology of the filler on the properties of the composite. Both the fillers can be dispersed well in the polyolefin blend matrix. The effects of nano fillers on the mechanical, thermal, rheological and morphological characteristics of nanocomposites were evaluated. In both cases significant improvement in mechanical properties are obtained. The interfacial interactions between these porous fillers and the polymer matrix improve the mechanical properties even without any surface modification to both the filler and the matrix. Further, the composites show a higher thermal stability with respect to the neat blend. The reinforcement effect of the nanofiller and the polymer matrix is found to be due to the mechanical interlocking between the polymer chain and the porous filler particles, as observed from the FTIR studies of the nanocomposites. The micro structure investigation of the nanocomposite through SEM also confirms enhanced interactions of polymer chains and the filler. Irrespective of their crystalline phase, size and morphology, both fillers are capable of producing a similar enhancement of composite features.

5.B.1 Introduction

Nanotechnology has contributed to the creation of smart functional materials, devices and systems through manipulation of matter in the nanometer scale, and exploitation of novel phenomena and properties which arise because of the nanometer size. Polymer nanocomposites (PNCs) are a class of composite material comprising of two phases, a continuous

phase that is the organic polymer matrix and a discontinuous phase that is the filler which is having at least one dimension in nanometer length scale [1]. Nanomaterials have emerged as the ultimate reinforcing agents for polymers and modification of polymer blends with nanofillers is an exciting area because of the myriad number of choices available. Significant improvements in properties were observed for PNCs with low filler loading compared to the pure polymers or conventional particulates composites [2].

The uniqueness of nanoparticles is that their properties can be tuned by controlling the size, morphology and composition of constituents. There is a wide spectrum of nanomaterials which include metal oxides (nanosilica nanoalumina, nanozirconia, nanozincoxide, etc.) nanoclay, nanocellulose, carbon nanotubes, graphene etc. Many researchers have paid attention to the role of these nanofillers on the thermoplastics, because the significant improvement in properties at very low concentrations [3-8].

Polyolefins are extensively used as a matrix for PNCs has become the general norm due to their wide spectrum of properties finding applications in diverse fields. Among thermoplastic polymers, polyethylenes are of technological interest since they can be easily processed. Polyolefins can be further subdivided into several grades for different applications depending on density, crystallinity and molecular weight. High molecular weight high density polyethylene (HMHDPE) is extensively used due to its versatile properties like mechanical strength, low cost, and resistance to chemical and biological attack. Linear low density polyethylene (LLDPE) is a substantially linear polymer with significant numbers of short branches. The major application of LLDPE is in packaging industry for film

production, because of its high tear and impact strength. In recent years blends of various polyolefins have received much attention due to the improved processability and mechanical properties. Many authors have already reported the improvements of the physicomechanical properties of the polyethylene blends by the incorporation of various inorganic nanofillers [9-11].

Nanozirconia is a versatile material with diverse applications due to its innate mechanical property and thermal stability. The use of nanozirconia (n-ZrO$_2$) on the performance of polyethylene blend is a very creative research area these days. n-ZrO$_2$ has generated a greater amount of research interest owing to its fascinating properties [12-14]. Good chemical and dimensional stability, mechanical strength, toughness, and Young's modulus similar to that of stainless steel alloys make zirconia an excellent ceramic biomaterial. Zirconia has been shown as to be biocompatible as titanium and it has been widely used to build prosthetic devices due to its good mechanical strength [15-17]. Zirconia has three crystalline phases: monoclinic, tetragonal, and cubic. Monoclinic phase is thermodynamically stable at room temperature, while tetragonal and cubic phases exist at high temperatures (>1170 $^{\circ}$C and >2370 $^{\circ}$C, respectively) [18,19].

Mishra *et al.* [20] studied the effect of n-ZrO$_2$ on mechanical and thermal stability of PEEK nanocomposites and they found improvement in both areas with the increase of the nanozirconia content. The inclusion of zirconium particles into a UHMWPE matrix can effectively reduce the wear rate of the component without sacrificing the impact toughness [21]. Epoxy-ZrO$_2$ nanocomposites with good particle distribution improve the overall toughening mechanism of the neat epoxy [22]. R.V. Kurahatti *et al.*

investigated effect of the friction and dry sliding wear behavior of nanozirconia filled bismleimide (BMI) composites, and they concluded that hardness and wear resistance of BMI nanocomposites considerably improve with increasing content of ZrO_2 [23].

In the present study it is proposed to investigate the use of two different zirconia nano fillers (m- ZrO_2 and t- ZrO_2) synthesized by PVA assisted sol-gel method (as described in Chapter 3) to modify the properties of HMHDPE/LLDPE blends.

5.B.2 Methodology
5.B.2.1 Materials and sample preparations

80% HMHDPE/ 20% LLDPE were blended with 0.5, 1, 1.5, 2, 2.5, 3 wt % of the synthesized zirconia (NZR) fillers (m- ZrO_2 and t- ZrO_2) separately. The blends containing 0 weight% filler are designated as HL-2. The blends containing monoclinic crystallite form of zirconia (m-ZrO_2) are designated as HL-2-XmNZR, where X is 0.5, 1, 1.5, 2, 2.5, 3 wt% of m-ZrO_2 (e.g., HL-2-0.5mNZR) and for the composite containing tetragonal crystallite form of zirconia (t-ZrO_2) were designated as HL-2-XtNZR, where X is 0.5, 1, 1.5, 2, 2.5, 3 wt% of t-ZrO_2 (e.g., HL-2-0.5tNZR). For the fabrication of polymer blend nanocomposites first the polymer pellets were fed into the mixing chamber of Thermo Haake Rheomix Poly Lab system equipped with roller type rotors at 50rpm set at a temperature of 160 ^oC. A mixing time of 8 minutes was allowed to complete the reaction; and the torque to become steady. After 2 minutes of mixing, required quantities of zirconia filler were added according to their corresponding weight%. Procedure for

the preparation of polymer blend nanocomposites strategy is shown in Scheme 5. B.1
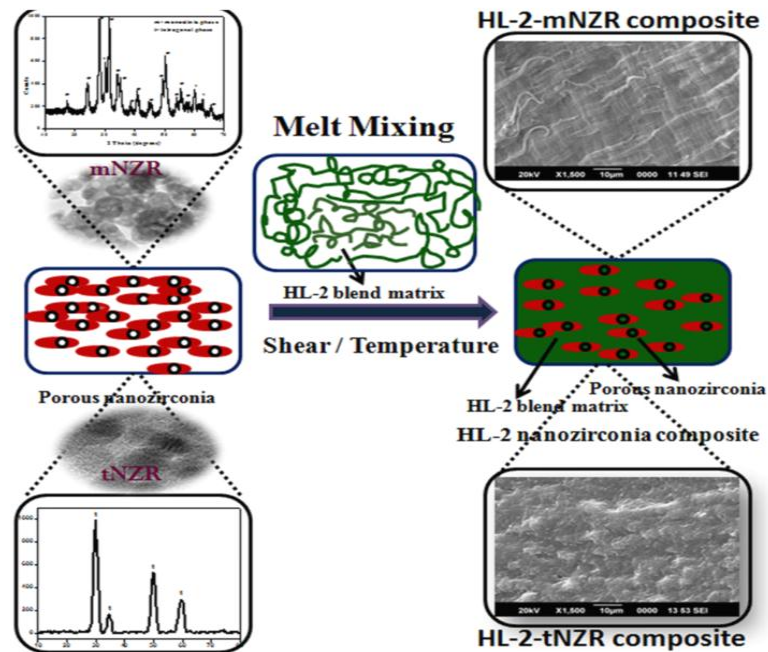
Scheme 5.B.1 Schematic diagram of polymer nanozirconia composites

5.B.3 Results and discussion

5.B.3.1 Mechanical properties

5.B.3.1.1 Tensile properties

Nanozirconia has high intrinsic strength which helps to act as excellent filler for the fabrication of composites with superior thermo-mechanical properties. Large surface area and porosity are the highlights of nano sized zirconia which facilitates dispersion of fillers and enables it to act as reinforcement in the composite. Besides, the matrix/filler interface interactions facilitates mechanical load transfer from matrix to filler improvising the

stiffness and strength. The influence of NZR on the mechanical performance of HL-2-NZR composites was evaluated in terms of the tensile, flexural, notched impact and hardness property measurements. Substantial improvements in the mechanical properties were obtained as expected, even without any surface modification. The development in mechanical properties of the HL-2-NZR composites was similar to the behavior reported earlier by Panaitescu *et al.* [24]. They observed an increase in the tensile performance with the incorporation of nanoSiO$_2$ and Al$_2$O$_3$ in low density polyethylene.
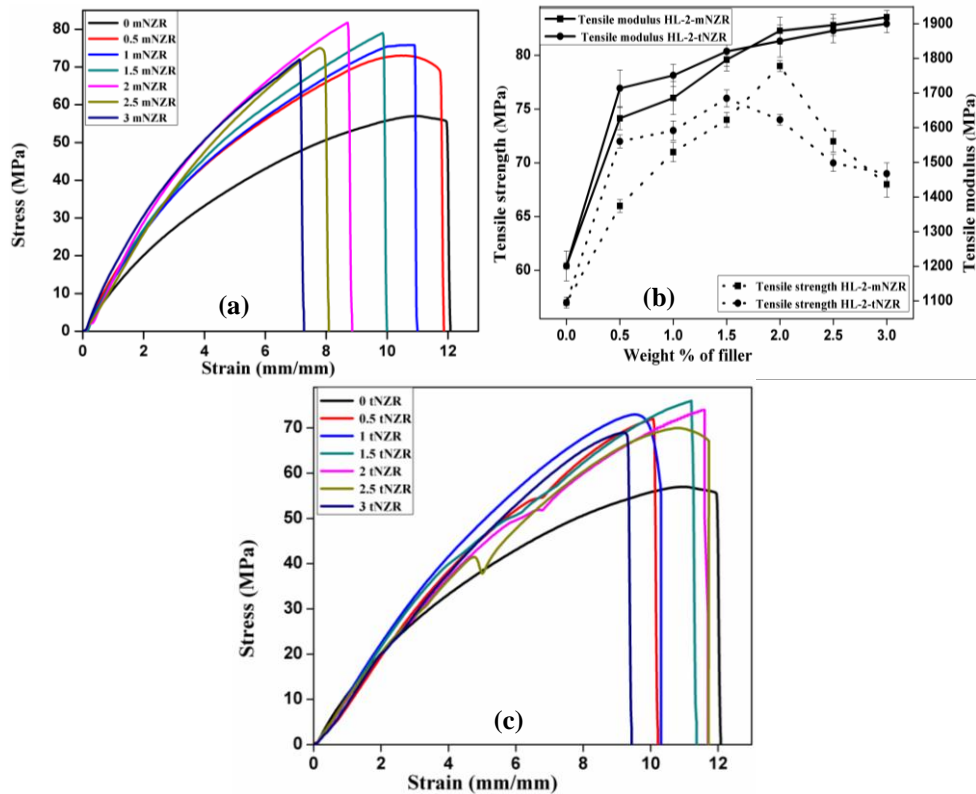
Figure 5B.1 **Tensile properties of HL-2-NZR composites (a) stress-strain curves of HL-2-mNZR composites (b) stress-strain curves of HL-2-tNZR composites (c) variation of tensile strength and tensile modulus of both m-ZrO$_2$ and t-ZrO$_2$ composites**

The tensile stress-strain curves of the pure HL-2 blend and the nanocomposite filled with different loadings of m- ZrO_2 and t- ZrO_2 are shown in Figure 5(a) and (b) respectively. As the NZR loading increases in both cases ultimate tensile strength increases and attains a maximum for the composite loaded with 2 weight % of m-ZrO_2 and with 1.5 weight % of t-ZrO_2 and then decreases. An increase of 38% in tensile strength is observed for HL-2-2mNZR and 33% for HL-2-1.5tNZR. This can be attributed to good filler dispersion and effective interaction of nanozirconia with HL-2 blend matrix at this composition leading to an effective stress transfer. [25]. The decrease in tensile strength after reaching the peak value can be due to the aggregation of filler which leads to stress field concentration in and around the aggregates in matrix leading to speedy propagation of the initiated crack [26, 27].

The elastic modulus of the composites almost doubles with respect to that of neat HL-2 blend matrix at 3 weight % NZR loading, in agreement with literature data concerning various thermoplastic matrices reinforced with various ceramic fillers [28-32]. Increase in the elastic modulus is that the filler can restrain the mobility of the polymer chains in the vicinity of each particle. In addition, elongation at break (EB) value decreases steadily with increasing filler loading as evident from the stress-strain plot which are in accordance with previous studies on HDPE-hydroxyapatite system [28, 29, 32]. The variation in strain to failure for nanocomposite is different for different systems. Typically addition of hard and rigid nanofiller to a moderately crystalline polymer irrespective of filler matrix interaction arrests the elongation and hence the deformation [33].

5.B.3.1.2 Flexural properties
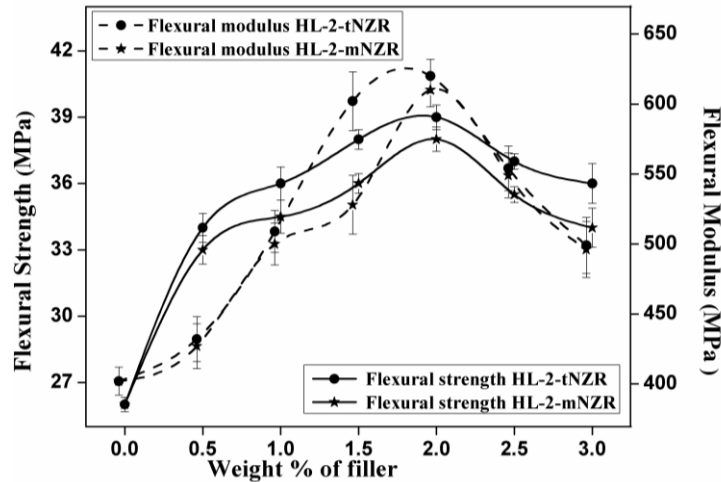
**Figure 5 B.2 Variation of flexural strength and flexural modulus
of both m- ZrO$_2$ and t- ZrO$_2$ composites**

An increasing trend is observed in the flexural strength and flexural modulus with increase of NZR content till 2 wt % for both the cases and thereafter a slight decrease is noted. Enhancement in flexural strength by 46% is achieved by the addition of 2wt% m- ZrO$_2$ and 50% for tNZR. Here modulus increases by 52% for m- ZrO$_2$ composites and 54% for t- ZrO$_2$ composites. Better filler dispersion and effective interaction of nanoparticles results in behavior at this particular level of filler loading. At higher particulate loadings, nanoparticles tend to form agglomerates and aggregates leading to diminished physicals, still better than that for the neat blend. The better development in flexural properties strongly supports the enhanced load bearing capacity of the composites.

5.B.3.1.3 Impact strength

Impact strength denotes the ability of the composite to resist the fracture under stress applied at high speed. The notched izod impact strength of the composites is represented in Figure 5.B. 3.
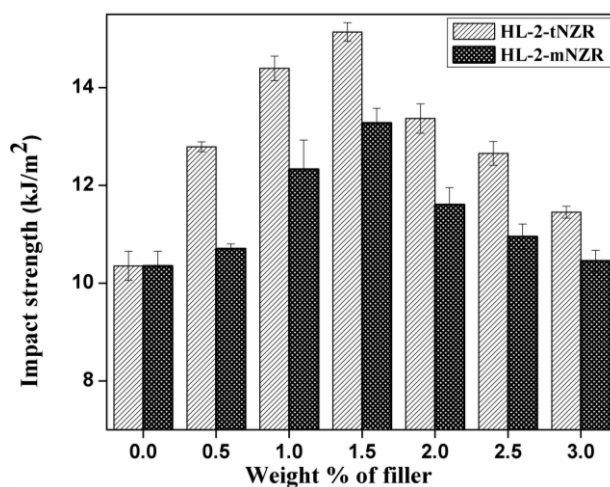
Figure 5 B.3 Variation of impact strength of both m-ZrO₂ and t-ZrO₂ composites

The effect of both m-ZrO$_2$ and t- ZrO$_2$ on the notched izod impact strength values of HL-2 blends is particularly of great interest; the nanocomposite achieved about a 33%, enhancement in impact strength compared to pure blend for m-ZrO$_2$ filler at 1.5 weight % loading and 46% for t-ZrO$_2$ loading at the same composition. The impact properties of a material, especially a polymer is directly proportional to the overall toughness of that material. Application of rigid fillers to toughen polymers has also been received ample attention [34]. This states that when a nanocomposite is under impact loading, the interfacial region resists crack propagation more effectively than the neat polymer matrix. This is due to

the large surface area provided by the nanoparticles and its improved dispersion in the polymer matrix. At higher NZR loading the nanoparticles form aggregates and these act as points of stress concentration where cracks get initiated and the critical crack size increases that cause composite failure.

5.B.3.1.4 Surface hardness (Shore D)
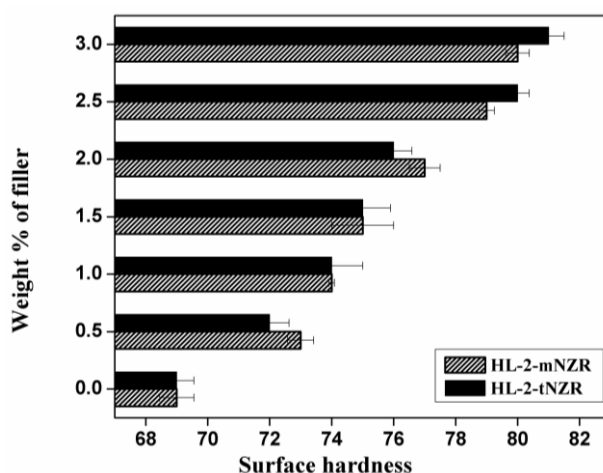
Figure 5 B.4 Variation of Surface hardness values obtained from a hand operated durometer of both m-ZrO$_2$ and t- ZrO$_2$ composites

The hardness value indicates the ability of a material to stand firm to the local surface deformation and it stands for the degree of compatibility. There is a substantial rise in hardness with the addition of both NZR loadings. The enhancement in hardness by the addition of NZR is due to the inherent characteristics of the ZrO$_2$ particle; it possesses strong inter atomic ionic bonding, resulting in desirable material properties. The increased confinement of PE chain in the nanocomposites also contributes to the hardness. In the case of matrix reinforced with

nanoparticles, the size of the nanoparticles around ~10nm is comparable with average random coil size (~10nm) of polymers [35].

5.B.3.2 FTIR spectroscopy

Figure 5 B.5 shows the FTIR spectra of the HL-2 blend, NZR, and the HL-2-2-mNZR composite.
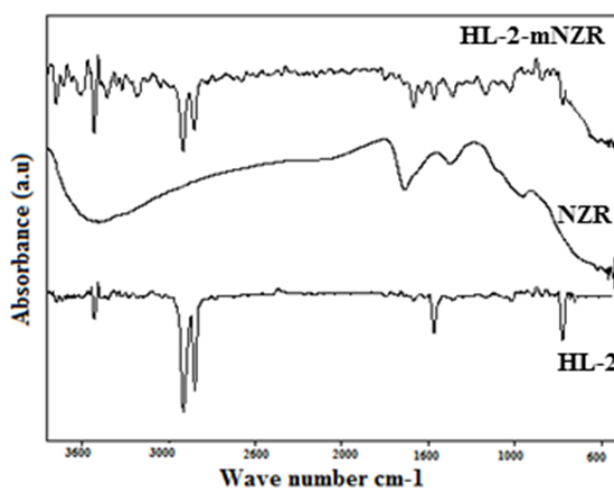
Figure 5 B.5 FTIR analysis of HL-2-mNZR composites

The strong peaks at 2912 and 2848 cm^{-1} represent the symmetric and asymmetric -C-H stretching modes of the -CH$_2$ groups in the PE blend. Weak bands around 1464cm^{-1} and 3429cm^{-1} indicate -C-H deformation and skeletal -C-H stretching frequency respectively. The weak bands around 1200–800 cm^{-1} correspond to the C-C stretching frequency. The characteristic peaks of m-ZrO$_2$ as explained in chapter 3 and also the peaks of pure HL-2 blend remain unaltered in HL-2-2mNZR composite, which suggests there exist mechanical interlocking (physical interaction) between the filler and the matrix.

5.B.3.3 Microstructure analysis

5.B.3.3.1 SEM analysis

Morphological analysis of tensile fractured surfaces of neat HL-2 blend and HL-2-2mNZR and HL-2-2tNZR composites are given in Figure 5 B.6.
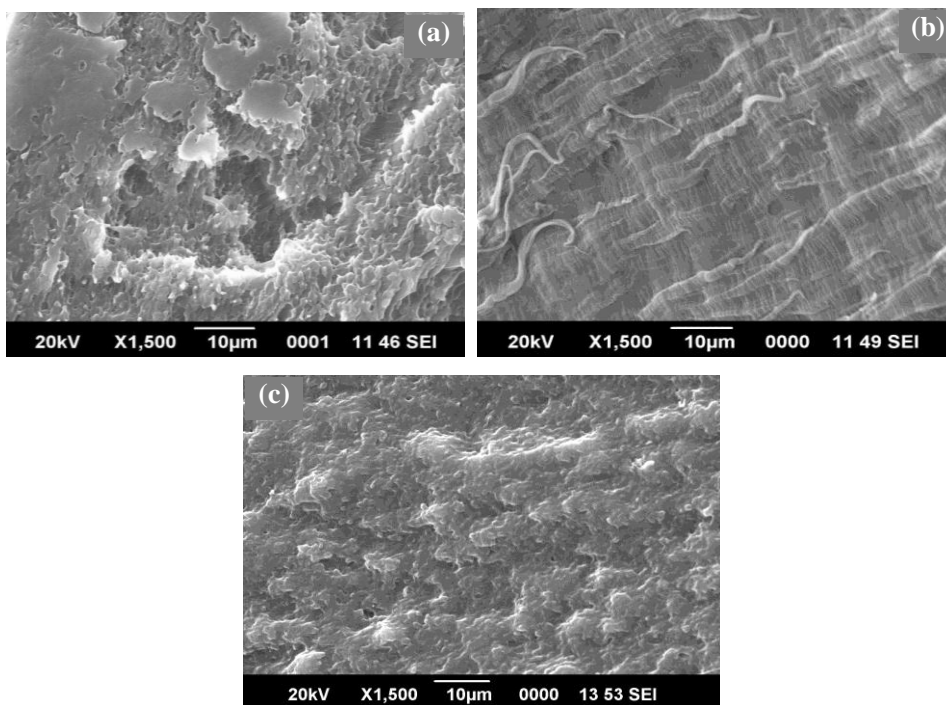
Figure 5 B.6 SEM images of tensile fractured surfaces of (a) HL-2 (b) HL-2-2mNZR and (c) HL-2-2tNZR

SEM is a significant measure of the morphological changes of PNCs. It can be seen in Figure 5 B. 6 (a) that for tensile fractured surface, neat HL-2 blend exhibits a relatively smooth surface with occasional valley patterns with several voids. These voids may adversely affect the physicomechanical properties of the matrix polymer. Fractured specimen of HL-2-2mNZR composites [Figure 5 B.6 (b)] supports that when the

filler (m-ZrO$_2$) is added; the fine, porous particles will occupy the voids uniformly, providing more reinforcement to the base polymer. The failure surface of the composites shows signs of higher energy absorption by the presence of irregularities (dark and bright regions) and wavy texture. Thus the improved homogeneity increases the tensile and flexural properties. This result is in complete agreement with the observed mechanical properties. Figure 5. B 6(c) is the SEM images of tensile fractured surface of HL-2-2tNZR composite which show that the surface is much rougher compared to neat HL-2 matrix with larger number of undulations and there is a drastic reduction in micro voids. The increased ductility is an indication of good interaction of t-ZrO$_2$ particles with the HL-2 matrix.
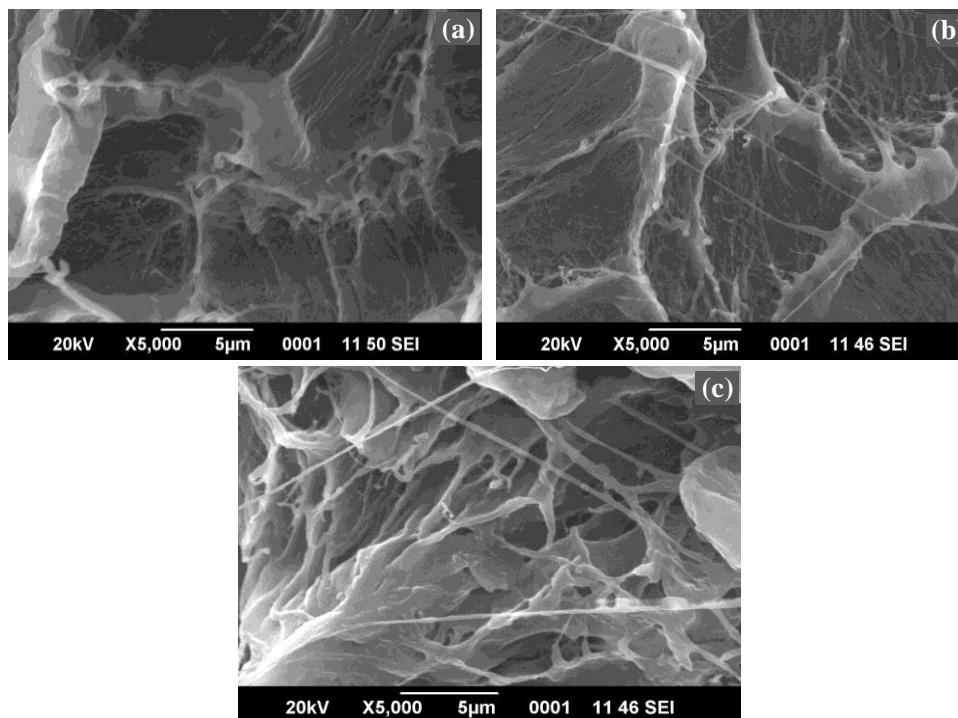
Figure 5 B.7 SEM images of impact fractured surfaces of (a) HL-2 (b) HL-2-2tNZR and (c) HL-2-2mNZR

The SEM micrographs of the impact fractured surface for the pure blend and the composites are shown in Figure 5 B.7 (b) and (c). Considerable difference is noticed between failure surface of neat blend and that of the NZR composite system. On the addition of NZR, the failure surface becomes rough which indicates that the crack propagation is difficult and there is increased energy absorption. Hence the crack propagation follows a much difficult track for failure and leads to high strength.

5.B.3.3.2 TEM analysis

Figure 5 B.8 present a general sight on the dispersion of t-ZrO_2 nanoparticles in the HL-2 matrix. TEM bright field images of 2 weight % t-ZrO_2 in the HL-2 matrix are shown in Figure 5 B.8 (a) and (b).
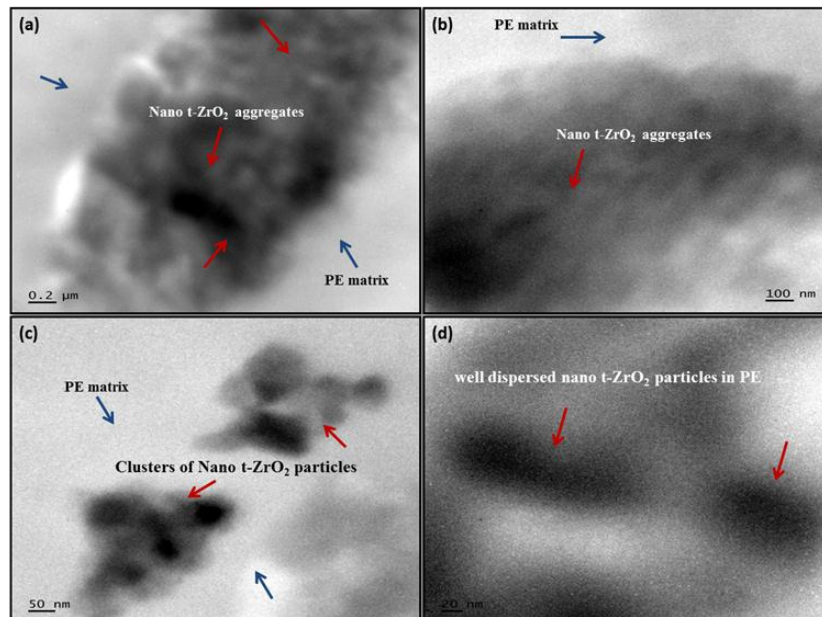
Figure 5 B.8 Bright field TEM images of HL-2-2tNZR nanocomposite at different magnifications. (a) and (b) showing PE matrix and dispersed t-ZrO_2 nanoparticles in the matrix along with some aggregates, well dispersed individual spherical t-ZrO_2 nanoparticles in the PE matrix are seen in (c) and (d)

The dark phase indicated by red arrows is the filler and the bright phases denoted by blue arrows are the PE matrix phase. TEM micrograph of the nanocomposite evidenced that the t-ZrO_2 nanoparticles are randomly dispersed in the polymer matrix. Highly magnified TEM micrographs [Figure 5 B.8 (c) and (d)] clearly depict the well dispersed spherical t-ZrO_2 nanoparticles in the PE matrix.

5.B.3.4 Melt rheological analysis
5.B.3.4.1 Melt flow index (MFI)

Figure 5 B.9 shows the variation of the melt flow index of HL-2 blend upon NZR loading.
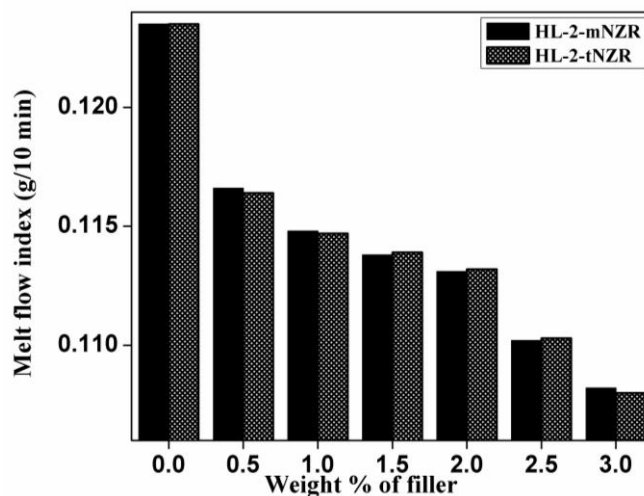
Figure 5 B.9 Variation of MFI of HL-2-NZR composites with m-ZrO_2 and t-ZrO_2 loading

It is evident that the incorporation of both types of NZR to HL-2 blend decreases the MFI values of the composites. Low melt flow index indicates higher melt viscosity of matrix. The addition of NZR to the blend increases the viscous as well as elastic response of the system due to

better filler-matrix interaction. Also, when solid particles are present in the matrix, they restrict the melt movement by increasing viscosity, which implies the hardening effect of the filler [36]. The melt flow index (MFI) also throws light on the degree of chain entanglement of the polymer via formation of physical or chemical cross links [37]. The low melt flow indices at higher concentration of the fillers are apparently due to the increased entanglement of the polymer chains of HL-2 blend and the filler. The results are in good agreement with the identified ability of the filler to increase the intermolecular forces between the polymer chains via physical bonds and also to restrict chain mobility by the presence of these filler in the vicinity of the polymer chains.

5.B.3.4.2 Dynamic rheological analysis (DRA)

Rheological properties of polymer are very sensitive to the variations of polymer composition and structure. For HL-2-NZR composites the molten HL-2 matrix, solid NZR particles can each have appreciable effect on the rheological behavior of the composite materials. Figure 5 B.10 shows the complex viscosity, storage (G'), loss (G") moduli and tan δ as a function of frequency for neat HL-0, LH-0, HL-2 blend and the HL-2-2mNZR composites. First, it can be noted that the addition of m-ZrO_2 marginally improves storage modulus and loss modulus than HL-2 matrix in the entire frequency range. The HL-2-mNZR composites exhibit significantly higher storage and loss modulus than LH-0 but much lower values than HL-0 at lower frequency region. These observations are in consistent with the result obtained by M. Zhang and U. Sundararaj for LLDPE/PEMA/clay system [38]. Both storage and loss modulus gradually approach those of LH-0 and HL-0 at high frequency region.
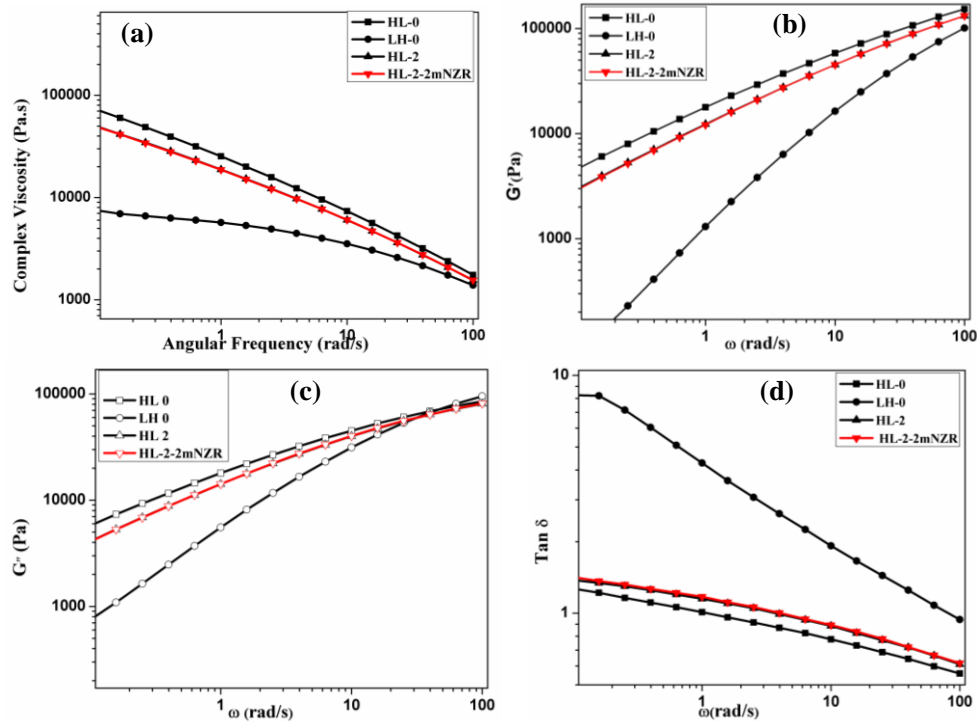
Figure 5 B.10   Rheological observations of HL-2-2mNZR composites
(a) Variation of complex viscosity as a function of frequency
(b) Variation of storage modulus as a function of frequency
(c) Variation of loss modulus as a function of frequency and
(d) Variation of tanδ as a function of frequency

Figure 5 B.9 (a) shows logarithmic plots of complex viscosity versus frequency for neat LH-0, HL-0, HL-2 blend and HL-2-2mNZR nanocomposites. Complex viscosity of the nanocomposite has slightly higher value over entire frequency region, while that has lower value than HL-0 and higher value than LH-0 at lower frequency region. The enhancement in complex viscosity of the nanocomposite at lower frequency region clearly indicates enhanced interaction between the filler and the HL-2 matrix by interfacial reactions in the melt. These results are in accordance with what was already observed for other similar systems [39-42].

The variations of storage modulus (G'), loss modulus (G") with frequency for the pure polymers, blend as well as blend containing t- ZrO_2 are shown in Figure 5 B.11 (b) and (c).
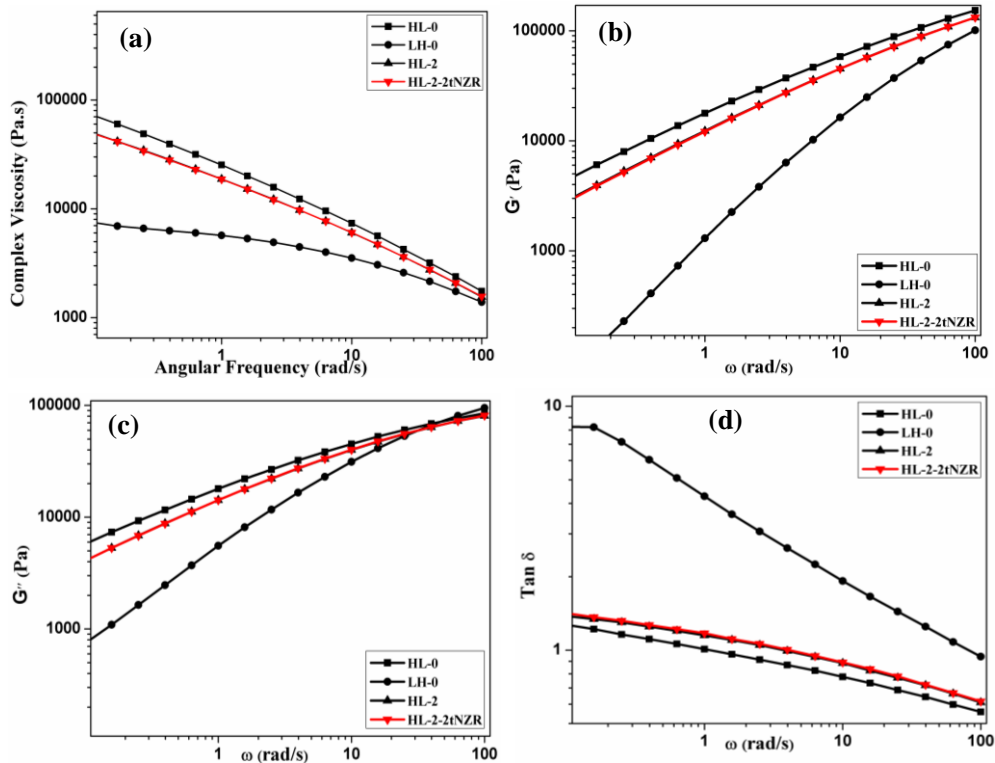
Figure 5 B.11 Rheological observations of HL-2-2tNZR composites
        (a) Variation of complex viscosity as a function of frequency
        (b) Variation of storage modulus as a function of frequency
        (c) Variation of loss modulus as a function of frequency and
        (d) Variation of tanδ as a function of frequency

The composite prepared at uniform melt compounding conditions and contain 2 weight% t-ZrO_2. A slight improvement is observed for the nanocomposites for the storage and loss modulus than pure blend at lower frequency region, as observed in the case of composites containing m-ZrO_2 loading.

Figure 5 B.11 (a) shows the variations of complex viscosity with frequency on a log scale for the pure polymers, blend as well as the blend nanocomposites containing 2 weight% t-ZrO$_2$. As it can be seen, for all nanocomposites, complex viscosity is decreasing with increasing frequency. For composite containing t-ZrO$_2$, the complex viscosity is above that of pure blend. This is attributed to particle-particle interaction as an important parameter in increasing the viscosity. The improvement in complex viscosity than the blend indicates more filler-matrix interaction and better dispersion of t-ZrO$_2$ particles in the polymer matrix.

From these observations it can be clearly observed that both m-ZrO$_2$ and t-ZrO$_2$composites have lower complex viscosity, storage modulus as well as loss modulus than HL-2 matrix can be easily processable.

5.B.3.5 Thermal properties
5.B.3.5.1 Thermogravimetric analysis
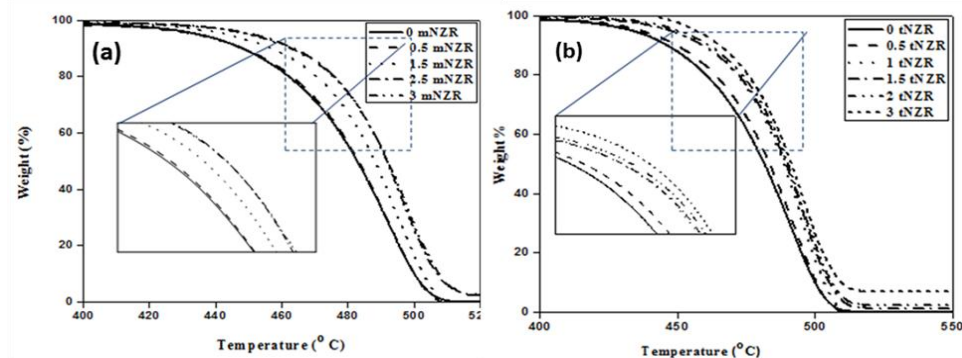
Figure 5 B.12   Thermogram of (a) HL-2-mNZR composites and (b) HL-2-tNZR composites

TGA was performed on neat HL-2 blend and NZR filled HL-2 composite to study the effects of NZR on the thermal stability of the composite. The TGA results of the m-ZrO$_2$ nanocomposites are shown in

Table 5.1. Figure 5. B.12 (a) shows weight loss vs temperature curve for the m-ZrO_2 nanocomposites. All the nanocomposites have improved thermal stability than that of virgin HL-2 blend matrix. Degradation of pristine HL-2 blend starts at 426 °C. This is mainly due to pyrolysis of polymer chains. On addition of m-ZrO_2, degradation of the composite shifts to a higher temperature compared to neat blend. This indicates that there is a good interaction between the PE matrix and m-ZrO_2 nanofillers. There is considerable enhancement in T_{onset} (onset thermal degradation temperature), T_{10} (temperature for 10% mass loss) and T_{50} (temperature for 50% mass loss) for HL-2-NZR composites with m-ZrO_2 loading. The incorporation of a low concentration of m-ZrO_2 promotes thermal stability, increasing the degradation temperature by about 23 °C at 3 weight%. Since zirconia is a thermally stable ceramic material, the rigid and hard nano m-ZrO_2 particles act as barriers arresting volatile degradation of polymer matrix. Incorporation of nanozirconia reduces the chain mobility of the polymer matrix by generating numerous restriction sites which reduces the intrinsic thermal vibration of skeletal C–C bonds [43-45]. This results in high demand of thermal energy for the decomposition of polymer matrix which in turn enhances the thermal stability. Char formation, which act as a physical barrier between the polymer and the superficial zone where the polymer combustion is taking place also enhances the thermal stability by limiting the entry of oxygen [46]. Finally, the residues of the m-ZrO_2 based composites are in good agreement with their initial composition.

Table 5.1 Thermal properties of HL-2-mNZR nanocomposites

m-ZrO$_2$ content (wt%)	Temperature at different mass losses (°C)			Peak max (T$_{max}$, °C)	Residue at 600 °C (%)
	T$_{Onset}$	T$_{10\%}$	T$_{50\%}$		
0	426	448	483	491	0.08
0.5	436	448	484	492	0.64
1.5	444	457	488	495	1.70
2.5	448	463	492	498	2.24
3	449	465	493	499	3.10

Figure 5 B.12 (b) represents the thermogram of neat HL-2 blend and (b) HL-2-tNZR composites and the results are tabulated in Table 5.2.

Table 5.2 Thermal properties of HL-2-tNZR nanocomposites

t-ZrO$_2$ content (wt%)	Temperature at different mass losses (°C)			Peak max (T$_{max}$, °C)	Residue at 600 °C (%)
	T$_{Onset}$	T$_{10\%}$	T$_{50\%}$		
0	426	448	483	491	0.08
0.5	434	450	483	493	0.66
1	437	457	488	494	1.02
1.5	445	458	489	494	1.70
2	449	459	491	496	2.24
3	450	461	492	450	3.14

As in the case of m-ZrO$_2$ composites addition of t-ZrO$_2$ improves the thermal stability of neat HL-2 blend. By the addition of 3 weight % of t-ZrO$_2$, the temperature at which maximum degradation (T$_{max}$) takes place is increased by 23 °C for HL-2 matrix. Temperature required for weight loss at different percentage is higher for the HL-2-tNZR composite compared to neat HL-2 blend at all stages of degradation. The enhanced stability as in the case of HL-2-mNZR composites can be explained by the restricted mobility of polymer chains due to the strong interaction with

t-ZrO$_2$ particles limiting the diffusion of the volatile combustion products throughout the composites. The residual weight loss is almost proportional to the initial t-ZrO$_2$ content introduced into the composite. Yet again, the improvement of the thermal stability is unaffected by the nature of filler (whether it is monoclinic or tetragonal) dispersed in the polymer matrix.

5.B.3.5.2 Differential Scanning Calorimetry

DSC is used for studying the crystallization characteristics of polymers and their composites. The effect of size and morphology of the zirconia fillers on T$_m$ and crystallinity of HL-2 matrix was evaluated. DSC cooling and heating curves of neat HL-2 blend and 2 weight% loaded m- ZrO$_2$ and t- ZrO$_2$ nanocomposites are shown in Figure 5.B.13. The crystallization temperature (T$_c$), apparent melting temperature (T$_m$), corresponding enthalpies (ΔH_c and ΔH_m) and percentage crystallinity (χ_c) of the composites and the neat blend are given in Table 5.3.
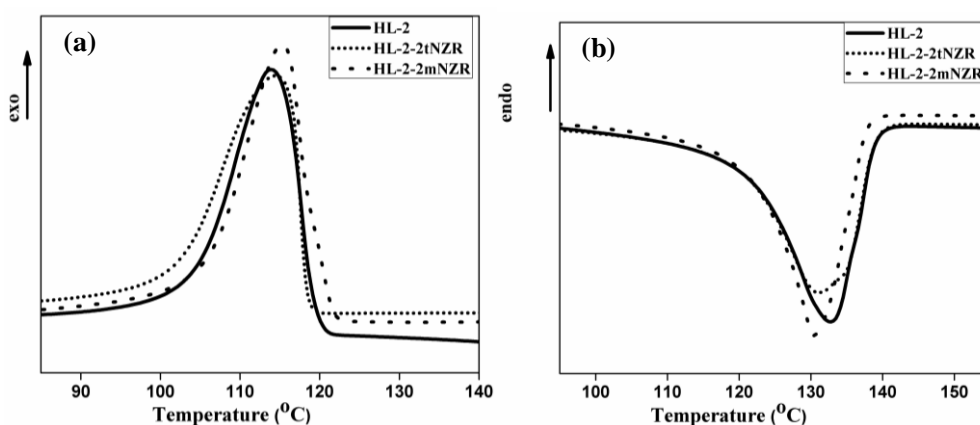
Figure 5 B.13 Non-isothermal crystallization studies (a) Cooling (b) Melting behavior of HL-2-mNZR and HL-2-tNZR composites

Table 5.3 **Non-isothermal crystallization characteristics of HL-2-NZR composites**

Sample	T_m (°C)	ΔH_f (J/g)	T_c (°C)	ΔH_c (J/g)	χ_c (%)
HL-2	133	145	109	162	61.86
HL-2-2mNZR	130	148	111	138	63.19
HL-2-2tNZR	131	137	115	137	58.4

DSC shows no remarkable change in T_m. At the same time, T_c is slightly improved. This confirms weak nucleating effect of NZR on HL-2 matrix.

5.B.4 Conclusions

HL-2-NZR nanocomposites were fabricated by incorporating NZR into the PE matrix through melt mixing followed by injection moulding. The NZR fillers used differed in size, crystalline phase, morphology and specific surface area. Static mechanical, rheological and thermal properties of m-ZrO$_2$ and t- ZrO$_2$ reinforced nanocomposites were analysed. The HL-2-mNZR nanocomposites with 2 weight% m-ZrO$_2$ loading showed an enhancement of 38% in tensile strength, 43% in tensile modulus, 46% in flexural strength and 52% in flexural modulus compared to pure matrix. While HL-2-tNZR nanocomposites furnished an improvement of 33% in tensile strength, 53% in tensile modulus, 50% in flexural strength and 54 % in flexural modulus at 1.5weight % t-ZrO$_2$ loading. Impact strength shows a 33% and 46% improvement at 1.5 weight % m-ZrO$_2$ and t-ZrO$_2$ filler addition. The entanglement between the polymer chains and the porous nanozirconia was substantiated by the FTIR studies and MFI analysis. Morphological characterization by SEM on the fractured surface of the nanocomposite shows the better dispersion and interfacial addition of both

types of NZR in the HL-2 matrix and is correlated with their mechanical performance. With the inclusion of NZR into the HL-2 matrix the thermal stability has been drastically increased, as evidenced from the TGA analysis. Thus, HL-2 blend matrix can be considerably reinforced by the incorporation of small amounts of zirconia nano fillers even without any surface modification. Both types of NZR fillers act as a weak nucleating agent for HL-2 matrix. The study also proves that the addition of NZR has a salutary effect on the thermo mechanical properties of PE matrix. Regardless of the zirconia nanofillers properties, the rheological properties are also modified. Both types of fillers gave a similar enhancement of the composite feature. The results give credence to the dependence on NZR dispersion for any significant improvement in properties.

References

[1] Giannelies EP. Polymer layered silicate nanocomposites, J. Adv. Mater.1996; 8:29–35.

[2] Paul DR, Robeson LM. Polymer 2008; 49:3187-204.

[3] Meng J, Hu X. Polymer. 2004; 45:9011-8.

[4] Dorigato A, Pegoretti A, Penati A. Express Polym. Lett. 2010; 4:115-29.

[5] Panaitescu D, Ciuprina F, Iorga M, Frone A, Radovici C, Ghiurea M, Sever S, Plesa I. J. Appl.Polym. Sci. 2011; 122:1921-35.

[6] Zhao H, Li RK. Polymer. 2006; 47:3207-17.

[7] Fang L, Leng Y, Gao P. Biomaterials. 2005; 26:3471-8.

[8] Zhang J, Wang X, Lu L, Li D, Yang X. J. Appl.Polym. Sci. 2003; 87:381-5.

[9] Scaffaro R, Mistretta MC, La Mantia FP. Polym.Degrad. Stab. 2008; 93:1267-74.

[10] Ren X, Wang XQ, Sui G, Zhong WH, Fuqua MA, Ulven CA. J. Appl.Polym. Sci. 2008; 10:2837-45.

[11] Zonder L, Ophir A, Kenig S, McCarthy S. Polym. 2011; 52:5085-91.

[12] Tanabe K, Yamaguchi T. Catal. Today. 1994; 20:185-97.

[13] Xu BQ, Yamaguchi T, Tanabe K. Appl.Catal. 1991; 75:75-86.

[14] Yokoyama T, Yamagata N. Appl.Catal. A.2001; 221:227-39.

[15] Silva VV, Domingues RZ, Lameiras FS. Compos. Sci. Technol. 2001; 61:301-10.

[16] Denry I, Kelly JR. Dental mater. 2008; 24:299-307.

[17] Manicone PF, Iommetti PR, Raffaelli L. J. Dent. 2007; 35:819-26.

[18] Chraska T, King AH, Berndt CC. On the size-dependent phase transformation in nanoparticulate zirconia. Mater. Sci. Eng. A. 2000; 286:169-78.

[19] Luo TY, Liang TX, Li CS. Stabilization of cubic zirconia by carbon nanotubes. Mater. Sci. Eng. A. 2004; 366:206-9.

[20] Mishra TK, Kumar A, Verma V, Pandey KN, Kumar V. Compos. Sci. Technol. 2012; 72:1627-31.

[21] Plumlee K, Schwartz CJ. Wear. 2009; 267:710-7.

[22] Medina R, Haupert F, Schlarb AK. J. Mater. Sci. 2008; 43:3245-52.

[23] Kurahatti RV, Surendranathan AO, Srivastava S, Singh N, Kumar AR, Suresha B. Mater. Des. 2011; 32:2644-9.

[24] Panaitescu D, Ciuprina F, Iorga M, Frone A, Radovici C, Ghiurea M, Sever S, Plesa I. J. Appl.Polym. Sci. 2011; 122:1921-35.

[25] Li Y, Yu J, Guo ZX. J. Appl.Polym. Sci. 2002; 84:827-34.

[26] Akita H, Kobayashi H. J.Polym. Sci. Part B Polym. Phys. 1999; 37:209-18.

[27] Chang JH, An YU. J.Polym. Sci. Part B Polym. Phys. 2002; 40:670-7.

[28] Fang L, Leng Y, Gao P. Biomaterials. 2006; 27:3701–3707.

[29] Shahbazi R, Javadpour J,Khavandi AR. Adv. Appl. Ceram. 2006; 105:253–257.

[30] Kontou E, Niaounakis M.Polymer. 2006; 47:1267–1280.

[31] Misra RDK, Nerikar P, Bertrand K, Murphy D. Mater. Sci. Eng.A. 2004; 384:284–298.

[32] Wang M, Joseph R. Bonfield W.Biomaterials. 1998; 19:2357–2366.

[33] Wang J, Severtson SJ, Geil PH. Mater. Sci. Eng. A. 2007; 467:172-80.

[34] Zhao H, Robert K, Li Y. Polymer. 2006; 47:3207.

[35] Jancar J, Douglas JF, Starr FW, Kumar SK, Cassagnau P, Lesse AJ, Sternstein SS, Buehler MJ. Polym. 2010; 51:3321-3343.

[36] Albano C, Karam A, Domínguez N, Sánchez Y, González J, Aguirre O, Cataño L. Compos.Struct. 2005; 71:282-8.

[37] Jang BC, Huh SY, Jang JG, Bae YC. J. Appl.Polym. Sci. 2001; 82:3313-20.

[38] Zhang M, Sundararaj U. Macromol. Mater. Eng. 2006; 291:697-706.

[39] Scaffaro R, La Mantia FP, Canfora L, Polacco G, Filippi S, Magagnini P. Polymer. 2003; 44:6951.

[40] La Mantia FP, Scaffaro R, Valenza A, Marchetti A, Filippi S. Macromol.Symp. 2003; 198:173.

[41] La Mantia FP, Canfora L, TzankovaDintcheva N. Polym. Eng. Sci. 2004; 44:1732.

[42] Canfora L, Filippi S, La Mantia FP. Polym.Degrad. Stab. 2005; 45:1297.

[43] Wong CP, Bollampally RS. J. Appl.Polym. Sci. 1999; 74:3396-403.

[44] Pan G, Guo Q, Zhang W, Tian A. Wear. 2009; 266:1208-15.

[45] Lozano K, Barrera EV. J. Appl.Polym. Sci. 2001; 79:125-33.

[46] Beyer G. Fire Mater. 2001; 25:193-7.

.....ೞೕೞ.....

FIBRILLAR NANOSILICA REINFORCED HMHDPE/LLDPE BLEND: PREPARATION AND EVALUATION OF NOVEL NANOCOMPOSITES

Part A

HMHDPE/LLDPE/CGS NANOCOMPOSITES

Nanocomposites of 80/20 HMHDPE/LLDPE blend reinforced with silica nanofibers isolated from Indian grass (CGS) were fabricated through melt mixing in a Thermo Haake rheocord mixer. CGS was isolated from a renewable source by a cost effective route. The mechanical, morphological, rheological and thermal properties of the nanocomposites have been evaluated. Mechanical properties are improved with the incorporation of CGS fibers without any surface modification of both the filler and the polymer matrix. Morphological analysis of tensile fractured surface of the nanocomposite reveals that the silica fibers are well dispersed and distributed as individual fibers in the polymer matrix. FTIR analysis confirms that there is no chemical interaction between the filler and the matrix.TGA analysis shows that thermal stability of the nanocomposites increases with increasing CGS content. DSC analysis suggests a weak nucleating effect of the filler.

6.A.1 Introduction

Nanotechnology is currently a subject of much research and study, and as a result it is developing rapidly. It has great potential for producing improvements and innovations in many areas of life, with benefits of cleaner, faster and safer manufacturing, quicker and smaller device fabrication, increased life of products. The rapid expansion of nanoscience and nanotechnology can be seen from its diverse fields of applications in the physics, biology, engineering, chemistry and computer science [1].

Polymer nanocomposites (PNC) offer the possibility for new patterns in material properties. PNC is a class of hybrid materials consisting of an organic polymer matrix with dispersed inorganic nanofillers embedded in it. The fillers have at least one dimension in nanometer range. Modification with nanofillers results in spectacular improvement in performance at low filler loading without sacrificing the processability of the polymer detrimentally [2, 3].

Among various nanofillers, two of the most extensively investigated particulates are layered silicates and carbon nanotubes. Recently, growing consideration is being paid to low aspect ratio fillers like nanosilica, nanoalumina, nano hydroxyapatite because of their immense applications and low cost. PNC based on nanofillers isolated from natural material have attracted a great deal of interest in fields ranging from the scientific community to the industry because of their renewable origin [4,5]. Natural fillers like natural fibers, fly ash, wood ash, rice husk ash and sawdust offer comparable or superior properties than the commercial fillers such as precipitated silica, carbon black and talc [5, 6].

Recently, nanosilica has received a great deal of importance in various fields. Especially much attention was given to their use in biomedical field for different applications like separation and adsorption of protein, molecular imaging, nucleic acid detection, drug delivery, gene therapy, and for the preparation of scaffolds [7-10]. Nanosilica particulates are used for regenerative medicine applications and tissue engineering [10]. For large scale industrial applications, enormous quantity of nanosilica is needed. The synthetic method is energy extensive and costly; therefore development of an economically viable method to fabricate nanosilica from a silicon-containing biomass material has become inevitable. Silica has long been known to be present in plants; it is one of the macro nutrients in plants, which exist in opal phytolith or silica phytolith. Some agricultural residues are sources of silica and silica-based materials, including silicon, silicon nitrite, silicon carbide, and zeolite [7, 11, 12]. In continuing attempts to reduce processing cost and time, many authors have published the use of rice husk as a raw material for producing silica nano particles [13-16]

Polyolefins polymer blends are important matrix materials for the fabrication of polymer nanocomposites owing to their wide spectrum of specific applications [2]. A vast number of blends of polyolefin have been used in agricultural and packaging industries in the form of extrudates. Among polyolefins or polymer blend nanocomposites, polyethylene plays a major role because of their good mechanical properties, high chemical resistance and low cost. Mechanical properties of HDPE/HA nanocomposites have been investigated by K. Li and S. C. Tjong [17]. Panaitescu *et al.* investigated the effect of SiO_2 and Al_2O_3 on

polyepropelene (PP) and they found considerable change in morphological, mechanical and electrical properties of PP [18]. The effects of synthetic boehmite alumina (BA) on the morphology, thermal, thermo oxidative and rheological behavior of polyethylenes like LDPE and HDPE was extensively studied by Khumalo *et al.* They found that BA does not influence the crystallization and rheological properties of HDPE and LDPE but work as a powerful thermo oxidative stabilizer for LDPE and HDPE [19]. The flexural strength modulus and yield strength of PP was improved by the incorporation of nanoCaCO$_3$ [20].

The blends of high molecular weight high density polyethylene (HMHDPE) and linear low density polyethylene (LLDPE), with short chain branching has been reported as miscible polymers. However their properties can be modified with the incorporation of isolated nano fibrous silica. Lu *et al.* demonstrated the effect of fiber characteristics and polymer melt flow index on the mechanical properties of sugar cane fiber/HDPE composites [21]. Different fibers had a variable performance on HDPE matrix due to their specific fiber characteristics. The reinforcing effect of cellulose nanofibers in different polyethylene matrices like LDPE, LLDPE and PP was studied by Navin Chand *et al.*[22].

In the present study, 80/20 blend of HMHDPE/LLDPE is proposed to reinforce with fibrous nano silica from the tip of Indian grass (CGS). The objective of the study is to upgrade HMHDPE/LLDPE blend using unmodified nanosilica thus to make the composite suitable for high performance applications. The modification of HMHDPE/LLDPE blends

with CGS is anticipated to generate a variety of morphology and improvement in mechanical properties.

6.A.2 Methodology

The polymers used for the study are discussed in Chapter 2.

6 A.2.1 Preparation of HL-2 CGS nanocomposites

HMHDPE and LLDPE granules were placed in an air oven set at 100°C for four hours to remove any moisture present and were then allowed to cool to room temperature in a desiccator. 80% HMHDPE/ 20% LLDPE (HL-2) were blended with 0.5, 1, 1.5, 2, 2.5, 3 weight% of the isolated silica fibers CGS. The blends containing 0 weight % filler is designated as HL-2. The blend containing different dosages of CGS were designated as HL-2-XCGS, where X is 0.5, 1, 1.5, 2, 2.5, 3 weight% of CGS (e.g., HL-2-0.5CGS) For the fabrication of polymer blend nanocomposites the polymer pellets were fed into the mixing chamber of Thermo Haake Rheomix Poly Lab system equipped with roller type rotors operating at 50 rpm at a temperature of 160°C. After 2 minutes of mixing, required quantities of CGS were added to the melted and homogenized polymer mix. A time of 6 minutes was allowed for complete the mixing. To ensure proper mixing, the torque in the Haake mixing chamber was stabilized in all the batches.

The samples were injection moulded and characterized. The detailed description of the characterization techniques are discussed in Chapter 2.

6.A.3 Results and discussion

6.A.3.1 Mechanical properties

6.A.3.1.1 Tensile properties
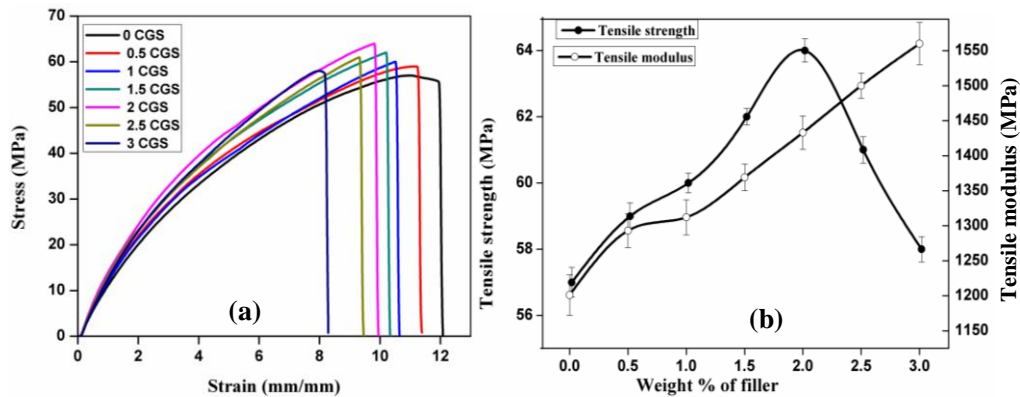
Figure 6 A.1   Tensile properties of HL-2-CGS composites with CGS loading (a) stress-strain curves (b) variation in tensile strength and tensile modulus

The stress-strain curves of neat HL-2 blend and the corresponding CGS composites are given in Figure 6 A.1(a) and Figure 6 A.1(b) respectively. The strength and modulus of the composites improve with the incorporation of silica fibers to the HL-2 matrix. All the composites show a tensile yield point after which the strength drops. The maximum tensile strength was obtained at 2 weight % CGS loading 13% improvement and that too without any surface modifications of either the filler or the matrix. The improvement in tensile properties may be due to the sacrificial bearing of the appied stress by the fibrous filler and the distribution of it evenly throughout the matrix, which in turn delay the rupture of the material. The decrease in tensile strength beyond the optimum filler loading may be due to the agglomeration of CGS fibers. As expected, irrespective of the filler concentrations, tensile modulus was increased with increase in filler

dosage, since hard and rigid fillers have a tendency to restrict the mobility of polymer chains [23]. Elongation at break drops off with increasing CGS content, because in addition to filler-matrix interaction, addition of nanofillers moderately reduces the maximum strain [24].

6.A.3.1.2 Flexural properties
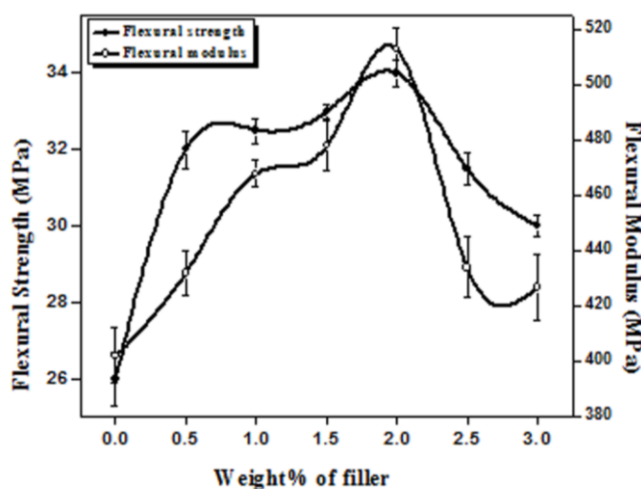
Figure 6 A.2   Variation of flexural strength and flexural modulus with CGS loading

As shown in Figure 6 A.2 both flexural strength and flexural modulus increased upto 2weight % CGS addition and there after decreased. Here flexural strength increased by 31% while flexural modulus was increased by 22%. This observation underlines the percolating behavior of the filler at this composition, due to the effective dispersion and distribution of fibrous CGS filler in the matrix. The enhancement in flexural properties confirms the superior load bearing capacity of HL-2-CGS nanocomposite.

6.A.3.1.3 Impact strength
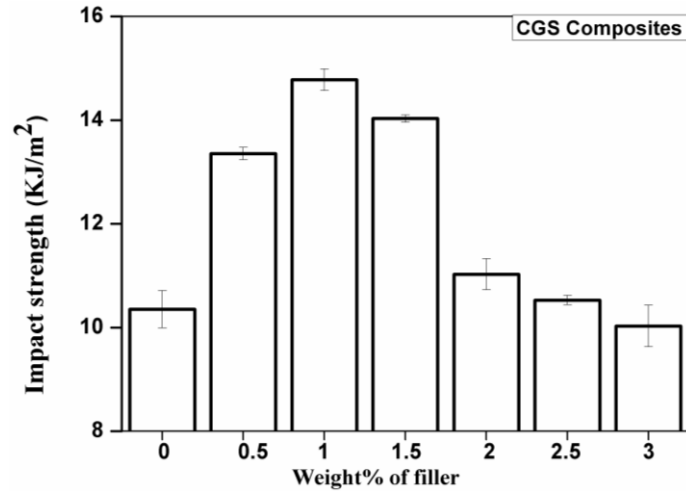
Figure 6 A.3 Variation of impact strength of HL-2-CGS composites

The effect of fibrous silica on the notched impact strength of HL-2-CGS composites with increasing CGS loading is given in Figure 6 A.3. The impact strength increases with CGS addition, reaches a maximum and decreases thereafter. The improvement in impact strength may be attributed to the improved interaction between fibrous filler and the matrix, which inturn helps in superior stress transfer. Thus the fibrous filler hinder the crack path produced upon impact.Similar observation was obtained for glass fiber reinforced nanocomposites where the fibers arrest crack propagation and act as a medium for effective load transfer [25, 26]. A maximum of 40% improvement in impact strength was observed at 1 weight % CGS loading. However, at higher filler loading, impact strength decreased since the agglomerates obstruct the efficient stress transfer.

6.A.3.1.4 Hardness
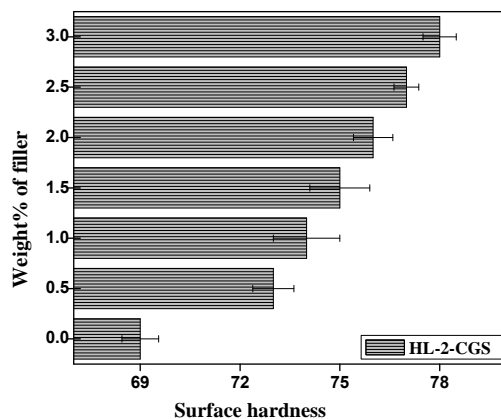
Figure 6 A.4 Variation of surface hardness of HL-2-CGS composites

Variation of surface hardness with CGS loadings is shown in Figure 6 A.4. Hardness of the composite material indicates the ability of a material to stand firm during local surface deformation. Hardness is also a measure of degree of compatibility. A regular improvement in hardness was observed for CGS addition, confirming the enhanced reinforcing effect of the filler.

6.A.3.2 FTIR Spectrum
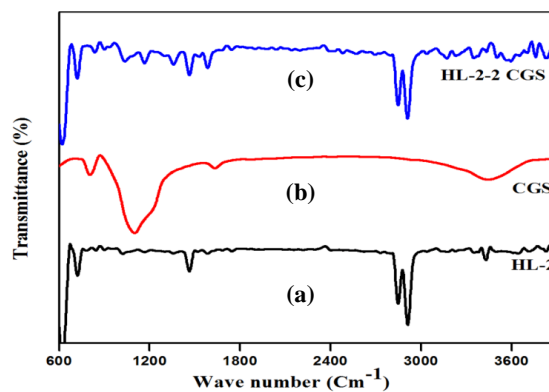
Figure 6 A.5   FTIR analysis of (a) HL-2 blend, (b) CGS and (c) HL-2-2CGS composite

Figure 6 A.5 shows the FTIR spectrum of HL-2 blend, pure CGS, and the HL-2-2CGS composite. The characteristics peak of   polyethylene

was observed in both neat HL-2 blend as well as in the composite. Weak band [Figure 6 A.5 (a)] around 1464 cm^{-1} and 3429 cm^{-1} indicate –C-H bending and skeletal –C-H stretching respectively. The strong peaks at 2910 cm^{-1} and 2848 cm^{-1} in Figure 6 A.5 (a) represent the symmetric and asymmetric –C-H stretching modes of the –CH$_2$ groups in the PE blend. The weak bands in around 1200 – 800 cm^{-1} correspond to the C-C stretching frequency. The characteristic peaks of CGS and pure HL-2 blend remain unaltered in HL-2-2CGS composite, which shows that there is no chemical interaction between the filler and matrix.

6.A.3.3 Microstructure analysis

6.A.3.3.1 SEM Analysis
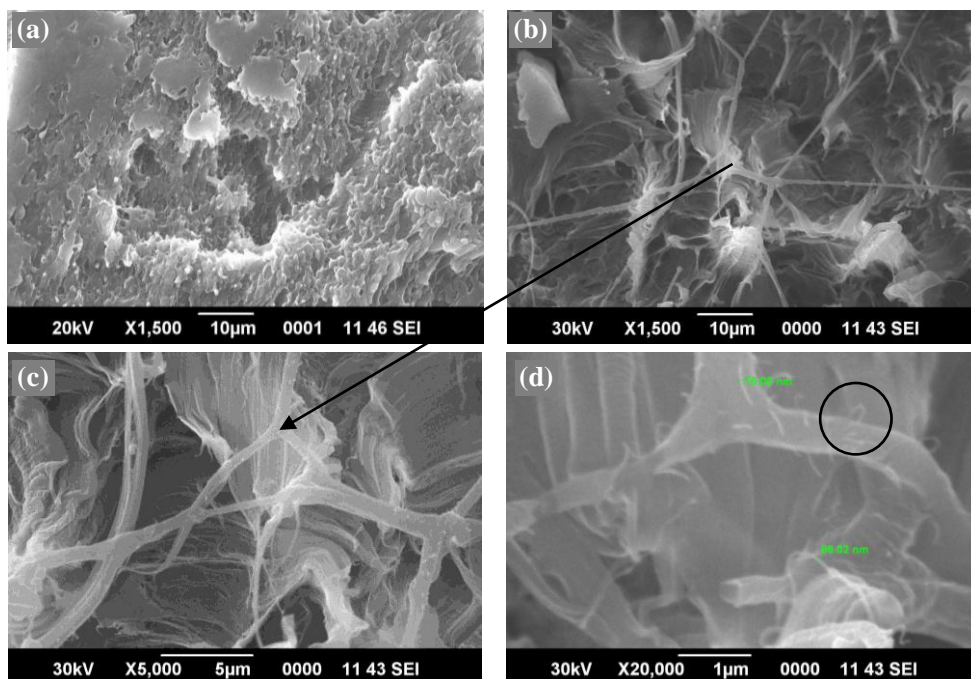
Figure 6 A.6 SEM images of tensile fractured surfaces of (a) HL-2 blend (b), (c) and (d) HL-2-2CGS composite at different magnifications

Figure 6 A.6 reveals the microstructure analysis of the tensile fractured surface of the neat blend and the HL-2-2CGS composite. The fractured surface of neat HL-2 blend shows a number of voids. An entirely different morphology was observed in the SEM images (Figure 6 A.6 (b), (c), and (d)) of the composite. At higher magnification of the composite, semi tubular CGS fiber bundles [as discussed in chapter 4, Figure 4.6 (a) and (b) and Figure 4.12 (a) and (b)] were found as woven individual nano fibers. The debundling of CGS fibers may have occurred during the melt mixing stage, with an individual fiber width of approximately 70 nm. Pictorial representation of the fabrication of CGS nanocomposite is shown in Scheme 6 A.1.
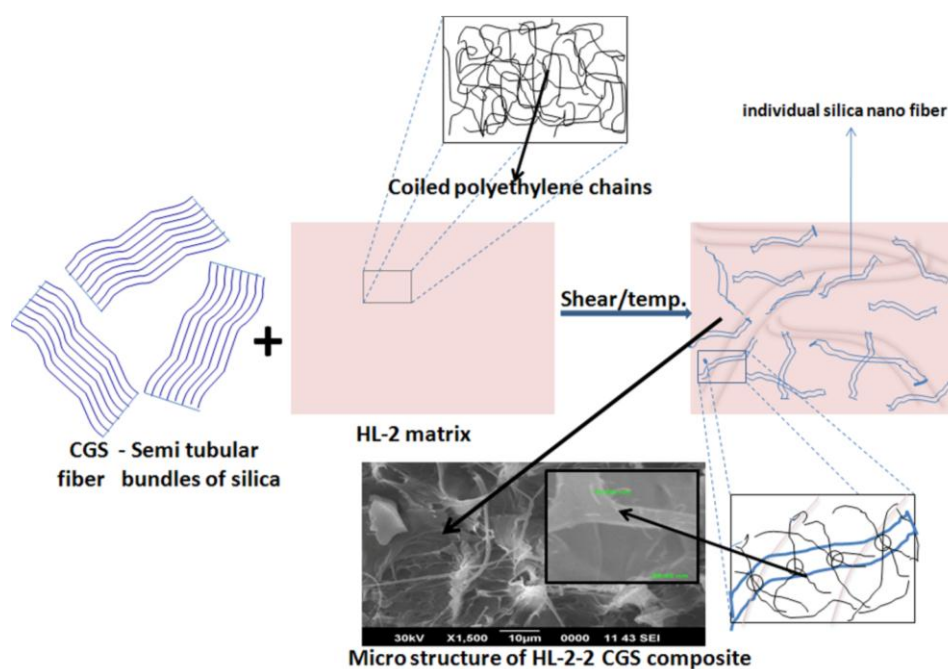
Scheme 6 A.1: Pictorial representation of the preparation of HL-2-2 CGS composite
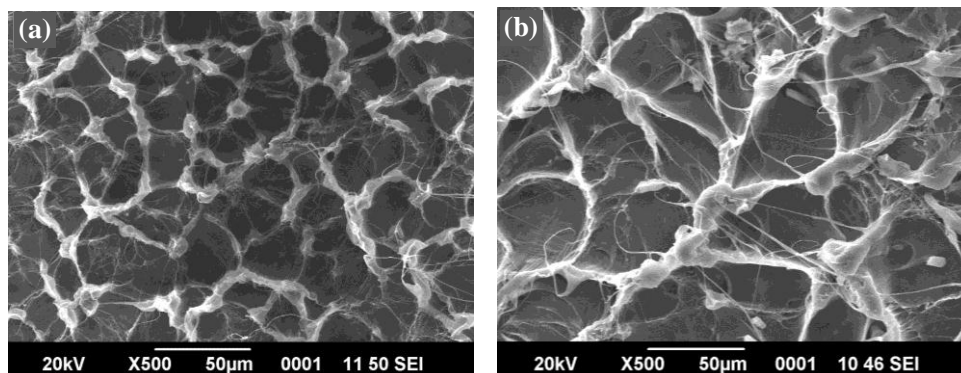
Figure 6 A.7 SEM images of impact fractured surfaces of (a) HL-2 (b) HL-2-1CGS

The SEM micrographs of the impact fractured surface for the pure blend and the composite loaded with 1 weight % CGS are given in Figure 6 A.7 (a) and (b). Significant difference was noticed between failure surface of neat blend and that of the composite. With the addition of CGS, the failure surface became rough and show evidences of increased energy absorbtion. The tedious crack propagation path in the composite may be attributed to the energy absorption mechanisms like crack pinning and crack arresting, which in turn leads to high strength.

6. A.3.4 Melt rheological analysis

6. A.3.4.1 Melt flow index (MFI)

The effect of CGS in the melt flow of HL-2-CGS composite is given in Figure 6 A.8. A marginal decrease in the MFI indicates a higher viscosity of the melt due to CGS loading. The results also substantiate the better interaction of the fibrous filler with the polyethylene matrix. The improved interaction of fibrous CGS with the polymer matrix restricts chain mobility and decreases the flow rate.
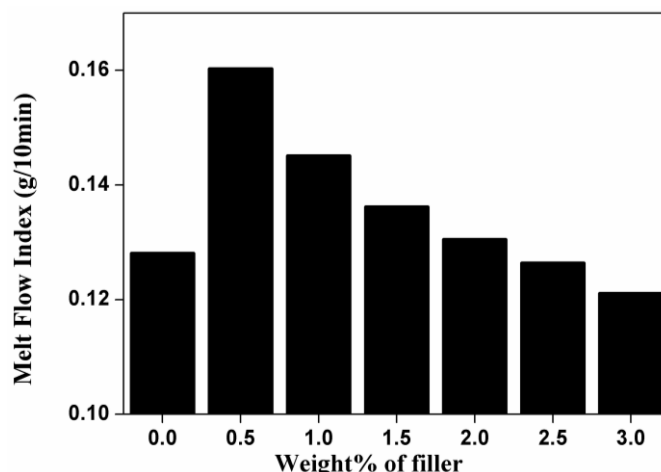
Figure 6 A.8   Variation of MFI of HL-2-CGS composite with CGS loading

6.A.3.4.2 Dynamic rheological analysis (DRA)

Polymer rheological properties are extremely sensitive to the variations of polymer composition and structure. Generally in the case of polymer nanocomposites, a noticeable increase in the melt viscosity is observed atleast in the low frequency region. In thermoplastic nanocomposites a pseudo solid-like transition is usually observed due to the dispersed nanoparticles in the matrix. Furthermore the enhanced interaction between nanoparticles and polymer molecule will obstruct the mobility of the polymer chains, boost up the friction between the polymer molecule and the filler particles which in turn enhances both elasticity and viscosity of the composite [27-29].
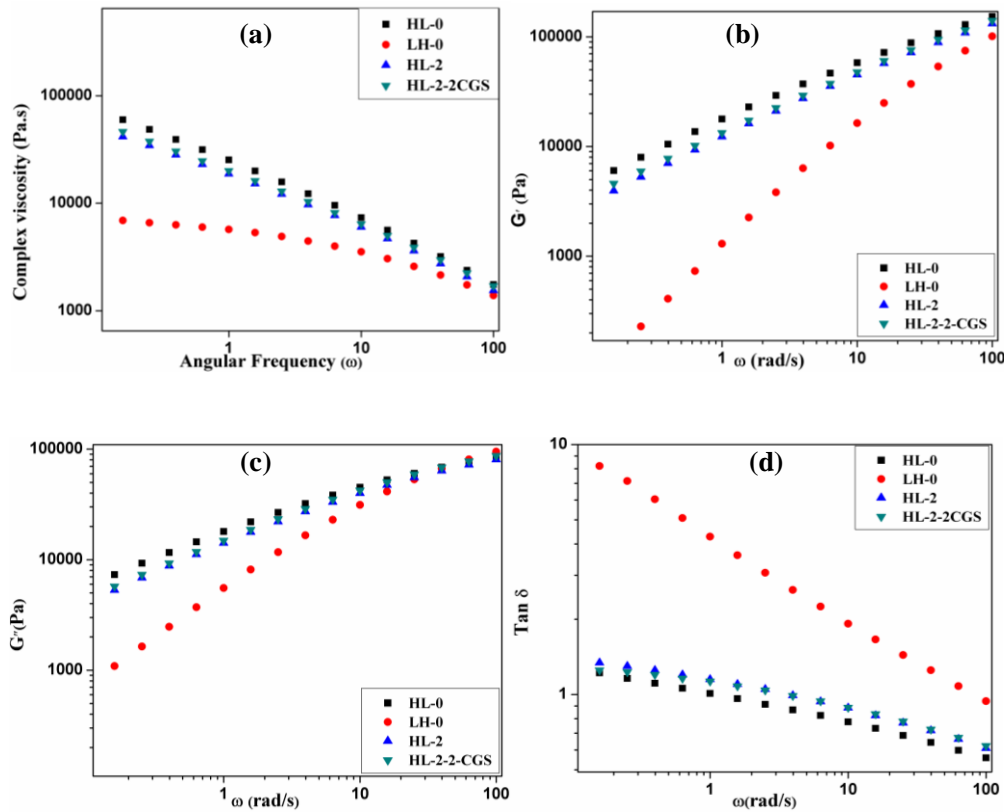
Figure 6 A.9 Rheological observations of HL-2-2CGS composite
(a) Variation of complex viscosity as a function of frequency
(b) Variation of storage modulus as a function of frequency
(c) Variation of loss modulus as a function of frequency and
(d) Variation of tanδ as a function of frequency

In HL-2-CGS composites, the molten HL-2 matrix and solid CGS particles can each have appreciable effect on the rheological behavior of the composite materials. Figure 6 A.9 (a), (b), (c) and (d) shows complex viscosity, storage modulus (G'), loss modulus (G") and tan δ as a function of frequency for neat HL-0, LH-0, HL-2 blend and the HL-2-2CGS composites respectively. From the figure, it is clear that there is noticeable improvement in the complex viscosity, storage modulus and loss modulus

of the composite compared to the neat blend. But these values were still lower than the pure HL-0. This clearly shows that the nanocomposites offer better processability than the pure HL-0. The improvement in dynamic rheological properties gives credence to the fact that there is fine dispersion of CGS filler in the matrix with a strong interaction between them. Dorigato *et al.* also have reported similar observations for micro and nano silica reinforced LLDPE composites [29].

6.A.3.5 Thermal properties

6.A.3.5.1 Thermo gravimetric analysis

Thermal stability and degradation characteristics of polymers and their composites have been studied for the better selection of suitable processable conditions and applications [30-32].
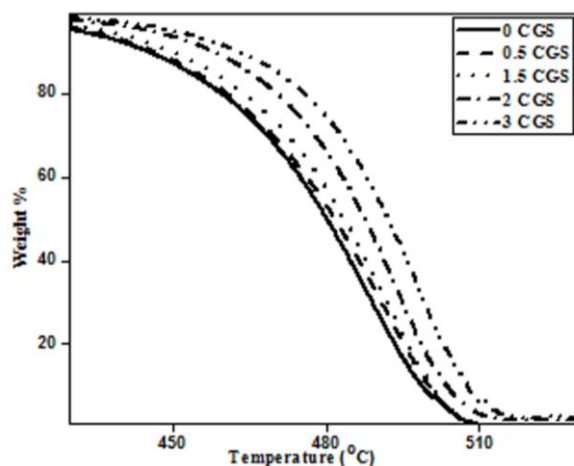
Figure 6 A.10 Thermogram of HL-2-CGS composites

Figure 6 A.10 shows the thermogram of neat HL-2 blend and HL-2-CGS composites. T_{onset}, T_{max}, T_{10}, T_{50} values (onset degradation temperature, maximum degradation temperature, temperatures at which 10

and 50% weight loss respectively, are achieved) and residue at 600°C of the composites are tabulated in Table 6 A.1.

Table 6 A.1 Thermal analysis of HL-2-CGS composites

CGS content (wt%)	Temperature at different mass losses (°C)			Peak max (T_{max}, °C)	Residue at 600 °C (%)
	T_{onset}	$T_{10\%}$	$T_{50\%}$		
0	426	448	483	491	0.08
0.5	433	452	485	492	0.6
1.5	440	454	486	493	1.61
2	442	458	488	494	2.2
3	446	460	490	497	3.07

With the addition of 0.5 weight % CGS, the onset degradation temperature (T_{onset}) of the blend was increased by 7 °C. Temperature required for 10 and 50% weight loss was higher for the HL-2-CGS composite compared to the neat blend. The enhanced thermal stability may be due to the restricted mobility of polymer chains because of the strong interactions with the fibrous silica particle (CGS) [33], which limit the diffusion of the volatile degradation products from the composites. The residual weight loss was comparable to the increment in the CGS content in the composite.

6.A.3.5.2 Differential Scanning Calorimetry

Differential scanning calorimetry (DSC) is the most widely accepted technique for studying the crystallization characteristics of polymers and their composites. DSC analyses were used to evaluate the effect of size and morphology of the silica fibers on melting temperature and crystallinity of HL-2 matrix. DSC cooling and heating curves of neat HL-2 blend and 2

weight% CGS loaded nanocomposite are shown in Figure 6.A.11. The crystallization temperature (T_c), apparent melting temperature (T_m) and the corresponding enthalpies (ΔH_c and ΔH_m) of the neat blend and the composites are summarized in Table 6 A.2.
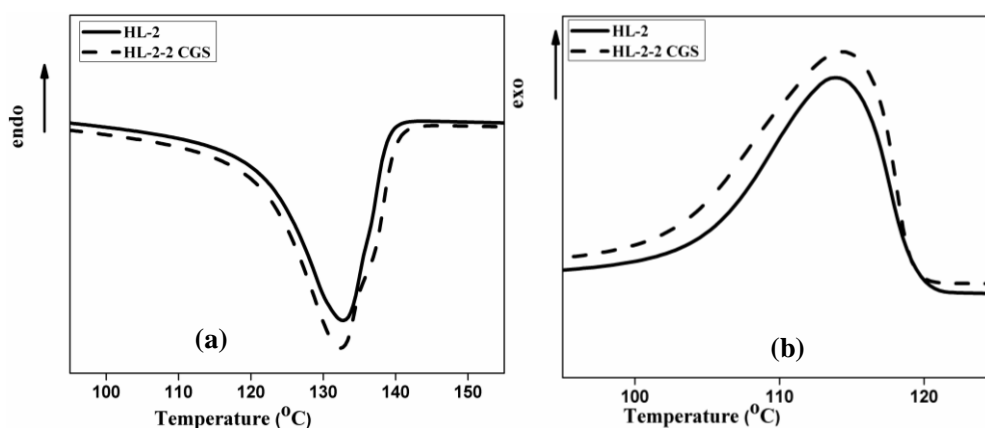
Figure 6 A.11 **Non-isothermal crystallization studies (a) Cooling (b) Melting behavior of HL-2-2CGS composites**

Table 6 A.2 **Non-isothermal crystallization characteristics of HL-2-CGS composites**

Sample	T_m (°C)	ΔH_f (J/g)	T_c (°C)	ΔH_c (J/g)	X_c (%)
HL-2	133	145	109	162	61.86
HL-2-2CGS	132	143	110	140	61

There was no remarkable change in T_m but a slight change in T_c was observed. This shows that fibrous CGS has a little effect on the crystallization characteristics of HL-2 matrix. Since there is only a minor change in the crystallization temperature it may be concluded that CGS acts as a very weak nucleating agent.

6.A.4 Conclusions

HL-2-CGS nanocomposites were fabricated by incorporating the isolated fibrous silica (CGS) into the HL-2 blend through melt mixing. Static, mechanical, rheological and thermal properties of the CGS reinforced nanocomposites were analyzed. The HL-2-CGS nanocomposites with 2 weight% loading showed an increase of 13% in tensile strength, 31% in flexural strength and 22% in flexural modulus compared to pure matrix without any surface modification in either filler or matrix. A regular increase in tensile modulus was also noted. Impact strength showed a 40% improvement at 1 weight % CGS dosage. Absence of any chemical interaction between filler and matrix was confirmed by the FTIR studies. Rheological analysis showed better processability for the nanocomposites than HL-0. SEM analysis of CGS filer revealed bundle fiber morphology with few micrometers in diameter. Morphological characterization of the fractured surface of the nanocomposite by SEM shows the debundling of micrometer sized fibers into individual nanofibers with the application of shear forces during processing. With the inclusion of CGS into the HL-2 matrix, the thermal stability improves. DSC studies suggest that CGS act as a very weak nucleating agent due to a slight change in T_C.

References

[1] Ajayan PM, Schadler LS, Braun PV. Nanocomposite Science and Technology, Wiley; 2003.

[2] Jordan J, Jacob KI, Tannenbaum R, Sharaf M, Jasiuk I. J. Mater. Sci. Eng. A. 2005; 393:1-11.

[3] Jeon IY, Baek JB. Mater. 2010; 3: 3654-3674.

[4]   Emmanuel PG. Appl.Organometal. Chem. 1998; 12:675.

[5]   Ayswarya EP, Abraham BT, Thachil ET. J. Appl.Polym. Sci. 2012; 124:1659–1667.

[6]   Chaudhary DS, Jollands MC, Cser F. Silicon Chem. 2002; 1:281.

[7]   Liou TH, Yang CC. Mater. Sci. Eng. B. 2011; 176:521–529.

[8]   Dongmin A, Yupeng G, Yanchao Z, Zichen W. Chem. Eng. J. 2010; 162:509–514.

[9]   Lin YS, Haynes CL. Chem. Mater. 2009; 21:3979–3986.

[10]   Jugdaohsingh R, Katherine LT, Ning Q, Cupples LA, Douglas PK, Powell JJ. J. Bone Miner. Res. 2004; 19:297–307.

[11]   Sun L, Kecheng G. Ind. Eng. Chem. Res. 2001; 40:5861–5877.

[12]   Athinarayanan VS, Periasamy M, Alhazmi AA, Alshatwi. J. Biomed. Mater. Res. Part B Appl.Biomater.2017; 105:340-349.

[13]   Zaky RR, Hessien MM, El-Midany AA. Powder Technol. 2008; 185:31–35.

[14]   Carmona VB, Oliveria R.M, Silva WT, Mattoso, LH, Marconcini JM. Ind. Crop Prod. 2013; 43:291- 296.

[15]   Li D, Chen D, Zhu X. BioresTechnol 2011; 102:7001–7003.

[16]   Liou TH, Yang CC. Mater. Sci. Eng. B. 2011; 176:521–529.

[17]   Li K, Tjong SC.J.Macromol. Sci. B.2011; 50:1325–1337.

[18]   Panaitescu D, Ciuprina F, Iorga M, Frone A, Radovici C, Ghiurea M, Sever S, Plesa I. J. Appl.Polym. Sci. 2011;122:1921–1935.

[19]   Khumalo VM, Karger-Kocsis J, Thomann R. Express Polym. Lett. 2010; 4:264–274.

[20]   Yang K, Yang Q, Li G, Sun Y, Feng D. Mater. Lett. 2006; 60:805–809.

[21]   Lu JZ, Wu Q, Negulescu II, Chen Y. J. Appl.Polym. Sci. 2006; 102:5607–5619.

[22] Chand N, Prajapati SC, Singh RK. Journal of Scientific Research and Reviews. 2012; 1:026 – 032.

[23] Nielsen. LE, Robert RF. Mechanical properties of polymers and composites. Newyork; 1974.

[24] Wang J, Severtson SJ, Geil PH. Mater. Sci. Eng. A. 2007; 467:172-80.

[25] Leguet X, Ericson M, Chundury D, Baumer G. ANTEC, SPE, Toronto. 1997; 2117.

[26] Barbosa SE, Kenny JM.J. Vinyl Additive Tech.1995; 1:269.

[27] Durmus A, Kasgoz A, Macosko CW. Polym. 2007; 48:4492–4502.

[28] Rezanavaz R, RazaviAghjeh MK, Babaluo AA. Polym. Compos.2010;31:1028-1036.

[29] Dorigato A, Pegoretti A, Penati A. Express Polym. Lett. 2010; 4:115–129.

[30] Jin-hua T, Guo-qin L, Huang C, Lin-jian S. Mat. Res. 2012; 15:1050-6.

[31] Pedrazzoli D, Ceccato R, Karger-Kocsis J, PegorettiA. Express Polym. Lett. 2013; 7:652–666.

[32] Malucelli G. Palmero, Ronchetti P, Delmastro S, Montanaro L. Polym. Int.2010; 59:1084–1089.

[33] Gilman.J.W. Appl. clay science 1999; 15:31-49.

Part B

HMHDPE/LLDPE/PGNS NANOCOMPOSITES

Isolated fibrous silica from Pampas grass flowers (PGNS) was used for the reinforcement of 80/20 HMHDPE/LLDPE blend. The nanocomposites were prepared through melt mixing in a Thermo Haake Rheocord mixer. The mechanical, morphological, rheological and thermal properties of the composites were evaluated. The mechanical properties improve by the addition of fibrous silica. The morphological analysis of tensile fractured surface of the composite shows uniform distribution of the fibrous filler. The improved interaction between the filler and matrix is established by rheological analysis. FTIR analysis confirms that there is no chemical interaction between filler and the matrix. TGA results show an improved thermal stability for the nanocomposites compared to that of the pure blend. DSC analysis shows a weak nucleating effect of the fibrous filler PGNS.

6.B.1 Introduction

Polymer nanocomposites are usually prepared by reinforcing organic polymer matrix with dispersed nanoscale reinforcing materials. With the introduction of nanofillers, many value added properties are obtained for the composites without sacrificing the polymer's inherent advantageous properties. This enables PNCs to stand firm in engineering and other high performance applications. PNC based on nanofillers from natural material have attracted a great deal of interest in fields ranging from the scientific community to the industry because of remarkable improvement in properties they can offer to polymers.

Among various polymers, polyethylene has a major role in plastic industry, with diversified applications from house hold to aeronautical sectors as well as in biomedical engineering. Bonefield and co-workers have extensively studied HDPE-hydroxy apatite composite for bone implant applications [1-3]. Countless investigations and numerical modeling studies have been reported on the enhancements in mechanical properties of nano clay reinforced with elastomers, thermoset resins, and thermoplastics [4-9].

Significant enhancement in the synergetic effect of both bioactive and bioinert ceramic fillers like HA and Al_2O_3 on the mechanical and biocompatibility properties of a bioinert polymer like HDPE has been demonstrated [10]. The mechanical and antibacterial properties of HDPE containing silica nanoparticles with immobilized nanosilver and nanocopper have been investigated [11].

Reinforcing effect of precipitated silica and nanosilica synthesized from conventional synthesis methods has long been explored. But the reinforcing effect of fibrous silica in polyethylene matrix has not been the focus of research till date. Therefore in the present investigation, the potential of silica nanofibers (PGNS) isolated from Pampas grass flowers in 80/20 HMHDPE-LLDPE blend (HL-2) is proposed to be investigated.

6.B.2 Methodology

6.B.2.1 Preparation of HL-2-X PGNS composites

HMHDPE and LLDPE granules were placed in an air oven set at $100^{\circ}C$ for four hours to remove any moisture present and allowed to cool to room temperature in a desiccator. 80% HMHDPE/ 20% LLDPE (HL-2) were blended with 0.5, 1, 1.5, 2, 2.5, 3 wt% of the isolated silica fibers PGNS. The blend containing 0 weight % filler is designated as HL-2. The blends containing PGNS were designated as HL-2-XPGNS, where X is the dosage of PGNS used (0.5, 1, 1.5, 2, 2.5, 3 wt%; e.g., HL-2-0.5 PGNS). For the fabrication of polymer blend nanocomposites first the polymer pellets were fed into the mixing chamber of Thermo Haake Rheomix Poly Lab system equipped with roller type rotors operating at 50 rpm set at a temperature of $160^{\circ}C$. The polymers were melted and homogenized for 2 minutes after which required quantities of PGNS were added. A mixing time of 6 minutes was allowed to complete the reaction. In all the cases to ensure proper mixing the torque in the Haake mixing chamber was stabilized. The hot mix taken from the chamber was immediately pressed in a hydraulic press and then cut into small pieces. These were then injection moulded at $170\ ^{\circ}C$. The characterization of the nanocomposites were done by appropriate ASTM standards, the details of which are given in section 6.A.2.2

6.B.3 Results and discussion

6.B.3.1 Mechanical properties

6.B.3.1.1 Tensile properties
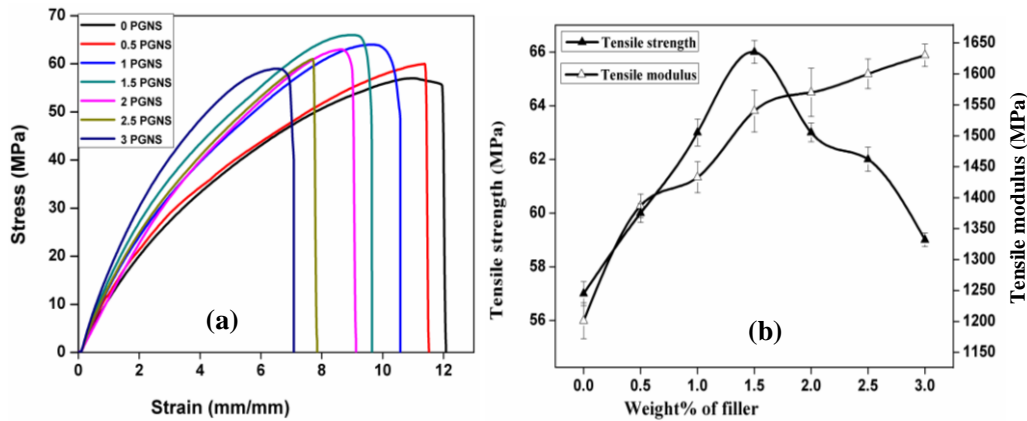
Figure 6 B.1 Tensile properties of HL-2-PGNS composites (a) stress-strain curves of HL-2-PGNS composites (b) variation of tensile strength and tensile modulus with PGNS loading

The response of pure HL-2 blend and HL-2-PGNS composites towards tensile performance is given in Figure 6 B.1. The stress strain curves of pure blend and the composites are identical in nature. The addition of PGNS leads to a significant improvement in tensile properties up to 1.5 weight % PGNS loading and was thereafter decreased. 16% improvement in tensile strength was noticed for HL-2-1.5PGNS composites as compared to the neat blend. The nano fibrous silica at this composition effectively transfers the stress throughout the matrix and delays early rupture of the material. However at higher loading, wettability of the filler with the matrix decreases considerably due to formation of agglomerates leading to easy breakage. [12]

The tensile modulus increases progressively with increasing PGNS loading. Relative stiffness of the material is indicted by the tensile modulus. Neilsen has suggested that the addition of rigid fillers would increase the modulus of the composites since they restrict the mobility of polymer chains [13]. With increasing filler loading elongation at break decreases, since under a stress cracks can propagate through weak interfacial regions leading to composite rupture at lower elongation values.

6.B.3.1.2 Flexural properties
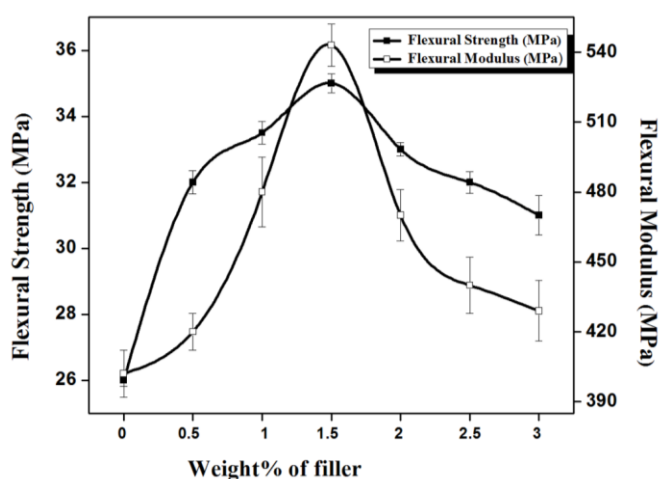
Figure 6 B.2 Variation of flexural strength and flexural modulus with PGNS loading

Effect of PGNS on the flexural properties of the nanocomposites is presented in Figure 6 B.2. Both flexural strength and flexural modulus increase upto 1.5 weight% PGNS loading and there after decreases. This shows that there is optimum interaction between filler and the matrix at 1.5 weight% PGNS loading. Flexural strength and flexural modulus of the HL-

2-1.5 PGNS composite improves by 26% and 35% respectively as compared to the neat blend.

6.A.3.1.3 Impact strength
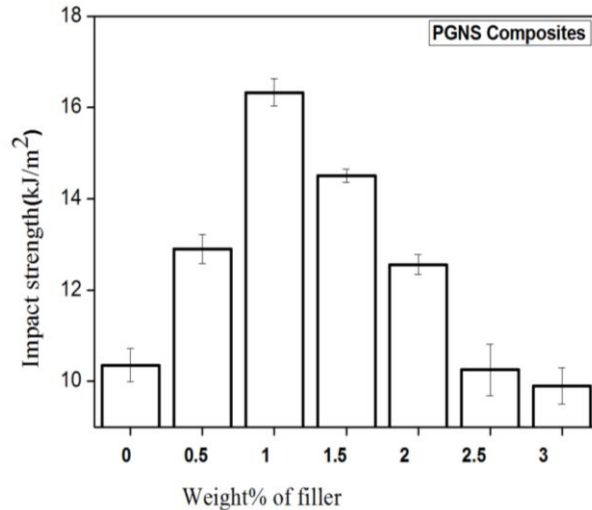
Figure 6 B.3 Variation of impact strength of HL-2-PGNS composites

Impact strength of the composite is a measure of the total energy dissipated in the material before it fails. Figure 6 B.3 shows the variation of notched impact strength with fibrous silica (PGNS) loading. The impact strength increases with increase in fiber loading up to 1 weight %. The impact strength of a polymer nanocomposite depends upon many factors like stiffness of the reinforcing filler, nature and mode of frictional work involved in pulling out the fiber from the matrix and character of the interfacial region. When the composite material is subjected to an impact stress, a large number of crazes are formed and some of these crazes are turned into cracks upon further applied stress finally breaking down the specimen. In HL-2-PGNS composite system the PGNS fibers play a

significant role in increasing the impact resistance of the composites as they resist the crack propagation and act as efficient load transfer medium due to effective interfacial bonding [14]. A maximum of 62% improvement in impact strength was obtained for the composite at 1 weight% PGNS loading. The reduction in impact strength after 1 weight % filler loading is due to formation of filler agglomerates in the matrix, leading to non-uniform stress transfer [15].

6. B.3.1.4 Hardness
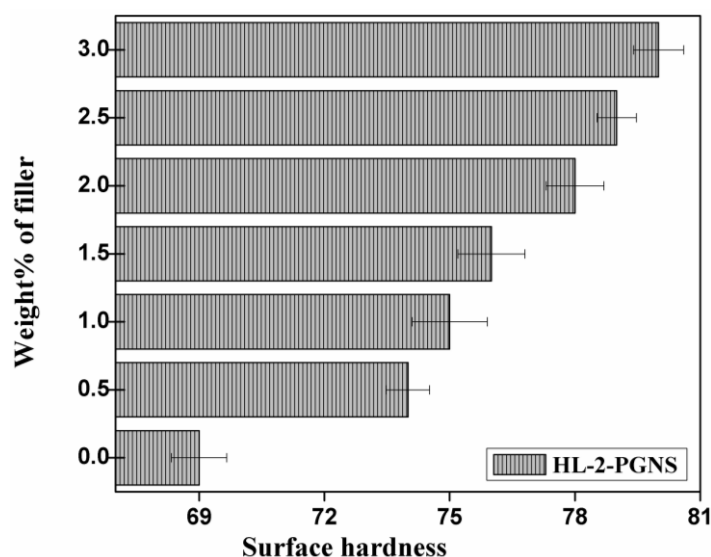
Figure 6 B.4 Variation of surface hardness of HL-2-PGNS composites

Variation of hardness of HL-2-PGNS composites with PGNS loading is given in Figure 6 B.4. The addition of 3 weight% PGNS improves the hardness of the composite by 16% as compared to pure matrix. The increase in hardness may be due to the stiffening of the composite caused by the incorporation of fibrous silica.

6.B.3.2 FTIR spectroscopy
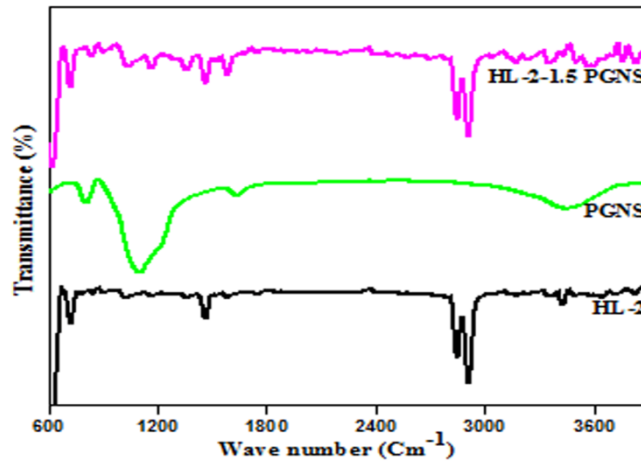
Figure 6 B.5 FTIR spectra

Figure 6 B.5 represents the FTIR spectrum of HL-2 blend, pure PGNS and HL-2-1.5 PGNS composite. The characteristic peaks of polyethylene remain unshifted in the composite. The characteristic FTIR peaks of PGNS were also unshifted in the FTIR spectrum of the composite. This confirm the absence of any chemical interaction between the filler and the matrix

6.B.3.3 Microstructure analysis

6.B.3.3.1 SEM analysis

The morphological analysis of the tensile fractured surfaces of neat HL-2 blend (6 B.6 (a)) and the composite loaded with 2weight % of PGNS (6 B.6 (b), (c) and (d)) at different magnifications are shown in Figure 6 B.6. The voids seen in the HL-2 matrix are not observed in the SEM micrograph of the composite. Moreover Figure 6 B.6 (c) and (d) illustrate a

more homogeneous morphology for the composites which reveals better stress transfer between the components.
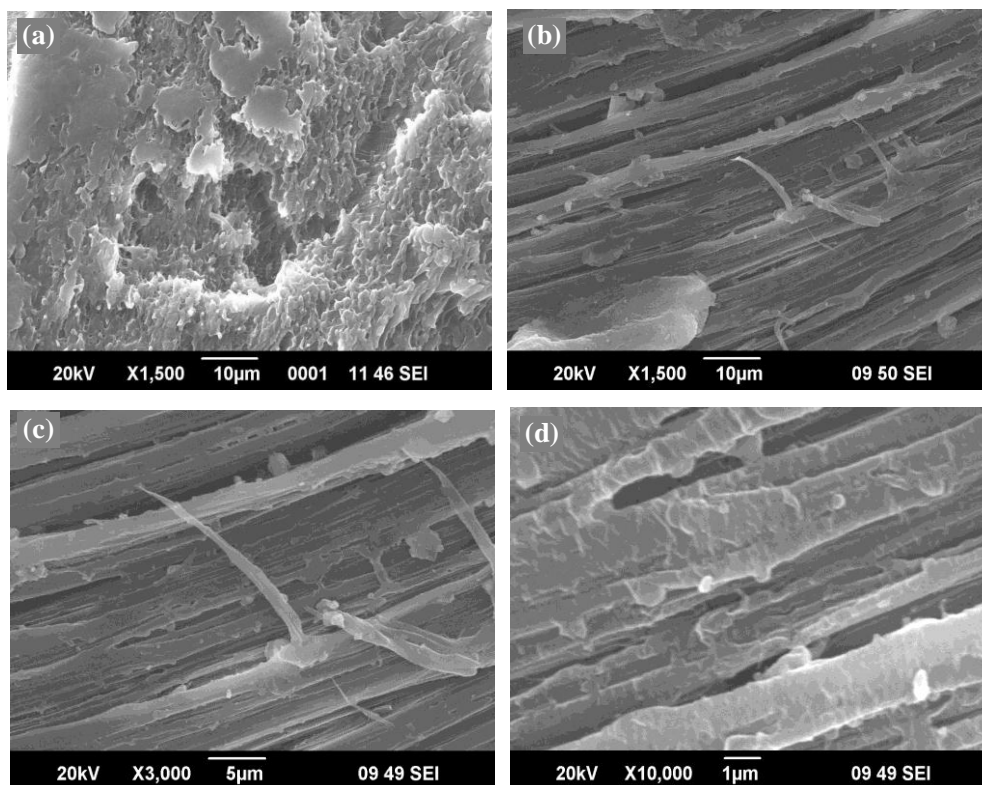
Figure 6 B.6 SEM images of tensile fractured surfaces of (a) HL-2 blend, (b),(c) and (d) HL-2-2 PGNS composite at different magnifications

The images also show that PGNS fibers are well dispersed in the matrix. The mechanical interlocking between the fibrous filler and the matrix is evident from the SEM images of the composite. Scheme 6 B.1 shows the pictorial representation of the transformation of PGNS fiber bundles into individual fibers (as evidenced from SEM images) under the application of shear forces during processing.
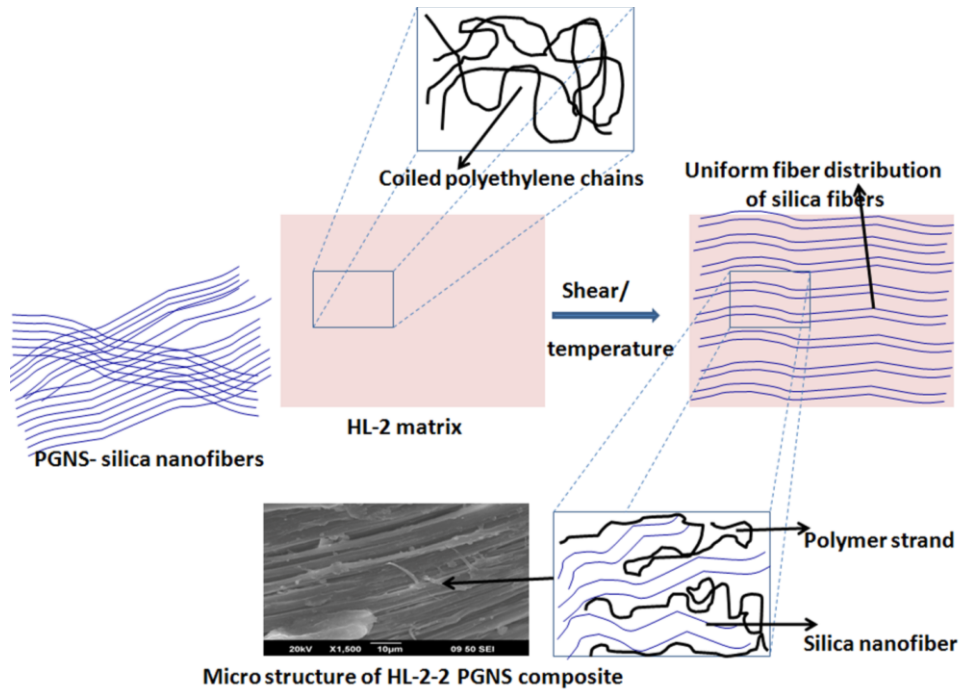
Scheme 6 B.1: Schematic representation of the preparation of PGNS nanocomposite
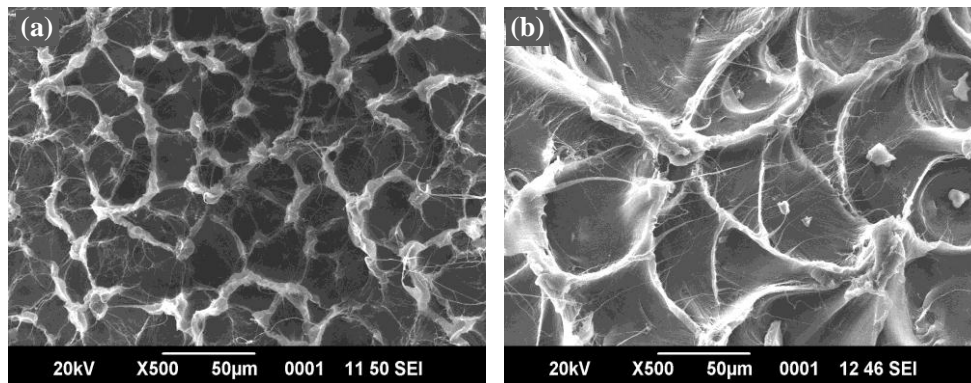
Figure 6 B.7   SEM images of impact fractured surfaces of (a) HL-2 (b) HL-2-1PGNS

SEM images of impact fractured surfaces of neat HL-2 blend and the composite loaded with 1 weight % PGNS are given in Figure 6 B.7. A

rough morphology with more energy absorbed interfaces is noticed in the HL-2-1PGNS. These rough surfaces create a tortuous path for the crack propagation thus increasing the impact strength.

6.B.3.3.2 TEM analysis

Figure 6 B.8 demonstrates the TEM image of the HL-2-2 PGNS nanocomposite. PGNS nanofibers were found homogeneously dispersed in the HL-2 matrix with some nanofiber aggregates [Figure 6 B.8 (a) and (b)]. The well dispersed individual silica nanofibers in the matrix are clearly visible in Figure 6 B.8 (c) and (d). The proposed schematic representation of fabrication strategy illustrated in Scheme 6 B.1. is well supported by the TEM micrograph of the nanocomposite shown in Figure 6 B.8.
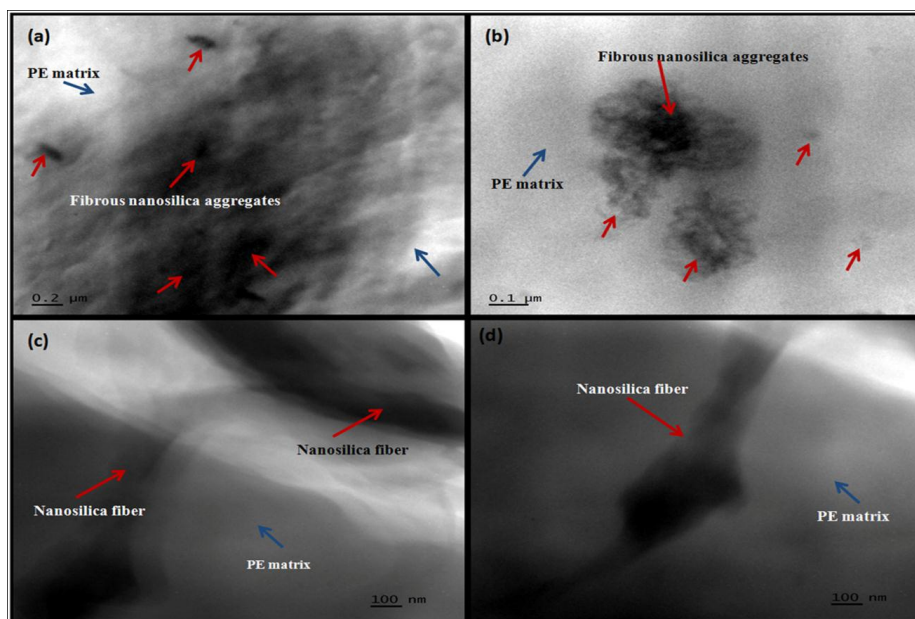
Figure 6 B.8 Bright field TEM images of HL-2-2PGNS nanocomposite (a) and (b) showing PE matrix and dispersed silica nanofibers in the matrix along with some aggregates (c) and (d) single nanosilica fiber in the PE matrix

6.B.3.4 Melt rheological analysis

6.B.3.4.1 Measurement of melt flow index (MFI)
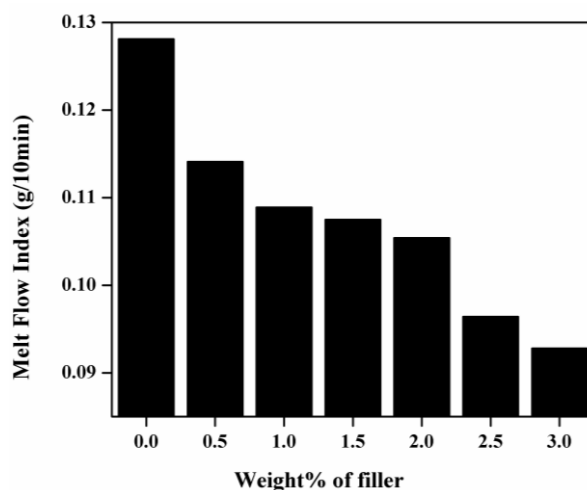
Figure 6 B.9   Variation of MFI of HL-2-PGNS composite with PGNS loading

The effect of PGNS loading on the melt flow index is illustrated in Figure 6 B.9. The result shows that increased PGNS loading furnish a marginal decrease in MFI. This indicates a nominal increase in the melt viscosity of the polymer melt upon the addition of PGNS. The addition of filler increases the elastic as well as elastic response of the system due to enhanced filler matrix interaction. Moreover, due to the presence of rigid and hard filler in the polymer matrix results in the restricted mobility of polymer chains thus amplify the viscosity of the melt. The results are in good agreement with the identified ability of the filler to increase the intermolecular forces between the polymer chains via physical bonds, which also restrict the mobility of polymer chains. The possibilities of the mechanical inter locking of the CGS and the polymer chains can be best supported by the suggested Scheme 6 B.1.

6.B.3.4.2 Dynamic rheological analysis (DRA)
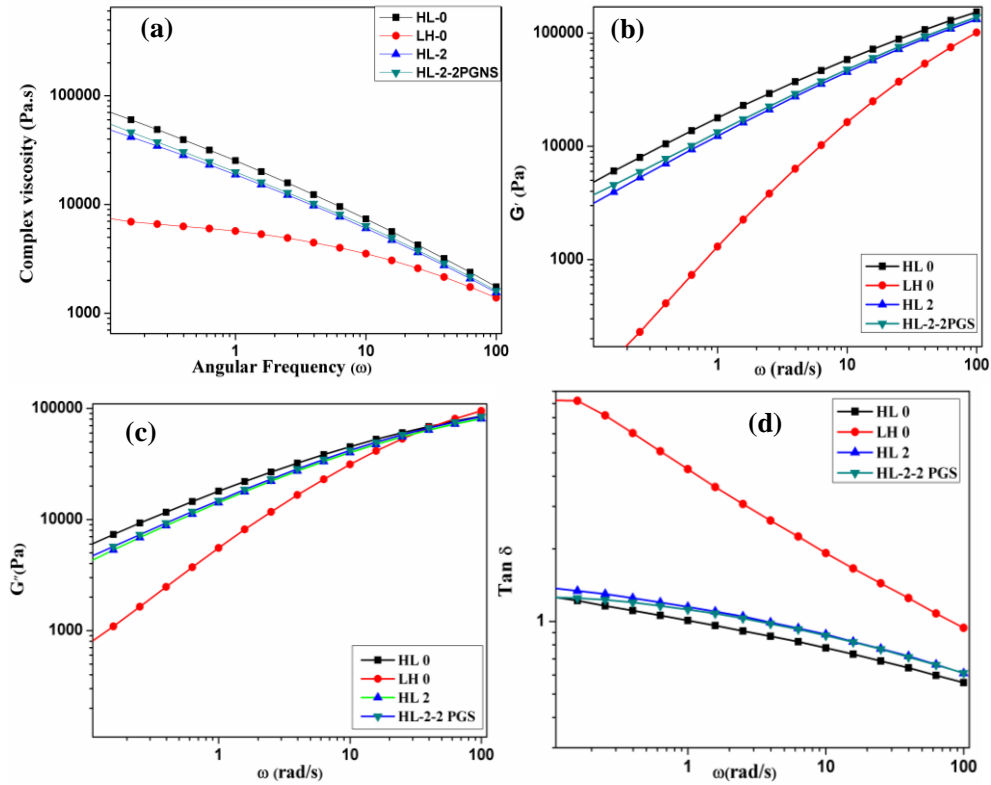
Figure 6 B.10   Rheological observations of HL-2-2PGNS composite
        (a) Variation of complex viscosity as a function of frequency
        (b) Variation of storage modulus as a function of frequency
        (c) Variation of loss modulus as a function of frequency and
        (d) Variation of tanδ as a function of frequency

Rheological measurements were made in the linear visco elastic region at a constant temperature of 200°C. Figure 6 B.10 show the complex viscosity, storage modulus (G') loss modulus (G") and tan δ as a function of frequency for neat HL-0, LH-0, HL-2 blend and the HL-2-2PGNS composites. Rheological behavior of the composite has affected by the molten HL-2 matrix and solid PGNS particle. A slight increase in G' and G" is observed with the addition of PGNS than the neat blend. Also a notable improvement

for the complex viscosity is also observed. Generally the addition of nano fillers offer improves G', G" and complex viscosity [16, 17]. It is evident that by the addition of rigid fillers into polyethylene matrix reduced the flow ability of polymer, and hindered the disentanglement of the molecular chains of polyethylene. Moreover fine dispersion of the filler particle thus offers strong interaction between filler and matrix credit enhancement in complex viscosity and all other properties of the composite than the blend. Furthermore from the results it is evident that nanocomposites have lower melt viscosity than HL-0 depict nanocomposite has good processability.

6.B.3.5 Thermal analysis

6.B.3.5.1 Thermo gravimetric analysis

The thermal data obtained are tabulated in the Table 6 B.1. Onset of degradation temperature for neat HL-2 matrix is lower than those of its nanocomposites, demonstrating that the thermal stability of the nanocomposites has been enhanced because of the addition of PGNS filler. Further the residual weight of HL-2-PGNS nanocomposites left increases steadily with the increase of PGNS loading. Peak max temperature and temperature for the degradation at different weight percentage of the composites increase with increased PGNS content. Enhancement of thermal stability of the PGNS composites is attributed to the interaction between the organic polymer matrix and inorganic filler PGNS where the thermally stable inorganic filler delays the chain scission of carbon–carbon bond of the polymer matrix [18]. Moreover presence of the filler hampers the mobility of the polymer chains and thus delays the degradation [19] Figure 6 B.11 shows the thermogram of neat blend and the HL-2-PGNS composites.
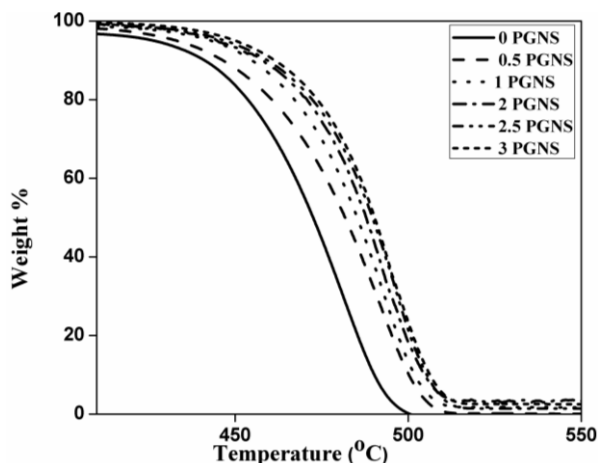
Figure 6 B.11 Thermogram of HL-2-PGNS composites

Table 6 B.1 Thermal analysis of HL-2-PGNS composites

PGNS content (wt%)	Temperature at different mass losses (°C)			Peak max (T_{max}, °C)	Residue at 600 °C (%)
	T_{onset}	$T_{10\%}$	$T_{50\%}$		
0	426	448	483	491	0.08
0.5	433	459	484	492	0.7
1	442	456	485	493	1.2
2	443	459	488	495	2.1
2.5	445	460	489	496	2.45
3	446	461	490	497	2.96

In addition to that char produced during the degradation process can also absorb the heat generated in the degradation and assist to slow down the overall degradation process. The reduction in MFI of the composites compared to the HL-2matrix is also suggestive of this.

6.B.3.5.2 Differential Scanning Calorimetry

It is of immense importance to study the melting and crystallization behavior of neat blend and its nanocomposites since crystallinity and crystal structures play a major role in the mechanical and other properties

of crystalline polymers. The mechanical properties of the HL-2 can be significantly enhanced by the addition of fibrous PGNS, if there is any change in the crystallization characteristics of the neat blend by the addition of nanofillers can be well explored by DSC. DSC analyses were used to evaluate, if any, the effect of size and morphology of the silica fibers on T_m and crystallinity of HL-2 matrix. DSC cooling and heating curves of neat HL-2 blend and 2 weight% loaded PGNS nanocomposite are shown in Figure 6.B.12.
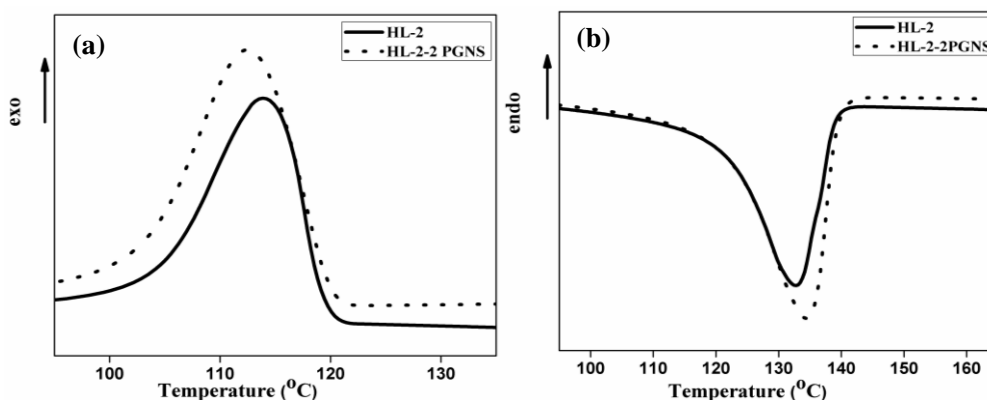
Figure 6 B.12   Non-isothermal crystallization studies (a) Cooling (b) Melting behavior of HL-2-2PGNS composites

The crystallization temperature (T_c), apparent melting temperature (T_m), corresponding enthalpies (ΔH_c) and ΔH_m of the composites and the neat blend are summarized in Table 6 B.2

Table 6 B.2   Non-isothermal crystallization characteristics of HL-2- PGNS composites

Sample	T_m ($^\circ$C)	ΔH_f (J/g)	T_c ($^\circ$C)	ΔH_c (J/g)	X_c (%)
HL-2	133	145	109	162	61.86
HL-2-2 PGNS	135	146	110	145	62.28

The addition of PGNS, in general does not alter the crystallinity. Similar observation has shown by *et al.* that addition of untreated or polymer grafted silica nanoparticles does not have considerable effect on the crystallinity and crystallization temperature of PP [20].

6.B.4 Conclusions

HL-2-PGNS nanocomposites were fabricated by incorporating the isolated fibrous silica, PGNS into the PE matrix melt mixing followed by injection moulding. Static mechanical, rheological and thermal properties of the PGNS reinforced nanocomposites were analyzed. The HL-2-PGNS nanocomposites with 1.5 weight% loading show an enhancement of 16% in tensile strength, 26% in flexural strength and 35% in flexural modulus compared to pure matrix without any surface modification to both the filler and the matrix. Tensile modulus increases progressively with increasing PGNS loadings. Impact strength shows a 62% enhancement at 1weight % PGNS addition. Absence of any chemical interaction is proved by the FTIR studies. The mechanical interlocking between the polymer chains and the fibrous filler is clear from MFI analysis and it was confirmed by morphological investigation through SEM of tensile fractured surface of the nanocomposite. SEM images also show that PGNS fibers are distributed well in the matrix without any surface modifications. Thus the enhanced mechanical performance is well correlated with their morphological investigations. Rheological analysis confirms better interaction between the filler and PE matrix. Lower complex viscosity than HL-0 confirms better processability than HL-0. With the inclusion of PGNS into the HL-2 matrix the thermal stability has been drastically increased, as evidenced from the

TGA analysis. DSC studies show the PGNS acts as weak nucleating agent for PE matrix. The results support the need for good dispersion of fibrous nanosilica in the blend for any significant improvement in properties.

References

[1]   Bonafield WJ. Biomed. Eng. 1988; 10:522-6.

[2]   WangM, Joseph R, Bonafield W. Biomaterials. 1988; 19:2357-66.

[3]   Di Silvio L, Dalby M, Bonfield WJ. Mater. Sci. Mater. Med .1998; 9:845-8.

[4]   Fornes TD, Paul DR. Polymer. 2003; 44:4993-5013.

[5]   Sheng N, Boyce MC, Parks DM, Rutledge GC, Abes JI, Cohen RE. Polymer. 2004; 45:487-506.

[6]   Shia D, Hui CY, Burnside SD, Giannelis EP. Polym. Compos.1998;19:608-17.

[7]   Luo JJ, Daniel IM. Compos. Sci. Technol. 2003; 63:1607-16.

[8]   Zhu L, Narh KA. J.Polym. Sci. Part B Polym. Phys. 2004; 42:2391-406.

[9]   Jo C, Fu J, Naguib HE. Polym. Eng. Sci. 2006; 46:1787-96.

[10]   Nath S, Bodhak S, Basu B. J. Biomed. Mater. Res. Part B Appl. Biomater. 2009;88:1.

[11]   Jeziórska R, Zielecka M, Gutarowska B, Żakowska Z. Int. J.Polym. Sci. 2014; 2014.

[12]   Lin N, Dufresne A. Macromolecules. 2013; 46:5570–5583.

[13]   Nielsen LE, Robert RF. Mechanical properties of polymers and composites, New York; 1974.

[14]   Rahman NA, Hassan A, Yahya R, Lafia-Araga RA, Hornsby PR. J. Reinf. Plast. Compos. 2012; 31:269-81.

[15]   Amuthakkannan P, Manikandan V, Jappes JW, Uthayakumar M. Mater. Phys. Mech. 2013; 16:107-17.

[16]   Ares A, Pardo SG, Abad MJ, Cano J,Barral L. Rheol. Acta .2010; 49:607-18.

[17]   Rezanavaz R, RazaviAghjeh MK, Babaluo AA. Polym. Compos. 2010; 31:1028-36.

[18]   BiswalManoranjan, MohantySmita, Sanjay Nayak K. Polym. Compos. 2011; 32:1190–201.

[19]   Ren F, Ren PG, Di YY, Chen DM, Liu GG. Polym. Plast. Technol. Eng. 2011; 50:791-6.

[20]   Rong M Z, Zhang M Q,Zheng YX, Zeng HM, Walter R, friedrich K. Polymer. 2001; 42:167.

Part C

HMHDPE/LLDPE/BMS NANOCOMPOSITES

Nanocomposites based on 80/20 HMHDPE/LLDPE blend (HL-2) reinforced with silica nanofibers isolated from Bamboo (BMS) was fabricated through melt mixing in a Thermo Haake Rheocord mixer. The amount of filler was varied from 0 to 3 weight %. The mechanical properties, thermal stability and rheological properties of the nanocomposites have been evaluated. BMS reinforced nanocomposites show considerable improvement in mechanical properties without any surface modification to both the filler and the matrix. SEM analysis of the tensile fractured surface clarifies how bundles of fiber in micrometer range separate into nanofibers and reinforce the HL-2 matrix. FTIR analysis confirms the absence of chemical interaction between the filler and matrix. Rheological analysis of the nanocomposite reveals enhanced interaction between BMS and the HL-2 matrix. Thermo gravimetric analysis (TGA) shows improved thermal stability of HL-2-BMS nanocomposites. DSC analysis suggests weak nucleating effect of the filler.

6.C.1 Introduction

Polymer nanocomposites are innovative materials due to their light weight with significant improvement in properties. With unique properties and diversified applications, thermoplastics are most extensively used matrix for polymer nanocomposite preparations. Among thermoplastic polymers polyethylene plays a major role and occupies the topmost positions. Depending on the crystallinity, density and molecular weight polyethylenes are classified into a large number of varieties.

Many attempts have been done to enhance the properties of polyethylenes or their blends with nano fillers for specific applications. Silica containing immobilized nanosilver was used to improve the addition between maleated HDPE and wood fiber by R. Jezi' orsaka *et al.* They found that silica nanoparticles increase the eleastic and flexural moduli of wood fiber reinforced HDPE [1]**.** S. H Lee *et al.* found that PP containing MWCNT composites shows drastic improvement in electrical properties [2]. Mechanical properties of LLDPE have been enhanced by the incorporation of nanoclay as reported elsewhere [3, 4]

Owing to the recyclability and low cost, polymer industry gave immense attention to natural fibers and industrial byproducts. Since the end of 20th century, interest has been focused on the applications of natural fibers like wood fibers and non-wood plant fibers like jute, kenaf and bagasse, with thermoplastic fibers for the manufacture of natural fiber-polymer composite for value added products [5-13]. Lu *et al.* studied the influence of sugar cane fibers on the mechanical properties of HDPE and they reported that improved properties were observed by the addition of sugar cane fibers and it was well influenced by the nature, dimension and aspect ratio of the fiber [14].

Reinforcing effect of fibrous silica having natural origin on the properties of PE has not been reported earlier. Bamboo, the fastest growing grass species and the effect of bamboo charcoal for the synthesis of multiwalled carbon nanotubes were studied by Jiangtao Zhu *et al.* and the role of minerals on the growth of CNTs was also explored [15]. S. Nahar *et al.* studied reinforcing effect of bamboo fiber as such on the mechanical

and interfacial properties of polypropylene (PP) and they compared the properties of jute fiber reinforced PP [16]. They revealed that bamboo fiber reinforced PP had higher tensile properties and the degradation studies in soil showed that bamboo fiber/PP composite retained its original mechanical properties than jute fiber/PP composite.

In the present study it is proposed to investigate the reinforcing effect of fibrous silica isolated from bamboo (BMS) on 80/20 blend of HMHDPE-LLDPE (HL-2).

6.C.2 Methodology

6.C.2.1 Materials and sample preparations

HMHDPE and LLDPE granules were placed in an air oven set at $100^{o}C$ for four hours to remove any moisture present and allowed to cool to room temperature in a desiccator. 80% HMHDPE/20% LLDPE (HL-2) were melted with 0.5, 1, 1.5, 2, 2.5, 3 wt % of the isolated silica fibers BMS. The blends containing 0 weight % filler are designated as HL-2. The blends containing BMS were designated as HL-2-XBMS, where X is 0.5, 1, 1.5, 2, 2.5, 3 wt% of BMS (e.g., HL-2-0.5BMS). For the fabrication of polymer blend nanocomposites first the polymer pellets were fed into the mixing chamber of Thermo Haake Rheomix Poly Lab system equipped with roller type rotors operating at 50 rpm set at a temperature of 160 °C. After 2 minutes of mixing, required quantities of BMS were added to the polymer melt. A mixing time of 6 minutes was allowed to complete the reaction. In all the cases to ensure proper mixing the torque in the Haake mixing chamber was stabilized. The hot mix taken from the chamber immediately pressed in a hydraulic press and then cut into small pieces and

finally subjected to injection moulding at 170 °C. The detailed characterization techniques are discussed in Chapter 2.

6.C.3 Results and discussion

6.C.3.1 Mechanical properties

6.C.3.1.1 Tensile properties
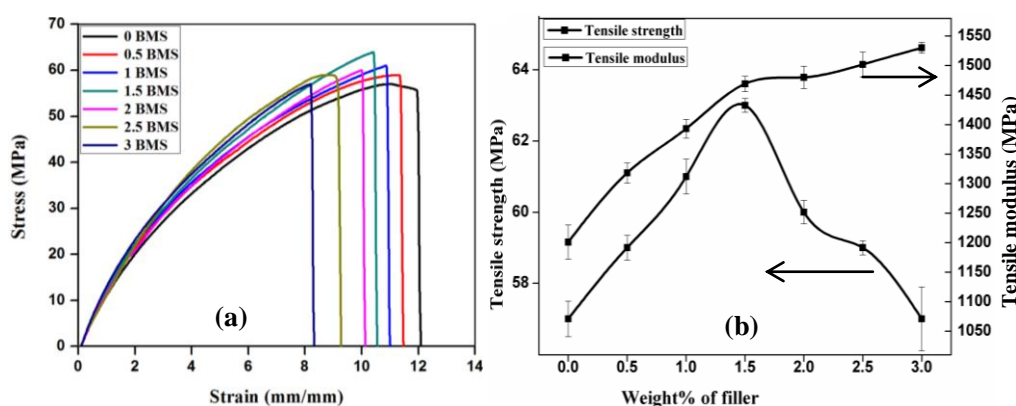
Figure 6 C.1 Tensile properties of HL-2-BMS composites (a) stress-strain curve of HL-2-BMS composites (b) variation of tensile strength and tensile modulus with BMS loading

The stress-strain curves of HL-2 blend matrix and the BMS loaded composites are shown in Figure 6 C.1(a). The entire sample shows same fracture behavior with clear yield point after that sudden breaks occur. Variation of tensile strength and tensile modulus with increasing BMS loading is given in Figure 6 C.1(b). Initially tensile strength increases with increasing filler loading, reaches a maximum and after that begins to decrease. The decrease in tensile properties may be due to agglomeration of filler particles. When the agglomerates are present stress concentration on these agglomerates leads to easy failure. Tensile strength shows a

marginal increase with BMS loading, reaches a maximum at 1.5 weight % BMS loading. The improvement in strength is mainly attributed to the absorption of stress by the fibrous filler and its uniform distribution throughout the matrix. Tensile modulus steadily increases with increasing BMS addition as expected. The elongation at break decreases with increasing filler loading, because the crack propagates via much weaker interfacial regions leading to the fracture of the composites at lower elongation values [17].

6.C.3.1.2 Flexural properties
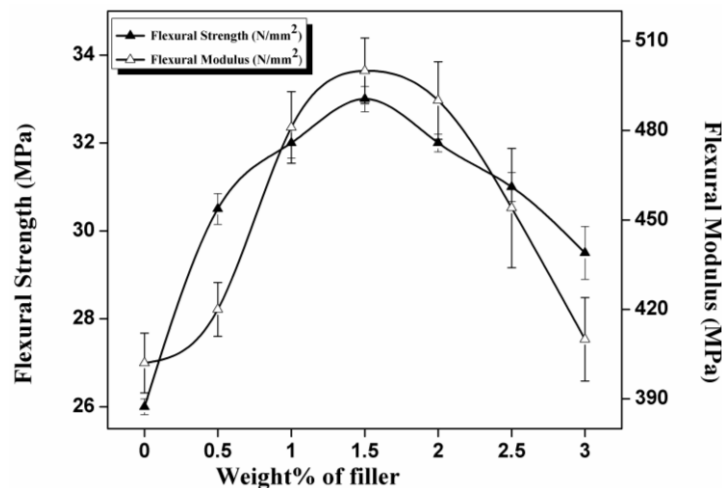
Figure 6 C.2 Variation of flexural strength and flexural modulus with BMS loading

The improved flexural properties of the HL-2-BMS composites are evident from Figure 6 C.2. Maximum enhancement is achieved for the composite loaded with 1.5 weight % BMS with 30% improvement for flexural strength and 25% for flexural modulus substantiating the better resistance towards bending forces. After that a decrease in both

the flexural strength and modulus is noted, which is mainly due to the weaker filler matrix interaction produced by the overcrowding at higher filler loadings.

6.C.3.1.3 Impact strength
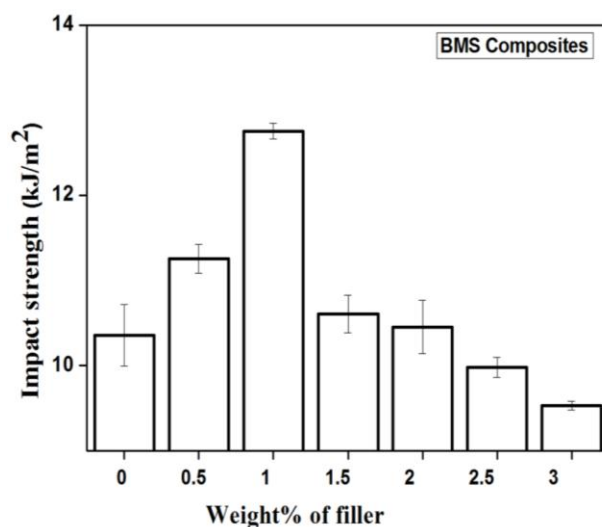
Figure 6 C.3 Variation of impact strength of HL-2-BMS composites

Figure 6 C.3 shows the variation of notched impact strength with BMS loading. The impact strength increases with increase in BMS addition up to 1 weight % and after that it decreases. The improvement in the impact strength is credited due to the enhanced interfacial adhesion between fibrous filler and polymer matrix, which require more energy to de-bond the fiber from the matrix. Moreover fibers also absorb the external stress applied during impact loading, which delays the rupture. However, a decreasing trend is observed for the impact strength with higher BMS addition due to poor interfacial adhesion between the fibrous filler and matrix.

6.C.3.1.4 Hardness
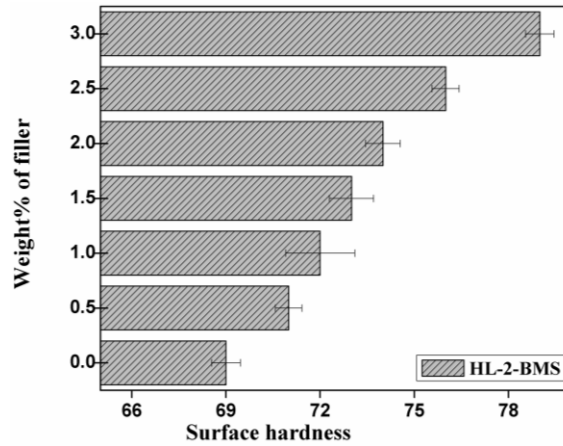
Figure 6 C.4 Variation of surface hardness of HL-2-BMS composites

The effect of BMS on the hardness is shown in from Figure 6 C.4. Surface hardness of the material is a measure of its resistance to indentation and it indicates the degree of compatibility and crosslink density. A regular improvement in hardness is observed. The increase in hardness may be due to the higher stiffness of the silica particle. The hardness increment of nanocomposites can lead to an improvement in their wear resistance.

6.C.3.2 FTIR spectrum
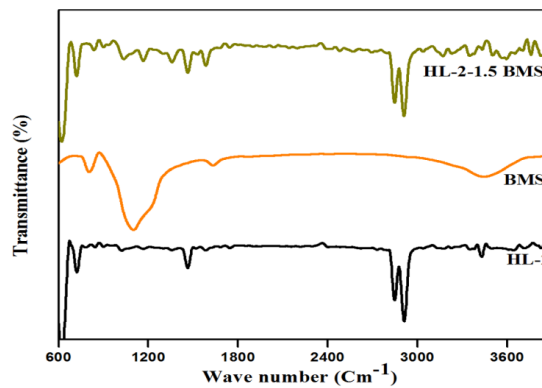
Figure 6 C.5 FTIR analysis of HL-2-1.5BMS composites

FTIR spectra of HL-2 matrix, pure BMS and the HL-2-1.5BMS composites are given in Figure 6 C.5. There is no significant shift in the characteristic peaks of HL-2 in the HL-2-1.5BMS composite, which shows that there is no chemical interaction between the filler and the matrix. The inclusion of BMS in the HL-2 matrix is confirmed from the FTIR spectrum of the HL-2-1.5BMS.

6.C.3.3 Microstrure analysis
6.C.3.3.1 SEM analysis
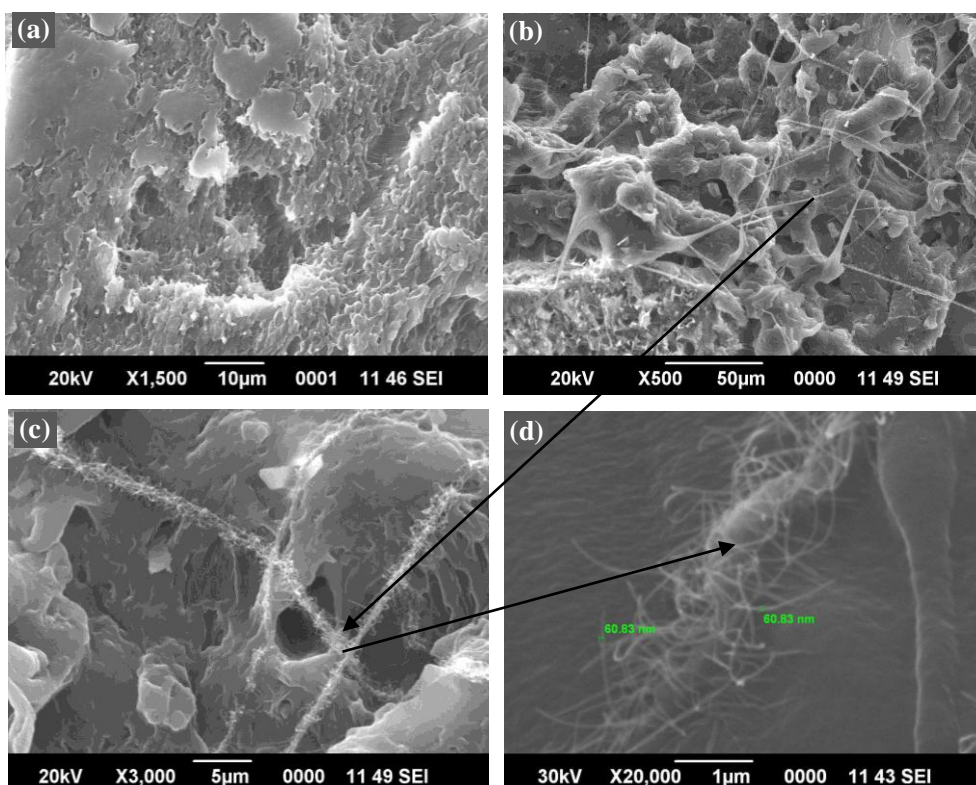
Figure 6 C.6 SEM images of tensile fractured surfaces of (a) HL-2 blend, (b), (c) and (d) HL-2-2BMS composite at different magnifications

The morphological difference of the tensile fractured surface of neat HL-2 blend (a) and HL-2-BMS composite loaded with 2 weight % of BMS

at different magnifications ((b), (c), and (d)) are illustrated in the Figure 6 C.6. Commendable difference is noticed in the composite than the blend. The surface of neat blend shows voids. In the microstructure of composite the bundles of silica, (shown in chapter 4 Figure 8 (e) and (f) SEM images; and also in Figure 14 (a) and (b) TEM images) release the individual nano fibers with an average fiber diameter of 60 nm which reinforces the polymer. During composite preparation how the individual fibers are separated from the fiber bundles of BMS and strengthen the HL-2 matrix is demonstrated from Scheme 6 C.1. This mechanical interlocking between the filler and the matrix without any surface modification can enhance the mechanical properties of the blend.
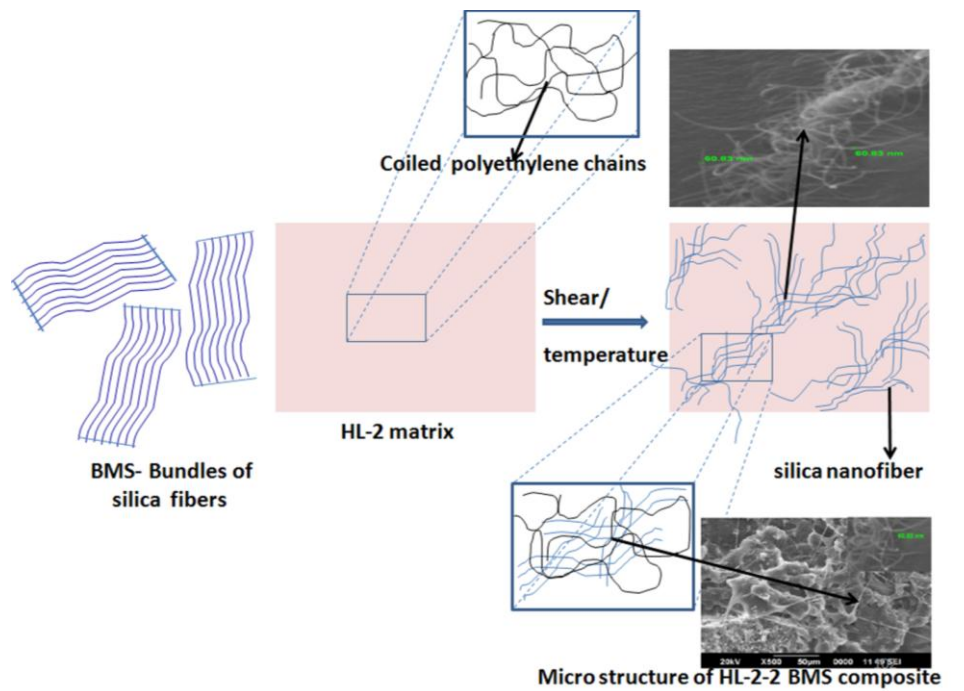
Scheme 6 C.1: Pictorial representation for the preparation and microstructure of HL-2-2 BMS composite
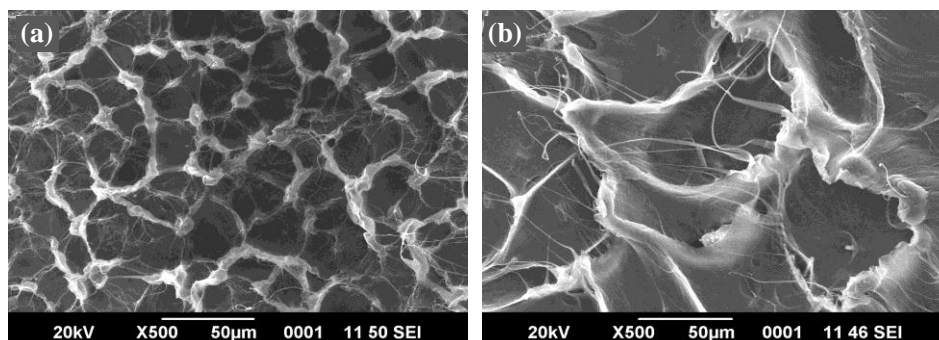
**Figure 6 C.7 SEM images of impact fractured surfaces of (a) HL-2
(b) HL-2-1BMS**

The morphological difference of the impact fractured surface of the neat HL-2 blend and the composite loaded with 1 weight % of BMS is illustrated in Figure 6 C.7 (a) and (b) respectively. Compared to neat blend the SEM images of HL-2-BMS composite have edge like structure with large interface. Moreover the failure surface becomes rougher which indicates that the propagation of crack during impact loading is very difficult. Thus the elevated interfaces possibly absorb more energy thus improving the property.

6.C.3.4 Melt rheological analysis
6.C.3.4.1 Melt flow index (MFI)
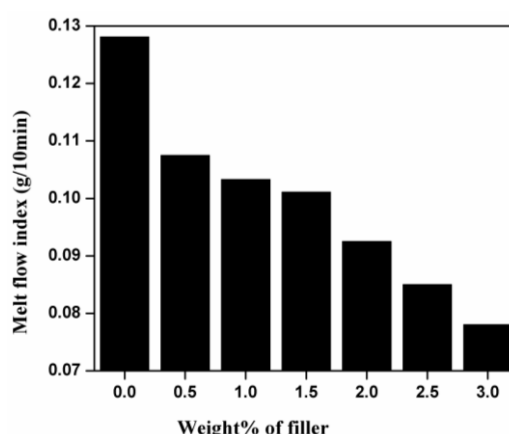
Figure 6 C.8 Variation of MFI of HL-2-BMS composite with BMS loading

The influence of BMS loading on the melt flow rate is represented in Figure 6 C.8. MFI value decreases with the increasing BMS content showing reduced flow properties of the composites. A steady decrease in MFI is credited mainly to the increasing entanglements, which also leads to the restricted mobility of the polymer chains in the vicinity of the effective interaction of BMS with HL-2 polymer matrix.

6.C.3.4.2 Dynamic rheological analysis (DRA)
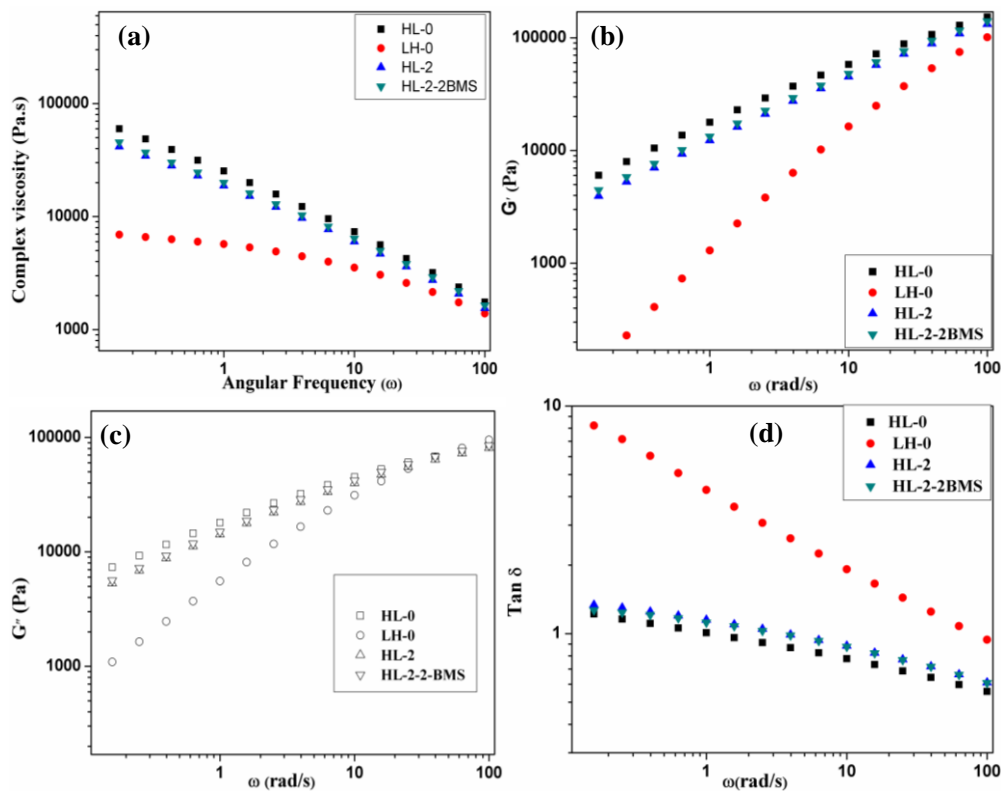
Figure 6 C.9 Rheological observations of HL-2-2BMS composite
(a) Variation of complex viscosity as a function of frequency
(b) Variation of storage modulus as a function of frequency
(c) Variation of loss modulus as a function of frequency and
(d) Variation of tanδ as a function of frequency

Polymer rheological properties are often sensitive to the variations of polymer composition and structure. In the case of polymer nanocomposites both the rigid filler particles and the molten polymer matrix can have a commendable role on the rheological behavior of the composite material. Figure 6 C.9 shows the complex viscosity, storage modulus (G'), loss modulus (G") and tan δ as a function of frequency for neat HL-0, LH-0, HL-2 blend and the HL-2-2BMS composites. First, it can be noted that the addition of BMS has slightly enhanced storage modulus and loss modulus than the matrix blend HL-2 in the entire frequency region. Furthermore HL-2-2BMS composites exhibit significantly higher storage and loss modulus than LH-0 but much lower value than HL-0 at lower frequency region. Both storage and loss modulus gradually approach those of LH-0 and HL-0 at high frequency region. The enhancement in these properties depicts the better interaction of filler and the matrix due to the effective dispersion of filler particles.

Figure 6 C.9 (a) shows logarithmic plots of complex viscosity versus frequency for neat LH-0, HL-0, HL-2 blend and HL-2-2BMS nanocomposites. Complex viscosity of the nanocomposite has slightly higher value over entire frequency region, while that has lower value than HL-0 and higher value than LH-0 at lower frequency region. The enhancement in complex viscosity of the nanocomposite at lower frequency region clearly indicates enhanced interaction between the filler and the HL-2 matrix by interfacial reactions in the melt. These results are completely in accordance with what was already observed for other similar systems.

6.C.3.5 Thermal properties
6.C.3.5.1 Thermogravimetric analysis
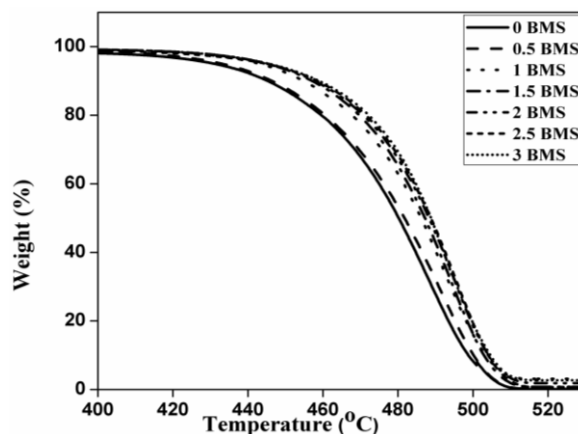
Figure 6 C.10 Thermogram of HL-2-BMS composites

Figure 6 C.10 shows the dependence of the decomposition temperatures (T_{onset}, T_{max}, T_{10} and T_{50}) on BMS content for HL-2-BMS composites and the corresponding thermal analysis data are tabulated in Table 6 C.1.

Table 6 C.1 Thermal analysis of HL-2-BMS composites

BMS content (wt%)	Temperature at different mass losses (°C)			Peak max (T_{max}, °C)	Residue at 600 °C (%)
	T_{onset}	$T_{10\%}$	$T_{50\%}$		
0	426	448	483	491	0.08
0.5	434	456	489	492	1.02
1	437	457	487	494	
1.5	441	458	489	495	1.8
2	444	459	489	496	2.24
3	446	460	490	497	2.96

The presence of BMS shifts the degradation temperatures towards higher values, signifying a higher thermal stability of the nanocomposites with respect to the neat blend. Neat HL-2 starts to lose weight at 426 °C, whereas addition of even 0.5 weight% BMS causes the decomposition temperature of

HL-2 to rise by more than 8 °C. It can be seen that the thermal stability of the nanocomposites is improved compared with neat HL-2 matrix. The enhancement in thermal stability of HL-2-BMS nanocomposites may be due to the factors: presence of inorganic fillers like BMS restricts the polymer chain mobility which declines the pyrolysis of carbon-carbon scission in HL-2 matrix; the dense char formed absorbs more heat than the organic polymer matrix and thereby hinders thermal degradation [18, 19].

6.C.3.5.2 Differential scanning calorimetry

DSC analysis is a convenient method for the analysis of first order transitions like melting and crystallization of polymers and their composites. Non isothermal crystallization curves of HL-2 blend and HL-2-2BMS composite are shown in Figure 6 C.11. The crystallization curve is represented in (a) and the corresponding melting curve in (b). The apparent melting point (T_m), crystallization temperature (T_c), enthalpy of fusion (ΔH_m), enthalpy of crystallization (ΔH_c), and the percentage of crystallinity (X_c) are reported in Table 6 C.2.
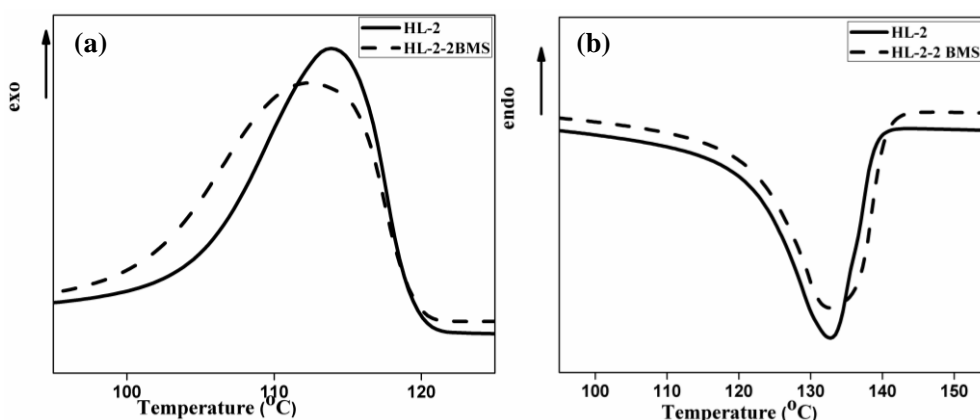
Figure 6 C.11 Non-isothermal crystallization studies (a) Cooling (b) Melting behavior of HL-2-2BMS composites

Table 6 C.2 Non-isothermal crystallization characteristics of HL-2-BMS composites

Sample	T_m (°C)	ΔH_f (J/g)	T_c (°C)	ΔH_c (J/g)	X_c (%)
HL-2	133	145	109	162	61.86
HL-2-2BMS	133	142	111	146	60.5

From the DSC analysis data it is obvious that the T_m is unaffected but there is slight increase in the crystallization temperature T_c. This confirms a weak nucleating effect of fibrous BMS in HL-2 matrix. Comparable results were found in previous work on LLDPE-AIN composites and on HDPE-CaCO$_3$ composites [20].

6.C.4 Conclusions

HL-2-BMS nanocomposites were fabricated by incorporating the isolated fibrous bamboo silica BMS, into the PE matrix through melt mixing followed by injection moulding. The isolated fibrous silica exists as bundles of fibers with few micrometers in size as per SEM analysis of BMS filler alone. Static mechanical, rheological and thermal properties of the BMS reinforced nanocomposites were analyzed. The mechanical properties of HL-2 blend are improved by the addition of fibrous BMS. A marginal improvement in tensile and flexural properties is observed for the composite with1.5 weight% loading. Regular increase in tensile modulus is also noted. Impact strength shows a 28% improvement at 1 weight% BMS addition. Thermal stability is significantly improves by the addition of BMS. Absence of chemical interaction is confirmed by FTIR analysis and the entanglement between the polymer chains and the fibrous filler is indicated by MFI analysis. Rheological analysis confirms enhanced

interaction between the filler and PE matrix. Individual nanofibers get separated from the fiber bundles of BMS during composite preparation and reinforce the HL-2 matrix as observed in the SEM micrographs of the fractured surface of the nanocomposite. This is further correlated with their mechanical performance. DSC studies show that BMS acts as a very weak nucleating agent.

References

[1] Jeziórska R, Zielecka M, Szadkowska A, Zakowska Z, Gutarowska B. J.Biobased Mater. Bio. 2012; 6:370-9.

[2] Lee SH, Kim MW, Kim SH, Youn JR. Eur.Polym. J. 2008; 44:1620-30.

[3] Durmus A, Kaşgöz A, Macosko CW. J.Macromol. Sci. B. 2008; 47:608-19.

[4] Hotta. S, Paul DR. Polymer. 2004; 45:7639-54.

[5] Krzysik AM, Youngquist JA. Int. J.Adhes. Adhesives. 1991; 11:235-40.

[6] Youngquist JA, Krzysik AM, Muehl JH, Carll C. Forest Prod. J. 1992; 42:42-8.

[7] Rowell RM, Keany FM, Wood Fiber Sci..1991; 23:15.

[8] McLaughlin EC. J. Mater. Sci. 1980; 15:886-90.

[9] Raj RG, Kokta BV. Eur.Polym. J. 1991; 27:1121-3.

[10] Nada A, Hassan M. L. J. Sci. Ind. Res. 1999; 58:616.

[11] Hassan ML, Rowell RM, Fadl NA, Yacoub SF, Christainsen AW. J. Appl.Polym. Sci. 2000; 76: 575-86.

[12] Stael GC, Tavares MI, d'AlmeidaJR. Polym. Testing. 2001; 20:869-72.

[13] Paiva JM, Frollini E. J. Appl.Polym. Sci. 2002; 83:880-8.

[14] Lu JZ, Wu Q, Negulescu II, Chen Y. J. Appl.Polym. Sci. 2006; 102:5607-19.

[15]   Zhu J, Jia J, Kwong FL, Ng DH, Tjong SC. Biomass Bioenergy. 2012; 36:12-9.

[16]   Nahar S, Khan RA, Dey K, Sarker B, Das AK, Ghoshal S. J.Thermoplast. Compos. Mater. 2012; 25:15-32.

[17]   Ahmad Fuad MY, Shikor R, MohdIshak ZA, Mohd Omar AK. Plast. Rubber Compos. Process Appl. 1994; 21:225-35.

[18]   Sanchez-Valdes S, Mendez-Nonell J, Ramos de valle L.F, Lozano-Ramierz T, Ramirez-Vargas E, Lopez-Quintanilla M L, Gutierrez-Rodriguez JM.e-Polymers. 2009; 126.

[19]   Sharma SK, Nayak SK.Polymer Degradation and Stability. 2009; 94:132-8.

[20]   Gu J, Zhang Q, Dang J, Zhang J, Yang Z. Polym. Eng. Sci. 2009; 49:1030-4.

.....ജാള.....

Chapter 7

POLYMER BLEND NANOCOMPOSITES FOR HIGH PERFORMANCE APPLICATIONS

Polymer nanocomposites based on 80/20 blend of HMHDPE-LLDPE (HL-2) reinforced with nanozirconia (m-ZrO_2 and t-ZrO_2) and silica nanofibers (CGS, PGNS and BMS) were fabricated through melt mixing. Potential of these nanocomposites for high performance applications was investigated by studying the mechanical properties like compressive property, fracture toughness and tribological properties. Wear resistance was tested by pin-on-disc method and the corresponding worn surfaces were analyzed through SEM. It is found that both the compressive properties and SEN-TB fracture toughness of the pure HL-2 blend were improved by the addition of nanofillers, indicating better load bearing capability of the material. It is also found that nanocomposites exhibit lowest coefficient of friction in comparison with HL-2 blend. The SEM photographs of the wear traces indicate that a uniform thin layer of inflexible coating is formed on the surface of the disc. These coating may be a major facts for the lower value of the coefficient of friction.

7.1 Introduction

Metals and ceramics are generally used for high performance biomedical applications. In the current scenario with the advancement in nanoscience and nanotechnology polymer nanocomposites are potential candidate for such special application. By the incorporation of nanofillers the properties of the polymers can be tuned for specific high end applications. Wear resistance, the key property in such load bearing applications can be improved by the incorporation of nanofillers since the nano phase in the polymer composite forms a homogeneous and inflexible transfer coating on the surface of the load bearing materials. The most extensively studied nanofillers for this special purpose are $nanoZrO_2$, nanohydroxy apatite (HA), nanoZnO, $nanoAl_2O_3$ due to their intrinsic strength and biocompatibility. More over short aramid (AF), carbon fibers (CF) or glass fibers (GF) are also used to boost the creep resistance and the compressive strength of the polymer matrix [1-4].

Due to outstanding wear resistance, chemical resistance, extreme toughness, low frictional property, and relatively low cost, polyethylenes (PE) such as HDPE, UHMWPE, and other PE composites are widely used in various high performance applications [5]. UHMWPE is a choice polymer in many engineering applications and in the biomedical field such as wheels, runners for bottling production lines, gears, bearings, lining for coal chutes, orthopedic implants and even in bullet resistant vests [6]. HDPE has enormous tribological applications including automotive industry, low speed bearings, pressure pipes etc [7-9]. Along with UHMWPE and HDPE, highly stable polymeric systems like PTFE [10] and PEEK [11] have been

investigated for orthopedic implant applications due to their excellent mechanical properties. Out of these polymers, UHMWPE, HDPE and PE composites are the most promising materials as well as widely accepted.

The major problem associated with the use of PEs as acetabular cups is not only the wear of the cups themselves but also the wear of interfacial adhesion between the tissue and the implant. Thus the debris created by wear of PE articulating surfaces is attacked by the body's immune system and lead to bone loss, known as osteolysis. Therefore debris accumulates in the area close to implant; leads to loosening of the implant system, resulting in a repeated surgery. Lifetime of implant systems can improve by enhancing the wear resistance of the polymeric portion of the implant, especially through the use of suitable biocompatible nanofillers.

Excellent results offered by UHMWPE makes it the best candidate for load bearing medical devices [12]. The complex processing of pure UHMWPE by conventional manufacturing practices is very intricate because of its high melt viscosity [13]. Furthermore this high viscous matrix could result in poor dispersions of the nanoparticles during the fabrication of nanocomposite, resulting in poor mechanical performances of the composites [14]. As a result an alternative to UHMWPE for loadbearing medical devices is of paramount importance under economical conditions. Compared with UHMWPE, HDPE has essentially the same chemical structure, comparable mechanical properties, relatively low cost, excellent creep resistance, good processability, and biocompatibility. A number of researchers have investigated the significance of HDPE as matrices in bone implant applications. From 1980 onwards HDPE was

used and examined to develop low-wear and low-friction bone analogue materials [15,16]. However, it was reported that with the long time use, HDPE exhibited a lower wear resistance than that of UHMWPE.

Ever since Bonfield et al. introduced HA reinforced HDPE (HAPEX), there has been a constant attempt to develop bone-analogue nanocomposites for biomedical applications [17-21]. With the advancement of nanotechnology and innovative manufacturing techniques for the preparation of nanocomposites, HDPE based nanocomposites were recently investigated for the utilization in total hip artificial joints [22-24].

Recently a big window of opportunities has opened for HDPE based nanocomposites by the introduction of nanoclay, CNTs and CNFs, [25, 26-28] for total joint replacement applications. Fouad and Elleithy [24] developed HDPE -graphite nanocomposites as load bearing biomaterials, by utilizing the solid lubricant potential of graphite nanoparticles (GNPs). Bodhak and coworkers [29] deliberated the friction and wear properties of HDPE–HA–Al_2O_3 bio-composites and resulted in enhanced properties for the composite. Same type of work was performed by Nath et al. [30] and demonstrated how the stiffness, hardness as well as the biocompatibility property of bioinert HDPE can be extensively enhanced by the combined addition of both bioactive and bioinert ceramic fillers like Al_2O_3 and HA. Pettarin and coworkers [31] modified HMWHDPE by the incorporation of nanoMoS_2 and studied the ability of these fillers to reduce the wear rate and friction of the composites.

The important parameter essential for polymeric counterpart in load bearing joint components in biomedical field is high degree of crystallinity.

Higher crystallinity gives a larger modulus of elasticity, superior yield strength, improved resistance to creep deformation and enhanced fatigue strength. Reduced cost with specific property requirements is a challenge for a polymer technologist, to develop strong biocompatible materials through incorporation of suitable biocompatible fillers. So the modification of commodity low cost polymers by simple blending is of special interest.

Along with other mechanical properties of the polymer nanocomposites used for load bearing medical devices, special attention should given on the compressive property, fracture toughness and wear resistance of the material. In the present part of the work, it is proposed to study the potential of nanozirconia and silica nanofibers in enhancing the load bearing properties of HMHDPE-LLDPE blend.

7.2 Methodology

7.2.1 Sample preparations

80% HMHDPE/ 20% LLDPE (HL-2) were melt mixed with 0.5, 1, 1.5, 2, 2.5,3 wt % of nanozirconia (both m-ZrO_2 and t-ZrO_2) and the isolated silica fibers (CGS, PGNS and BMS) in a Thermo Haake Rheomix poly lab system fitted with roller type operating at 50 rpm for 8 minutes at 160. The hot mix from the chamber was immediately fed into the hydraulic press, cut into small pieces and then injection molded at $170^{o}C$ in a semi automatic type injection moulding machine (Model JIM 1 H series, 4508). Cylindrical specimens for compressive test, rectangular shaped test specimens for fracture toughness and a pin shaped specimens for Pin on disc wear analysis using appropriate moulds.

The characterization methods employed are discussed in Chapter 2.

7.3   Results and discussion

7.3.1 Mechanical properties

7.3.1.1 Fracture toughness

7.3.1.1.1 Fracture toughness of HL-2- nanosilica composites

The SEN-TB fracture toughness (K_{IC}) of fibrous nanosilica filled HL-2 blend nanocomposites is given in Figure 7.1. (a) represent HL-2-CGS nanocomposites, (b) HL-2-PGNS nanocomposites and (c) HL-2-BMS nanocomposites respectively. These figures show how the fibrous silica effectively influences the fracture toughness of the pure HL-2 blend.
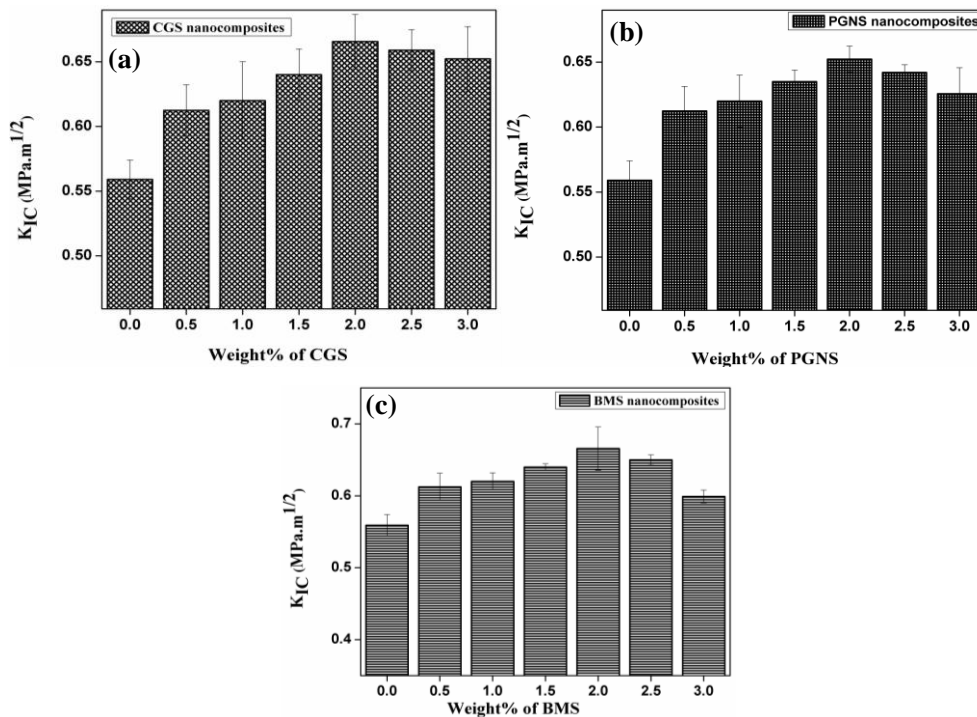
Figure 7.1   Fracture toughness properties of HL-2 nanosilica composites (a) K_{IC} of HL-2-CGS nanocomposites (b) K_{IC} of HL-2-PGNS nanocomposites and (c) K_{IC} of HL-2-BMS composites, against filler loading

In all the cases fracture toughness shows an enhancement of 20% for CGS nanocomposites, 17% for PGNS nanocomposites and 19% for BMS nanocomposites at 2 weight % loading. The increase in fracture toughness of the nanocomposites is mainly due to the ability of the nanofillers to oppose the crack propagation prior to the fracture has taken place [32]. As the silica loading increases, the agglomeration of the filler particle results in the decrease of the resistance of the material against the propagation of crack, accordingly fracture toughness of the composite drop off. Still the K_{IC} value, even at 0.5 weight % filler loading in all the respect is higher than pure HL-2 blend.

7.3.1.1.2 Fracture toughness of HL-2-nanozirconia composites
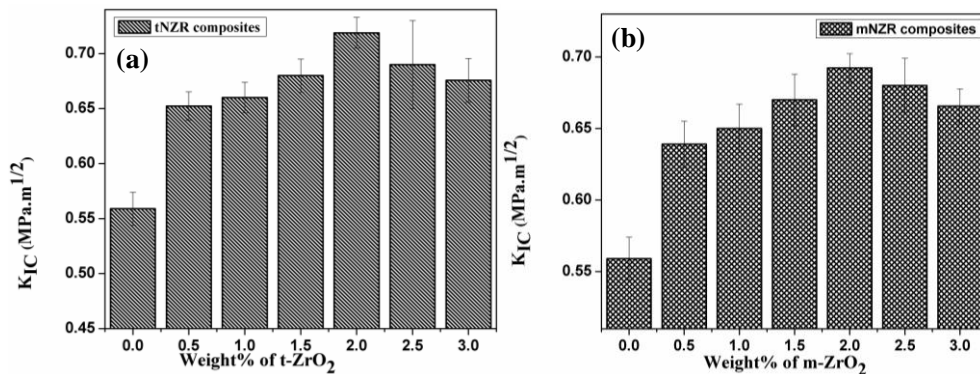
Figure 7.2 Fracture toughness properties of HL-2-nanozirconia composites (a) K_{IC} of HL-2- t-ZrO$_2$ nanocomposites and (b) K_{IC} of HL-2- m-ZrO$_2$ nanocomposites, against filler loading

Fracture toughness of the composites as a function of nanozirconia loading is given in Figure 7.2, where (a) represents the fracture toughness of t-ZrO$_2$ and (b) fracture toughness of m-ZrO$_2$ respectively. Zirconia, being a ceramic material well known for its hardness, once it is used as filler, a reinforced composite with better fracture mechanical properties can be

expected. The improvement in K_{IC} is observed at 2 weight % filler loading in both the cases, after that it decreases. HL-2-t-ZrO_2 composite at 2 weight % t-ZrO_2 loading shows 29% improvement in fracture toughness and 23% increase at the same loading by the addition of m-ZrO_2. This shows that the introduction of nanozirconia appreciably enhances the fracture toughness properties at a particular loading due to better filler matrix interaction, while at higher filler loading agglomeration acts as stress concentrator which allows propagation of crack path much easier way, resulting in decrease in K_{IC}.

7.3.1.2 Compressive properties

7.3.1.2.1 Compressive modulus of HL-2 nanosilica composites

Figure 7.3 Variation of compressive modulus of HL-2-nanosilica composites (a) compressive modulus of HL-2-CGS nanocomposites (b) compressive modulus of HL-2-PGNS nanocomposites and (c) compressive modulus of HL-2-BMS composites, with filler loading

Figure 7.3 shows the variation of compressive modulus with silica loading. In the case materials like polyethylenes that do not burst under compressive force, ultimate compressive strength cannot be evaluated. In this contest compressive modulus is taken to evaluate the load bearing capability of the material. In all the three cases compressive modulus shows a considerable improvement of 37% at 1.5 weight percentage CGS addition and there after it decreases with filler loading. A substantial enhancement of 44% is obtained at 2 weight% PGNS addition and a 33% improvement at 2 weight% BMS addition. After that particular filler loading compressive modulus decreases with increasing filler loading. The enhancement in compressive property is mainly due to the ability of the fibrous nanosilica particles to lock the crack and flaws which are perpendicular to the applied load which further promotes better filler-matrix interaction due to the good dispersion of filler particles in the PE matrix [33]. As a result, compared to neat HL-2 blend HL-2-nanosilica composite can endure more load. The improved compressive modulus is a sign of increased load bearing ability of the material.

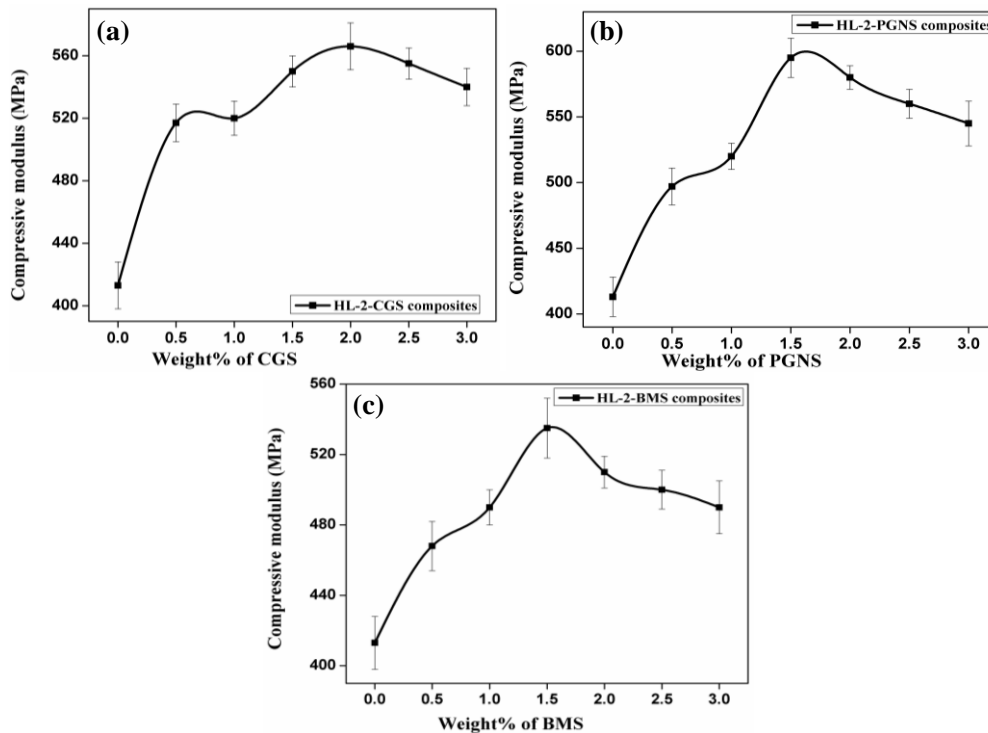### 7.3.1.2.2 Compressive modulus of HL-2 nanozirconia composites
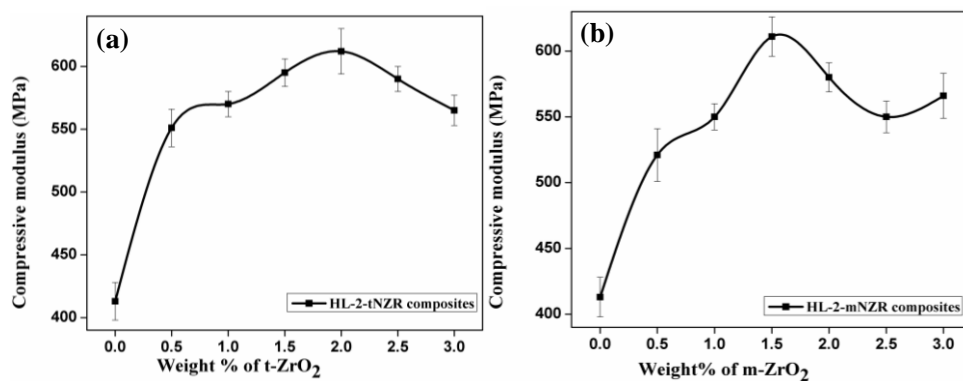

Figure 7.4 Variation of compressive modulus of HL-2-nanozirconia composites (a) compressive modulus of HL-2- t-ZrO$_2$ nanocomposites (b) compressive modulus of HL-2- m-ZrO$_2$ nanocomposites with filler loading

Compressive modulus increases with increase in both types of nanozirconia loading and reaches a maximum at 1.5 weight percentage m-ZrO$_2$ loading and 2 weight percentage t-ZrO$_2$ as observed in the figure. The improvement in compressive modulus by the incorporation of nanozirconia results from the ability of the nanoparticulates to close the crack and defects in the PE matrix during compressive load. 48% enhancement in compressive modulus is observed for HL-2-1.5 m-ZrO$_2$ and HL-2-2 t-ZrO$_2$ composites. The reduction in compressive modulus at higher loading can be due to the agglomeration of nanoparticulates which restrict the insertion into the voids due to larger size.

7.3.1.3 Compressive properties and flexural properties of the HL-2 nanocomposites

Table 7.1 Compressive and flexural mechanical properties of the polymer and HL-2-nanocomposites, where mNZR represent m-ZrO$_2$ and tNZR as t-ZrO$_2$

	Compressive mechanical property		Flexural mechanical property	
	Compressive modulus (MPa)	Offset yield strength (MPa)	Flexural modulus (MPa)	Flexural strength (MPa)
HL-0	527 ± 20	24.78 ± 1.2	505 ± 16	33 ± 0.9
LH-0	170 ± 18	11.58 ± 0.5	80 ± 22	8 ± 1.3
HL-2	413 ± 15	23.13 ± 0.9	402 ± 24	26 ± 0.7
Silica nanocomposite				
HL-2-0.5CGS	517 ± 12	24.01 ± 0.82	432 ± 8	32 ± 0.49
HL-2-2CGS	566 ± 15 (37%)	26.2 ± 1.5 (13%)	478 ± 9 (19%)	33 ± 0.2 (27%)
HL-2-3CGS	540 ± 12	25.1 ± 2.3	427 ± 12	30 ± 0.3
HL-2-0.5PGS	497 ± 14	23.3 ± 2.3	420 ± 8	32 ± 0.35
HL-2-1.5PGS	595 ± 15 (44%)	29.6 ± 0.68 (28%)	543 ± 9 (35%)	35 ± 0.29 (35%)
HL-2-3PGS	545 ± 17	24.96 ± 1.2	429 ± 13	31 ± 0.6
HL-2-0.5BMS	468 ±14	22.9 ± 3.1	420 ± 9	30.5 ± 0.35
HL-2-1.5BMS	535 ±17 (30%)	25.85 ± 1.1 (12%)	500 ± 11 (24%)	33 ± 0.29 (27%)
HL-2-3BMS	490 ±15	23.66 ± 0.5	410 ± 14	29.5 ± 0.6
Zirconia nanocomposite				
HL-2-0.5mNZR	521 ± 20	23.9 ± 1.5	527 ± 16	33 ± 0.65
HL-2-1.5mNZR	611 ± 15 (48%)	31.15 ± 2.1 (35%)	610 ± 12 (52%)	38 ± 0.55 (46%)
HL-2-3mNZR	566 ± 17	27.2 ± 1.2	496 ± 20	34 ± 0.89
HL-2-0.5tNZR	551 ± 15	25.6 ± 0.91	532 ± 16	34 ± 0.65
HL-2-2tNZR	612 ± 18 (48%)	33.22 ±1.9 (44%)	620 ± 12 (54%)	39 ± 0.55 (50%)
HL-2-3tNZR	565 ± 12	26.7 ± 1.3	499 ± 20	36 ± 0.89

The mechanical properties like compressive modulus and flexural properties are equally important for load bearing applications especially for bone tissue engineering applications [34]. The compressive and flexural mechanical properties of the pure polymers, HL-2 blend and their nanocomposites with varying filler (different type of silica nanofibers and nano zirconia) concentrations are listed in table 7.1. The incorporations of nanofillers reinforced the mechanical properties of the HL-2 blend and also the pure polymer HL-0 and LH-0 in a qualitatively similar manner, i.e., the mechanical properties increase with the initial concentrations of both silica and zirconia nanofillers, peaks between 1.5 and 2 weight%, then decreases at higher filler loadings. There are significant enhancements in compressive modulus and flexural modulus for the different groups of the nanocomposites. Similar increases are observed for the flexural strength. However, not much significant reinforcements in offset compressive yield strength are observed for the different nanocomposites tested. Both flexural modulus and strength increase with the incorporation of nanozirconia and silica nanofibers.

7.3.1.4 Wear resistance studies

7.3.1.4.1 Wear resistance of the HL-2 nanosilica composites

Zirconia being a ceramic material well known for its hardness, tribological properties like wear resistance was tests for neat HL-0, LH-0, the blend HL-2 and the nanocomposites according to the pin on disc method. Usually, the wear property of a composite material is illustrated by the coefficient of friction and wear rate.

Figure 7.5 **Variation of coefficient friction of pure polymers HL-0, LH-0, blend HL-2 and the HL-2-nanosilica composites (a) HL-2-CGS nanocomposites (b) HL-2-PGNS nanocomposites (c) HL-2-BMS nanocomposites against sliding distance**

Variation of coefficient friction against sliding distance is shown in figure 7.5. Coefficient of friction is an important factor for deciding the material's tribological properties. Coefficient of friction of CGS filled composites [Figure 7.5 (a)] shows lower value than the pure polymer and the blend matrix. Evidently, the nanocomposites with 3 weight% CGS filled HL-2 blend has lowest coefficient of friction, which indicates that as the filler concentration increases the corresponding nanocomposites become more wear resistant. During the course of wear experimentation,

the removed nanoparticles might also perform as solid lubricants. These account for the lower specific wear rates and friction coefficients of the nanocomposites [35]. In these fibrous silica based nanocomposites HL-2-3PGNS composite shows lowest coefficient of friction hence most wear resistant.

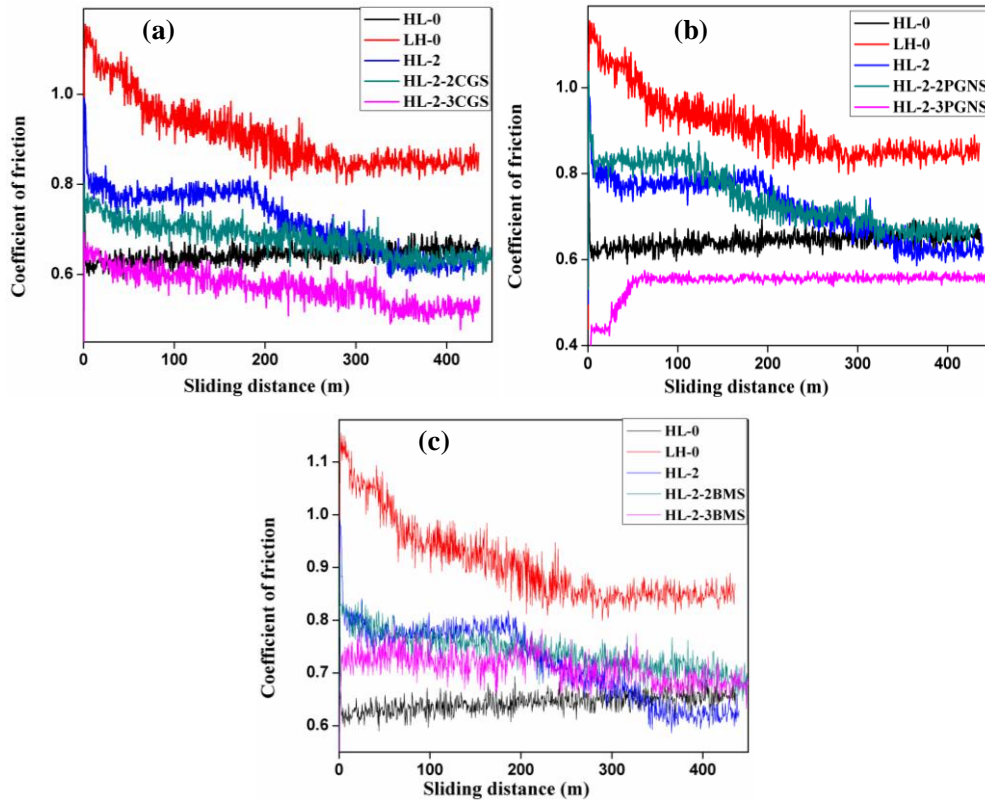## 7.3.1.4.2 Wear resistance of the HL-2 nanozirconia composites
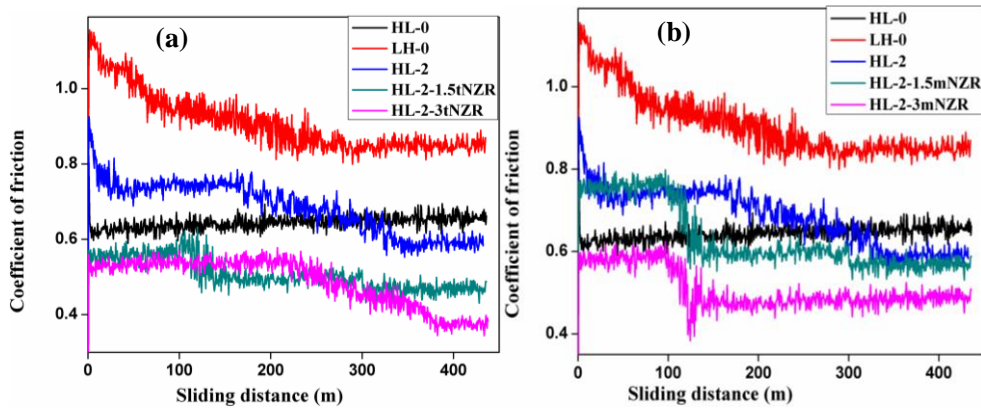
Figure 7.6 Variation of coefficient friction of pure polymers HL-0, LH-0, blend HL-2 and the HL-2-nanozirconia composites (a) HL-2-m-ZrO₂ nanocomposites (b) HL-2-t-ZrO₂ nanocomposites against sliding distance

Figure 7.6 shows the wear behavior of raw polymers, the blend HL-2 and the nanozirconia reinforced HL-2 blend nanocomposites and it was investigated by determining the change in friction coefficient as a function of wear distance. It is observed that both types of zirconia reinforced HL-2 blend nanocomposite show lower coefficient of friction than that of the pure polymers and the blend. Lower friction coefficient indicates increased wear resistance of the composite material. Results show that the nanocomposites exhibit better dispersion and which results in much stronger interfacial

bonding between the nanoparticulates and the PE blend matrix. As the nanozirconia loading increases the friction coefficient again decreases, because a positive rolling effect of the nanoparticles between the materials and the filler is proposed due to the presence of more wear resistant ceramic counterpart. Similar result is observed for the two composites (m-ZrO_2 and t-ZrO_2 composites), due to the extremely uniform distribution of both fillers in the PE matrix, although independent of the type of crystallinity whether monoclinic or tetragonal zirconia [36].

Table 7.2 Wear rate of the sample

Sample name	Specific wear rate ($10^{-5}*$ $mm^3N^{-1}m^{-1}$)
HL-2 blend	1.4
HL-2-2 CGS	1.3
HL-2-3 CGS	1.2
HL-2-2 PGNS	1.19
HL-2-3 PGNS	1.01
HL-2-2 BMS	1.2
HL-2-3 BMS	1.1
HL-2-2 m-ZrO_2	1.2
HL-2-3 m-ZrO_2	1.1
HL-2-2 t-ZrO_2	1.1
HL-2-3 t-ZrO_2	0.9

Table 7.2 shows the wear rate of the material. Wear rate was assesed from the profiles of the trace on materials surface. The nanocomposites posesses minimum wear rate than the blend. As the nanofiller loading increases, the wear rate decrease in all the trials.

7.3.2 Morphological analysis by SEM

7.3.2.1 Morphological analysis of the fracture toughness specimen

Figure 7.7 SEM photographs of SEN-TB fracture toughness specimens (a) pure blend HL-2 (b) HL-2-2PGNS nanocomposite (c) HL-2-2BMS nanocomposite (d) HL-2-t-ZrO$_2$ nanocomposite

Microstructure analysis of the TPB fractured surface of the fracture toughness specimens of pure blend and the nanocomposites were examined by SEM analysis and the resultant micrographs are shown Figure 7.7. The SEM images of the pure blend [(Figure 7.7(a)] show smooth and weak surface which makes the characteristic ineffective brittleness and low results for K$_{IC}$. A different morphology was observed for nanocomposites [Figure 7.7 (b-d)]; much rougher surface is noticed in contrast to the pure blend. Presence of nanofillers in the PE matrix makes fracture to extend along a very twisted route by the formation of matrix plastic deformation,

which makes longer time to break and more absorption of energy resulting enhanced K_{IC} [37].

7.3.2.1 Morphological analysis of the worn surface of the wear resistance test specimens
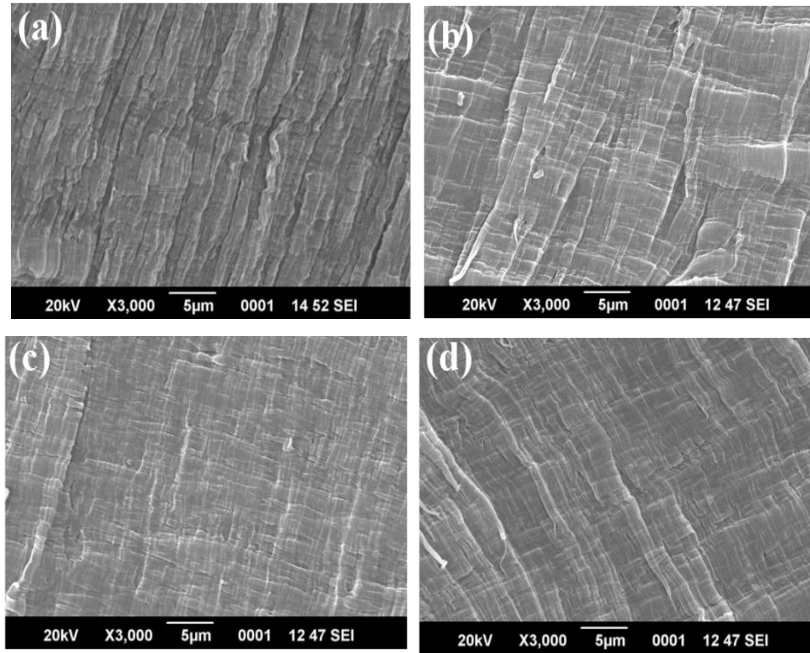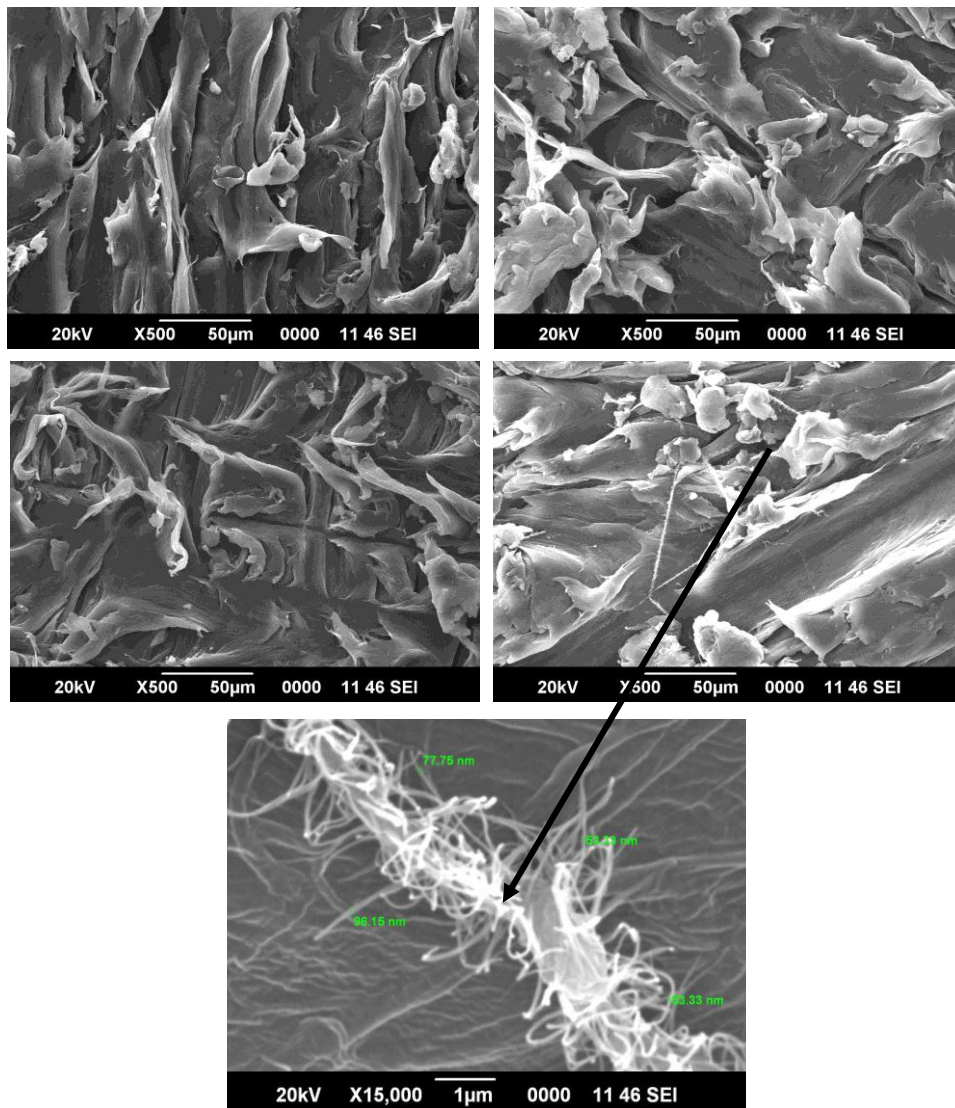

Figure 7.8 SEM photographs of SEN-TB fracture toughness specimens (a) pure blend HL-2 (b) HL-2-2PGNS nanocomposite (c) HL-2-2BMS nanocomposite (d) HL-2-t-ZrO$_2$ nanocomposite

SEM analysis of the worn surfaces of the neat blend and the nanocomposite are shown in Figure 7.8. SEM micrographs of the worn surfaces provide knowledge about both, the role that nanoparticles play in the reduction of wear rate, and the wear mechanisms. The SEM image of the worn surface of the blend is more rough indicates that the micrometers size of the polymer fragments detach from the surface of the HL-2 blend during the course of the experiment and leaves small craters behind. These polymer fragments might be captured between the counterface and the pin sample, abrade the sample surface leading to even more substantial loss of material. In the case of filled nanocomposites, the SEM images are completely different and become rather smooth. Noticeable difference is noticed for the SEM images of HL-2-2 m-ZrO$_2$, HL-2-2 t-ZrO$_2$ [Figure 7.8 (b) and (c)] and also for the HL-2-2 PGNS composite [Figure 7.8 (c)] . the micro structure investigation of the PGNS loaded nanocomposite of the worn surface also show the debundling of the fibers of PGNS into individual nanofibers, which has been already stated in the Chapter 6 B.

7.4 Conclusions

The effect of fibrous nanosilica and nanozirconia on the mechanical and tribological properties of HL-2 blend nanocomposite has been studied. It is found that the mechanical properties improve with nanofiller (both nanosilica and zirconia) content upto a particular loading and then decreases. The progress in mechanical properties is supposed to be due to the presence of more contact positions offered by the small sized nanoparticulates and the PE matrix. SEN-TB fracture toughness improves by 20% in HL-2-2CGS composite, 17% in HL-2-2PGNS and 19% in HL-2-2BMS composite.

Moreover the zirconia based nanocomposite exhibits an improvement of 23% in HL-2-2mZrO$_2$ and 29% in HL-2-2tZrO$_2$ composite. The high compressive strength of brittle ceramic nanoparticles coupled with efficient stress transfer results in superior compressive properties for both the silica and zirconia based nanocomposites. Compressive modulus shows an enhancement of 37% in HL-2-2CGS composite, 44% in HL-2-1.5PGNS and 33% in HL-2-1.5BMS composite. The zirconia based nanocomposite shows an increase of 48% in both HL-2-1.5mZrO$_2$ and HL-2-2tZrO$_2$ composite. This enhanced compressive modulus is an indication of superior load bearing capacity of the material. Tribological properties like wear resistance based on pin in a disc analysis reveal lower coefficient of friction for the nanocomposites than the corresponding blend indicating enhanced wear resistance for the composite. More pronounced wear resistance is observed for PGNS and zirconia based nanocomposites.

References

[1]   Friedrich K. Advances in composite tribology. Composite materials series, vol. 8: Elsevier. 1993; 107–57.

[2]   Friedrich K. Friction and wear of polymer composites. Composite materials series, vol. 1: Elsevier. 1986; 363–96.

[3]   Friedrich K. Advances in composite tribology. Composite materials series, vol. 8: Elsevier. 1993; 3–15.

[4]   Friedrich K. Wear performance of high temperature polymers and their composites, CRC Press. 1997; 221–46.

[5]   Suh N, Moseleh M, Arinez J. Wear. 1998; 214:231.

[6]   Kurtz SM. UHMWPE biomaterials handbook, Academic Press; 2009.

[7] Sahebian S, Zebarjad S, Sajjadi S, Sherafat Z, Lazzeri A. J. Appl.Polym. Sci. 2007; 104:3688.

[8] Guermazi N, Elleuch K, Ayedi H, Fridrici V, Kapsa P. Mater. Des. 2009; 30:3094.

[9] Anderson J. Tribol. Int. 1982; 15:43.

[10] Chowdhury S, Mishra A, Pradhan B, Saha D. Wear. 2004; 256:1026.

[11] Bakar MA, Cheng MH, Tang SM, Yu SC, Liao K, Tan CT, Khor KA, Cheang P. Biomaterials. 2003; 24:2245.

[12] Westby M, Backman C. BMC Health Serv. Res. 2010; 10:119.

[13] Chen J, Yang W, Yu GP.et.al. J. Mater. Process Technol. 2008; 202:165.

[14] Wood W, Maguire R, Zhong W. Compos. Part B 2011; 42:584.

[15] Wroblew B, Lynch M, Atkinson J, et al. J. Bone Joint Surg. Br. 1987; 69:61.

[16] Isaac G, Atkinson J, Dowson D, Wroblewski B. Eng. Med. 1986; 15:19.

[17] Wang M, Ladizesky NH, Tanner KE, Ward IM, Bonfield W. J. Mater. Sci. 2000; 35:1023-30.

[18] Bonfield WJ, Grynpas MD, Tully AE, Bowman J, Abram.J. Biomaterials. 1981; 2:185.

[19] Huang J, Di Silvio L, Wang M, Tanner K.E, Bonfield WJ. Mater. Sci. Mater. Med. 1997; 8:775.

[20] Suwanprateep J, Tanne. KE, Turner S, Bonfield. WJ. Biomed. Mater. Res. 1998; 39:16.

[21] Ladizesky NH, Ward IM, Bonfield. WJ. Appl.Polym. Sci. 1997; 65:1865.

[22] Johnson B, Santare M, Novotny J, Advani S. Mech. Mater. 2009; 41:1108.

[23] Fouad H, Elleithy R, Al-Zahrani S, Ali M. Mater. Des. 2011; 32:1974.

[24] Fouad H, Elleithy R. J. Mech.Behav. Biomed. Mater. 2011; 4:1376.

[25] Liu S, Xu J. Int.Commun. Heat Mass Transfer. 2011; 38:734.

[26] Zeng J, Saltysiak B, Johnson W, Schiraldi D, Kumar S. Composites Part B. 2004; 35:173.

[27] Benitez R, Fuentes A, Lozano K. J. Mater. Process Technol. 2007; 190:324.

[28] Hammel E, Tang X, Trampert M, et al. Carbon 2004; 42:1153.

[29] Bodhak S, Nath S, Basu B. J.Biomater. Appl. 2009; 23:407-33.

[30] Nath S, Bodhak S,Basu B.J. Biomed. Mater. Res. B Appl.Biomater. 2009; 88B:1–11.

[31] Pettarin V, Churruca M, Felhos D, Karger-Kocsis J, Frontini P. Wear. 2010; 269:31.

[32] TK BS, Nair AB, Abraham BT, Beegum PS, Thachil ET. Polymer. 2014; 55:3614-27.

[33] Mallick PK, Broutman LJ. Mater. Sci. Eng. 1975; 18:63.

[34] Athanasiou KA, Zhu CF, Lanctot DR, Agrawal CM, Wang X .Tissue Eng. 2000; 6:361–81.

[35] Kurahatti RV, Surendranathan AO, Srivastava S, Singh N, Kumar AR, Suresha B. Mater. Des. 2011; 32:2644-9.

[36] Malucelli G, Palmero P, Ronchetti S, Delmastro A, Montanaro L. Polym. Int. 2010; 59:1084-9.

[37] Sharmila TK, Antony JV, Jayakrishnan MP, Beegum PS, Thachil ET. Mater. Des. 2016; 90:66-75.

.....ಬಿಐ.....

Chapter 8
SUMMARY AND CONCLUSIONS

The major findings of the study are presented in this chapter.

Polymer nanocomposites (PNC) have opened a new window in achieving a much higher realm of performance which cannot be attained by neat polymer alone. PNC is a class of hybrid materials comprising of an organic polymer matrix with dispersed inorganic nanofillers, having at least one dimension in nanometer range. Value added properties are obtained without sacrificing the processability or adding too much weight. Dispersion of fillers at the nanometer length scale leads to improved filler − matrix interaction. When compared with the economical and technical uncertainties associated with synthesizing new polymeric materials, these nanocomposites have the potential to combine the attractive properties of the component present.

The major thrust of this study is to evaluate the effect of nanozirconia and nanosilica, on various physico-mechanicals, rheological and thermal properties of polyethylene based polymers and its blends. Upgradation of HMHDPE-LLDPE blend using those biocompatible nanofillers is described in detail for developing materials for high performance applications like load bearing biomaterials has been proposed.

The synthesis of the nanoparticulates like nanozirconia and silica nanofibers is the first part of this study. Monodispersed tetragonal nanocrystalline zirconia (t- ZrO_2) with spherical morphology and monoclinic zirconia (m- ZrO_2) with spheroid morphology were synthesized by adopting a facile template assisted sol-gel method. The medium assisting the growth of nanoparticles mainly consisted of $ZrOCl_2.8H_2O$ and NH_4OH as reactants in a 1:2 mixture of Isopropyl alcohol (IPA)-polyvinyl alcohol (PVA) as the dispersing agent. The calcined nanopowders were characterized by X-ray diffraction (XRD), Fourier transform infrared spectroscopy (FTIR), Scanning electron microscopy (SEM), Transmission electron microscopy (TEM), Nitrogen adsorption (BET), Particle size distribution , Zeta potential measurement and Thermogravimetric analysis (TGA). The studies reveal that the size of the particle has highly dependent on PVA content and calcination temperature. Moreover, reacting medium and calcination temperature have vital roles in determining the crystallinity and morphology of ZrO_2. The sample prepared under optimized conditions (2% w/v PVA) show pure tetragonal crystallite phase with an average particle size of 5 nm, surface area of 56 m^2 g−1, and mesoporous structure after calcination at 600 ^{o}C for 5 h. Changing the mode of addition of the reacting medium followed by calcination provides mesoporous, spheroid, m-ZrO_2 with an average particle size of 15nm and surface area 73.5 m^2 g−1. The particle size of t- ZrO_2 is 4nm and that for m-ZrO_2 is 16nm from TEM. These values are in good agreement with XRD results.

Increasing demand and inflexible performance requirements have given thrust for finding new sources for the isolation of silica for the preparation of nanocomposites. Silica has long been known to be present in

plants. It is stored primarily as opaline phytoliths in the epidermis of plant tissue. A novel green chemical route by exploiting the vast and abundant grass varieties are suggested for the production of silica nanofibers. The three different grass varieties namely Indian grass (Sorghastum nutans, CG), Pampass grass (Cortaderia selloana, PG), and Bamboo (BM) have been selected for the isolation of nanosilica via an acid pre treatment followed by calcination method. The concentrations of acid (HCl) pretreatment were optimized from SEM and EDS analysis as 0.01N HCl for CG and 0.1N HCl for FPG and 1N HCl for BM to get highly pure, white, mesoporous nanosilica powder having fibrillar morphology. The chemical purity, crystallinity and morphology are confirmed by FTIR, XRD, and TEM analysis. Thermal stability of the fiber was investigated by TGA analysis and surface area was measured by BET surface area analyzer. HR-TEM analysis reveals that the actual morphology of isolated silica is rich in nano fibrillar channel network for PGNS silica and bundles of fibers for silica from Indian grass and Bamboo. Thus the study suggests a breakthrough route for preparing high-purity mesoporous fibrous silica materials by utilizing an abundant bio-precursor like tip of Indian grass, flowers of pampas grass and stem of Bamboo. The silica obtained has good potential for the preparation of polymer nanocomposites.

The isolated biocompatible fillers were used for the upgradation of a polyethylene blend matrix for high performance applications. High molecular weight high density polyethylene (HMHDPE) and Linear low density polyethylene (LLDPE) based blend was prepared by melt mixing in a Thermo Haake Rheocord mixer. HMHDPE and LLDPE are sufficiently compatible to take advantage of the attractive properties of the both. All

mechanical properties other than impact strength are higher for HMHDPE than LLDPE. Blending HMHDPE with LLDPE enhances the toughness of HMHDPE with only slight decrease in the yield stress. Thermal stability and processability are improved by blending. To take advantages of the high mechanical performance with better processability, 80/20 blend was selected as the base for composite preparation.

Polymer nanocomposites based on 80/20 blend of HMHDPE-LLDPE (HL-2) were prepared by melt mixing using nanozirconia and silica nanofibers followed by injection moulding. Two different crystalline forms of nanozirconia (m-ZrO_2 and t-ZrO_2), fillers were dispersed in the HL-2 matrix to evaluate the effect of the crystalline form, size and morphology on reinforcement. Both the fillers got dispersed well in the PE blend matrix. The effects of nanofillers on the mechanical, thermal, rheological and morphological characteristics of nanocomposites were evaluated. Composites show higher thermal stability with respect to the neat blend. Independent of their crystalline phase, size and morphology, both fillers give significant improvement in desirable properties. The entanglement between the polymer chains and the nanozirconia was seen from the FTIR studies and MFI analysis. Microstructure investigations on the HL-2-2t-ZrO_2 nanocomposite by TEM illustrate well dispersed nano t-ZrO_2 in the PE matrix. Morphological characterization by SEM on the fractured surface of nanocomposites shows better dispersion and interfacial addition of both types of zirconia in the HL-2 matrix and this can be correlated with their mechanical performance. With the addition of nanozirconia into the HL-2 matrix the thermal stability has been significantly improved, as evidenced from the TGA analysis. Both types of nanozirconia act as weak

nucleating agents for HL-2 matrix. The study proves that addition of zirconia nano fillers has a salutary effect on the thermo mechanical properties of PE matrix without any surface modification to both the filler and the matrix.

HL-2 blend reinforced with silica nanofibers isolated from Indian grass (CGS), Pampas grass (PGNS) and Bamboo (BMS) was prepared separately by melt mixing. Significant improvement in mechanical properties is observed by the addition of fibrous silica to PE matrix without any surface modification. Absence of chemical interaction is evident from FTIR analysis and the entanglement between the polymer chains and the fibrous filler is from the MFI analysis. Rheological analysis confirms enhanced interaction between the fibrous silica and PE matrix. FTIR analysis confirms that there is no chemical interaction between the filler and the matrix.TGA analysis shows that thermal stability improves with increasing nanosilica content. DSC analysis shows a weak nucleating effect of the filler. TEM micrographs of HL-2-2PGNS nanocomposites prove homogeneous fibrous silica distribution in the PE matrix with some aggregates. Microstructure analysis of the tensile fractured surface of the nanocomposite by SEM gives evidence for the dispersion of silica fibers. SEM micrographs reveal the separation of individual silica fibers from the fiber bundles of CGS and BMS during melt mixing, which can efficiently reinforce the polymer matrix.

An attempt was made to test the suitability of PNCs in high performance applications. PE based nanocomposites has long been used for load bearing applications in biomedical field for bone implants. PNCs

may be potential candidates for such applications due to their versatility. The potential of nanozirconia and silica nanofibers in enhancing the load bearing properties of HMHDPE-LLDPE blend has already been considered in this thesis. The improved properties of the HL-2 blend nanocomposites widen the application spectrum of this composite for the replacement of PE based composite used for load bearing bone implants. Apart from the properties already discussed in the earlier portion of the work, other important parameters essential for polymeric materials to be used for load bearing joint components in biomedical field are compressive property, fracture toughness and wear resistance. Accordingly the effect of nanozirconia and fibrous nanosilica on these mechanical and tribological properties of HL-2 blend nanocomposite has been studied. It was exposed that an increase in the ceramic content results in the enhancement in the mechanical properties. The improvement in mechanical properties is supposed to be due to the presence of more contact positions offered by the small sized nanoparticulates and the PE matrix. An improvement in fracture toughness is observed for nanosilica and nanozirconia based composites. The high compressive strength of brittle ceramic nanoparticles coupled with efficient stress transfer results superior in compressive properties for both the silica based and zirconia based nanocomposites. The enhanced compressive modulus is an indication of superior load bearing capacity of the material. Tribological properties like wear resistance based on pin in a disc analysis reveal lower coefficient of friction for the nanocomposites than the corresponding blend indicating better wear resistance for the composite. Improved wear resistance is observed for PGNS and zirconia based nanocomposites.

The isolation of silica nanofibers and synthesis of zirconia nanoparticles and the identification of their potential to develop useful nanocomposites based HMHDPE-LLDPE blend to generate a spectrum of useful engineering material for critical applications.

The major contributions of the work are

- Using a surfactant assisted sol-gel method monodispersed tetragonal nanozirconia was synthesized at a comparatively low cost.

- A new source of biomass was explored for the synthesis of fibrous nanosilica, which may have commercial applications.

- Using nanozirconia and fibrous nanosilica high performance composites based on PE blend was prepared.

Future Scope

a) Evaluating biological response of the blend nanocomposites by 'in vivo' and 'in vitro' test, using simulated body fluid (SBF) or in the actual implant conditions

b) Introduction of random crosslinking by radiation for further development in the mechanical and tribological properties of the nanocomposites.

.....ৡ৹ঙ.....

List of Publications

Journals Paper

[1] "On the Facile Poly vinyl alcohol assisted Sol-gel synthesis of Tetragonal zirconia nanopowder with mesoporous structure" **Shadiya M. A.**, Nisha Nandakumar, Rani Joseph, George K.E. (**'Advanced powder technology'** 28 (2017) 3148–3157; https://doi.org/10.1016/j.apt.2017. 09.029)

[2] "Carbon nanofiber reinforced thermoplastic elastomer based on polypropylene/polybutadiene blend: theoretical modeling of Young's modulus of the nanocomposites with respect to the orientation and agglomeration of carbon nanofibers" Sreedevi P.G, **Shadiya M. A.,** Rani Joseph. (**'Journal of Polymer Engineering',** Published online 2018-05-22; DOI: https://doi.org/10.1515/polyeng-2017-0408)

[3] "Isolation and characterization of Mesoporousfibrillarnanosilica of floral origin: Cortaderiaselloana flowers as the Silica source" **Shadiya M. A.**, NishaNandakumar, MidhunDominic.C.D, Rani Joseph, George K.E. (Communicated to **'International Journal of Nanoscience and Nanotechnolog'**)

[4] "Fabrication and Characterisation of Nano Zirconia Reinforced High Molecular Weight High Density Polyethylene – Linear Low Density polyethylene Blend Nanocomposites" **Shadiya M. A.** [1], Dennymol P.V, Rani Joseph*[1], George K.E.[1,2] (Communicated to **'Composite science and technology'**)

[5] "Effects of olivine nanosilica on the rheological, mechanical, transport and thermal properties of natural rubber nanocomposites" Julie chandraC.S, **Shadiya M. A.**, Bipinbal P.K, Sunil. K. Narayanankutty. (Communicated to '**Journal of Applied Polymer science**')

[6] "A facile route for the synthesis of nano fibrous silica from Indian grass: A promising biofiller for HMHDPE-LLDPE blend" **Shadiya M. A.**, K. E. George, Rani Joseph. (Proceedings of **27**[th] **Kerala Science Congress, 2015, ISBN:81-86366-88-1**)

[7] "Mechanical and Melt Rheological Properties of Nano Zirconia Reinforced HMHDPE-LLDPE Blend" **Shadiya M. A.**, K.E.George, Rani Joseph. (Proceedings of **13th Prof. K V Thomas endowment National Seminar 2014** on New frontiers in Chemical Research, **ISBN: 978-81-930558-0-9**)

[8] "Fibrous nano silica from bamboo: Excellent biofiller in HMHDPE-LLDPE blend" **Shadiya M. A.**, Rani Joseph, K.E.George (Proceedings of **24thSwadeshi Science congress, 2014, ISBN: 978-81-928129-2-2**)

Papers presented in National/International Conferences

[1] "Fibrous nano silica from bamboo: Excellent biofiller in HMHDPE-LLDPE blend", **Shadiya M. A.**, Rani Joseph, K. E. George. 24th SwadeshiScience congress, National Seminar, ThunchathEzhuthachan Malayalam University, Thirur, MalappuramDist, Kerala, November 6-8, 2014.

[2] "A Green Source for the Synthesis of Structurally Controlled Silica Nano Fibers and Its Mechanical Reinforcement in HMHDPE-LLDPE Blend", **Shadiya M. A.**, K.E. George, Rani Joseph. National Conference on Stimulating concepts in green chemistry , SNM College Maliankara, Ernakulum Dist, kerala, November 13-14, 2014.

[3] "Extraction of Silica with Diverse Morphology from Different Grass Sources and Its Role as Mechanical Reinforcement in HMHDPE-LLDPE Blend", **Shadiya M. A.**, K. E. George, Rani Joseph. National Conference on Biopolymers & Green composites- Emerging Science & Technology, BPGC 2014-2nd Series, CBPST, CIPET, Kalamassery, Ernakulum Dist, kerala, November 14, 2014. (**2nd Prize, Best Oral Presentation**)

[4] "Mechanical and Melt Rheological Properties of Nano Zirconia Reinforced HMHDPE-LLDPE Blend" **Shadiya M. A. [1*]**, K.E.George, Rani Joseph.13th Prof. K V Thomas endowment National Seminar on New frontiers in Chemical Research, S.H, College Thevara, Ernakulamdist, kerala, December 4-5, 2014. (**2nd Prize, Best Oral Presentation**)

[5] "Mechanical and Thermal Properties of Nano Zirconia Reinforced HMHDPE-LLDPE Blend", **Shadiya M. A.**, K.E.George, Rani Joseph. National Seminar on Characterisation Techniques in chemistry, KKTM College, Kodungallur, ThrissurDist, Kerala, December 16 & 17, 2014.(**3rdPrize, Best Oral Presentation**)

[6] "A facile route for the synthesis of nano fibrous silica from Indian grass: a promising biofiller for HMHDPE-LLDPE blend", **Shadiya M. A.**, K. E. George, Rani Joseph. 27th Kerala Science Congress, Alappuzha, January 27-30,2015.

[7] "Isolation of Silica with Structurally Controlled Morphology from a Green Source and Its Role as Mechanical Reinforcement in HMHDPE-LLDPE Blend", **Shadiya M. A.**, K.E.George, Rani Joseph. National Seminar on Modern trends in Chemistry, Sree Kerala Varma College, Thrissur, Kerala. November 12 &13, 2015.

[8] Effect of Zirconia nano-fillers on HMHPE-LLDPE blend: Mechanical, Thermal and Morphological Evaluations, **Shadiya M. A.**, K. E. George, Rani Joseph. National Seminar on Colloquium on exotic materials and its implication in societal life, SreeVyasa NSS College, Wadakanchery, ThrissurDist.,Kerala. December 17&18, 2015.

[9] Fabrication and Characterisation of Nano Zirconia Reinforced HMHDPE-LLDPE blend Nanocomposites, **Shadiya M. A.**, K.E.George, Rani Joseph. International Conference on Advances in Polymer technology APT, Dept.of Polymer Science and Rubber Technology, CUSAT, Cochin, Kerala. February 25-26, 2016.

[10] High Performance Tetragonal Nanozirconia Reinforced HMHDPE-LLDPE Blend Nanocomposite with Improved Tribological Properties, **Shadiya M. A.**, K. E. George, Rani Joseph. International conference on New Trends in Applied Chemistry, NTAC-2017, S.H College, Cochin, Kerala. February 9-11.

.....ോരു.....

Curriculum Vitae

Shadiya M A
Thaiparambil House
Chapel Lane
Aluva, Pin-683101
Ernakulam

Mob. 9947014094, 8281818795
E mail: shadhiya.ashraf@gmail.com

Educational Qualification

- MSc Chemistry, School of Chemical Sciences, M G University, Kottayam.
- MPhil Chemistry, School of Chemical Sciences, M G University, Kottayam.

Teaching and Training Experience

2 years of Teaching experience
8 years of Research experience

a) C-MET, Thrissur
b) Department of Polymer Science and Rubber Technology, CUSAT.

Achievement Awards

- KSCSTE Research fellowship
- UGC-BSR Research fellowship
- Best Oral Presentation (2nd Prize) in BPGC 2014-2nd Series , CBPST, CIPET, Ernakulam
- Best Oral Presentation (2nd Prize) in 13th Prof. K V Thomas endowment National Seminar on New frontiers in Chemical Research, S.H, College Thevara, Ernakulam, Kerala.
- Best Oral Presentation (3nd Prize) in National Seminar on Characterisation Techniques in chemistry, KKTM College, Kodungallur, Thrissur, Kerala

Personal Details

Nationality	:	Indian
Marital Status	:	Married
Father's Name	:	Muhammad Ashraf M.S
Husband's Name	:	Imthiyas T A
Language Proficiency	:	English, Hindi, Malayalam.

…..ഇരു…..